ECOLOGICAL MODELLING OF THE PHYTOPLANKTON COMMUNITY IN THE NORTHERN ADRIATIC SEA

Ivano Vascotto

Doctoral Dissertation
Jožef Stefan International Postgraduate School
Ljubljana, Slovenia

Supervisor: Dr. Janja Francé, National Institute of Biology, Ljubljana, Slovenia

Evaluation Board:
Prof. Dr. Vlado Malačič, Chair, IPS and National Institute of Biology, Ljubljana, Slovenia
Prof. Dr. Patricija Mozetič, Member, IPS and National Institute of Biology, Ljubljana, Slovenia
Dr. Ioanna Varkitzi, Member, Hellenic Centre for Marine Research (HCMR), Institute of Oceanography, Attica, Greece.

MEDNARODNA PODIPLOMSKA ŠOLA JOŽEFA STEFANA
JOŽEF STEFAN INTERNATIONAL POSTGRADUATE SCHOOL

Ivano Vascotto

ECOLOGICAL MODELLING OF THE PHYTOPLANKTON COMMUNITY IN THE NORTHERN ADRIATIC SEA

Doctoral Dissertation

EKOLOŠKO MODELIRANJE FITOPLANKTONSKE ZDRUŽBE V SEVERNEM JADRANSKEM MORJU

Doktorska disertacija

Supervisor: Dr. Janja Francé

Ljubljana, Slovenia, January 2025

our time will come... (the nuggets)

Acknowledgments

I wish to thank all the people of the Marine Biology Station Piran for the support and friendship during my years of study and work there. Their kind presence was crucial to preserve my ease and serenity every time the most discouraging and frustrating aspects of the research popped up. I thank Assoc. Prof. Dr. Patricija Mozetič who got me *off the streets* and gave me the chance of finding my way. I thank Dr. Timotej Turk Dermastia for our challenging conversations and for keeping our door open to the most recent scientific and social novelties. Finally, I wish to thank my supervisor Dr. Janja Francé, whose scientific trustworthiness and commitment stands for me as a role model. Her guidance and encouragement represented the pillar of my professional flourishing.

I acknowledge the following funding grants: ARIS (P1-0237), ARIS young researchers (51986), Horizon 2020 - ASSEMBLE Plus (No 730984), Open access CRUI-CARE Agreement (Istituto Nazionale di Oceanografia e di Geofisica Sperimentale).

Abstract

This dissertation examines the ecological dynamics of phytoplankton communities in the northern Adriatic Sea, focusing on phenology, environmental drivers, and trophodynamics. The complexity of the region, characterized by the richness of phytoplankton communities, environmental variability and intensive human activities, is not seen as an obstacle but as an opportunity to gain new ecological insights. Building on existing knowledge, the research combines established data analysis techniques with innovative ecological modeling methods to unravel the complicated and paradoxical nature of phytoplankton life.

The dissertation comprises three interlinked studies conducted at the Slovenian Long-Term Ecological Research (LTER) site in the Gulf of Trieste. The first study examines the phenology of the phytoplankton community using a time series of monthly taxa abundances collected between 2005 and 2017. By reducing the complexity of the community into constituent assemblages, the study evaluates techniques for species selection, community structure analysis and assemblage definition, highlighting their strengths and limitations.

The second study investigates how atmospheric (winds, temperature, precipitation) and hydrospheric (river inputs, water column stability, salinity) factors shape the ecological niches of the phytoplankton assemblages described in the previous study. Through linear and nonlinear numerical modeling, the study identifies the main niche-forming parameters and their properties. The resulting models are then applied to assess the connectivity of the northern Adriatic Basin at the mesoscale. These results are placed in the context of current ecological theories.

The third study extends phytoplankton research to individual-based biological data collected in the Gulf of Trieste between April 2020 and March 2021. It investigates the differences between taxonomic and trait-based classifications and between abundance and biomass metrics. By scaling individual-level data to community-level dynamics, the study provides insights into the trophic structure of the planktonic food web.

The dissertation concludes by summarizing the main results in a conceptual model that improves the understanding of phytoplankton dynamics in a highly dynamic coastal environment. In summary, the distribution of phytoplankton communities in the Gulf of Trieste exhibits a partially predictable seasonal succession driven by environmental forces and mesoscale connectivity. The baseline community is dominated by nano-sized phytoflagellates, with cell size and biomass distribution following a power law during times of resource scarcity or grazing pressure. Diatoms dominate during biomass peaks in spring and autumn, which is associated with larger cells and multimodal distributions. These shifts reflect the influence of both top-down and bottom-up processes. Phenology is influenced by periodic events such as stratification and river discharge, as well as non-periodic disturbances such as climatic anomalies, which promote the occurrence of short-lived assemblages. At the mesoscale, the Gulf of Trieste is partially connected to the northern Adriatic by cyclonic gyres and wind-driven circulations, especially in winter and autumn, while in spring and summer local phenomena dominate and reduce connectivity.

Povzetek

Doktorska disertacija preučuje ekološko dinamiko fitoplanktonskih združb v severnem Jadranu s poudarkom na fenologiji, okoljskih dejavnikih in trofodinamiki. Kompleksnost območja, ki ga zaznamujejo pestrost fitoplanktonskih združb, velika spremenljivost okolja in intenzivne človekove dejavnosti v tej disertaciji ni obravnavana kot ovira, temveč kot priložnost za pridobitev novih ekoloških spoznanj. Disertacija gradi na podlagi obstoječega znanja in uveljavljene tehnike analiz podatkov združuje z inovativnimi metodami ekološkega modeliranja, da bi razkrila zapleteno in paradoksalno naravo fitoplanktona.

Disertacija vključuje tri medsebojno povezane prispevke, izvedene na mestu dolgoročnih ekoloških raziskav (LTER) v Tržaškem zalivu. Prvi prispevek preučuje fenologijo fitoplanktonske združbe, kjer uporabi mesečne podatke o sestavi in abundanci fitoplanktona, ki so bili zbranih med letoma 2005 in 2017. Prispevek kritično ovrednoti in prilagodi metode izbire značilnih taksonov, analize sestave fitoplanktonske združbe in metode določitve osnovnih, časovno ločenih skupin značilnih taksonov, s katerimi je mogoče zmanjšati kompleksnost fitoplanktonske združbe, ob tem pa tudi osvetli prednosti in slabosti teh metod.

Drugi prispevek raziskuje, kako atmosferski (veter, temperatura, padavine) in hidrološki dejavniki (pritoki rek, stabilnost vodnega stolpca, slanost) oblikujejo ekološke niše fitoplanktonskih združb, opisanih v prvem prispevku. Z uporabo linearnega in nelinearnega numeričnega modeliranja prispevek določi glavne parametre, ki oblikujejo ekološke niše, in opredeli njihove lastnosti. Rezultati modelov so nato uporabljeni za oceno povezljivosti severnojadranskega bazena na mezoskalnem nivoju. Ti rezultati so nato umeščeni v kontekst sodobnih ekoloških teorij.

Tretji prispevek razširja raziskave fitoplanktona s podatki na ravni posameznega organizma. Ti podatki so bili zbrani v Tržaškem zalivu med aprilom 2020 in marcem 2021. Prispevek preučuje razlike med taksonomsko klasifikacijo in klasifikacijo na podlagi drugih lastnosti, kot je oblika celice, ter med metrikami na podlagi abundance in biomase. S prenosom spoznanj pridobljenih na ravni posameznih organizmov na raven celotne združbe se odpira vpogled v trofično strukturo planktonske prehranske mreže.

Disertacija se zaključi s povzetkom glavnih ugotovitev, ki izboljšuje razumevanje dinamike fitoplanktona v zelo dinamičnem obalnem okolju in jih združi v konceptualni model. Na kratko, fitoplanktonska združba v Tržaškem zalivu kaže delno predvidljivo sezonsko sukcesijo, ki jo definirajo okoljski dejavniki in mezoskalna povezljivost. V fitoplanktonski združbi večinoma prevladujejo nanoflagelati, pri čemer frekvenčna porazdelitev velikosti in biomase celic pogosto sledi potenčnemu zakonu in nakazuje na obdobja pomanjkanja virov ali pritiska plenilcev. Diatomeje prevladujejo med spomladanskim in jesenskim viškom biomase, večinoma z večjimi celicami čigar frekvenčne porazdelitve težijo k multimodalnosti. Ti spremembe v združbi odražajo vpliv procesov, ki delujejo od zgoraj navzdol (top-down) in od spodaj navzgor (bottom-up). Na fenologijo fitoplanktona vplivajo periodični pojavi, kot na primer razslojenost vodnega stolpca in dotoki rek, ter neperiodičnih motenj, kot so na primer podnebne anomalije, ki spodbujajo pojav kratkoživečih združb. Na mezoskalnem nivoju je Tržaški zaliv delno povezan s

severnim Jadranom prek ciklonskih vrtincev in z vetrom gnanih tokov, zlasti pozimi in jeseni, medtem ko spomladi in poleti prevladujejo lokalni pojavi, ki zmanjšujejo povezljivost.

Contents

List of Figures

Chapter 1

Introduction

1.1 Phytoplankton Ecology

1.1.1 Overview

In ecology, phytoplankton is one of the collection of organisms into which aquatic life is divided. Of the two parts that make up the word phytoplankton, the first, phyto, refers to the biological property of being able to convert light energy into chemical energy, while the second, plankton, refers to the physical compliancy to water currents. Apart from this simple and clear definition of phytoplankton, there are many caveats. This is because, of the many taxa commonly referred to as phytoplankton, many also exhibit heterotrophic or mixotrophic behaviors (Mansour and Anestis 2021) and are then also representatives of another aquatic group, the zooplankton, while others spend part of their lives on the bottom, mainly as different kinds of resting stages (Reynolds 2006). On the contrary, some microalgae can be introduced into the water column from adjacent habitats by chance (tychoplankton; Reynolds 2006). The fact that planktonic organisms live suspended in water does not mean that they have no way of determining their position in the water column. Indeed, many planktonic organisms have flagella, while others can slow their sinking or speed their ascent. Nevertheless, planktonic organisms cannot resist most of the broad spectrum of movements of the water (Reynolds 2006).

Besides the autotrophic nutrition mode and the inability to resist most currents, the size of the cells of the phytoplankton is the third common characteristic of this group and is commonly used to distinguish its classes (Sieburth et al. 1978). Cells that fall in the 2-20 µm size range define the nanofraction of phytoplankton, while cells between 20 and 200 µm define the microfraction. Phytoplankton cells smaller than 2 μm define the picophytoplankton which is constituted by the smallest possible free-living cells (Raven 1998), while cells larger than 200 µm should be counted as mesoplankton (Sieburth et al. 1978). These ranges are usually referred to as phytoplankton size classes (PSC).

From a cladistic perspective, phytoplankton is a paraphyletic group, meaning that species belonging to phytoplankton have no common ancestor. In fact, there are representatives of classes from different phyla in this ecological compartment (Archibald et al. 2017), and, moreover, there are many existing algal classifications, still evolving (Adl et al. 2019). Perhaps the most studied phytoplankton group are diatoms, which according to Medlin (2016) belong to three classes: Coscinodiscophyceae, Mediophyceae and Bacillariophyceae (phylum Ochrophyta). Other not less important groups of phytoplankton include coccolithophorids belonging to the Haptophyta phylum, and the Dinophyceae, corresponding to dinoflagellates and belonging to Alveolata supergroup (Archibald et al. 2017). Other common phytoplankton classes include: the Raphidophyceae, the

Euglenophyceae, the Chlorophyceae, the Cryptophyceae, the Chrysophyceae, the Dictyochophyceae, and the Prasinophyceae.

Phytoplankton often occurs as single cells, but colonies are also not uncommon. In both cases, the specimens are too small to observe and identify with the naked eye. Then, the most common method for examining these organisms is to observe and count them with an inverted light microscope using the Utermöhl method (Utermöhl 1958). Worldwide, in a pool of around 50.000 marine and freshwater microalgae (Guiry 2024), at least 4000 marine phytoplankton species can be distinguished morphologically, most of which belong to the three main groups: diatoms (~1700 species), dinoflagellates (~1600 species) and coccolithophorids (~300 species) (Sournia et al. 1991), but recent genetic studies estimated the total number of species higher by one order of magnitude (De Vargas et al. 2015). Whether such a number is to be considered large or small depends on the approach taken in considering it. From the perspective of the first pioneering ecological studies on the subject, the oceans do not contain enough niches to explain such a large diversity of species (Hutchinson 1961), while from the perspective of genetic diversity, such a number is very small considering the population size (Filatov 2019).

Marine phytoplankton is present in the upper layer of all earth's oceans and seas, where the amount of radiation light is sufficient for these organisms to thrive. Locally the measured abundance of phytoplankton species varies greatly between a few thousand to millions of cells per litre. Such variations are often abrupt and driven by the exponential growth in favoring conditions (Huppert et al. 2002), which can ultimately result in phytoplankton blooms. Often the gradients of cell density between blooms and low abundance areas are steep and not at all smooth, because phytoplankton finds the proper growth condition only in certain water bodies which are then shaped by currents. Inside eddies and current fronts, the phytoplankton cells accumulate, whereas beyond eddies and fronts the abundance may remain very low (Condie and Condie 2016). Discontinuities in physical water properties, such as those driven by temperature (thermocline) and salinity (halocline), as well as their dissipation then determine the dispersal of phytoplankton cells in the seas (Franks 1992, D'asaro et al. 2011). All these forces combined result in a highly patchy spatial distribution of phytoplankton. In nearshore upwelling areas and estuaries, phytoplankton cells accumulate along persistent fronts (McManus and Woodson 2012) and in thin layers below the water surface (Sullivan et al. 2010). The main factor driving the phytoplankton distribution in such nearshore areas is the nutrient input, since upwelling brings enriched deep water to the surface (Margalef 1978), while rivers discharge transport nutrients away from land (Horner-Devine et al. 2015). These nutrient-rich areas are critical for the phytoplankton primary production (Martin et al. 2002) and they are also a prerequisite for the energy transfer to higher trophic levels that would not be possible in a perfectly mixed ocean (Mullin and Brooks 1976).

Another important aspect in which phytoplankton patchiness plays a role is sexual reproduction. Phytoplankton alternates between repetitive asexual reproductive phases, during which population density increases (if there are no external losses), and rare sexual reproductive events (Rengefors et al. 2017), during which it is easier for phytoplankton to find a mate if cell density is high (Durham et al. 2013). Phytoplankton life cycles may include also a dormant phase corresponding to the production of resting stages or cysts that can buffer environmental fluctuations on a time scale of up to years (von Dassow and Montresor 2011). In recent years, the importance of this phytoplankton life strategy in coastal waters has been highlighted by Belmonte and Rubino (2019) and proposed as a solution to explain the high phytoplankton diversity in these areas.

1.1.2 Role in biogeochemical cycling

Phytoplankton communities play an important role in marine ecosystems, as they are the gateway to the food chain and are critical to biogeochemical cycling in the seas and oceans (Falkowski et al. 2003, Hays et al. 2005). One of the main characteristics of phytoplankton is its ability to convert light energy into chemical energy, i.e., it can produce the organic matter necessary for its maintenance, growth, and reproduction through photosynthesis. Unlike land plants, phytoplankton do not lose water when they acquire carbon from external sources, but this does not mean that phytoplankton cells do not need to uptake other important chemical components from external sources. Such chemical elements are the so-called nutrients, which are critical for phytoplankton life. The important nutrients include sodium (Na), potassium (K), calcium (Ca), magnesium (Mg) and chlorine (Cl), which are ubiquitous in seawater, while two macronutrients (phosphorus - P and nitrogen - N) and two micronutrients (iron - Fe and silicon - Si) are usually the limiting factors for phytoplankton growth (Reynolds 2006). The main source of phosphorus in the marine environment is the weathering on land. This element is then transported to the sea in particulate and dissolved forms via rivers (Paytan and McLaughlin 2007). Rivers play a role in the nitrogen cycle as well, which is also transported to the sea via rivers (Fogg 1982), but the main non anthropogenic source of this element is the upwelling of deep water and, in coastal seas, the nitrification reaction in the anoxic sediment layer (Herbert 1999). Iron is a limiting factor, especially in surface oceanic waters, whereas in nearshore environments it is adequately supplied by freshwater and dust inputs (Reynolds 2006). Finally, silicon, an important micronutrient for diatoms and silicoflagellates (Dictyochophyceae), is transported either by rivers to the sea or supplied to the surface layer by upwelling (Treguer and De La Rocha 2013). Thus, phytoplankton is not only the entry point for organic carbon into the marine food chain, but also one of the most important nodes in the biogeochemical cycles for nitrogen, phosphorus, iron, and silicon. The direct contribution of phytoplankton to biogeochemical cycles extends beyond the boundaries of the marine environment. In fact, phytoplankton are responsible for a significant portion of oxygen production at the planetary scale (Field et al. 1998).

Moreover, phytoplankton, along with microzooplankton, bacteria, and viruses, play an important ecological role in marine biogeochemistry as part of the so-called “microbial loop” (Azam and Malfatti 2007). Bacteria assimilate organic compounds formed and excreted by phytoplankton in the form of dissolved organic matter, while zooplankton directly graze on phytoplankton and bacterioplankton (Azam et al. 1983). Conditions favourable for a phytoplankton bloom can be interpreted as physical or chemical perturbations that disrupt predator-prey control, which usually operates at the level of microbial cycling. In such "loopholes," populations of some phytoplankton species can increase exponentially (Irigoien et al. 2005). Cell lysis triggered by viral infection, the viral shunt, is also thought to be an important factor in preventing and terminating such blooms (Brussaard 2004). Recycling of organic components from lysed cells then occurs via microbial cycling, which is estimated to be responsible for 2-10% of the total export of phytoplankton primary production (Wilhelm and Suttle 1999). Another important factor affecting the faith of the phytoplankton primary production and its organic compounds is the cell size. Larger phytoplankton cells escape the prey range of the microzooplankton, but not the range on which the mesozooplankton feed. The trophic pathway through the microzooplankton results in a reduction in export of primary production both by sinking and by consumption at higher trophic levels. Grazing by the microzooplankton also helps maintain nutrient concentrations in seawater as nutrients rapidly regenerate and circulate (Mitra et al. 2007). Microzooplankton grazing exerts the greatest predatory pressure on planktonic primary production, consuming about 60-70% of it (Calbet and Landry 2004).

Mesozooplankton, on the other hand, generally consume 10-40% (Calbet 2001). These proportions depend on the size structure of the phytoplankton community, which in turn depends on the chemical and physical factors of the water column.

1.1.3 Phytoplankton environment

1.1.3.1 Ecosystem definition

An ecosystem can be defined as a functional unit with recognizable boundaries and an internal homogeneity (Boje and Tomczak 1978). Because of the dynamic nature of the marine environment, it is particularly difficult to recognize these boundaries and to draw spatial and temporal units on which define the marine ecosystems, especially in the pelagic zone (Clayton et al. 2013). Such units are connected to the idea of defining relevant spatial and temporal scales, which is a common and consistent theme across ecology and biogeography. Ecological studies typically address time spans ranging from generation times to longer population cycles (Jenkins and Ricklefs 2011). The intermediate scales for temporal and spatial dimensions on which ecology and biogeography converge are considered relevant to population dynamics (Jenkins and Ricklefs 2011). In the specific case of phytoplankton biogeography, it has been shown that the distribution of this biological compartment is generally patchy and that the current inability of prediction models to resolve ecosystems at the mesoscale (1-500 km) is a major obstacle to understanding the marine ecosystem as a whole (Martin 2003).

Then the above definition of the ecosystem can be expanded to include a self-regulating system of interactions between organisms and their inorganic environment (Boje and Tomczak 1978). In the case of coastal ecosystem, a ubiquitous and definite definition has not been formulated so far (Hossain et al. 2020). Yet, the intertwined relationship between space, time, environment, and phytoplankton suggests that it would be highly interesting to study variation in all these dimensions simultaneously to partition the known variation in community composition into proportions explained by factors related to dispersal, community succession, and environmental influences (Soininen 2010).

1.1.3.2 Coastal characteristics affecting phytoplankton

Freshwater runoff from rivers and sewers is one of the characteristics of coastal marine ecosystems. The complex dynamics of phytoplankton become even more complex in areas where rivers discharge large volumes of freshwater, in low-volume basins (Franco and Michelato 1992, Groß et al. 2022). In such cases, when multiple freshwater sources are present in a shallow basin, the area is simply referred to as a region of freshwater influence (Horner-Devine et al. 2015). Shallow coastal waters are particularly influenced by such natural and anthropogenic freshwater sources, and these ecosystems, which include tidal rivers, estuaries, lagoons, and coastal river basins, are distinct from offshore ecosystems (Cloern 1996). In such waters, especially near river mouths, dissolved nitrogen and dissolved silica appear to be abundant and rarely limit phytoplankton growth. Riverine inputs are sources of sediment, nutrients, and live phytoplankton cells that together form large spatial gradients along the river-sea axis. The ecosystem impact of a single river plume depends on the dilution rate and transport processes within the plume. The dilution process is controlled by vertical mixing, while horizontal transport is controlled by horizontal advection, driven in large part by buoyancy (Horner-Devine et al. 2015). Increased stratification and high nutrient levels promote phytoplankton bloom formation, which may in evolve in harmful algal blooms (Margalef 1978). Persistent fronts between saltwater and freshwater have a similar promoting effect on the phytoplankton community,

favouring only some of the taxa present in the community (Franks 1992, Mangolte et al. 2022). Another relevant coastal characteristic is the intrusion of relatively cold and nutrient-rich deep water into the photic zone near the coast, also known as coastal upwelling. This phenomenon typically occurs near the coast and is due to offshore winds; the deep-water swells near the surface to compensate for the advection of surface water caused by these winds. When coastal winds subside, mixing becomes less intense and warmer, nutrient-poorer water begins to accumulate at the surface (Reynolds 2006). The transition from well-mixed water to stratified conditions is associated with a decrease in production and a transition from a community dominated by diatoms to smaller or mobile coccolithophorids and dinoflagellates (Smayda and Reynolds 2001). In addition to river runoff and wind-induced mixing, nutrients are released in the coastal ecosystem by sewage and industry (Stirn 1993, Rangel-Buitrago et al. 2024). The additional release of nutrients and the process of enrichment is referred to as eutrophication and can have disastrous consequences for coastal ecosystems, including loss of true oligotrophic species, loss of biodiversity, and mass mortality in the benthic community (Stirn 1993, Akinnawo 2023).

1.1.3.3 Benthic-pelagic coupling

Benthic biogeochemical fluxes are important in all marine ecosystems, and in shallow waters a tight coupling exists between the water column and the benthic habitats. Benthic-pelagic coupling is the relationship between processes, events and responses in sediments and in the water column (Soetaert et al. 2000). The coupling between the two ecosystems favors the exchange of mass, energy, and nutrients (Griffiths et al. 2017), where the transport between these ecosystems is not limited to dead cells and nutrients, but also includes living organisms that are part of the phytoplankton. In fact, not all phytoplankton organisms spend their entire lives suspended in the water column; and in many cases, a portion is spent on the seafloor. These taxa are particularly important nearshore, in fact, in coastal systems, many putative holoplankton organisms also have benthic resting stages (Marcus and Boero 1998). Environmental forces and meteorological drivers can trigger blooms of these taxa in shallow coastal waters. For example, diatom resting stages germinate in bottom sediment when light penetrates deep enough (Shikata et al. 2008), and dinoflagellate cysts can be transported into the water column by storm-induced currents (Kremp 2001). Overall, in temperate seas, unfavorable periods are avoided by accumulation of dormancy forms in seed banks on the seafloor, and, seasonally, communities are restored by germination of these biodiversity storages (Belmonte et al. 1997). In addition, phytoplankton seed banks in coastal waters offer a possible explanation for the paradoxical coexistence of many species in the marine environment (Belmonte and Rubino 2019).

1.1.4 Theory of phytoplankton distribution

The earliest studies on the distribution of phytoplankton by Cleve (1900) and Gran (1902) advocate two different theses (Smayda and Reynolds 2001). The first stated that the presence of species was determined by their "thermal type" in relation to the thermal zone (season), while the second stated that the presence of species was determined by the prior composition of the autochthonous community and water mass conditions (Smayda and Reynolds 2001). A common feature in the results of these and later studies (Reynolds 1980, Platt and Sathyendranath 1999, Reynolds 2006), was the high degree of redundancy of life forms among co-occurring species and the fact that some aggregations of species occur cyclically along spatial and temporal gradients. Such repetitive aggregations are referred to as phytoplankton assemblages (Reynolds 2006). Rojo and Alvarez-Cobelas (2000)

suggest that phytoplankton assemblages and their assembly rules should be one of the most important tools phytoplankton ecologists should look for in their studies, and that assemblage studies have the potential to distinguish population fluctuations caused by exogenous contributions (autecology) from those caused by internal processes (synecology). At the 11th International Association of Phytoplankton Taxonomy and Ecology (IAP) workshop, 10 rules for the formation of such a community were proposed (Reynolds et al. 2000)

I. Provided suitable inocula are available, planktonic algae will grow wherever and whenever they can and to their best potential under the conditions given

II. Then, of those present, the species which are initially likely to become dominant are those able to sustain the fastest net growth rates and/or those arising from large inocula;

III. The species with the largest autochthonous inocula are generally those which have been abundant at the same location in the recent past.

IV. Environments may select preferentially for certain algal attributes or traits;

V. Species with preferred attributes are likely to build bigger populations and, where appropriate, to found larger inocula to carry forward;

VI. Phytoplankton assemblages become biased in their species composition with respect to the conditions obtained in individual water bodies;

VII. The species most frequently characterizing specific environments share common advantageous attributes;

VIII. The outcome of community assembly is subject to food-web and other interactions;

IX. Of those species present (and quite independently of the initial conditions), the ultimate dominant is likely to be the one with the most advantageous adaptations;

X. Assembly is always subject to the overriding effects of environmental variability and of the resetting of assembly processes.

The above rules have been proposed as a model for the selection mechanisms of phytoplankton assemblages along trophic gradients in lakes. The reader should not dwell on the undeniable differences between marine and lake ecosystems; such differences exist, but they relate here mainly to the sixth rule, which applies to individual water bodies, i.e. lakes, whereas in the marine environment such "individualization" of water masses is less stringent. The reader should notice instead that the authors have emphasized the role of the prior state of the community and stochasticity (Reynolds et al. 2000). To underscore the applicability of such rules to the marine environment, it is also important to note that the same authors applied a modified version of such rules to dinoflagellate communities in

the marine environment a few years later (Smayda and Reynolds 2003). These rules take into account all three key aspects of phytoplankton distribution: the former autochthonous community, the advantage of a particular life form or trait, and the redundancy of such a life form among many species.

The idea that each species has a unique set of optimal ecological conditions for growth, survival, and reproduction was summarized in the concept of the ecological niche (Hutchinson 1941). According to niche theory, species with higher fitness thrive under similar ecological conditions at the expense of species with similar ecological roles but lower fitness. In this context, a paradox has been noted in phytoplankton: there are too many species for apparently similar ecological conditions. Many explanations have been proposed for this paradox in plankton. Hutchinson suggested that the excessive species richness of phytoplankton is related to the fact that equilibrium conditions are not achieved in the pelagic habitat because habitat characteristics change at the same rate as the phytoplankton reproduction (Hutchinson 1961). Other explanations for the paradox have been found in nested competition models for multiple limiting resources (Huisman and Weissing 1999), in models simulating periodic fluctuations of disturbances (Elliott et al. 2001), and in the feedback relations between phytoplankton and viruses (Flynn et al. 2022). Recently, a new theory of species distribution has emerged, i.e. the neutral theory, which undermines the basic assumption of the niche theory of competitive advantage (Hubbel 2005). According to neutral theory, each individual has the same chance of survival and reproduction as all other individuals in a community. The dynamics of the community follow a random walk process where only prior history and stochasticity determine the success of a particular species (Hubbel 2005).

The observable importance of niches in determining species distributions led to the formulation of the theory of lumpy coexistence, to which both the niche and neutral theories contribute (Scheffer and van Nes 2006). In this theory, all species have the same fitness, but only within a specific niche of ecological conditions**.** Similarly to the rules proposed by the IAP, a combination of environmental conditions, history, and stochasticity determines community composition according to lumpy coexistence. Knowledge of the characteristic niches of phytoplankton communities is greater than knowledge of the stochastic processes that determine community dynamics. This is mainly due to historical reasons, as the niche theory was accepted and developed earlier than the neutral and lumpy coexistence theory, for which there are few research results so far (Roelke and Spatharis 2015, Sakavara et al. 2018). Therefore, the niche model remains the main interpretive key for studying the distribution of the phytoplankton assemblage.

1.1.5 Phytoplankton niches

For our understanding of oceanic biogeochemical cycles, trophic interactions and, in general, the ecology of the marine environment, it is important to know how phytoplankton is distributed in the pelagic habitat (Ptacnik et al. 2008, Vallina et al. 2014). In the marine environment, the dynamicity of the sea makes particularly difficult to define areas or, better, defined spatial and temporal units on which any analysis and sampling would be performed (Clayton et al. 2013). In the specific case of phytoplankton biogeography, it has been shown that the distribution of this biological compartment is generally patchy. Platt and Denmann confirmed the nonuniformity of phytoplankton by spectral analysis when they showed that marine phytoplankton are distributed in space according to the Kolmogorov 5/3 dissipation rule (Platt and Denmann 1975). In contrast, temporal patterns of phytoplankton range from stable annual fluctuations in certain biomes to the absence of a repeating pattern in others (Cloern and Jassby 2010).

Margalef's model of the distribution of phytoplankton assemblages along nutrient and turbidity gradients formed the cornerstone of phytoplankton ecological modelling. Margalef's "mandala" (Figure 1, left) positions species along a successional pathway from very turbulent and nutrient-rich waters to calm and nutrient-poor waters. R-strategists, such as diatoms of the genera *Thalassiosira* and *Chaetoceros*, thrive at the first end, while K-strategists, such as dinoflagellates, thrive at the other end. In the middle, the community transitions to a mixed assemblage of coccolithophorids, diatoms, and dinoflagellates. In highly turbulent but nutrient-poor water, no species finds the optimal conditions, whereas in calm and nutrient-rich water, red tides (harmful algal blooms) can be expected (Margalef 1978). The turbulence gradient selects semimobile species for calm waters, while the second gradient selects rounded shapes for lower nutrient concentrations . The Margalef's mandala has been modified by other authors several times over the years, often with dubious success (Kemp and Villareal 2018).

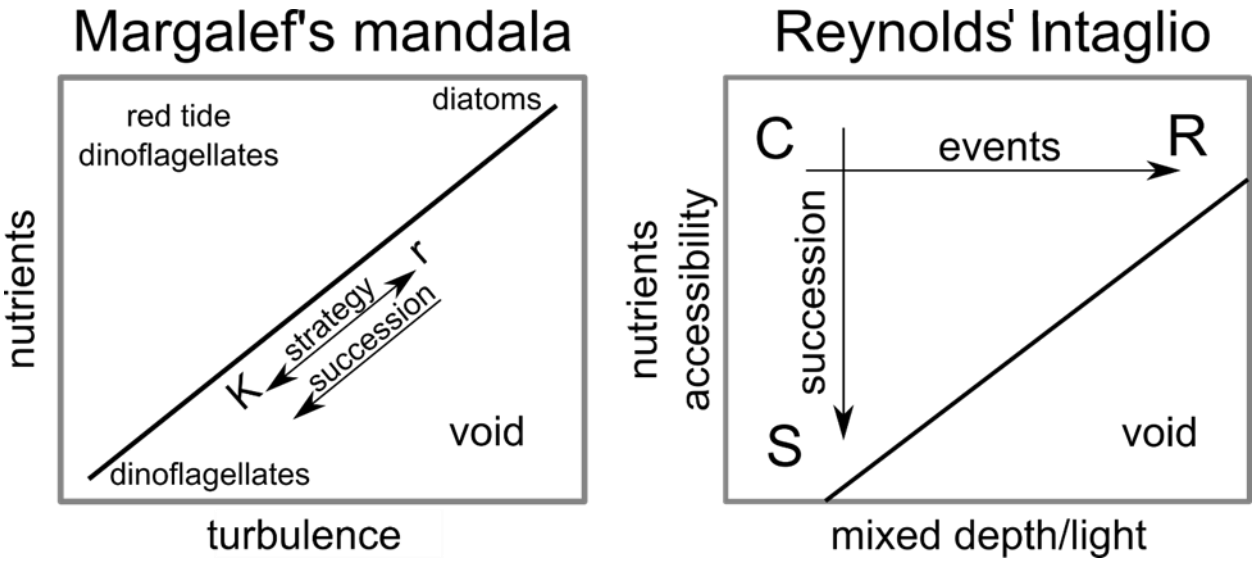

Figure 1: Models of the distribution of phytoplankton assemblages along environmental gradients: (left) the Margalef's mandala, (right) the Reynolds' intaglio

Perhaps the most important subsequently developed model of the succession and distribution of phytoplankton assemblages is the so-called Reynolds' Intaglio (Reynolds 2006) (Figure 1, right). Influenced by the work of Grime on C-S-D plant strategies (Grime 1977), Reynolds first developed this model for freshwater phytoplankton and then extended it to the marine environment (Smayda and Reynolds 2001). In this model, three adaptive strategies are defined: i) the C species (colonists), which are invasive, r-selected, small, fast growing, and have a high surface area to volume ratio; ii) the S species (nutrient stress tolerants), which are acquisitive, large, slow growing, but biomass conserving, and K-selected; and iii) the R species (ruderal), which are adaptive, light-gathering, restrained, and resistant to disturbance. In relation to Margalef's mandala, nutrient concentration and turbulence are recognized as independent variables and are substituted: the "turbulence" axis is replaced by a vector reflecting the vertical extent of mixing relative to light intensity and its attenuation with depth, while the "nutrient" axis becomes one reflecting the state of its depletion and the accessibility of the remaining resource (Smayda and Reynolds 2001). Like the Margalef's mandala, a portion of the intaglio represents unfavorable conditions for any species, corresponding to a water body low in light and nutrients. C species thrive in nutrient-rich, highly stratified waters and are displaced by S species in

the environment without physical disturbance when nutrients become scarce. This succession is typical of summer nutrient depletion, when the community evolves from naked dinoflagellates typical of red tides to migratory species (Smayda and Reynolds 2001). R species thrive in mixed waters or low light conditions and are displaced by C species as light increases, or the water column stabilizes. This succession is typical of the transition from the bloom-forming diatom community in early spring to the dinoflagellate species in early summer. The annual cycle for the phytoplankton community in temperate habitats involves a final transition from S to R species during autumn and winter mixing (Reynolds 2006). Reynolds' Intaglio model also accounts for other possible successions, such as nutrient depletion in the upwelling system and coastal currents, as well as the interruption of typical successions by physical events such as storms. The Reynolds' Intaglio model has two major advantages over the Margalef's Mandala: First, the low-turbulence, high-nutrient conditions are not treated as a disfunction of the system, but as systemic conditions of the marine environment typical of nearshore and coastal areas. Second, a greater diversity of successions is possible in the model.

1.1.6 Phenology

Variations in coastal ecosystem properties play an important role in the distribution of phytoplankton taxa. The temporal variability of this distribution (i.e. phenology) is of particular research interest because such knowledge allows us to distinguish between expected (natural) fluctuations in the phytoplankton community and long-term trends or shifts. The most striking feature of phytoplankton phenology is its cyclic behaviour (Winder and Cloern 2010). As already mentioned above, early attempts to link phytoplankton phenology and periodicity of environmental variables were made in the 1970s when Margalef introduced the concept of phytoplankton succession, the mandala (Fig. 1), in which the main stages of succession are determined by turbulence and nutrient availability (Margalef 1978). Based on his work, Reynolds developed the concept of the "phytoplankton year" for lake communities, separating succession from simple seasonality and calling the cyclical behaviour of environmental factors "periodicity" (Reynolds 1980).

In general, the spectrum of dynamics of ecological systems is broad, encompassing all stages between regular cycles and chaotic oscillations (May 1976, Stone 1993). Patterns of phytoplankton phenology in different ecosystems also range from stable annual fluctuations in certain biomes to the absence of a repeating pattern in others (Winder and Cloern 2010). The most common frequencies of phytoplankton biomass fluctuations are 12 and 6 months; higher frequencies are also common, but the usual sampling frequency of one month is a limiting factor in their determination (Winder and Cloern 2010). In this case, it is not the stochasticity inherent in IAP rules (Reynolds et al. 2000) or the assumptions of the lumpy coexistence theory (Scheffer and van Nes 2006) that explains the presence or absence of repeating patterns. The answer should lie in the oscillating behaviour of environmental parameters that contribute to the formation of phytoplankton communities. Such fluctuations define an attractor-like pathway in the Reynolds' Intaglio model, in which communities typically switch from R to C species following stratification and from C to S species following nutrient depletion (Reynolds 2006). Inter- and intra-annual recurrences of these communities follow the cycling of environmental parameters, while a prolonged deviation from these cycles can cause a shift in the community toward new compositional equilibria by altering recruitment equilibria (Reynolds and Elliott 2002).

In addition, within the framework of the intermediate disturbance hypothesis (Connell 1978), the fluctuation frequency of niche-forming parameters, such as mixing events, has been shown to be critical in explaining species diversity in phytoplankton (Elliott et al. 2001). Similarly, numerical simulations in the framework of neutral ecology (Hubbel 2005)

and lumpy coexistence theory (Scheffer and van Nes 2006) have shown that phytoplankton community richness and succession are influenced by nature, gradual or sudden, of resource fluctuations (Roelke and Spatharis 2015). Finally, Sakavara et al. (2018) showed that assemblage-like structures occur numerically in a wide range of spectral modes of resource fluctuations. For the nearshore environment, the usual fluctuation frequency of environmental factors, which drive the access to resources, is expected to be in the order of 2 to 4 months (Winder and Cloern 2010).

1.2 From Observations to Data

1.2.1 Introduction

Phytoplankton studies pose significant challenges in data acquisition and analysis. In fact, the temporal and spatial variability of phytoplankton communities (Cloern & Jassby, 2010) complicates consistent sampling efforts requiring high-frequency and broad-scale sampling to capture the dynamics accurately. Also, differentiating and counting the diverse phytoplankton species often requires profound taxonomical knowledge and can be resource-intensive (Thompson and Carstensen 2023). Despite the rise of alternative methods, the use of the inverted microscope is so far the most common sampling method in routine monitoring programs (Alster et al. 2024). This method produces quantitative (abundance and biomass) and qualitative (size and shape) assessment of phytoplankton, providing detailed information on species abundance and diversity. This data is crucial for understanding phytoplankton dynamics, ecological interactions, and responses to environmental changes.

1.2.2 Phytoplankton abundance

The simplest parameter for phytoplankton is abundance or number of individuals, which is usually converted to density data (number of cells/L) and is probably the most common format for phytoplankton data in ecology. The prevailing estimation method for this important parameter is counting with an inverted microscope using the Utermöhl method (Utermöhl 1958). Count data is one of the possible statistical data types and has some special properties; in particular, it is always positive and discrete. Each individual contributes equally to the total abundance, regardless of differences in size, productivity, or other relevant ecological characteristics. Consequently, the only information that is retained for a particular individual of a certain species is whether it was present or not. The total number of individuals or total abundance of a given species/taxon or group is then calculated for each species. In a sample, a particular species may contribute more to the total abundance than other species. Analysing the distribution of species proportions in a community is a goal of diversity studies, and there are many functions for evaluating such distributions (Rao 1982, Rocchini et al. 2021). Such functions attempt to assess for a given community how the overall abundance is distributed among many species, based on the ecological assumption that diversity, evenness, and dominance are relevant characteristics of an ecological system (Pielou 1977). When many samples are evaluated together, counts can be organised on what is called a contingency table. Such contingency tables are a type of multivariate data set and require specific mathematical tools to be analysed (Legendre and Legendre 2012).

1.2.3 Phytoplankton traits

Recent trends in the study of the structure and functioning of the phytoplankton communities are aimed at the research of traits able to act as non-taxonomic “descriptors of community” (Weithoff and Beisner 2019). The large number of phytoplankton species populating the oceans and the stochasticity embedded in their local recruitment success present a challenge for describing and forecasting the community structure. A possible solution to the diversity of responses in terms of taxa composition is to use simpler alternative descriptors to group phytoplankton organisms; this solution is known as the trait-based approach and it has been increasingly used in recent years (Kruk et al. 2017, Weithoff and Beisner 2019). Functional traits are morphological, biochemical, physiological, behavioural, and life history characteristics of an organism that define an ecological niche (McGill et al. 2006, Salmaso et al. 2015, Glibert 2019). These conceptual groupings of species under similar functional characteristics regardless of their taxonomic affiliation should still contain ecological information (Abonyi et al. 2018).

Cell size is considered a "master trait" in phytoplankton ecology (Litchman et al. 2007) that is closely related to other traits (nutrient and light uptake, predator avoidance) and is a good candidate for understanding and predicting responses to climate-induced changes in the nutrient regime (Nock et al. 2016). According to the metabolic theory of Brown (2004), body size is one of the three key factors affecting individual metabolism and consequently community ecology, along with temperature and stoichiometry. In addition, body size offers potential advantages over standard taxonomic descriptors in community organisation studies (Vadrucci et al. 2007), and is, along with the associated value of biovolume, of critical importance in allometric studies (Niklas 2004, Beardall et al. 2009, Verdy et al. 2009). Phytoplankton exhibit a cell size range of several orders of magnitude but is usually classified into the three phytoplankton size classes (PSC): pico plankton (0.2-2 µm), nano plankton (2-20 µm) and micro plankton (20-200 µm) (Sieburth et al. 1978). It is important to mention that such a definition, which according to Sieburth goes back to Lohmann from the early 20th century, is only a necessity caused by sampling procedures. Nowhere, in fact, is it claimed that the PSCs have ecological significance. Rather, Sieburth showed that phytoplankton comprise at least four of such classes, pico-, nano-, micro-, and meso-classes and emphasised that within the range of phytoplankton PSCs, other ecologically distinct organisms also exist, namely mycoplankton and protozooplankton.

Other morphological traits that are important for acquiring resources and avoiding predators include cell behavioural and physiological traits such as mixotrophy, motility, shape, life forms (single cell vs. colony), and surface-to-volume ratio (Weithoff and Gaedke 2016, Roselli and Litchman 2017, Durante et al. 2019). Finally, phytoplankton can be classified based on the characteristic roles in biologically mediated biogeochemical transformations. This classification produces typically broad phytoplankton functional types (PFTs) (Le Quéré et al. 2005), which are widely integrated into large scale biogeochemical ocean models (Aiken and Navarette 2014). The grouping of often taxonomically diverse organisms, based on all above listed traits, gives rise to the so-called functional groups (Reynolds et al. 2002). The research on the proper context and of the constraints in the usage of functional trait and groups is still ongoing and such methods should not be considered a substitute for taxonomic knowledge (Salmaso et al. 2015). In fact, while the trait-based approach has the potential to describe and explain functional diversity, the commonly used taxonomic affiliation can still provide complementary insights (Litchman and Klausmeier 2008, Titocci et al. 2022).

1.2.4 Phytoplankton biomass

Phytoplankton biomass is an essential parameter in biogeochemical cycle analyses and ecosystem modelling (Falkowski et al. 2003, Aumont et al. 2015), and is closely related to biovolume, from which it can be calculated using standard conversion factors (Menden-Deuer and Lessard 2000, Socal et al. 2010). The biovolume, in turn, depends on the cell size of phytoplankton, which, as we have seen, plays an important role in phytoplankton physiology and has relevant implications for marine ecology and biogeochemical cycles (Finkel et al. 2009).

Currently, the most used method for estimating the biovolume of phytoplankton is to assign to each species a three-dimensional shape that most closely resembles the actual shape of the organism (Olenina et al. 2006, Vadrucci et al. 2007). The dimensions of these shapes are measured under the inverted microscope using the Utermöhl method (Utermöhl 1958), in parallel with taxonomic identification and enumeration. One is often faced with the dilemma of whether to assign the shape of a phytoplankton cell to a complex but similar geometric model or to a simple, easily measured but dissimilar shape (Olenina et al. 2006). Because of the geometric relationship between size and volume, there is a wide range of nine orders of magnitude for the cell biovolume of phytoplankton (Sieburth et al. 1978), so the choice of shape formula to apply to each species and the accuracy of the measurement are critical. It should also be noted that microscopy methods for some phytoplankton species are costly, either due to the time required for analysis or the difficulties in implementing the analytical protocol (Vadrucci et al. 2007).

In addition to direct measurement, pigment-based methods can also be used to estimate phytoplankton biomass. The most widely used proxy for phytoplankton biomass is the concentration of chlorophyll-a in the water, which is also extensively used as an indicator for assessing the environmental status of European and other seas (Francé et al. 2021). Identification and quantification of other main algal pigments, which are then used as chemical markers for phytoplankton groups, is possible with the High-Performance Liquid Chromatography (Jeffrey and Vesk 2005). HPLC can be used to estimate the contribution of diatoms, dinoflagellates, coccolithophores, and other important groups to total chlorophyll content, and recently improved performance has allowed characterization of the spectral response of individual species (Zapata et al. 2004, Zapata et al. 2012). In addition, the optical properties of phytoplankton pigments provide the possibility to partition biomass among the three PSCs (Claustre 1994, Vidussi et al. 2001, Uitz et al. 2006).

These optical signatures have been also used in conjunction with satellite data on ocean colour to estimate the biomass of main phytoplankton groups and PSCs from space (Brewin et al. 2011, Ciavatta et al. 2019). Such estimates from satellite data have been used in modelling the offshore dynamics of the Mediterranean Sea at larger scales, but coastal waters are optically very complex, which hamper the adequate modelling due to the additional influences of the seafloor, suspended sediments, and river runoff (IOCCG 2000). The assessment of phytoplankton biomass and its partition into phytoplankton groups or size classes is still being intensively researched (Brewin et al. 2011, Di Cicco et al. 2017) and promises to overcome major drawbacks, such as the lack of in situ data to allow comparison (Anderson 2005).

In addition to the bulk measurements or estimates of phytoplankton biomass, considerations can also be made about the distribution of the biomass parameter among individual phytoplankton cells, as each individual can contribute differently to the total biomass. It is often assumed that the biomass distribution among individuals of any species follows a power law distribution (Niklas 2004, Kostadinov et al. 2009, Kostadinov et al. 2010), and this assumption has been shown to be correct at the global scale (Perkins et al.

2019). In such a distribution, a few large cells contribute as much to the total as many small ones, so the average cell biomass is not a meaningful value (Sheldon et al. 1972). Moreover, in such a distribution, the biomass is uniformly distributed on a logarithmic scale and describes a line on a logarithmic graph (Clauset et al. 2009). Since the literature on power law distribution of phytoplankton biomass uses the term "size" in the sense of "body size" or "biovolume" or "biomass" (Marquet et al. 2005, Finkel et al. 2009, Andersen et al. 2016, Heneghan et al. 2019), it is not clear whether the phytoplankton trait “body size” also follow a power law. When biomass is assessed at the local scale, deviations from the power law are found in nearshore marine waters (Witek and Krajewska-Soltys 1989). Such deviations raise important questions because they indicate ecological processes that operate at specific ranges and scales (Armstrong 1999, Cavender-Bares et al. 2001, Hatton et al. 2021).

1.3 Study Area (Northern Adriatic)

1.3.1 Environmental characteristics

The northern Adriatic basin is defined as the area north of the 100-metre isobath of the Adriatic Sea and represents the largest shelf area in the Mediterranean Sea (Gačić et al. 2001). This area can be divided into oligotrophic, mesotrophic, and eutrophic regions, with two main gradients from east to west and from nearshore to offshore (Brush et al. 2021). This basin is under the influence of strong lateral (river discharge and transport to the south) and surface (wind and air temperature) stresses (Poulain et al. 2001). The easternmost part is mainly influenced by the Soča River (Malačič and Petelin 2001) and occasionally by the Po River plume (Viličić et al. 2013), while the western part is mainly influenced by the Po River plume (Poulain et al. 2001). Rivers such as Tagliamento, Livenza, Piave, Brenta, and Adige contribute to runoff in the western northern Adriatic, but overall account for only a small fraction as compared to the Po River runoff (Cozzi and Giani 2011). Due to the large number of rivers, high runoff, and topography of the basin, nutrient concentrations in this part of the Adriatic are generally higher than in other parts of the Mediterranean (Cozzi and Giani 2011).

The water column of the northern Adriatic is seasonally mixed and stratified (Poulain et al. 2001), and in many areas the euphotic zone exceeds the depth of the upper mixed layer for most of the year (Talaber et al. 2014). Very low transparency values have also been observed due to input of particles from rivers and other nearshore sources, as well as resuspension processes, active lateral advection in lower water layers, and storms (Bernardi Aubry et al. 2004).

The northern Adriatic is under the influence of two main winds, the "bora" and the "jugo" (scirocco), the first of which blows from the northeast and the second from the southeast. The bora is a strong katabatic wind that affects the water column in two ways, i.e. by mixing and cooling. Jugo, on the other hand, is a constant wind and in the eastern part of the basin has a chaotic effect on the current circulation (Malačič and Petelin 2001). The general circulation in the northern Adriatic is divided into three persistent sub-gyres (Poulain et al. 2001, Petelin et al. 2013). The circulation in the northernmost part of the basin is characterized by cyclonic advection of water, which is even enhanced during bora events (Boicourt et al. 2021), when this circulation moves the surface water masses alongshore towards the western coasts. The surface outflow from the basin is balanced by the inflow of cold deep water. Thus, this bora-driven circulation results in upwelling in the GoT (Crise et al. 2006). The surface water from the GoT reaches the western part of the northern Adriatic, while deeper water from the Gulf of Venice (GoV) is transported back

to the eastern part, with one branch flowing into the GoT (Malačič et al. 2012). Cyclonic circulation is also responsible for the occasional advection of river water, nutrients, and phytoplankton from the western to the eastern side of the Adriatic (Viličić et al. 2013). In contrast, during sirocco events, the surface circulation usually splits into two branches, one of which enters the GoT and the other circulates in a cyclone in the basin area (Boicourt et al. 2021). When the winds die down, the stratification in the northern Adriatic shifts eastward, beginning in the western part at the end of spring and reaching the strongest stratification state at the end of summer (Degobbis et al. 2000). In the GoT, however, the strongest stratification occurs at the end of spring; at this time, the Soča River outflows in the Gulf remain blocked in the surface layer moving clockwise (Malačič and Petelin 2009).

1.3.2 The phytoplankton community

The environmental forces in the northern Adriatic, like mixing, river discharge, and benthic influences described so far, create a complex environment for the phytoplankton community, which here exhibits all the life strategies of the Reynolds' Intaglio. This basin is generally considered as one of the most productive areas in the Mediterranean (d'Ortenzio and Ribera d'Alcalà 2009), but with considerable spatial differences. Chlorophyll-a concentrations in the northern Adriatic mimic the nutrient gradient, with higher values in the north and west and lower in the south and east, usually exhibiting two seasonal peaks, one in spring and one in autumn (Brush et al. 2021). At the basin scale, an oligotrophication trend was observed in the 2000's (Mozetič et al. 2010), following the reduction of freshwater discharge between 2003 and 2007 and improved control of nutrient inputs with waste waters. This decline in phytoplankton biomass was probably the consequence of intensified nutrient imbalance in the northern Adriatic, since the reduction of phosphates were not accompanied by a concomitant reduction in nitrates leading to an even more intensified P-limitation (Grilli et al. 2020, Brush et al. 2021). In some parts of the northern Adriatic, however, there are signs of a reversal of this trend. For example, in the southern part of the basin, an increase in inorganic phosphorus and nitrogen concentrations has been observed in recent years, followed by an increase in phytoplankton abundance and biomass, but also with concomitant changes in the seasonality of the main groups (Totti et al. 2019). So far, no reversal of the biomass trend has been observed in the Gulf of Trieste (Flander-Putrle et al. 2021), but changes in seasonality have been observed, as the bloom in late winter-early spring has almost disappeared, while the spring bloom is most pronounced (Cerino et al. 2019).

These significant differences in the structure of the phytoplankton community between different areas of the northern Adriatic were depicted also by Brush et al. (2021). In the western part, diatoms dominate the phytoplankton community, accounting for 67% abundance and 81% of biomass (Bernardi Aubry et al. 2004). The dominance of diatoms follows the same gradient of nutrients and chlorophyll-a levels, which decrease with distance from the Po River plume (Mangoni et al. 2008). In fact, in the eastern part of the basin, nanoflagellates dominate the community in terms of abundance (66%), while diatoms contribute only a smaller part (29%) to the total abundance (Brush et al. 2021). Chlorophyll-a values show that biomass in the eastern part of the basin is more evenly distributed among the main phytoplankton groups, again with a lower proportion of diatoms than in the western part (Flander-Putrle et al. 2021).

In the western part, relatively small species with high surface-to-volume ratios generally predominate (Brush et al. 2021). Diatoms such as *Skeletonema marinoi*, *Cerataulina pelagica* and species of the genera *Cylotella*, *Thalassiosira*, *Chaetoceros*, *Pseudo-nitzschia*, as well as nanoflagellates thrive here (Bernardi Aubry et al. 2006). It has been suggested that the blooms occur at the same time of year in the area, probably due to the modulation

of large-scale meteorological characteristics mentioned above (Brush et al. 2021). Indeed, a regular seasonal pattern was observed in the phytoplankton community of the northern western Adriatic (Bernardi Aubry et al. 2012). However, after 2006, a shift in the seasonal succession of species and an increase in irregularities with sudden diatom blooms were observed in the southernmost area, reflecting the increasing variability of meteorological events (Totti et al. 2019).

The eastern part of the basin has been suggested as the area of the seed population for spring phytoplankton blooms in the western part of the basin (Godrijan et al. 2013), so the phytoplankton communities are similar in terms of typical phytoplankton taxa in the eastern and western northern Adriatic (Brush et al. 2021). However, even here, some differences in taxa composition have been described between the northernmost part, the Gulf of Trieste (GoT) and the Istrian coast (Brush et al. 2021). The common pattern of the eastern phytoplankton community is the importance of non-diatom groups in the seasonal succession, especially those in the nano-size fraction (Cabrini et al. 2012, Marić et al. 2012, Mozetič et al. 2012, Godrijan et al. 2013). Nevertheless, the seasonality of phytoplankton taxa in different parts of the eastern north Adriatic basin is diverse and subject to high interannual variability due to meteorological influences, changes in circulation pattern and river discharge (Brush et al. 2021). In summary, the phytoplankton community in the northern Adriatic shows fast response to environmental perturbations, making the phytoplankton studies a good tool for early indication of changes in the pelagic habitat.

1.4 Purpose of the Dissertation

Phytoplankton research is crucial for deciphering the marine ecosystem, which is a multilevel network of several biotic compartments and abiotic drivers. Specifically, shifts in community composition of phytoplankton can alter also other trophic levels, which can be in turn reflected in altered ecological services (e.g. changes in biogeochemical pathways, influences on mariculture productivity). A thorough understanding of the ecological and physiological characteristics of phytoplankton in dynamic coastal environments is, however, difficult due to the variability of processes and the complexity of anthropogenic influences (Cloern and Jassby 2008). The extensive but still insufficient knowledge of phytoplankton community composition and the ever-increasing amount of data implies the need to integrate relevant environmental processes into standard biological models (Margalef 1978, Kemp and Villareal 2018) through modelling. Ecological modelling is one of the essential and increasingly necessary steps in the ocean management process, as it can greatly improve the understanding of the pressure-response relationship also for phytoplankton communities (Ford et al. 2017).

Appropriate models of the relationship between environmental conditions and phytoplankton are critical for accurate predictions of community structure. These predictive models in combination with forecasts of environmental conditions in turn provide tools for effective management. With climate change on the horizon, deciphering these relationships becomes even more important. Also, understanding the representativeness of current sampling strategy and the limitations of current analytical tools in describing phytoplankton characteristics and dynamics will contribute to a cost-benefit analysis of future monitoring and research planning.

The ecology of phytoplankton is an extensively studied subject. Still several open questions remain. The definition of the phytoplankton assemblages as well as the ecological interpretation of their succession is uncertain. Clear rules for the prediction of species' appearance and disappearance are hidden in the huge variability of local phenomena while

the redundancy in the biology of the species is still partially inexplicable given the known set of relevant environmental variables. Finally, a wide spectrum of promising alternatives for measuring phytoplankton such as, for example, the size and the shape remain poorly investigated. The main ecological questions on which the dissertation will dig in are:

I. Reduce the complex mosaic of coastal phytoplankton community into assemblages defined by the main co-occurring species.

II. Interpret the phenology of the found assemblages in light to the relation with environmental variables, disentangling the influence of mesoscale patterns from local species succession.

III. Describe the seasonal dynamics in terms of biomass and diversity, starting from individual-traits.

Thus, the purpose of this dissertation is to test and evaluate the accuracy of established and new phytoplankton distribution models. By effectively describing the relationship between phytoplankton and the environment, as well as several key ecological aspects such as bloom phenology, seasonality of assemblages, and biomass distribution, the dissertation will provide a comprehensive portrait of the phytoplankton key components in the pelagic habitat of the Gulf of Trieste and broader in the northern Adriatic. In addition, through new approaches (e.g., relevance of taxa, assemblages' determination, individual based data), the dissertation will provide methodological guidance for data preparation, analysis and modelling.

Chapter 2

Community Structure and Phenology

2.1 Paper: Phytoplankton Time-Series in a LTER Site of the Adriatic Sea: Methodological Approach to Decipher Community Structure and Indicative Taxa

This chapter presents a detailed study on the variability of phytoplankton phenology at a Long-Term Ecological Research (LTER) site in the Gulf of Trieste, from 2005 to 2017. The study aimed to decipher the community structure and identify indicative taxa using two multivariate analysis protocols, one found in literature and a modified version of it. This chapter highlights the importance of using appropriate methodologies to avoid losing critical information and provided insights into the complex seasonal patterns and variability of a phytoplankton community.

The key differences between the original and modified protocols in the study revolve around several methodological adjustments. In the original protocol, taxa selection was based on their frequency of appearance, with a threshold set at 12%. In contrast, the modified protocol introduced the FREVE index, which combines frequency and evenness to better preserve the information from the original dataset. The ordination method has also been modified. The original protocol employed Principal Component Analysis (PCA), which preserves Euclidean distance. The modified protocol, however, used Correspondence Analysis (CA), which preserves chi-square distance and is more suitable for species frequency tables. Clustering was handled differently as well. The original protocol relied on a Bayesian probability-based criterion to evaluate partitions, whereas the modified protocol used k-means Calinski pseudo-F and Ratkowsky indices, which are based on the analysis of variance. Finally, the identification of indicative taxa differed between the protocols. The original protocol relied solely on the IndVal index, while the modified protocol supplemented IndVal with a likelihood ratio method (Xproj) to better identify taxa responsible for cluster formation. These modifications aimed to improve the accuracy and reliability of the analysis, better preserving the dataset's information and providing a more realistic representation of phytoplankton community structure and seasonal patterns.

Key findings include:

I. Phenology: Seasonal phytoplankton dynamics showed a cyclic behaviour with diatom peaks in spring and autumn.
II. Assemblages structure: Two significant partitions of the time series were possible, into four and eighteen assemblages. The average lifespan of the phytoplankton assemblages was short (2-4 months).

III. Inter- and intra-annual variability: The study identified typical seasonal assemblages and bloom events, with significant changes observed in the second half of the year and towards the end of the series.

The findings emphasize the importance of long-term monitoring for detecting ecological shifts and understanding the impact of environmental drivers. The observed variability in phytoplankton dynamics underscores the sensitivity of coastal ecosystems to climatic and anthropogenic pressures. The clustering partition find will be the starting point for the subsequent association with environmental variables.

Goal:

I. Determine the phenology of the recurrent phytoplankton assemblages in the Gulf of Trieste.

Hypothesis:

I. The phytoplankton community in the Gulf of Trieste follows a predictable succession of assemblages (temporal co-occurrence of taxa), which are characterized by indicative species or taxa.

The goal is accomplished, and hypothesis is confirmed by the results presented in this chapter.

The research work is presented in the following publication and is listed below:

Vascotto, I., Mozetič, P., & Francé, J. (2021). Phytoplankton time-series in a LTER site of the Adriatic Sea: methodological approach to decipher community structure and indicative taxa. *Water*, *13*(15), 2045.

Ivano Vascotto contributed to this paper as follows: conceptualisation, data curation, methodology, formal analysis, writing the original draft, revising and editing.

water

MDPI

Article

Phytoplankton Time-Series in a LTER Site of the Adriatic Sea: Methodological Approach to Decipher Community Structure and Indicative Taxa

Ivano Vascotto [1,2,*], Patricija Mozetič [1] and Janja Francé [1]

[1] National Institute of Biology, Marine Biology Station Piran, Fornače 41, 6330 Piran, Slovenia; patricija.mozetic@nib.si (P.M.); janja.france@nib.si (J.F.)
[2] Jozef Stefan International Postgraduate School, Jamova Cesta 39, 1000 Ljubljana, Slovenia
* Correspondence: ivano.vascotto@nib.si; Tel.: +356-(0)59-232-935

Abstract: In the shallow and landlocked northeast Adriatic Sea, environmental factors have changed in recent decades. Their influence on seasonal and inter-annual variability of phytoplankton has been documented in the recent literature. Here, we decipher the long-term variability of phytoplankton phenology at a Long-Term Ecological Research site (Gulf of Trieste, Slovenia). Structural changes in the phytoplankton community (period 2005–2017) were analysed using a multivariate protocol based on Bayesian clustering. The protocol was modified from the literature to fit the needs of the study, using correspondence analysis and k-means clustering. A novel index for ordination and selection of taxa based on frequency and evenness was developed. The Total Inertia analysis showed that this index better preserved the available information. Typical seasonal assemblages were highlighted by applying the Indicative Value index in conjunction with likelihood ratio values. We obtained a rough picture of the seasonal separation of the diatom-dominated community from the mixed community and a refined picture of the phenology of the assemblages and bloom events. The spring diatom peak proved to be inconstant and short-lived, while the autumn bloom was generally long and diverse. As expected for nearshore environments, the average life span of the assemblages was found to be short-periodic (2–4 months). The second part of the year and the last part of the series were more prone to changes in terms of typical assemblages.

Keywords: phytoplankton; phenology; assemblages; LTER; Adriatic Sea

Citation: Vascotto, I.; Mozetič, P.; Francé, J. Phytoplankton Time-Series in a LTER Site of the Adriatic Sea: Methodological Approach to Decipher Community Structure and Indicative Taxa. *Water* **2021**, *13*, 2045. https://doi.org/10.3390/w13152045

Academic Editor: Genuario Belmonte

Received: 10 June 2021
Accepted: 21 July 2021
Published: 27 July 2021

1. Introduction

The theory behind the spatio-temporal distribution of phytoplankton species in the pelagic habitat [1] has long been debated and remains unresolved. Variations in coastal ecosystem properties play an important role in the distribution of phytoplankton taxa [2] and one of the most evident features of seasonal phytoplankton dynamics is cyclic behaviour [3–6]. Nevertheless, the core problem remains that phytoplankton taxa take on some paradoxical aspects when we consider their distribution in their hyperspace-niche [1]. The excess in phytoplankton taxa richness—the so-called Paradox of Plankton—has been associated with the permanent failure to reach the equilibrium state within the pelagic habitat, as the habitat properties vary at a similar rate as the phytoplankton reproduce [7]. Numerical simulations [8] have shown that nested competition for multiple limiting resources can lead to an unstable equilibrium, as described for phytoplankton by Hutchinson [1]. However, it is still unknown how much of the observed coexistence can be attributed to environmental heterogeneity and how much arises within the community [9].

In the 1970s, Margalef [10] introduced the concept of phytoplankton succession, the so-called Mandala, in which the main stages of succession are driven by turbulence and nutrient availability. Succession starts in highly turbulent waters where diatoms successfully proliferate (r strategy) and culminates in calm oligotrophic waters where

dinoflagellates dominate (K strategy). Coccolithophores thrive in intermediate conditions, while red tides occur in calm but nutrient-enriched waters. Successive attempts have been made to revise the original mandala, but with doubtful success [11].

For our understanding of oceanic biogeochemical cycles, trophic interactions and, in general, the ecology of the marine environment, it is important to know how phytoplankton diversity is distributed in the pelagic habitat [12,13]. In the marine environment, it is particularly difficult to define areas or, better, defined spatial and temporal units on which diversity is then calculated and assemblages defined. These difficulties arise from the dynamic nature of the sea [14]. Phytoplankton phenology patterns vary in the time domain from stable annual fluctuations in certain biomes to the absence of a repeating pattern in others [15]. The usual pattern for estuarine and coastal environments is a short period with fluctuations on the order of 2–4 months [16]. Although it is often difficult to access data with spatial and temporal coverage, data from LTER (Long-Term Ecological Research) sites are ideal for studying phytoplankton phenology because they cover large time windows. Such data allow us to capture the basic community structure and its variability [16].

In the northernmost part of the Adriatic Sea, the Gulf of Trieste (GoT), phytoplankton community composition has been described as nanoflagellate-dominated, with seasonal outbursts of diatoms in spring and autumn in correlation with freshet periods and water column mixing [5,17]. This community is also sensitive to freshwater inputs [3], and some characteristic shifts in taxa composition have been observed following freshwater pulses [18,19].

One approach to analysing phytoplankton phenology is to use time series of species composition coupled with fidelity-specificity indices to describe indicative species phenology. Such an analysis has already been applied in studies in the northern Adriatic [5,20–22], based on fixed time intervals (seasons, months, years) used to find indicative species and describe the phenology of co-occurring species (assemblages). In this work, we propose a different approach with the reverse order of steps: species composition within time series is first used to define time intervals, and then it is possible to find the groups of indicative species within time intervals. For this purpose, we applied and modified the protocol proposed by Souissi et al. [23] and used by Anneville et al. [24] in a study on the phytoplankton community of Lake Geneva and tested for marine phytoplankton communities in the GoT [25,26].

In addition to co-occurrences, we were also interested in describing the major abundance peaks and the taxa responsible for these peaks. To estimate the distributional structure of a group of taxa, diversity indices of various kinds can usually be used to estimate, for each sample, how much abundance is concentrated or even across taxa [27]. Again, we used the same approach, but in reverse, to estimate how much the abundance is concentrated or uniform across samples for each taxon. The taxa that would be uniform would be those that have constant abundance across samples; the more they would be uneven the more their abundance would be concentrated in a few samples. In this way, we tried to be careful not to discard any important taxa during the selection process.

Upon re-analysis of the long-term phytoplankton data series from the Slovenian LTER station, we found that several problematic passages resulted in the loss of relevant information about community structure, introduced incorrect ordinations of the data, and caused difficulties in assigning indicative taxa. Therefore, one of the two goals of this study is to refine the critical passages in the protocol of the analysis. The other objective of this study is to use the refined analysis steps to better characterize the temporal dynamics of phytoplankton with the determination of characteristic periods and species at the Slovenian marine LTER station in the GoT.

2. Materials and Methods

2.1. Area of Study

The Gulf of Trieste (GoT) is a basin surrounded by land at the northeastern tip of Adriatic Sea. Due to its shallow depth, 21 m on average [28], the GoT is largely influenced

by climatic conditions that cause variations in salinity and temperature. The GoT is seasonally stratified, and its euphotic zone significantly exceeds the depth of the upper mixed layer for most of the year [29]. The basin is under the influence of two main winds, the "bora" and the "jugo", which blow from the northeast and southeast, respectively. Bora is a strong catabatic wind whose effect on the water column is twofold: mixing and cooling, while Jugo is a constant wind that is thought to have a chaotic effect on the current circulation in the Gulf [30].

The Slovenian LTER station (45.53833° N, 13.55° E; 21 m depth) is located at the southern entrance to the GoT (Figure 1), where direct impact from freshwater inputs and other pressures are minimal. The waters around the station are usually traversed by the current North Adriatic Dense Water (NAdDW). Only occasionally, they are reached by the plume of the Soča (Isonzo) River (SO, Figure 1), one of the local freshwater sources that has the greatest influence on the basin [30]. The Slovenian LTER station represents the reference station for national monitoring purposes, but the bias of the representation should be taken into account when generalizing the results to the whole Gulf.

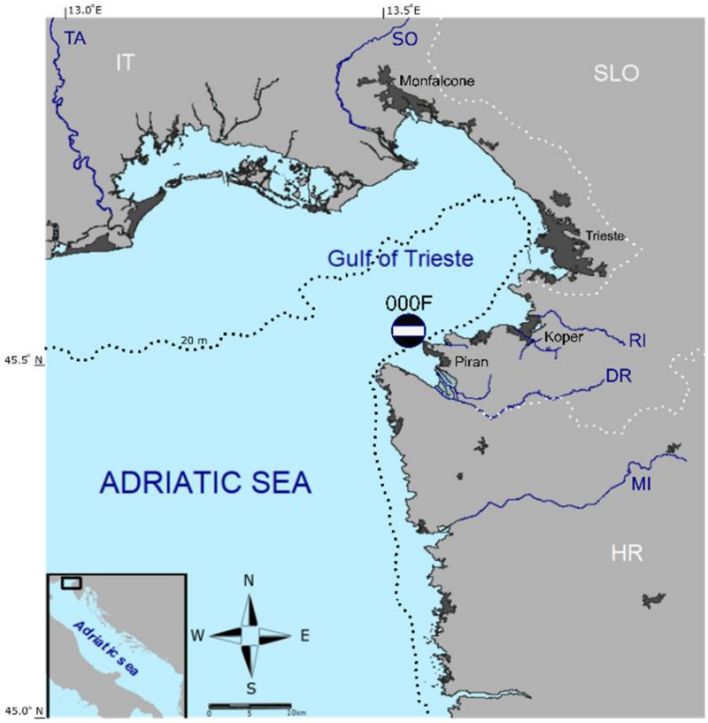

Figure 1. The map of the study site: The Slovenian LTER station 000F is marked with a black dot and a horizontal white bar. The dotted black line marks the 20 m isobath, the dotted white lines mark international borders while the blue lines mark the main rivers. SO Soča River, TA Tagliamento River, RI Rižana River, DR Dragonja River, MI Mirna River, IT Italy, SLO Slovenia, HR Croatia.

2.2. Data

Monthly data from Slovenian LTER sampling station 000F (Figure 1) were collected and stored as part of routine sampling in the Slovenian National Monitoring Program. In this work, a twelve-year time series from 2005 to 2017 was analysed. Phytoplankton was sampled with Niskin bottles (5 L) at different depths (0 m, 5 m, 15 m and near the bottom at 21 m). Phytoplankton samples were fixed with neutralized formaldehyde and stored until analysis. Subsamples of 50 mL were left to settle in a sedimentation chamber for 48 h and then examined using an inverted microscope ZEISS Axiovert 135, according to the Utermöhl method [31]. Phytoplankton taxa were determined to the lowest possible taxonomic level and counted in 50 to 100 microscope fields at 400× magnification. The final

dataset of phytoplankton composition and abundance included more than 100,000 entries. Taxonomic names were verified according to recent changes and consistency was checked for synonyms [32,33].

2.3. Analysis

Data analysis was performed using R-studio software (Version 1.1.456—© 2021–2018 RStudio, Inc., Boston, MA, USA). Table A1 in Appendix A shows the list of packages used in the analysis. Prior to analysis, data from different depths were merged in the Integrated Abundance (IA) using the trapezoidal rule. On the resulting matrix of taxa IAs (matrix X; Figure 2), a series of statistical methods for clustering the samples proposed by Anneville et al. [24] were applied (Figure 2A) and then modified (Figure 2B). The core idea was to create a clustering system of the samples based on the distribution of taxa and then obtain the indicative taxa for each cluster by the index of Fidelity and Specificity (IndVal) [34].

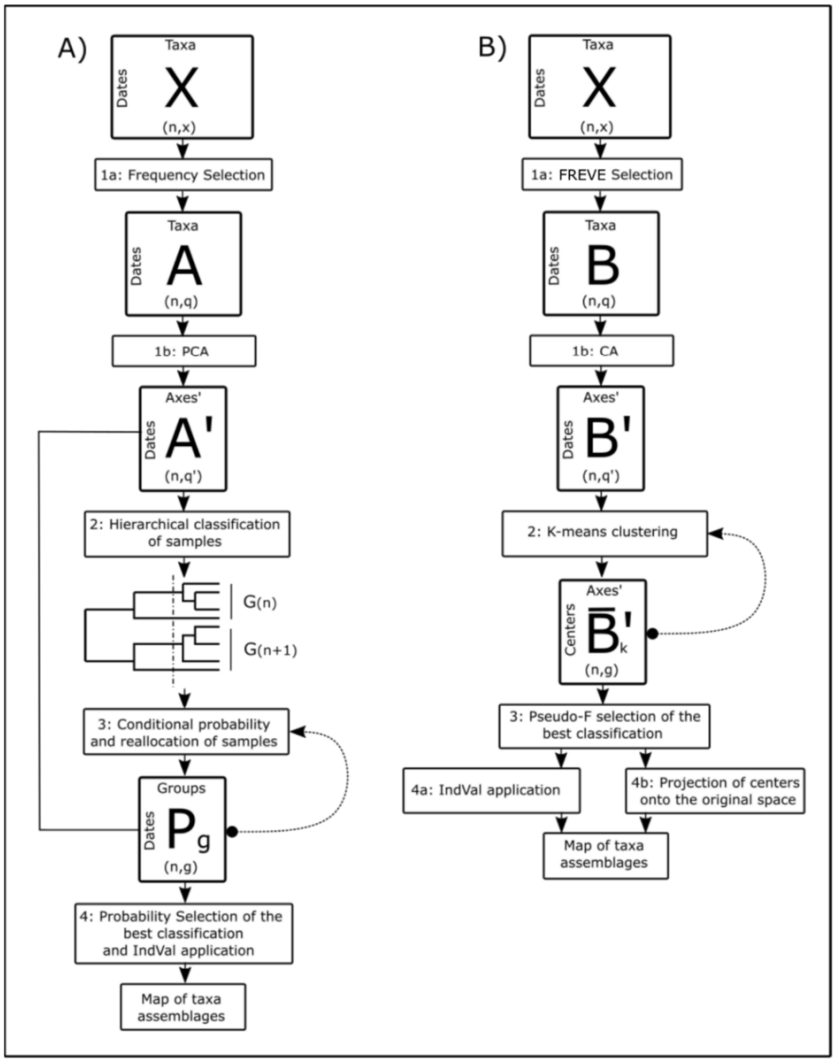

Figure 2. Flowchart of the (**A**) original and (**B**) modified protocol of data analysis.

2.4. Original Protocol

The first step consisted of the selection of the taxa on which to perform the successive analysis. Following Anneville et al. [24], taxa present in less than 12% of the samples were excluded (matrix A; Figure 2A, step 1a). A Principal Component Analysis (PCA) was

then applied to the log-transformed data (Figure 2A, step 1b). Principal components that accounted for 90% of the variance were retained and used to calculate PCA scores (matrix A'; Figure 2A). Multinormality was tested using the Dagnelie method [23]. From the matrix of PCA scores, hierarchical classification of samples (dates) was performed using Euclidean distance with a flexible clustering strategy (Figure 2A, step 2). Then, the probability that each sample belongs to each of the obtained clusters was calculated using Bayes' theorem. Here, the frequency of the cluster was used as the prior probability and the conditional probability was calculated using the χ^2 distribution estimator of the Mahalanobis distance of the object from the centroid of the cluster [24]. Since the probability was obtained for each samples' possible cluster, each sample could be reallocated to the cluster in which it had the maximum probability. Finally, new clusters were obtained and step 3 (calculation of P and reallocation of samples, Figure 2A) was repeated until the composition of the clusters remained stable and the final partition of the samples was obtained (matrix Pg, Figure 2A). Since it is possible to divide the samples into n clusters, where n varies from 1 to the total number of samples, a probability-based criterion was applied to characterize each partition (Figure 2A, step 4) as follows: a vector $P_{max}(k)$ representing the maximum probability for each sample was calculated. Each partition was evaluated on the basis of the median of the values of $P_{max}(k)$ This median was interpreted as the average measure of the within-cluster homogeneity [23]. The final clusters were used to create the map of taxa assemblages, in which each sample (i.e., each month) was assigned to a cluster (Figure 2A, step 4).

In each of these clusters, the IndVal index [34] was calculated for each taxon using the IA matrix obtained at the beginning (matrix A; Figure 2A). This index is a multiplication of two independently calculated values: the fidelity ($FI_{j,t}$) and the specificity ($SP_{j,t}$) of taxon t in the cluster of samples G_j (Equations (1) and (2), respectively).

$$FI_{j,t} = \frac{NS_{j,t}}{NS_{j+}} \quad (1)$$

$$SP_{j,t} = \frac{NI_{j,t}}{NI_{+j}} \quad (2)$$

where $NS_{j,t}$ is the number of samples in cluster G_j containing taxon t, NS_{j+} is the total number of samples in G_j, $NI_{j,t}$ is the mean abundance of taxon t in the samples belonging to G_j and NI_{+j} is the sum of the mean abundances of taxon t in all clusters. The fidelity of a taxon for a cluster is 1 if that taxon is present in all samples of the cluster, while the specificity of a taxon for a cluster is 1 if that taxon is present only in the cluster under consideration. The IndVal is calculated as in Equation (3) and has a range between 0 and 1.

$$IndVal_{j,t} = FI_{j,t} \times SP_{j,t} \quad (3)$$

As established by the authors in [34], an IndVal value greater than 0.25 is considered a threshold to describe a taxon as indicative of a particular cluster.

2.5. Modified Protocol

2.5.1. Frequency Selection

In step 1a (Figure 2A), taxa were selected for analysis based on their frequency with the threshold of 12%. The distribution of log cumulative abundances of the taxa along the frequency values is shown in Figure 3A. The dashed line representing the 12% presence shows no clear discontinuity in the data to support the setting of the threshold. Furthermore, any value of frequency used as a threshold would be arbitrary as there are no discontinuities along the frequency values. This is also supported by the frequency histogram showing the relative abundances (Figure 3B), where some of the rarely occurring taxa (<12%) showed relatively high abundances (darker colour). In contrast, some of the taxa with high frequency showed relatively low abundance (lighter colour).

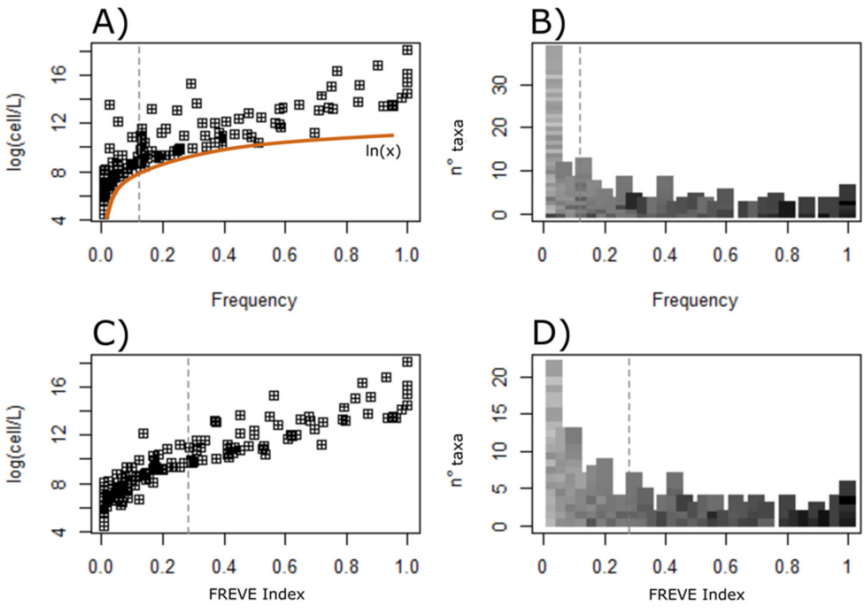

Figure 3. The rationale for the selection of taxa: (**A**) Frequency vs. log cumulative abundance distribution of taxa (points), dashed line represents the 12% threshold; (**B**) Frequency histogram of taxa, dashed line represents the 12% threshold, grey scale represents relative abundance of taxa; (**C**) FREVE index vs. log cumulative abundance distribution of taxa (points), dashed line represents the value of 0.28; (**D**) Histogram of FREVE index, the dashed line represents the 0.28 value of fluctuation index, grey scale represents the relative abundance of taxa.

The lower bound of the distribution of points in Figure 3A resembles the logarithmic function. A similar shape is obtained by the log transformation of the vector of positive naturals N^+ [1, 2, 3, . . .]. This distribution results from the taxa identification and counting method, during which some of the taxa were found only once per sample. This value of 1cell was then transformed per volume of sample and integrated. The resulting abundances were thus generated by a categorical process of presence/absence discrimination, even though the values look quantitative. The taxa abundances that occupy the lower limit of the distribution (those that are close to the ln(x) function, Figure 3A) are therefore the result of a scaled version of the log transformation of the presences' vector of rare taxa. This particular distribution of some taxa led to the postulation of the co-presence of two types of rarity and four types of distribution of taxa in our dataset. A taxon may be rare in terms of frequency (i.e., observed in a small number of samples) or rare in terms of abundance (i.e., having low abundances). The combination of rarities results in four distribution types: taxa that are rare in both presence and abundance (type 1), taxa that are rare in presence but not in abundance (type 2), taxa that are common in presence and abundance (type 3), and taxa that are common in presence and rare in abundance (type 4).

To measure the evenness of the abundances of each taxon, in order to exclude the type 1 (rare and even) taxa, we chose the Pielou Evenness index λ [27]. The idea was to scale the taxa frequency (f) to the taxa evenness (λ). In this way, we obtained a new index for the taxa, which we tentatively called FREVE (frequency and evenness), and which is shown in Equation (4):

$$\text{FREVE} = f^{\lambda} \tag{4}$$

and have the limits as in Equations (5)–(8):

$$\lim_{(f,\,\lambda)\to(0^+,1^-)} f^{\lambda} = 0 \tag{5}$$

$$\lim_{(f,\,\lambda)\to(0^+,0^+)} f^{\lambda} = 1 \quad (6)$$

$$\lim_{(f,\,\lambda)\to(1^-,0^+)} f^{\lambda} = 1 \quad (7)$$

$$\lim_{(f,\,\lambda)\to(1^-,1^-)} f^{\lambda} = 1 \quad (8)$$

Infrequent taxa with evenly distributed abundance would have frequency (f) close to 0 and evenness (λ) close to 1, then FREVE is close to 0 (Equation (5)). The other three cases, corresponding to distributions of type 2 (Equation (6)), type 3 (Equation (7)), and type 4 (Equation (8)), would yield FREVE values close to 1 (Figure 3C). The histogram of the FREVE index (Figure 3D) shows how the index shifted the taxa with the highest abundances to the right half. The cutting threshold we set to select taxa was the composite of two arbitrary thresholds. Because we wanted to retain taxa that were present at least once per year ($f = 1/12$) and whose abundance was less uniform than the level of intermediate evenness ($\lambda = 0.5$) [35], we obtained the threshold using the Equation (4) (0.28). Finally, taxa with FREVE > 0.28 were retained for subsequent analysis.

2.5.2. Component Space and Clustering

The choice of Principal Component Analysis (PCA) in the original protocol implies the preservation of Euclidean Distance between sample objects. The use of symmetric coefficients (as Euclidean distance) for the analysis of sample-taxa datasets is not the right choice in most cases [36]. This is due to the different information that a double presence or double absence of a given taxa brings, namely the "double-zero" problem [36]. Instead of PCA, a Correspondence Analysis (CA), which preserves χ^2 distance, was performed on the dataset after FREVE taxa selection (Figure 2B, step 1b). CA was also used to perform Inertia analysis [36] on the datasets selected by both protocols (Figure 2A, matrix A' and 2B, matrix B') to evaluate and confront the two selection methods (frequency-based vs. FREVE). To obtain clusters of samples, non-hierarchical k-means clustering [36] was then computed instead of Bayesian reallocation (Figure 2B, step 2). Each n-partition was evaluated using Calinski pseudo-F [36,37] and Ratkowsky index [38] (Figure 2B, step 3).

2.5.3. Indicative Taxa

The selection of the best clustering of samples was followed, as in the original protocol, by the application of the IndVal index (Figure 2B, step 4a). Dufrene and Legendre stated that "the use of IndVal removes any effect of the number of sites in the various clusters and also differences in abundance among sites belonging to the cluster" [34]. However, with the way IndVal is calculated, it is possible for a taxon to have the same IndVal value in two completely different hypothetical situations. In the first situation, the taxon whose cumulative abundance is split into two clusters and is present in half of the samples in both clusters would have the same IndVal value in both clusters (0.25). The IndVal value would also be the same (0.25) in a second situation where the taxon is present in two clusters, where in one it is present in every sample (FI = 1) and has 25% of the abundance (SP = 0.25) and in the other it is present in one third of the samples (FI = 0.33) and has 75% of the abundance (SP = 0.75). Theoretically, it should be possible to disentangle these biased cases using the *p*-values calculated according to the permutative method proposed by Dufrene and Legendre [34]. However, in the multivariate situation where each cluster is defined around several taxa, many if not all taxa are suboptimally described. As a result, many of the possible cluster permutations will produce higher IndVal values for each taxon, reducing the discriminatory power of the *p*-value. To facilitate interpretation of the IndVal results, the centroids of the clusters (CA centroids) obtained from k-means were projected onto the space of taxa (CA columns) (Figure 2B, step 4b), resulting in a vector of taxa likelihood ratios (Observed/Expected) for the centroids. This is justified in Appendix B. The higher the projected value of the taxa (Xproj), which represents the likelihood of the centroid, the stronger the association (Xproj > 0; Likelihood ratio > 1) between the column

(taxa) and the centroid (cluster). Xproj was used as the association index and the threshold was set to Xproj 1 (Likelihood ratio 2). A taxon with Xproj > 1 is strongly associated with the cluster, indicating that its observed abundance is more than twice as high as expected. The similarity of the two indicator matrices (IndVal and Xproj) was tested using the Mantel test over ranked indices (999 permutations) [36].

2.5.4. Log-Transformation

A final remark concerns the log transformation made at the beginning of the original protocol. In the modified protocol (Figure 2B), the raw data were not log-transformed because, as pointed out in the literature [39], this method, used on count data, is either redundant or wrong in most cases. In the context of extrapolating probabilities from Mahalanobis distances, multinormality was an issue and indeed, taxa abundances were log-transformed (see Section 2.4) and multinormality was tested using the Dagnelie method [23] before proceeding. However, no normality assumptions are required when using raw distances for clustering.

3. Results

3.1. Phytoplankton Community Composition and Taxa Selection

In the phytoplankton community at the Slovenian LTER station, a total of 130 taxa were determined during 2005–2017, including 53 diatom taxa, 50 dinoflagellate taxa and 15 coccolithophore taxa. The remaining 12 taxa were distributed among the classes Cryptophyceae, Chlorophyceae, Euglenophyceae, Prasinophyceae, Chrysophyceae, Dictyochophyceae and other undetermined nanoflagellates. Nanoflagellates accounted for the largest proportion of abundance (57%), while diatom cells accounted for 36%, coccolithophores 4% and dinoflagellates 3% of total abundance.

Abundance peaks above 1×10^6 cells L^{-1} were mainly recorded in late winter/spring and autumn and were mainly attributable to diatoms. Five diatom blooms were dominated by *Chaetoceros* spp. in February 2007 (2.2×10^6 cells L^{-1}), November 2011 (1.2×10^6 cells L^{-1}), November and December 2012 (up to 1.6×10^6 cells L^{-1}) and July 2015 (1.7×10^6 cells L^{-1}), while *Skeletonema* species were responsible for two February blooms in 2011 and 2012 (1.2×10^6 cells L^{-1}). The largest diatom bloom was recorded in November 2010, when species from the *Pseudo-nitzschia delicatissima* group reached 3.7×10^6 cells L^{-1}. Nanoflagellates caused two abundance peaks in July 2005 (1.5×10^6 cells L^{-1}) and in May 2016 (1.6×10^6 cells L^{-1}).

Out of a total of 130 taxa, 57 taxa were selected for further analysis based on the proposed FREVE (Table 1). Of these, 56 were already included in the frequency-based selection and one rare taxon was rescued. The major difference between the two selection methods was 17 common taxa that were discarded by FREVE but would have been retained based on frequency.

Table 1. Comparison of the number of retained and discarded taxa between two selection methods: frequency-based and FREVE.

			Frequency Selection	
			Common (f > 0.12)	**Rare (f < 0.12)**
			73	57
FREVE selection	(FREVE > 0.28)	57	56	1
	(FREVE < 0.28)	73	17	56

A comparison between selection methods was made using Inertia Analysis. Total Inertia (TI) was calculated as the sum of the eigenvalues of the χ^2 dissimilarity matrix. Taxa were sequentially removed from less abundant to abundant and TI was recalculated (Figure 4). The initial TI's value of the complete dataset (2.89) is closer to the TI value for the dataset obtained by FREVE selection (2.81) than the TI values obtained by frequency

selection (2.46). This means that FREVE retains more information from the original dataset. The one species rescued by FREVE (Table 1) was responsible for about 13% of the data TI, more than the 17 discarded taxa.

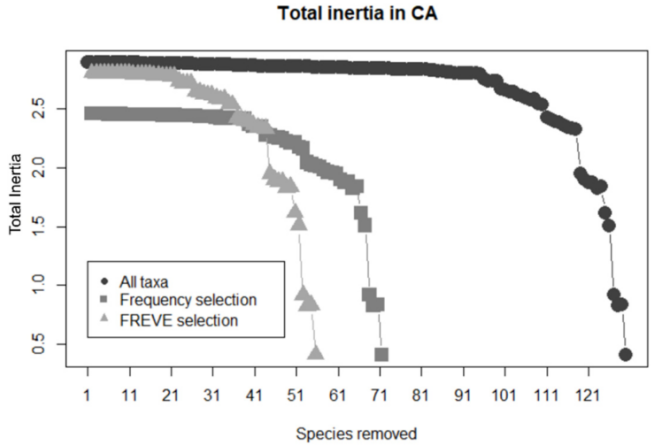

Figure 4. Inertia analysis for three datasets, the full dataset (All taxa), the dataset resulting from frequency selection, and the dataset resulting from FREVE selection. The taxa ordered by abundance were removed at each step and the Total Inertia was recalculated.

3.2. Evaluation of n-Partition

Among all possible partitions, the Calinski pseudo-F values peaked for the partition with four clusters and reached a second maximum for the partition with 18 clusters (Figure 5, left). The Ratkowsky *Between-Sum-of-square* increase rate was highest between partitions with three and four clusters (Figure 5, right), indicating that the best number of clusters was four. Between 18 and 20 clusters, the Ratkowsky's index reached the plateau. Finally, two partitions with 4 and 18 clusters were chosen to obtain a broad and a fine resolution in the data discontinuities, respectively.

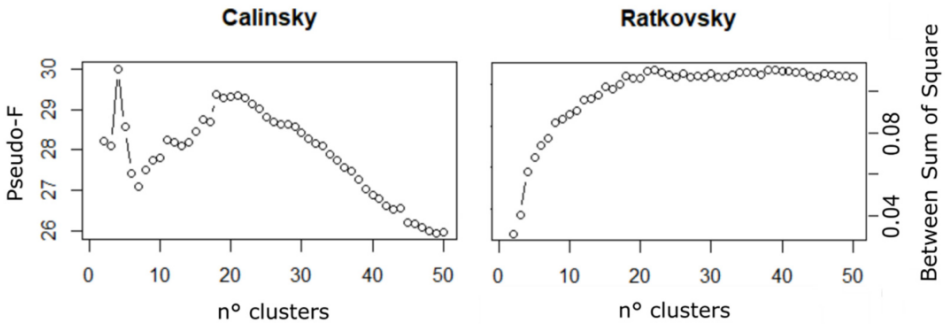

Figure 5. (**left**) Calinski Pseudo-F results plotted for each n-clustered possible partition and (**right**) the Ratkowsky index for each n-clustered possible partition.

3.3. Original Protocol Temporal Map

For the temporal map obtained with the original protocol (Figure 2A), the best of possible partitions with six clusters were used and the IndVal index was applied to select the indicative taxa of the clusters (Figure 6). A total of 43 out of 73 taxa were found to be indicative of at least one cluster (Table 2). The cluster map revealed a rough seasonal pattern except for the first two years (2005 and 2006). These two years and parts of 2007 and 2008 belonged entirely to Cluster I, in which no taxa exceeded the threshold (IndVal = 0.25) to be defined as indicative. From 2009 onwards, the winter (January–March) was mostly characterized by Cluster II with two indicative species, the diatom *Skeletonema*

costatum s.l. and the coccolithophore *Ophiaster hydroideus*. In 2009–2012, Cluster II extended into spring, whereas in recent years, it had already appeared in autumn. Cluster III almost always appeared before Cluster II, usually in autumn (October to December). This cluster was described by many indicative taxa, predominantly diatoms. Seven taxa had IndVal > 0.5: the diatoms *Asterionellopsis glacialis*, *Cylindrotheca closterium*, *Eucampia* spp., *Lauderia annulata*, *Pleurosigma normanii* and the *Pseudo-nitzschia seriata* group, as well as a coccolithophore *Calciosolenia murrayi*. Cluster III was generally anticipated by Cluster VI, typical of the summer (July to September) and occasionally extended into the autumn, which contained ten indicative taxa, mostly diatoms. Three taxa had IndVal > 0.5: the diatoms *Proboscia alata* and *Rhizosolenia* spp. and a coccolithophore *Rhabdosphaera stylifera*. Cluster IV was intermittently present in spring and summer and best described the temporal distribution for two diatom taxa: *Cyclotella* spp. and *Cerataulina pelagica*. Finally, Cluster V appeared in 2009 and characterized the spring from March to June. Cluster V was represented by a mixed phytoplankton community, but only one coccolithophore (*Calyptrosphaera oblonga*) had IndVal > 0.5.

Table 2. Composition of taxa in clusters derived from the original protocol sensu Anneville et al., (2002) with corresponding IndVal value. Only taxa with IndVal value higher than 0.25 are shown. The taxa are organized in descending order of IndVal value.

Cluster	Taxon	IndVal	Cluster	Taxon	IndVal
I	/	/	V	*Cyclotella* spp.	0.46
II	*Skeletonema costatum* s.l.	0.33		*Prorocentrum compressum*	0.44
	Ophiaster hydroideus	0.26		Euglenophyceae	0.42
III	*Eucampia* spp.	0.80		*Bacteriastrum delicatulum*	0.42
	Pseudo-nitzschia seriata gr.	0.62		*Prorocentrum balticum*	0.40
	Lauderia annulata	0.62		*Prorocentrum micans*	0.39
	Calciosolenia murrayi	0.61		Prasinophyceae	0.38
	Pleurosigma normanii	0.54		*Prorocentrum cordatum*	0.33
	Cylindrotheca closterium	0.53		*Alexandrium minutum*	0.32
	Asterionellopsis glacialis	0.50		Diatoms non ident.	0.31
	Leptocylindrus mediterraneus	0.49		*Leptocylindrus danicus*	0.29
	Thalassiosira spp.	0.43		*Nitzschia longissima*	0.29
	Chaetoceros spp.	0.43		Cryptophyceae	0.29
	Nitzschia spp.	0.43		*Gymnodinium* spp.	0.29
	Proboscia indica	0.41		*Prorocentrum triestinum*	0.28
	Cerataulina pelagica	0.37		*Amphora* spp.	0.28
	Pseudo-nitzschia delicatissima gr.	0.37	VI	*Rhizosolenia* spp.	0.54
	Leptocylindrus danicus	0.34		*Proboscia alata*	0.53
	Emiliania huxleyi	0.32		*Rhabdosphaera stylifera*	0.51
	Guinardia flaccida	0.31		*Pseudo-nitzschia delicatissima* gr.	0.49
	Thalassionema nitzschioides	0.28		*Dactyliosolen fragilissimus*	0.40
IV	*Cyclotella* spp.	0.29		*Syracosphaera pulchra*	0.37
	Cerataulina pelagica	0.25		*Thalassionema nitzschioides*	0.34
V	*Calyptrosphaera oblonga*	0.63		*Hemiaulas hauckii*	0.29
	Heterocapsa gr.	0.49		*Tripos fusus*	0.29
	Chlorophyceae	0.46		*Guinardia striata*	0.28

Five taxa were indicative of more than one cluster. Excluding the first two years, the typical sequence of phytoplankton during the study period was Cluster II—Cluster V—Cluster IV—Cluster VI—Cluster III.

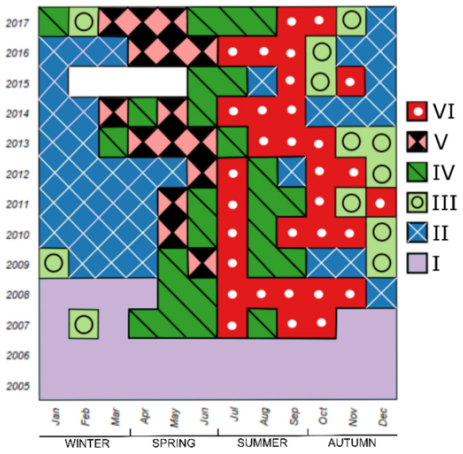

Figure 6. Temporal map of phytoplankton assemblages based on the original protocol sensu Anneville et al. (2002). The white area indicates missing data.

3.4. Modified Protocol Temporal Map

3.4.1. Four-Clustered Partition

The temporal map showing four clusters obtained with the modified protocol (Figure 2B) is shown in Figure 7 (left), while indicative taxa with Xproj and IndVal values for these clusters are summarized in Table 3. Two clusters showed some degree of seasonality. The "winter" Cluster II was strongly associated with the diatoms *Skeletonema costatum* s.l. and *Chaetoceros simplex* (Xproj 22.0 and 5.23, respectively, and IndVal > 0.5), but was restricted to February 2005, 2011, and 2012. The "summer and autumn" Cluster IV, which was also occurred sporadically in the early spring, was indicative of diatom blooms. Six diatom taxa had a meaningful Xproj > 1 for this cluster, while a variety of other taxa in a different order (though mainly diatoms) were indicated as typical by IndVal $\geq$ 0.25. Interestingly, the centroid of the Cluster IV was most associated with *Lauderia annulata*, which had IndVal < 0.25. Cluster III was present only in February 2017 and was associated with the diatoms *Chaetoceros curvisetus, Leptocylindrus danicus* and *L. annulata*. The largest of the clusters, Cluster I, was distributed across all other months and represented the mixed phytoplankton community of nanoflagellates, small diatoms and some coccolithophore taxa, although none of the Xproj or IndVal were particularly high. The Mantel test between the two ordination indices (Xproj and IndVal) showed a significant correlation (r = 0.78; *p*-value = 0.03).

Table 3. Taxa composition of the 4-clustered partition with corresponding Likelihood ratios (Xproj) for the centroids and IndVal values (IndVal). Taxa with Xproj > 1 or IndVal value > 0.25 are shown in bold. Taxa in both columns are organized in descending order of IndVal and Xproj. The term "Nanoflagellates" stands for flagellates in the nanoplankton size fraction that have not been identified as prasinophytes, cryptophytes, etc.

Cluster	Taxon (Ranked by Xproj)	Xproj	Taxon (Ranked by IndVal)	IndVal
I	*Meringosphaera mediterranea*	0.78	Prasinophyceae	**0.42**
	Diploneis crabro	0.68	Diatoms non ident.	**0.41**
	Diatoms non ident.	0.61	*Meringosphaera mediterranea*	**0.39**
	Cylindrotheca Closterium	0.56	*Diploneis crabro*	**0.36**
	Ophiaster hydroideus	0.53	Cryptophyceae	**0.33**
	Emiliania huxleyi	0.48	*Cylindrotheca closterium*	**0.33**
	Cryptophyceae	0.44	*Heterocapsa* gr.	**0.3**
	Dictyocha fibula	0.41	*Cyclotella* spp.	**0.29**
	Prorocentrum cordatum	0.39	nanoflagellates	**0.29**
	Nanoflagellates	0.37	*Ophiaster hydroideus*	**0.26**
	Gonyaulax spp.	0.37	*Emiliania huxleyi*	**0.26**

Table 3. *Cont.*

Cluster	Taxon (Ranked by Xproj)	Xproj	Taxon (Ranked by IndVal)	IndVal
II	*Skeletonema costatum* s.l.	**22.00**	*Skeletonema costatum* s.l.	**0.98**
	Chaetoceros simplex	**5.23**	*Chaetoceros simplex*	**0.55**
	Prorocentrum compressum	−0.25	*Emiliania huxleyi*	**0.29**
	Scrippsiella trochoidea	−0.25	*Scrippsiella trochoidea*	**0.28**
III	*Chaetoceros curvisetus*	**76.01**	*Chaetoceros curvisetus*	**1**
	Leptocylindrus danicus	**9.61**	*Leptocylindrus danicus*	**0.87**
	Lauderia annulata	**4.33**	*Prorocentrum micans*	**0.75**
	Prorocentrum compressum	**2.92**	*Lauderia annulata*	**0.75**
	Asterionellopsis glacialis	**2.85**	*Asterionellopsis glacialis*	**0.68**
	Prorocentrum micans	**2.51**	*Prorocentrum compressum*	**0.66**
	Prorocentrum cordatum	**2.22**	*Prorocentrum cordatum*	**0.66**
	Prorocentrum balticum	**1.68**	*Prorocentrum balticum*	**0.64**
	Bacteriastrum delicatulum	**1.42**	*Bacteriastrum delicatulum*	**0.58**
	Hemiaulas hauckii	**1.26**	*Hemiaulas hauckii*	**0.56**
	Nitzschia longissima	0.4	*Nitzschia longissima*	**0.53**
	Pleurosigma normanii	0.2	*Dictyocha fibula*	**0.52**
	Prorocentrum triestinum	0.19	*Prorocentrum triestinum*	**0.47**
	Guinardia striata	0.15	*Pleurosigma normanii*	**0.44**
	Dictyocha fibula	0.11	*Prorocentrum gracile*	**0.39**
	Pseudo-nitzschia seriata gr.	−0.08	*Guinardia striata*	**0.38**
	Cerataulina pelagica	−0.13	*Cyclotella* spp.	**0.37**
	Prorocentrum gracile	−0.27	*Pseudo-nitzschia seriata* gr.	**0.32**
	Gyrodinium. spp.	−0.27	*Gyrodinium* spp.	**0.32**
	Cyclotella spp.	−0.37	*Cerataulina pelagica*	**0.31**
	Thalassionema nitzschioides	−0.37	*Thalassionema nitzschioides*	**0.3**
	Rhizosolenia spp.	−0.38	*Rhizosolenia* spp.	**0.25**
IV	*Lauderia annulata*	**2.17**	*Pseudo-nitzschia delicatissima* gr.	**0.86**
	Asterionellopsis glacialis	**1.38**	*Chaetoceros* spp.	**0.81**
	Guinardia striata	**1.34**	*Proboscia alata*	**0.79**
	Leptocylindrus mediterraneus	**1.18**	*Dactyliosolen fragilissimus*	**0.64**
	Pseudo-nitzschia seriata gr.	**1.08**	*Nitzschia* spp.	**0.6**
	Bacteriastrum delicatulum	**1.05**	*Cerataulina pelagica*	**0.6**
	Chaetoceros spp.	0.92	*Syracosphaera pulchra*	**0.55**
	Cerataulina pelagica	0.8	Euglenophyceae	**0.54**
	Pleurosigma normanii	0.76	*Rhizosolenia* spp.	**0.49**
	Rhabdosphaera stylifera	0.75	*Rhabdosphaera stylifera*	**0.46**
	Dactyliosolen fragilissimus	0.75	*Tripos fusus*	**0.44**
	Hemiaulas hauckii	0.7	*Pseudo-nitzschia seriata* gr.	**0.41**
	Leptocylindrus danicus	0.67	*Guinardia flaccida*	**0.41**
	Guinardia flaccida	0.59	*Heterocapsa* gr.	**0.41**
	Coccolith. non ident.	0.59	*Cylindrotheca closterium*	**0.41**
	Pseudo-nitzschia delicatissima gr.	0.59	*Leptocylindrus mediterraneus*	**0.39**
	Proboscia alata	0.55	Prasinophyceae	**0.39**
	Syracosphaera pulchra	0.49	*Calciosolenia murrayi*	**0.38**
	Thalassiosira spp.	0.49	*Thalassionema nitzschioides*	**0.37**
	Tripos fusus	0.35	*Guinardia striata*	**0.36**
	Calciosolenia murrayi	0.3	*Diploneis crabro*	**0.35**
	Rhizosolenia spp.	0.3	*Thalassiosira* spp.	**0.34**
	Euglenophyceae	0.28	*Gymnodinium* spp.	**0.32**
	Nitzschia longissima	0.21	nanoflagellates	**0.3**
	Prorocentrum triestinum	0.21	*Calciosolenia brasiliensis*	**0.29**
	Dinobryon spp.	0.18	*Ophiaster hydroideus*	**0.26**
	Oxytoxum spp.	0.1	*Pleurosigma normanii*	**0.26**
	Protoperidinium spp.	0.08	Diatoms non ident.	**0.26**
	Calciosolenia brasiliensis	0.05	Cryptophyceae	**0.25**
	Nitzschia spp.	0.04	*Emiliania huxleyi*	**0.25**

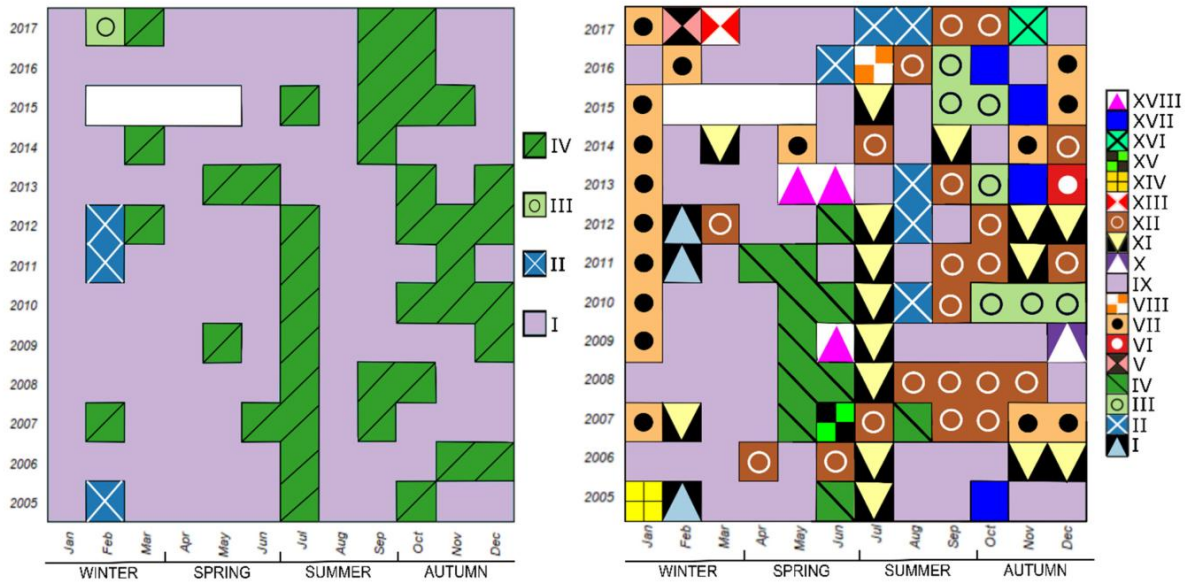

Figure 7. (**left**) Temporal map of phytoplankton assemblages of the 4-clustered partition. (**right**) Temporal map of phytoplankton assemblages of the 18-clustered partition. The white area indicates missing data.

3.4.2. Eighteen-Clustered Partition

The temporal map of 18 clusters obtained with the modified protocol is shown in Figure 7 (right), with the corresponding Xproj and IndVal values summarized in Table 4. It shows a more complex picture of seasonality, especially in autumn. Ten clusters included three or more samples/months, while the remaining eight included only one sample/month.

Table 4. Taxa composition of the 18-clustered partition with corresponding Likelihood ratios (Xproj) for the centroids and IndVal values (IndVal). Taxa with Xproj > 1 or IndVal > 0.25 are in bold. Taxa in both columns are organized in descending order of IndVal and Xproj. The term "Nanoflagellates" stands for flagellates in the nanoplankton size fraction that have not been identified as prasinophytes, cryptophytes, etc.

Cluster	Taxon (Ranked by Xproj)	Xproj	Taxon (Ranked by IndVal)	IndVal
I	*Skeletonema costatum* s.l.	**22.0**	*Skeletonema costatum* s.l.	**0.92**
	Chaetoceros simplex	**5.23**	*Chaetoceros simplex*	0.23
II	Diatoms non ident.	**10.1**	Diatoms non ident.	**0.38**
	Guinardia flaccida	**5.01**	*Dactyliosolen fragilissimus*	0.18
	Dactyliosolen fragilissimus	**4.20**	*Heterocapsa* gr.	0.12
	Prorocentrum triestinum	**4.12**	*Prorocentrum triestinum*	0.12
	Oxytoxum spp.	**1.82**	Chlorophyceae	0.11
	Heterocapsa gr.	**1.69**	*Guinardia flaccida*	0.10
	Pleurosigma normanii	**1.58**	*Cyclotella* spp.	0.07
	Prorocentrum gracile	**1.49**	*Thalassionema nitzschioides*	0.06
	Guinardia striata	**1.17**	*Prorocentrum balticum*	0.06
	Chlorophyceae	**1.16**	*Gyrodinium* spp.	0.06
	Thalassionema nitzschioides	**1.14**	*Prorocentrum gracile*	0.06
	Hemiaulas hauckii	**1.07**	Cryptophyceae	0.06

Table 4. *Cont.*

Cluster	Taxon (Ranked by Xproj)	Xproj	Taxon (Ranked by IndVal)	IndVal
III	*Calciosolenia murrayi*	**4.75**	*Pseudo-nitzschia delicatissima* gr.	**0.65**
	Pseudo-nitzschia delicatissima gr.	**4.37**	*Nitzschia* spp.	**0.28**
	Syracosphaera pulchra	**2.11**	*Syracosphaera pulchra*	**0.28**
	Tripos fusus	**1.87**	*Calciosolenia murrayi*	0.24
	Dactyliosolen fragilissimus	**1.63**	*Dactyliosolen fragilissimus*	0.20
	Tripos furca	**1.59**	*Gyrodinium* spp.	0.18
	Calciosolenia brasiliensis	**1.55**	*Tripos fusus*	0.18
	Nitzschia spp.	**1.39**	*Calciosolenia brasiliensis*	0.17
	Prorocentrum triestinum	**1.24**	*Ophiaster hydroideus*	0.16
	Rhabdosphaera stylifera	**1.12**	*Rhizosolenia* spp.	0.13
	Gyrodinium spp.	**1.12**	*Tripos furca*	0.13
	Leptocylindrus mediterraneus	**1.09**	*Pseudo-nitzschia seriata* gr.	0.11
IV	*Cyclotella* spp.	**5.28**	*Cyclotella* spp.	**0.44**
	Chaetoceros simplex	**4.02**	*Prorocentrum gracile*	0.20
	Prorocentrum gracile	**2.97**	*Prorocentrum cordatum*	0.13
	Heterocapsa gr.	**1.08**	*Chaetoceros simplex*	0.13
	Prorocentrum cordatum	**1.03**	Prasinophyceae	0.12
V	*Chaetoceros curvisetus*	**76.0**	*Chaetoceros curvisetus*	**0.95**
	Leptocylindrus danicus	**9.61**	*Prorocentrum cordatum*	**0.31**
	Lauderia annulata	**4.33**	*Prorocentrum balticum*	0.24
	Prorocentrum compressum	**2.92**	*Leptocylindrus danicus*	0.23
	Asterionellopsis glacialis	**2.85**	*Hemiaulas hauckii*	0.22
	Prorocentrum micans	**2.51**	*Prorocentrum micans*	0.21
	Prorocentrum cordatum	**2.22**	*Prorocentrum compressum*	0.20
	Prorocentrum balticum	**1.68**	*Bacteriastrum delicatulum*	0.12
	Bacteriastrum delicatulum	**1.42**	*Guinardia striata*	0.11
	Hemiaulas hauckii	**1.26**	*Nitzschia longissima*	0.11
VI	*Lauderia annulata*	**114.**	*Lauderia annulata*	**0.83**
	Leptocylindrus mediterraneus	**22.7**	*Leptocylindrus mediterraneus*	**0.54**
	Thalassiosira spp.	**7.94**	*Thalassiosira* spp.	**0.28**
	Guinardia flaccida	**5.54**	*Gonyaulax* spp.	0.20
	Cerataulina pelagica	**4.35**	*Guinardia flaccida*	0.18
	Leptocylindrus danicus	**2.89**	*Protoperidinium* spp.	0.12
	Thalassionema nitzschioides	**2.03**	*Thalassionema nitzschioides*	0.10
	Gonyaulax spp.	**1.76**	*Calciosolenia brasiliensis*	0.08
	Protoperidinium spp.	**1.63**	*Ophiaster hydroideus*	0.08
	Calciosolenia brasiliensis	**1.35**	*Pleurosigma normanii*	0.08
	Pleurosigma normanii	**1.34**	*Dactyliosolen fragilissimus*	0.08
	Nitzschia longissima	**1.01**	*Gyrodinium* spp.	0.07
VII	*Emiliania huxleyi*	**3.71**	*Emiliania huxleyi*	0.11
	Ophiaster hydroideus	**1.74**	*Ophiaster hydroideus*	0.07
	Diploneis crabro	**1.73**	*Diploneis crabro*	0.07
	Gonyaulax spp.	**1.66**	Prasinophyceae	0.06
	Cylindrotheca closterium	**1.24**	*Meringosphaera mediterranea*	0.06

Table 4. *Cont.*

Cluster	Taxon (Ranked by Xproj)	Xproj	Taxon (Ranked by IndVal)	IndVal
VIII 	*Dictyocha fibula*	**97.2**	*Dictyocha fibula*	**0.92**
	Rhabdosphaera stylifera	**10.2**	*Rhabdosphaera stylifera*	**0.54**
	Oxytoxum spp.	**10.1**	*Oxytoxum* spp.	**0.44**
	Calciosolenia brasiliensis	**5.17**	*Calciosolenia brasiliensis*	**0.27**
	Prorocentrum micans	**4.36**	*Tripos furca*	0.20
	Prorocentrum triestinum	**4.14**	*Prorocentrum triestinum*	0.18
	Diatoms non ident.	**3.04**	Diatoms non ident.	0.18
	Diploneis crabro	**2.90**	*Prorocentrum micans*	0.17
	Prorocentrum compressum	**2.71**	*Diploneis crabro*	0.17
	Tripos furca	**2.53**	*Heterocapsa* gr.	0.14
	Thalassionema nitzschioides	**2.25**	*Scrippsiella trochoidea*	0.14
	Scrippsiella trochoidea	**2.20**	*Thalassionema nitzschioides*	0.13
	Heterocapsa gr.	**1.85**	Chlorophyceae	0.12
	Cylindrotheca closterium	**1.10**	*Prorocentrum compressum*	0.10
IX 	*Meringosphaera mediterranea*	**1.05**	Cryptophyceae	0.08
X 	*Asterionellopsis glacialis*	**61.3**	*Asterionellopsis glacialis*	**0.79**
	Lauderia annulata	**3.51**	*Ophiaster hydroideus*	0.21
	Thalassiosira spp.	**2.66**	*Thalassiosira* spp.	0.16
	Cerataulina pelagica	**2.63**	*Guinardia striata*	0.13
	Ophiaster hydroideus	**2.14**	*Thalassionema nitzschioides*	0.13
	Leptocylindrus mediterraneus	**1.98**	*Leptocylindrus mediterraneus*	0.10
	Thalassionema nitzschioides	**1.69**	*Diploneis crabro*	0.09
	Guinardia striata	**1.21**	*Calciosolenia murrayi*	0.09
	Calciosolenia murrayi	**1.21**	*Cerataulina pelagica*	0.07
XI 	*Chaetoceros* spp.	**2.53**	*Proboscia alata*	**0.45**
	Proboscia alata	**1.78**	*Chaetoceros* spp.	**0.38**
XII 	Coccolith. non ident.	**4.43**	*Nitzschia* spp.	0.14
	Guinardia striata	**2.50**	*Guinardia striata*	0.12
	Oxytoxum spp.	**1.78**	*Dactyliosolen fragilissimus*	0.10
	Hemiaulas hauckii	**1.68**	*Syracosphaera pulchra*	0.09
	Dactyliosolen fragilissimus	**1.48**	*Hemiaulas hauckii*	0.09
	Rhabdosphaera stylifera	**1.27**	Coccolith. non ident.	0.09
	Nitzschia spp.	**1.14**	*Proboscia alata*	0.07
	Pleurosigma normanii	**1.05**	*Rhabdosphaera stylifera*	0.06
XIII 	*Dinobryon* spp.	**39.1**	*Dinobryon* spp.	**0.84**
	Leptocylindrus danicus	**19.9**	*Leptocylindrus danicus*	**0.46**
	Prorocentrum compressum	**5.51**	*Prorocentrum compressum*	**0.34**
	Chaetoceros curvisetus	**2.45**	*Scrippsiella trochoidea*	0.28
	Prorocentrum micans	**2.40**	*Prorocentrum micans*	0.21
	Scrippsiella trochoidea	**2.35**	*Nitzschia longissima*	0.18
	Nitzschia longissima	**1.35**	Prasinophyceae	0.18
XIV 	*Emiliania huxleyi*	**17.2**	*Emiliania huxleyi*	**0.41**
	Dinobryon spp.	**16.2**	*Meringosphaera mediterranea*	**0.30**
	Prorocentrum gracile	**6.36**	*Prorocentrum gracile*	0.21
	Meringosphaera mediterranea	**5.11**	*Diploneis crabro*	0.17
	Diploneis crabro	**4.91**	*Dinobryon* spp.	0.12
	Protoperidinium spp.	**2.33**	*Protoperidinium* spp.	0.12
	Chaetoceros simplex	**1.16**	*Chaetoceros simplex*	0.07
	Calciosolenia murrayi	**1.01**	*Calciosolenia murrayi*	0.05
XV 	*Cerataulina pelagica*	**20.7**	*Cerataulina pelagica*	**0.65**
	Leptocylindrus danicus	**7.56**	*Guinardia flaccida*	**0.26**
	Guinardia flaccida	**3.12**	*Tripos furca*	0.19

Table 4. *Cont.*

Cluster	Taxon (Ranked by Xproj)	Xproj	Taxon (Ranked by IndVal)	IndVal
XVI	*Cylindrotheca closterium*	**30.7**	*Cylindrotheca closterium*	0.53
	Calciosolenia murrayi	**11.9**	*Calciosolenia murrayi*	0.26
	Pleurosigma normanii	**9.42**	*Pleurosigma normanii*	0.26
	Nitzschia longissima	**6.55**	*Nitzschia longissima*	0.18
	Thalassionema nitzschioides	**5.11**	*Ophiaster hydroideus*	0.14
	Ophiaster hydroideus	**3.36**	*Thalassionema nitzschioides*	0.14
	Calciosolenia brasiliensis	**2.62**	*Tripos fusus*	0.09
	Diploneis crabro	**2.56**	*Calciosolenia brasiliensis*	0.09
	Tripos fusus	**1.80**	*Diploneis crabro*	0.09
	Diatoms non ident.	**1.55**	*Syracosphaera pulchra*	0.08
	Guinardia flaccida	**1.41**	*Nitzschia* spp.	0.08
	Syracosphaera pulchra	**1.20**	*Meringosphaera mediterranea*	0.07
	Nitzschia spp.	**1.17**	Diatoms non ident.	0.06
	Asterionellopsis glacialis	**1.10**	*Guinardia striata*	0.06
	Chaetoceros curvisetus	**1.07**	*Gyrodinium* spp.	0.05
XVII	*Pseudo-nitzschia seriata* gr.	**15.8**	*Pseudo-nitzschia seriata* gr.	**0.62**
	Protoperidinium spp.	**5.80**	*Protoperidinium* spp.	**0.29**
	Asterionellopsis glacialis	**4.03**	*Thalassiosira* spp.	**0.25**
	Nitzschia longissima	**3.72**	*Guinardia striata*	0.13
	Pleurosigma normanii	**2.98**	*Syracosphaera pulchra*	0.10
	Thalassiosira spp.	**2.57**	*Dactyliosolen fragilissimus*	0.09
	Cylindrotheca closterium	**2.10**	*Nitzschia longissima*	0.09
	Prorocentrum triestinum	**2.00**	*Pleurosigma normanii*	0.09
	Calciosolenia murrayi	**1.57**	*Nitzschia* spp.	0.09
	Diploneis crabro	**1.35**	*Calciosolenia murrayi*	0.08
	Guinardia striata	**1.27**	*Chaetoceros* spp.	0.08
	Oxytoxum spp.	**1.11**	*Asterionellopsis glacialis*	0.07
XVIII	*Bacteriastrum delicatulum*	**21.4**	*Bacteriastrum delicatulum*	**0.67**
	Prorocentrum micans	**4.60**	Euglenophyceae	**0.26**
	Prorocentrum compressum	**2.85**	*Heterocapsa* gr.	0.24
	Heterocapsa gr.	**2.52**	*Prorocentrum balticum*	0.18
	Euglenophyceae	**2.30**	*Prorocentrum micans*	0.17
	Prorocentrum balticum	**2.21**	*Prorocentrum triestinum*	0.13
	Prorocentrum gracile	**1.90**	*Prorocentrum compressum*	0.12
	Prorocentrum triestinum	**1.74**	*Scrippsiella trochoidea*	0.11
	Oxytoxum spp.	**1.28**	*Cyclotella* spp.	0.10
	Scrippsiella trochoidea	**1.04**	Chlorophyceae	0.10

During winter, the most important clusters were Cluster VII, strongly associated with the coccolithophore *Emiliania huxleyi*, and Cluster IX associated with the chrysophycean species *Meringosphaera mediterranea*. Cluster IX was also scattered in the other seasons.

In spring, the main clusters were IV and XVIII. From 2005 to 2012, late spring was characterized by Cluster IV associated with the diatoms *Cyclotella spp.* and *C. simplex* and the dinoflagellates *Prorocentrum gracile*, *Prorocentrum cordatum* and the *Heterocapsa* group. In 2009 and 2013, another late spring cluster (Cluster XVIII) formed, most strongly associated with the diatom *Bacteriastrum delicatulum*, as well as dinoflagellates from the genus *Prorocentrum*, the coccolitophore *Calyptrosphaera oblonga*, and undetermined euglenophytes.

The most important summer cluster, typical mainly of July during 2005–2012, was Cluster XI, which was also sporadically present in other seasons, especially in late autumn. This cluster was associated with the diatoms *Chaetoceros* spp. and *Proboscia alata*. From 2010, another summer cluster (Cluster II) appeared, characterized by a diverse community of diatoms (e.g., *Guinardia flaccida*, *Dactyliosolen fragilissimus* and undetermined species), dinoflagellates (e.g., *Prorocentrum triestinum, P. gracile*) and chlorophytes.

Autumn months were the most varied and richest for the occurrence of various clusters. Besides scattered occurrences of Cluster IX and Cluster XI, this season was charac-

terized by three clusters: Cluster XII, Cluster III and Cluster XVII. Cluster XII was most typical in October and November and was associated with undetermined coccolithophores and various diatoms such as *Guinardia striata*, *Hemiaulus hauckii* and *D. fragilissimus*. From 2010, the Cluster III appeared, associated with coccolithophores *Calciosolenia murrayi* and *Syracosphaera pulchra,* diatoms from the *Pseudo-nitzschia delicatissima* group and some dinoflagellates. Finally, Cluster XVII was associated with diatoms such as species from *Pseudo-nitzschia seriata* group, *Asterionellopsis glacialis*, *Nitzschia longissima* and *Pleurosigma normanii*.

A correlation of 0.87 with p-value = 0.001 was obtained between the two ordination indices (Xproj and IndVal).

4. Discussion

4.1. Review of the Critical Steps of Analysis

4.1.1. Taxa Selection, Ordination and Clustering

Plankton communities have complex and dynamic structure [40]. To unveil the temporal patterns of these communities it is often necessary to reduce the number of variates (i.e., taxa); however, preserving a representative amount of information is key when choosing different methods of taxa selection. Our results show that Total Inertia (TI), which was used as an indicator of the total amount of information present in the dataset [36] was higher when FREVE was used compared to the selection based on frequency of appearance. In other words, FREVE was more effective in preserving information (Figure 4). In the "real life" scenario of the GoT coastal ecosystem, the four distribution types we postulate can be interpreted as follows: Type 1 taxa can be considered occasional, e.g., only occasionally driven by currents or otherwise introduced; Type 2 taxa are also infrequent but may reproduce and bloom under favourable conditions; Type 3 taxa are common and bloom regularly; and Type 4 taxa are commonly present but always with low abundances. For the interpretation of phenology of the phytoplankton typical of the basin, the taxa of types 2 and 3 seemed to be more interesting because they contribute to the seasonal dynamics more than taxa of types 1 and 4. However, because taxa of type 4 are common, helping to define the baseline of the community and tending to structure the abundance matrix, the objective was then to eliminate only taxa of type 1 from the dataset. Taxa of types 1 and 4 share a common feature: in the samples in which they were present, they exhibited constant or quasi-constant abundance and are therefore found near or on the log distribution (Figure 3A). Taxa of types 2 and 3 also share a common feature: they exhibited fluctuating abundance in the samples in which they were present, so that the majority of abundance is concentrated in only a fraction of the samples. Considering again the FREVE index, instead of evenness we could have chosen dominance indices (like Simpson), which are invariant across the number of classes [41] but we were more interested in evaluating the space occupied by the classes (samples) over the disposable space (the whole time series). Moreover, Pielou's characteristic of variation between 0 and 1 made it ideal for coupling with frequency compared to other entropy indices.

The differences between temporal maps obtained by PCA (Figure 6) and CA (Figure 7) cannot be associated only with the selected number of clusters in which to divide the matrix (6 clusters vs. 4 clusters or 18 clusters) or the different taxa selection methods used in the two protocols, but they mostly express a qualitative difference between the two types of analysis. Legendre and Legendre [36] argue that Euclidean distance on which PCA relies is not a good distance method for studying species frequency tables because of the double-zero problem. We detected an increase in diversity over the years using Pielou's evenness index (data not shown). This increase could be due to a real increase in diversity or to better taxonomical skills of the expert who analysed the samples. Regardless of the reason, we observed a concentration of presences inside fewer taxa in the first years of the data series, which also means a high number of zero or near zero abundance values for other taxa. The large cluster covering the first years (2005–2006) of the series (see Cluster

I in Figure 6) with no seasonal structure and no indicative taxa was indeed the dataset region that contained most of the zeros.

With the use of a more adequate ordination method, i.e., CA that resulted in temporal maps in which diverse seasonal clusters were observed throughout the data series (Figure 7), we also confirmed the existence of seasonal patterns of phytoplankton community during the first years. The seasonality of the clusters was found in both partition levels (4 and 18) for this first part of the temporal series. The main difference between the two was that the 4-clustered and 18-clustered partitioning levels allowed us to observe seasonal patterns at two different degrees of complexity: a baseline structure of the phytoplankton community in the Gulf of Trieste (Figure 7, left) and a more detailed one (Figure 7, right), which will be further discussed.

As regards the clustering algorithm, we consider the method based on k-means clustering better than the method based on Bayes' rule proposed in the original protocol. Bayes' rule forces the clusters to achieve an equilibrium between dimension and homogeneity, but this would come at the cost of cutting off part of the complexity of the matrix. With the k-means method, the clusters are not weighted according to their relative dimension but only based on the fraction of variance that they explain. Thus, when using the k-means method, blooming events can form small outlying clusters easier than using Bayes' rule. Moreover, the k-means algorithm dictates the use of multiple random starts to avoid local maxima in the objective function, a problem that is not tackled in the original protocol. Finally, the use of the Calinski pseudo-F and Ratkowsky indices, which are both based on the analysis of variance, is preferable to the use of the probability vector $P_{max}(k)$ proposed in the original protocol. This is for the same reason that the k-means method is preferable to Bayes' rule.

4.1.2. Indicative Taxa

Characterization of the indicative species of clusters using the IndVal index resulted in some taxa that were indicative of more than one cluster. Examples include *Cyclotella* sp. in Clusters IV and V of the original protocol (IndVal 0.29 and 0.46, Table 2) and *Emiliania huxleyi* in Clusters I, II and IV of the modified protocol (IndVal 0.26, 0.29 and 0.25, Table 3). The fact that "IndVal removes any effect of the number of the sites in the various clusters and also differences in abundance among sites belonging to the cluster" [34] was in some cases a serious flaw of the method. Both the taxa in the example (*Cyclotella* sp. and *Emiliania huxleyi*) are very common in the phytoplankton community and consequently the fidelity term (Equation (1)) of the IndVal formula (Equation (3)) is, for many of the possible cluster, close to 1. The other term (Equation (2)), known as specificity, should counterbalance this by giving more weight to clusters that contain most of the average taxon's abundance. However, it is possible that the average abundance is quasi-constant between clusters, in particular when the clusters describe taxa distribution sub-optimally, which is often the case when the number of taxa is high while the number of clusters is low [36].

Another example of an IndVal computational flaw is given by the single-sample Cluster III (Table 3) and the corresponding Cluster V (Table 4). Those two clusters belong to two different partitioning levels of the same taxa selection (modified protocol) and were both indicative only for February 2017. However, they exhibit different species selection with high IndVal values. While more than 20 taxa were indicative of Cluster III of the 4-clustered partition, only two were indicative of Cluster V of the 18-clustered partition. This is explained by the way in which the IndVal index is calculated in both cases. The fidelity term for the taxa present in February 2017 is, in both cases, equal to 1 (Equation (1)). Instead, the denominator NI_{+j} (Equation (2)) of the specificity term varies since it is the sum of the mean abundances of all clusters [34]. With further refining in the 18-clustered partition and the division of big clusters from the 4-clustered partition into smaller clusters, the abundance peaks of more taxa were better defined by some of these smaller clusters. Consequently, the denominator NI_{+j} (Equation (2)) increased, the specificity term dropped,

and many taxa were no longer defined as indicative for February 2017, despite the fact that the cluster remained unchanged.

The likelihood ratio method (Xproj—Appendix B) served as a supplementary estimator of indicative taxa for a cluster because the arbitrary threshold (0.25) of the IndVal index was ambiguous. K-means clustering minimizes the within-cluster variance [36] which being expressed in χ^2 metric tends to separate similarly deviant samples from average profile samples [36]. In this way, the taxa with higher likelihood ratios are those most responsible for the formation of deviant clusters, while taxa with likelihood values close to zero are responsible for large average clusters. The likelihood ratios (Observed/Expected) present an advantage because they are not constrained between 0 and 1, which allows more precise identification of the taxa that are most important for the definition of a cluster. Below zero Xproj values indicate taxa that were present less than expected in a cluster and they also play a role in the definition of clusters. The single-sampled cluster of February 2017 can again serve as a good example. Two diatom species, *Chaetoceros curivesetus* and *Leptocylindrus danicus,* had similarly high IndVal values for Cluster III in 4-clustered partition (1 and 0.87, respectively, Table 3), which reveals that both are strongly indicative of this cluster. On the other hand, Xproj results show a substantial difference between the importances of the two species: in February 2017, the abundance of *C. curivesetus* was more than 70 times higher than expected (Xproj 76.0), while it was just ten times higher than expected for *L. danicus* (Xproj 9.61). Another important advantage of (Xproj) values is that the value for a taxon does not change between the different n-clustered partitions as long the centroid of the cluster remains the same (e.g., Cluster III in Table 3 and Cluster V in Table 4). As stated in the definition of methods, the deviation values (Xproj) are dependent only on the centroid of a cluster, which in this case is the same for both clusters (Appendix B).

Although the two indexing systems (IndVal and Xproj) have organized the indicative taxa in a similar way (as shown by highly significant correlation), substantial advantages have emerged for Xproj suggesting it as a preferred option in defining indicative taxa.

In summary, from an analytical point of view, for a correct representation of the assemblages we recommend to use (i) non log-transformed data, (ii) a selection method that preserves the information (like FREVE), (iii) distances that are not sensitive to the double-zero problem (such as the chi-square distance), (iv) a clustering method that minimizes the variance within clusters (such as k-means), and (v) more indices to define indicative taxa (the pair IndVal and Xproj seems effective).

4.2. Phytoplankton Phenology in the Period 2005–2017

In the 4-clustered partition (Figure 7, left), the main distinction that can be made between clusters represent two phytoplankton communities which are known to occur under different environmental conditions in the Gulf of Trieste [40]. In fact, the largest Cluster I is indicative of a mixed community composed mainly of nanoflagellates, diatoms and coccolithophores, while the remaining clusters (II, III and IV) represent the period of the year when diatom abundances increase and dominate the community. This alternation between the dominance of different phytoplankton groups is typical of the Gulf of Trieste [5,20] and the wider basin of the northern Adriatic [21,22,42], where nonetheless nanoflagellates contribute up to three thirds of total phytoplankton abundance [40]. The fact that in Cluster I none of the taxa exceeded the threshold pre-set for Xproj is not surprising, since in this large cluster the taxa are close to their expected (average) profile. In this sense Cluster I represents the "baseline" of the phytoplankton community in the GoT.

Cluster II and Cluster III both describe winter diatoms outbursts. For Cluster II, the highest Xproj was calculated for *Skeletonema costatum* s.l., which was identified as one of the characteristic taxa of the winter period in the northern Adriatic [5,20,21,43]. Since the taxonomy of the genus *Skeletonema* has not been resolved yet for our samples, all individuals were treated as *S. costatum* s.l. Possibly, most of the individuals belonged to *Skeletonema marinoi*, which was identified in the northern Adriatic [44], but more cryptic

species could be present [43]. Cluster II appeared only in three years, suggesting a very scattered appearance of *Skeletonema* species. This is in line with the observations of Cerino et al., in 2019 [5] who signalled a decrease in abundance of *Skeletonema* in the GoT after 2013. Some species from the genus *Chaetoceros* are also typical of the winter period in the area [20]. In our analysis, this was the case for *C. simplex* in Cluster II and *C. curvisetus* in the single-sample Cluster III. *C. curvisetus* was probably pooled with *Chaetoceros* spp. when present in low abundances, but during its bloom in February 2017 it was identified at species level, which then formed a specific cluster.

Cluster IV that was characterised by the highest diatom diversity was roughly divided into three periods: early spring, summer (mainly July) and autumn. At this level of partitioning, Cluster IV signals the phenology of diatom blooms, which during the study period had two conspicuous peaks, in July and in autumn [17,40]. Interestingly, diatoms at the LTER station in the Italian part of the GoT showed a different phenology in recent years, where between the years 2013 and 2017 the late spring peak of diatoms became the main one during the year, replacing the late winter-early spring bloom of *Skeletonema* spp. [5]. This type of shift was not observed in our data series, indicating differences in environmental conditions that determine community structure at the scale of a few km.

The division of the Cluster IV by 18-clustered partition (Figure 7, right) not only into large clusters, such as clusters III, XI, XII, XVII and XVIII, but also some of the single-sample clusters, such as VI, X, XIII and XV, helped to detail the phenology of diatoms. Pennate diatoms of the genus *Pseudo-nitzschia*, which are often mentioned as community-forming in the northern Adriatic [5,42,43] were characteristic of two autumn clusters, namely, Cluster III and Cluster XVII. Although species of this genus can bloom during different times of the year, they are mainly typical of autumn and winter [45,46]. Specifically, species from genus *Pseudo-nitzschia*, in our study period, lacked the early spring bloom described in other areas of the Mediterranean Sea [47]. The prolonged presence of Cluster III in Autumn 2010 describes an unusually long and intense bloom of species belonging to the *P. delicatissima* group, observed that year throughout the GoT [5]. The presence of *P. delicatissima* was recorded also in other coastal areas of the Mediterranean and were associated to higher concentration of silicate and nitrate [48]. In our study, *Pseudo-nitzschia* species were determined only at the level of two groups, the *P. seriata* group and the *P. delicatissima* group, while a recent study helped to resolve the diversity of *Pseudo-nitzschia* species in the GoT through integrative taxonomy [45]. The difficulties associated with the identification of *Pseudo-nitzschia* species as well as other taxa such as *Chaetoceros* in routine monitoring constitute a significant drawback for phenology studies. In fact, the consequent divergence of results when considering entire complexes or single species produces uncertainty in the description of taxa niches and community assemblages [45]. The last broad autumn cluster in the 18-clustered partition was represented by Cluster XII, which was characterised by undetermined coccolithophores in addition to large diatoms such as *Guinardia striata* and *Hemiaulus hauckii*. Similar co-dominance of large diatoms and coccolithophores during autumn has been reported by other studies carried out in the same area [20,21]. Finally, two single-sample clusters occurred twice in the month of December; Cluster X in 2009 with a peak of the diatom *Asterionellopsis glacialis*, and Cluster VI in 2013 with *Lauderia annulata*, which otherwise occurs rarely and in low numbers. Both species are considered as important community components in the western part of the northern Adriatic in the autumn and winter period [21,22].

Diatom dominance in autumn months was succeeded by winter Cluster VII, which emerged from Cluster I, i.e., the "baseline" community of the 4-clustered partition. Cluster VII was associated with the coccolithophores *E. huxleyi* and *Ophiaster hydroideus* and the diatom *Diploneis crabro*, all species also found elsewhere in the northern Adriatic in the autumn-winter period [5,21,42]. *E. huxleyi*, a cosmopolitan species that often forms blooms in the worlds' oceans [49], was found in most of samples of our time series but was the most abundant during winter. The only time when this cluster diverged from winter phenology was in May 2014, when a peculiar increase of *E. huxleyi* was also reported in

the neighbouring area [5]. Occasional blooms outside the winter period were described also in other areas of the Mediterranean [47], while a decrease in the winter blooms of *E. huxleyi* after 2002 was observed in the southern part of the northern Adriatic [22]. The "*Skeletonema*" Cluster I that succeeded Cluster VII during 2005, 2011 and 2012, was the same in both partitions.

Late winter and early spring were mostly defined by the remnants of the largest cluster in the 4-clustered partition, namely Cluster IX, which in this case consisted of only one indicative species (*Meringosphaera mediterranea*). The taxa with a higher-than-expected abundance (data not shown in Table 4) were similar to those of Cluster I in the 4-clustered partition, which means that Cluster IX can be interpreted as a mixed community with the dominance of nanoflagellates, which have a known spring peak in the GoT [40]. The fact that this cluster was less present in 2011 and 2012 than in other years seems to agree with the results of Cerino et al., 2019 [5], who described a low nanoflagellate density at the Italian LTER station in those two years.

Spring clusters Cluster IV and XVIII followed Cluster IX until 2013, thus signalling the late spring peak of dinoflagellates in the GoT [5,40]. Different species of the genus *Prorocentrum* and *Heterocapsa* group, indicative of these clusters are characteristic spring species in the northern Adriatic [21,22,42]. Similar to other areas of the Mediterranean [50], the *Bacteriastrum* genus was also found in association with dinoflagellates (Cluster XVIII). In mid-summer, Cluster XI emerged, especially in the first part of the time series, dominated by diatoms *Chaetoceros* spp. and *Proboscia alata*. This July peak of diatoms became a recurrent feature after the shift in the plankton community observed in 2002/2003 [17]. These summer blooms were tentatively linked to higher precipitations in June and July. A similar assemblage developed also in colder months when substantial precipitation is more common. The co-occurrence of *P. alata* with taxa from the genus *Chaetoceros* during summer has also been described in other coastal areas of the Mediterranean [51]. Both taxa representing the Cluster XI have been described to produce resting stages [52]. In addition to the consideration that they might bloom in response to summer precipitation, the recurrent July occurrence of Cluster XI could also be explained as a diapause phenomenon [53], e.g., germination of dormant spores after the summer irradiance peak. Another summer cluster (Cluster II) composed of diatoms, dinoflagellates and chlorophytes emerged alongside Cluster XI in 2010, eventually replacing the latter from 2013 onwards.

The diatom spring bloom was not constant and was short living, while the autumn bloom was usually longer and diverse. Dinoflagellates increased typically at the end of spring and in the summer, usually co-occurring with diatoms. The typical mixed community of the GoT, composed mainly of nano-sized phytoflagellates, was usually dominant the first part of the year, while coccolithophores were mostly present during the second part of the year with the exception of typically winter taxa. Considering the whole time series, we noticed a change in the middle part of the series (between year 2010 and 2013). In fact, in autumn, the importance of clusters associated with nanoflagellates decreased, while clusters associated with diatoms increased in number (see Figure 7, right). Brush et al., (2021) discuss these changes in relation to high inter-annual variability and alternation of drought periods with periods of higher freshwater discharge, which is connected with climate change at mesoscale in the northern Adriatic. It is possible that precipitation variability was also linked to the scattered presence in the summer of clusters associated with diatoms after 2013. Moreover, the occurrence of small clusters increased in number towards the end of the series. In fact, four of the eight existing single-sample clusters were present during the last two years 2016–2017 (Figure 7, right). This phenomenon could be explained by increased instability in community structure, possibly related to increased environmental disorder [22]. The results seem to be consistent with the irregularities expected for North Adriatic, which has been described as one of the less seasonal areas of the Mediterranean and more prone to irregular and interannual patterns [6].

The presence of resting stages has been described for many diatom species and for species in many other phytoplankton groups [52,53]. This reproductive strategy has been linked to seasonal succession in diatoms and to mechanisms of resilience in phytoplankton in general [53,54]. When considering the 4-clustered partition, Margalef's concept seems to be suitable to explain the succession of the two main assemblages (Cluster I vs. Clusters II, III, and IV), with diatoms thriving in nutrient enriched waters [10]. However, considering the detailed structure of the assemblages in the 18-clustered partition, the succession model based on resting stages may be better suited to reflect the dynamics for some taxa, for example, the indicative taxa of Cluster XI. This model is considered crucial for the demography of phytoplankton in confined coastal environments [53] and could represent a piece of the mosaic in explaining Hutchinson's plankton paradox [1].

As expected for coastal environments, the average lifetime of an assemblage was short, i.e., 2–4 months [16]; in fact, for the 4-clustered partition a cluster lasted 2.3 months on average (variance = 3.8 months), while it was shorter for the 18-clustered partition (mean = 1.4 months, variance = 0.68 months). January, March, April, May, August, September, and October were equal in terms of number of typical assemblages, and the most stable among all, since, during the thirteen years of the series, there were at most four different clusters for each of them (Figure 7, right). For August, September, and October, the assemblages sequence appeared to be more cyclical inter-annually, while for the rest of them it seems that a dominant cluster alternated sporadically with others. In general, the fact that a cluster appeared several times in the same month or season could signal recurring environmental conditions and underline the link between phytoplankton phenology and seasonality. This seems to be particularly true for January, March, April, and May. In these months, our data did not describe major changes possibly indicating stability either climatically, in connection with drivers such as river discharges, nutrients, etc., or other factors (physical properties, biotic interactions). In August, September, and October these conditions possibly alternated from year to year. For late autumn clusters, seasonality was harder to depict. Nonetheless, high diatom diversity and lack of a repetitive pattern of clusters can be considered a distinctive mark for this part of the year in the GoT. The variability of clusters became higher in two directions. On the one hand, the phytoplankton community became increasingly unstable from the beginning to the end of the time series. On the other, the second part of the year was more prone to changes in terms of typical assemblages following either cyclical or complex non-repetitive patterns, while the first part of the year was generally more stable.

5. Conclusions

The aim of our study was to analyse the phytoplankton community of the Gulf of Trieste and identify specific patterns of seasonal occurrence, which we assumed to be variable in time, thus mirroring variable environmental conditions [40]. We searched for characteristic bloom taxa, specific seasonal assemblages, and their variability in time. It was critical to use appropriate methodology for analysing such a complex dataset so to avoid losing important information. By modifying the original protocol, we approached a more realistic seasonal pattern.

The phytoplankton community at the Slovenian LTER station between years 2005 and 2017 showed a complex seasonal pattern. Some taxa maintained their phenology throughout the whole series and represented a more stable part of the phytoplankton community, e.g., winter and spring taxa. On the other hand, a high diversity of clusters and indicative taxa observed in autumn may indicate high variability of environmental conditions during this part of the year and/or higher interspecies competition for resources.

The occurrence of small clusters towards the end of the series reduced the predictability of phytoplankton phenology. A switch from more predictive to more irregular phytoplankton community dynamics was observed recently not only in the GoT but also in the entire northern Adriatic [22,55], probably triggered by climatic and hydrological drivers at mesoscale.

Author Contributions: Conceptualization, I.V. and J.F.; Data curation, I.V. and J.F.; Formal analysis, I.V.; Methodology, I.V.; Supervision, P.M. and J.F.; Writing—original draft, I.V.; Writing—review and editing, I.V., P.M. and J.F. All authors have read and agreed to the published version of the manuscript.

Funding: This research was funded by Slovenian Research Agency (ARRS), grant number P1-0237 and by the ARRS program for young researcher 51986.

Data Availability Statement: Phytoplankton data originates from the national monitoring program financed by the Slovenian Environment Agency of the Ministry of Environment and Spatial Planning.

Acknowledgments: Authors thank Milijan Šiško for microscopic analysis.

Conflicts of Interest: The authors declare no conflict of interest.

Appendix A

Table A1. List of R-packages and functions used in the analysis.

Package	Functions	Goal
vegan [56]	diversity	Pielou λ
ade4 [57]	dagnelie.test dudi.coa	Multinormality CA
cluster [58]	agnes	Hierarchical classification
Morpho [59]	typprobClass	Probability from Mahalanobis
cclust [38]	clustIndex	Calinski & Ratkowsky
labdsv [60]	indval	IndVal indexes
ape [61]	mantel.randtest	Mantel test

Appendix B

The following proves that Xprojare the likelihood ratio of the centroids: given that X is our sample-taxa matrix r × c, and Q the derived matrix of chi-square components χ_{ij} [36,57] with:

$$Q = \sum \chi_{ij} = \sum \frac{\text{Observed}_{ij} - \text{Expected}_{ij}}{\sqrt{\text{Expected}_{ij}}} \quad \text{(A1)}$$

we can apply singular value decomposition on Q:

$$Q = \hat{U}WU' \quad \text{(A2)}$$

where $\hat{U}$ and U' are the orthogonal matrices and W is the diagonal matrix of singular values. The position of the rows r in CA space is equal to the matrix F (Equation (A3)) and the position of the columns c is equal to matrix V (Equation (A4)) with:

$$F = D_{(p_{i+})^{-1/2}}\hat{U}W \quad \text{(A3)}$$

$$V = D_{(p_{+j})^{-1/2}}U \quad \text{(A4)}$$

where $D_{(p_{i+})^{-1/2}}$ and $D_{(p_{+j})^{-1/2}}$ are diagonal matrices of square roots of row weights and column weights, respectively. Those weights are the row (i+) and column (+j) components

of the $\sqrt{\text{Expected}_{ij}}$ term of the Equation (A1). Then the projection (Xproj) of the rows (samples) in respect to the columns (taxa) is given by the projection of F onto V:

$$\begin{aligned} \text{Xproj} &= D_{(p_{i+})^{-1/2}} \hat{U} W \left(D_{(p_{+j})^{-1/2}} U\right)' \\ &= D_{(p_{i+})^{-1/2}} \hat{U} W U' D_{(p_{+j})^{-1/2}} \\ &= D_{(p_{i+})^{-1/2}} Q D_{(p_{+j})^{-1/2}} \\ &= \sum \frac{1}{\sqrt{\text{Expected}_{i+}}} \times \frac{\text{Observed}_{ij} - \text{Expected}_{ij}}{\sqrt{\text{Expected}_{ij}}} \times \frac{1}{\sqrt{\text{Expected}_{+j}}} \\ &= \frac{\text{Observed}_{ij}}{\text{Expected}_{ij}} - 1 \end{aligned} \tag{A5}$$

The matrix F used here corresponds to the centroid matrix when each sample is a cluster, so each row of F is a centroid. Instead, when we use the centroids matrix obtained from k-means clustering on F we obtain the likelihood ratios for the clusters' centroids.

References

1. Hutchinson, G.E. The Paradox of the Plankton. *Am. Nat.* **1961**, *95*, 137–145.
2. Harding, L. Long-term trends in the distribution of phytoplankton in Chesapeake Bay: Roles of light, nutrients and streamflow. *Mar. Ecol. Prog. Ser.* **1994**, *104*, 267–291. [CrossRef]
3. Malej, A.; Mozetič, P.; Malačič, V.; Turk, V. Response of Summer Phytoplankton to Episodic Meteorological Events (Gulf of Trieste, Adriatic Sea). *Mar. Ecol.* **1997**, *18*, 273–288. [CrossRef]
4. Mozetič, P.; Fonda Umani, S.; Cataletto, B.; Malej, A. Seasonal and inter-annual plankton variability in the Gulf of Trieste (northern Adriatic). *J. Mar. Sci.* **1998**, *55*, 711–722. [CrossRef]
5. Cerino, F.; Fornasaro, D.; Kralj, M.; Giani, M.; Cabrini, M. Phytoplankton temporal dynamics in the coastal waters of the north-eastern Adriatic Sea (Mediterranean Sea) from 2010 to 2017. *Nat. Conserv.* **2019**, *34*, 343–372. [CrossRef]
6. Salgado-Hernanz, P.M.; Racault, M.F.; Font-Muñoz, J.S.; Basterretxea, G. Trends in phytoplankton phenology in the Mediterranean Sea based on ocean-colour remote sensing. *Remote Sens. Environ.* **2019**, *221*, 50–64. [CrossRef]
7. Hutchinson, G.E. Ecological Aspects of Succession in Natural Populations. *Am. Nat.* **1941**, *75*, 406–418. [CrossRef]
8. Huisman, J.; Weissing, F.J. Biodiversity of plankton by species oscillation and chaos. *Nature* **1999**, *402*, 407–410. [CrossRef]
9. Crawley, M.J. Plant population dynamics. In *Theoretical Ecology, Principles and Application*; May, R., McLean, A., Eds.; Oxford University Press: Oxford, UK, 2007; Chapter 6.
10. Margalef, R. Life-forms of phytoplankton as survival alternatives in an unstable environment. *Oceanol. Acta* **1978**, *1*, 493–509.
11. Kemp, A.E.S.; Villareal, T.A. The case of the diatoms and the muddled mandalas: Time to recognize diatom adaptations to stratified waters. *Prog. Oceanogr.* **2018**, *167*, 138–149. [CrossRef]
12. Ptacnik, R.; Solimini, A.G.; Andersen, T.; Tamminen, T.; Brettum, P.; Lepistö, L.; Willén, E.; Rekolainen, S. Diversity predicts stability and resource use efficiency in natural phytoplankton communities. *Proc. Natl. Acad. Sci. USA* **2008**, *105*, 5134–5138. [CrossRef] [PubMed]
13. Vallina, S.M.; Follows, M.J.; Dutkiewicz, S.; Montoya, J.M.; Cermeno, P.; Loreau, M. Global relationship between phytoplankton diversity and productivity in the ocean. *Nat. Commun.* **2014**, *5*, 4299. [CrossRef] [PubMed]
14. Clayton, S.; Dutkiewicz, S.; Jahn, O.; Follows, M.J. Dispersal, eddies, and the diversity of marine phytoplankton. *Limnol. Oceanogr. Fluids Environ.* **2013**, *3*, 182–197. [CrossRef]
15. Cloern, J.E.; Jassby, A.D. Patterns and scales of phytoplankton variability in estuarine-coastal ecosystem. *Estuar. Coasts* **2010**, *33*, 230–241. [CrossRef]
16. Winder, M.; Cloern, J.E. The annual cycles of phytoplankton biomass. *Philos. Trans. R. Soc.* **2010**, *365*, 3215–3226. [CrossRef]
17. Mozetič, P.; Francé, J.; Kogovšek, T.; Talaber, I.; Malej, A. Plankton trends and community changes in a coastal sea (northern Adriatic): Bottom-up vs. top-down control in relation to environmental drivers. *Estuar. Coast. Shelf Sci.* **2012**, *115*, 138–148. [CrossRef]
18. Malej, A.; Mozetič, P.; Malačič, V.; Terzić, S.; Ahel, M. Phytoplankton responses to freshwater inputs in a small semi-enclosed gulf (Gulf of Trieste, Adriatic Sea). *Mar. Ecol. Prog. Ser.* **1995**, *120*, 111–121. [CrossRef]
19. Mozetič, P.; Solidoro, C.; Cossarini, G.; Socal, G.; Precali, R.; Francé, J.; Bianchi, F.; De Vittor, C.; Smodlaka, N.; Fonda Umani, S. Recent Trends Towards Oligotrophication of the Northern Adriatic: Evidence from Chlorophyll a Time Series. *Estuar. Coasts* **2010**, *33*, 362–375. [CrossRef]
20. Cabrini, M.; Fornasaro, D.; Cossarini, G.; Lipizer, M.; Virgilio, D. Phytoplankton temporal changes in a coastal northern Adriatic site during the last 25 years. *Estuar. Coast. Shelf Sci.* **2012**, *115*, 113–124. [CrossRef]
21. Aubry, F.B.; Cossarini, G.; Acri, F.; Bastianini, M.; Bianchi, F.; Camatti, E.; De Lazzari, A.; Pugnetti, A.; Solidoro, C.; Socal, G. Plankton communities in the northern Adriatic Sea: Patterns and changes over the last 30 years. *Estuar. Coast. Shelf Sci.* **2012**, *115*, 125–137. [CrossRef]

22. Totti, C.; Romagnoli, T.; Accoroni, S.; Coluccelli, A.; Pellegrini, M.; Campanelli, A.; Grilli, F.; Marini, M. Phytoplankton communities in the northwestern Adriatic Sea: Interdecadal variability over a 30-years period (1988–2016) and relationships with meteoclimatic drivers. *J. Mar. Syst.* **2019**, *193*, 137–153. [CrossRef]
23. Souissi, S.; Ibanez, F.; Hamadou, R.B.; Boucher, J.; Cathelineau, A.C.; Blanchard, F.; Poulard, J.-C. A new multivariate mapping method for studying species assemblages and their habitats: Example using bottom trawl surveys in the Bay of Biscay (France). *Sarsia* **2001**, *86*, 527–542. [CrossRef]
24. Anneville, O.; Souissi, S.; Ibanez, F.; Ginot, V.; Druart, J.C.; Angeli, N. Temporal mapping of phytoplankton assemblages in Lake Geneva: Annual and interannual changes in their patterns of succession. *Limnol. Oceanogr.* **2002**, *47*, 1355–1366. [CrossRef]
25. Francé, J. Long-Term Structural Changes of the Phytoplankton Community of the Gulf of Trieste. PhD. Thesis, University of Ljubljana, Ljubljana, Slovenia, 2009; p. 160.
26. Virgilio, D. Studio Della Comunità Microfitoplanctonica del Golfo di Trieste (Mare Adriatico Settentrionale): Utilizzo di una Serie Storica con Particolare Riguardo al Fenomeno dell'Introduzione di Taxa Alloctoni. Ph.D. Thesis, Università Degli Studi di Trieste, Trieste, Italy, 2008.
27. Pielou, E.C. *Mathematical Ecology*; John Wiley & Sons: Hoboken, NJ, USA, 1977.
28. Malačič, V.; Celio, M.; Čermelj, B.; Bussani, A.; Comici, C. Interannual evolution of seasonal thermohaline properties in the Gulf of Trieste (northern Adriatic) 1991–2003. *J. Geophys. Res.* **2006**, *111*. [CrossRef]
29. Talaber, I.; Francé, J.; Mozetič, P. How phytoplankton physiology and community structure adjust to physical forcing in a coastal ecosystem (northern Adriatic Sea). *Phycologia* **2014**, *53*, 74–85. [CrossRef]
30. Malačič, V.; Petelin, B. *Physical Oceanography of the Adriatic Sea: Past, Present, and Future*; Benoit, C., Miroslav, G., Pierre-Marie, P., Antonio, A., Eds.; Kluwer Academic Publishers: Berlin, Germany, 2001; pp. 167–181.
31. Utermöhl, H. Vervollkommung der quantitativen Phytoplankton-Methodik. *Mitt. Int. Ver. Theor. Ange Wandte Limnol.* **1958**, *9*, 1–38.
32. WoRMS, World Register of Marine Species. Available online: https://www.marinespecies.org (accessed on 26 July 2021).
33. Guiry, M.D.; Guiry, G.M. *AlgaeBase*; World-Wide Electronic Publication; National University of Ireland: Maynooth, Ireland, 2019.
34. Dufrene, M.; Legendre, P. Species Assemblages and Indicator Species: The Need for a Flexible Asymmetrical Approach. *Ecol. Monogr.* **1997**, *67*, 345. [CrossRef]
35. Alatalo, R.V. Problems in the Measurement of Evenness in Ecology. *Oikos* **1981**, *37*, 199–204. [CrossRef]
36. Legendre, P.; Legendre, L. *Numerical Ecology*, 3rd ed.; Elsevier: Amsterdam, The Netherlands, 1983; Volume 24.
37. Calinski, T.; Harabasz, J. A dendrite method for cluster analysis. *Commun. Stat. Theory Methods* **1974**, *3*, 1–27. [CrossRef]
38. Weingessel, A.; Dimitriadou, E.; Dolnicar, S. An examination of indexes for determining the number of clusters in binary data sets. *Psychometrika* **2002**, *67*, 137–159.
39. O'Hara, R.B.; Kotze, D.J. Do not log-transform count data. *Methods Ecol. Evol.* **2010**, *1*, 118–122. [CrossRef]
40. Brush, M.J.; Mozetič, P.; Francé, J.; Aubry, F.B.; Djakovac, T.; Faganeli, J.; Harris, L.A.; Niesen, M. *Phytoplankton Dynamics in a Changing Environment*; John Wiley & Sons: Hoboken, NJ, USA, 2021.
41. Hill, M.O. Diversity and Evenness: A Unifying Notation and Its Consequences. *Ecology* **1973**, *54*, 427–432. [CrossRef]
42. Godrijan, J.; Marić, D.; Tomažić, I.; Precali, R.; Pfannkuchen, M. Seasonal phytoplankton dynamics in the coastal waters of the north-eastern Adriatic Sea. *J. Sea Res.* **2013**, *77*, 32–44. [CrossRef]
43. Marić, D.; Kraus, R.; Godrijan, J.; Supić, N.; Djakovac, T.; Precali, R. Phytoplankton response to climatic and anthropogenic influences in the north-eastern Adriatic during the last four decades. *Estuar. Coast. Shelf Sci.* **2012**, *115*, 98–112. [CrossRef]
44. Sarno, D.; Kooistra, W.H.C.F.; Medlin, L.K.; Percopo, I.; Zingone, A. Diversity in the Genus Skeletonema (Bacillariophyceae). II. An Assessment of the Taxonomy Ofs. Costatum-Like Species with the Description of Four New Species. *J. Phycol.* **2005**, *41*, 151–176. [CrossRef]
45. Turk Dermastia, T.; Cerino, F.; Stankovic, D.; France, J.; Ramsak, A.; Znidaric Tusek, M.; Beran, A.; Natali, V.; Cabrini, M.; Mozetic, P. Ecological time series and integrative taxonomy unveil seasonality and diversity of the toxic diatom Pseudo-nitzschia H. Peragallo in the northern Adriatic Sea. *Harmful Algae* **2020**, *93*, 101773. [CrossRef]
46. Mozetič, P.; Cangini, M.; Francé, J.; Bastianini, M.; Aubry, F.B.; Bužančić, M.; Cabrini, M.; Cerino, F.; Čalić, M.; D'Adamo, R.; et al. Phytoplankton diversity in Adriatic ports: Lessons from the port baseline survey for the management of harmful algal species. *Mar. Pollut. Bull.* **2019**, *147*, 117–132. [CrossRef] [PubMed]
47. Ribera d'Alcala, M.; Conversano, F.; Corato, F.; Licandro, P.; Mangoni, O.; Marino, D.; Mazzochi, M.G.; Modigh, M.; Montresor, M.; Nardella, M.; et al. Seasonal patterns in plankton communities in a pluriannual time series at a coastal Mediterranean site (Gulf of Naples): An attempt to discern recurrences and trends. *Sci. Mar.* **2004**, *68*, 65–83. [CrossRef]
48. Varkitzi, I.; Markogianni, V.; Pantazi, M.; Pagou, K.; Pavlidou, A.; Dimitriou, E. Effect of river inputs on environmental status and potentially harmful phytoplankton in a coastal area of eastern Mediterranean (Maliakos Gulf, Greece). *Mediterr. Mar. Sci.* **2018**, *19*, 326–343. [CrossRef]
49. Tyrrell, T.; Merico, A. Emiliania huxleyi: Bloom observations and the conditions that induce them. In *Coccolithophores*; Thierstein, H.R., Young, J.R., Eds.; Springer: Berlin/Heidelberg, Germany, 2004.
50. Gomez, F. Annual microplankton cycles in Villefranche Bay, Ligurian Sea, NW Mediterranean. *J. Plankton Res.* **2003**, *25*, 323–339. [CrossRef]

51. Aktan, Y. Large-scale patterns in summer surface water phytoplankton (except picophytoplankton) in the Eastern Mediterranean. *Estuar. Coast. Shelf Sci.* **2011**, *91*, 551–558. [CrossRef]
52. McQuoid, M.R.; Hobson, L.A. Diatom resting stages. *J. Phycol.* **1996**, *32*, 889–902. [CrossRef]
53. Belmonte, G.; Rubino, F. Resting cysts from coastal marine plankton. In *Oceanography and Marine Biology: An Annual Review*; CRC Press: Boca Raton, FL, USA, 2019; Volume 57, pp. 1–88.
54. McQuoid, M.R.; Hobson, L.A. Importance of resting stages in diatom seasonal succession. *J. Phycol.* **1995**, *31*, 44–50. [CrossRef]
55. Grilli, F.; Accoroni, S.; Acri, F.; Bernardi Aubry, F.; Bergami, C.; Cabrini, M.; Campanelli, A.; Giani, M.; Guicciardi, S.; Marini, M.; et al. Seasonal and Interannual Trends of Oceanographic Parameters over 40 Years in the Northern Adriatic Sea in Relation to Nutrient Loadings Using the EMODnet Chemistry Data Portal. *Water* **2020**, *12*, 2280. [CrossRef]
56. Oksanen, J.; Blanchet, F.G.; Friendly, M.; Kindt, R.; Legendre, P.; McGlinn, D.; Minchin, P.R.; O'Hara, R.B.; Simpson, G.L.; Solymos, P.; et al. *Vegan: Community Ecology Package*; CRAN: Wien, Austria, 2018.
57. Dray, S.; Dufour, A. The ade4 Package: Implementing the Duality Diagram for Ecologists. *J. Stat. Softw.* **2007**, *22*, 1–20. [CrossRef]
58. Maechler, M.; Rousseeuw, P.; Struyf, A.; Hubert, M.; Hornik, K. *Cluster: Cluster Analysis Basics and Extensions*; CRAN: Wien, Austria, 2021.
59. Schlager, S. Morpho and Rvcg–Shape Analysis in {R}. In *Statistical Shape and Deformation Analysis*; Academic Press: Cambridge, MA, USA, 2017; pp. 217–256.
60. Roberts, D.W. *Labdsv: Ordination and Multivariate Analysis for Ecology*; CRAN: Wien, Austria, 2016.
61. Paradis, E.; Schliep, K. ape 5.0: An environment for modern phylogenetics and evolutionary analyses in {R}. *Bioinformatics* **2018**, *35*, 526–528. [CrossRef] [PubMed]

Chapter 3

Assemblages' Ecology

3.1 Paper: Exploring the Mesoscale Connectivity of Phytoplankton Periodic Assemblages' Succession in Northern Adriatic Pelagic Habitats

This chapter explores the role of atmosphere (winds, temperature, and precipitation) and hydrosphere (river discharge, water column stability and salinity) in the formation of niches of the phytoplankton assemblages described in the previous chapter. Using the same long-term phytoplankton time series from the LTER site in the Gulf of Trieste, we determine the relevant niche-forming parameters. The linear analysis was performed using Linear Discriminant Analysis (LDA) while the non-linear analysis was performed using Neural Networks (NNets). These models were subsequently applied to assess the connectivity of the basin at the mesoscale, by predicting and validating assemblages in the Gulf of Venice (100km apart). To observe the role of the environmental periodicity, the prediction variables were split in periodic and non-periodic components using Moran eigenvector maps (MEMs).

Key findings include:

I. Periodic vs. non-periodic influence: Periodicity significantly structures the assemblages, while non-periodic events introduce variability.

II. Connectivity and synchronization: The mesoscale connectivity between the Gulf of Trieste and Gulf of Venice is driven by cyclonic circulation patterns and stratification. Winter assemblages are synchronized due to uniform environmental conditions, while summer assemblages reflect local variability.

III. Predictive modeling: Neural networks allow effective prediction of assemblages, demonstrating that non-linear relationships between environment and phytoplankton enhance forecasting. However, predictions are challenged by extreme events.

IV. Ecological implications: Increasing environmental anomalies, such as extreme meteorological events, could disrupt periodicity, weaken mesoscale connectivity, and possibly alter trophic and biogeochemical cycles.

Finally, the observed inconsistency in the composition of the assemblage under given environmental conditions is discussed in the light of the latest ecological distribution models. The lumpy coexistence theory seems to be supported by the results found in this chapter.

Goals:

I. Determine the relationships between phytoplankton assemblages and environmental factors, their explanatory power and harmonic properties.

II. Use linear and non-linear modelling approaches to determine the spatial and temporal extent of these relationships in the broader context of the northern Adriatic.

Hypothesis:

I. Using assemblages as the appropriate level of community organization/assembly in the analyses, a model based on the regularity of mesoscale environmental drivers can predict the phytoplankton community structure and distribution in the Gulf of Trieste and at the broader scale of the northern Adriatic.

The goals are accomplished, and the hypothesis is confirmed by the results presented in this chapter.

The research work is presented in the following publication and is listed below:

Vascotto, I., Aubry, F. B., Bastianini, M., Mozetič, P., Finotto, S., & Francé, J. (2024). Exploring the mesoscale connectivity of phytoplankton periodic assemblages' succession in northern Adriatic pelagic habitats. Science of the Total Environment, 913, 169814.

Ivano Vascotto contributed to this paper as follows: conceptualization, formal analysis, methodology, writing – original draft, writing – review & editing, visualization.

Science of the Total Environment 913 (2024) 169814

Contents lists available at ScienceDirect

Science of the Total Environment

journal homepage: www.elsevier.com/locate/scitotenv

Exploring the mesoscale connectivity of phytoplankton periodic assemblages' succession in northern Adriatic pelagic habitats

Ivano Vascotto [a,b,*], Fabrizio Bernardi Aubry [c], Mauro Bastianini [c], Patricija Mozetič [b], Stefania Finotto [c], Janja Francé [b]

[a] Jozef Stefan International Postgraduate School, Jamova cesta 39, 1000 Ljubljana, Slovenia
[b] National Institute of Biology, Marine Biology Station Piran, Fornače 41, 6330 Piran, Slovenia
[c] National Research Council—Institute of Marine Sciences (CNR—ISMAR), Arsenale Tesa 104, Castello 2737/F, 30122 Venice, Italy

HIGHLIGHTS

- The response of marine phytoplankton to temporal changes in the environment was analysed.
- Assemblages were a working model for describing the relationship between the environment and phytoplankton.
- Periodicity explained a between 39 and 46 % of the variance in environmental parameters.
- We predicted phytoplankton assemblages with more significant IndVal values using environmental periodic components.
- The northern Adriatic Sea is a connected mesoscale habitat for the phytoplankton community during autumn and winter.

GRAPHICAL ABSTRACT

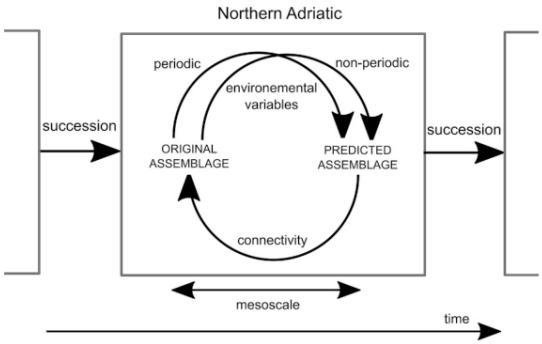

ARTICLE INFO

Editor: Julian Blasco

Keywords:
Phytoplankton
Assemblages
Northern Adriatic
Phenology

ABSTRACT

An appropriate model for phytoplankton distribution patterns is critical for understanding biogeochemical cycles and trophic interactions in the oceans and seas. Because phytoplankton dynamics in coastal waters are more complex due to shallow depth and proximity to land, more accurate models applied to the correct spatial and temporal scales are needed. Our study investigates the role of the atmosphere and hydrosphere in pelagic habitat by modelling phytoplankton assemblages at two Long Term Ecological Research sites in the northern Adriatic Sea using niche-forming environmental variables (wind, temperature, salinity, river discharge, rain, and water column stratification). To study the synchronization between the phytoplankton community and these environmental variables at the two LTER sites, we applied current linear and nonlinear numerical methods for ecological modelling. The aim was to use periodic and/or non-periodic properties of the environmental variables to classify the phytoplankton assemblages at one LTER site (Gulf of Trieste - Slovenia) and then predict them at another LTER site 100 km away (Gulf of Venice - Italy). We found that periodicity played a role in the explanatory and predictive power of the environmental variables and that it was more important than non-periodic events in defining the common structure of the two pelagic habitats. The non-linear classification functions of the neural networks further increased the predictive power of these variables. We observed partial synchronization of communities at the mesoscale and differences between the original and predicted assemblages under similar

* Corresponding author at: Jozef Stefan International Postgraduate School, Jamova cesta 39, 1000 Ljubljana, Slovenia.
E-mail address: ivano.vascotto@nib.si (I. Vascotto).

https://doi.org/10.1016/j.scitotenv.2023.169814
Received 11 May 2023; Received in revised form 22 December 2023; Accepted 29 December 2023
Available online 4 January 2024

environmental conditions. We conclude that mesoscale connectivity plays an important role in phytoplankton communities in the northern Adriatic. However, the loss of periodicity of niche-forming variables due to more frequent extreme meteorological and hydrological events could loosen these connections and affect the temporal succession of phytoplankton assemblages.

1. Introduction

Historically, ecology has addressed the causes of local population patterns, while biogeography has addressed large-scale patterns in the distribution of populations and the diversity of natural systems (Ricklefs and Jenkins, 2011). A theme common to both disciplines is the definition of temporal and spatial scales, from individual organisms and their lifespan activities (local scale) to population distributions (mesoscale and beyond). Ecological studies, in particular, typically address time spans ranging from generation times to longer population cycles (Jenkins and Ricklefs, 2011). The intermediate scales for temporal and spatial dimensions on which ecology and biogeography converge are considered relevant to population dynamics (Jenkins and Ricklefs, 2011). In the specific case of phytoplankton biogeography, it has been

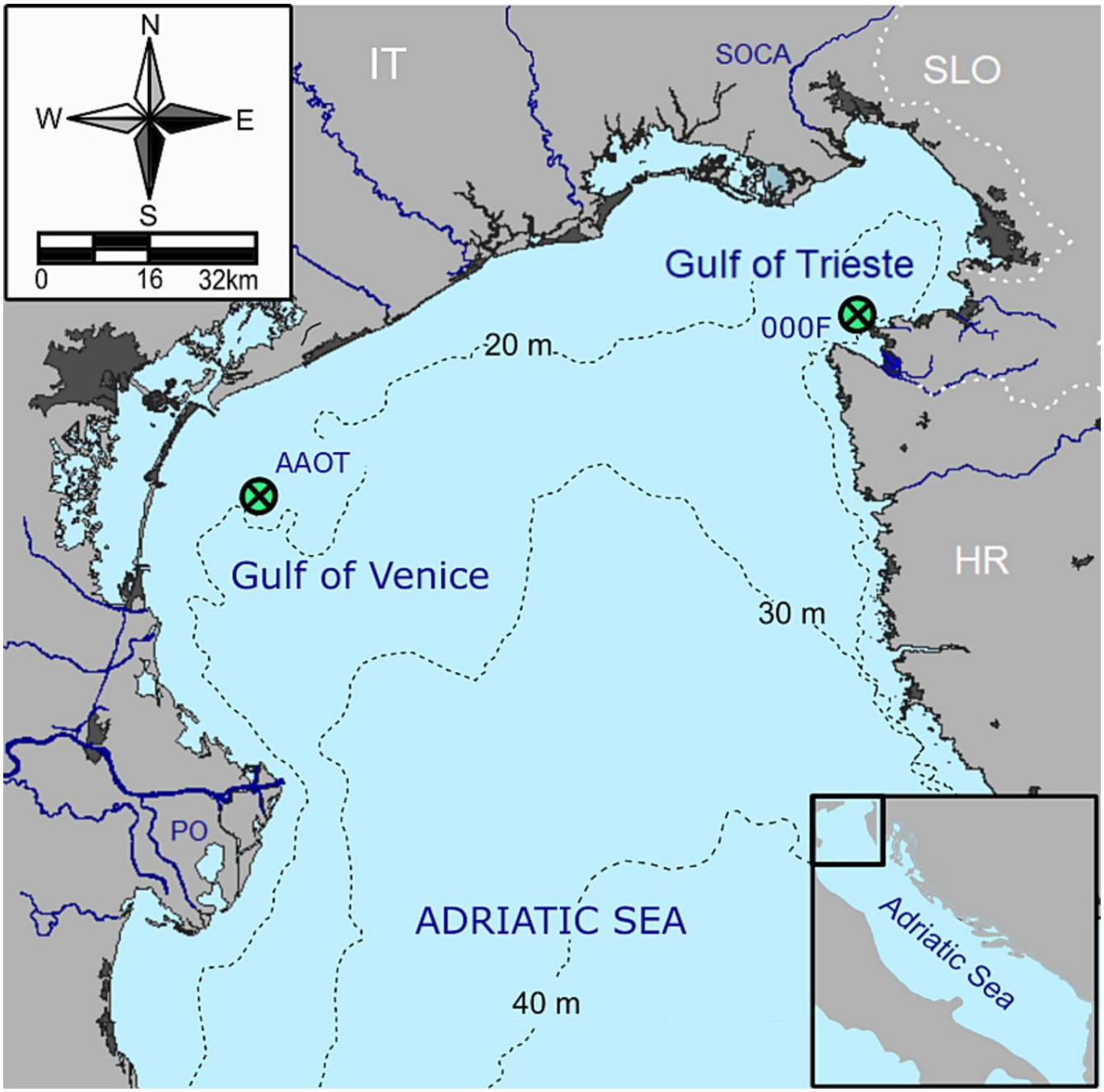

Fig. 1. Map of the study area. Both sampling stations, 000F and AAOT, represent respective LTER sites, i.e., Gulf of Trieste - Slovenia and Gulf of Venice – Italy IT12–001-M DEIMS).

shown that the distribution of this biological compartment is generally patchy and that the current inability of climate prediction models to resolve ecosystems at the mesoscale (1–500 km) is a major obstacle to understanding the marine ecosystem as a whole (Martin, 2003). Indeed, an appropriate model for phytoplankton distribution patterns is critical for understanding trophic interactions in the ocean, biogeochemical cycles, and more generally the ecology of the marine environment (Ptacnik et al., 2008; Vallina et al., 2014).

Environmental factors and top-down control by grazers shape phytoplankton dynamics, which experience greater complexity in coastal waters due to shallow water depth and proximity to land (Salgado-Hernanz et al., 2019). The intertwined relationship between space, time, environment, and phytoplankton suggests that it would be highly interesting to study variation in all these dimensions simultaneously to partition the known variation in community composition into proportions explained by factors related to dispersal, community succession, and environmental influences (Soininen, 2010). In general, the spectrum of dynamics of ecological systems is broad, encompassing all stages between regular cycles and chaotic oscillations (May, 1976; Stone, 1993). Platt and Denmann used spectral analysis to show that marine phytoplankton are distributed in space according to the Kolmogorov 5/3 dissipation rule (Platt and Denmann, 1975) while, temporally, patterns for phytoplankton range from stable annual variations in certain biomes to the absence of a repeating pattern in others (Cloern and Jassby, 2010).

Early attempts to link phytoplankton phenology and periodicity of environmental variables were made in the 1970s when Margalef introduced the concept of phytoplankton succession, the so-called mandala, in which the main stages of succession are determined by turbulence and nutrient availability (Margalef, 1978). Based on his work, Reynolds developed the concept of the phytoplankton year for lake communities, separating succession from simple seasonality and calling the cyclical behaviour of environmental factors "periodicity" (Reynolds, 1980). Within the framework of neutral ecology (Hubbel, 2005) and lumpy coexistence theory (Scheffer and van Nes, 2006), numerical simulations have shown that phytoplankton community richness and succession are affected by the nature of resource fluctuations (gradual or sudden) (Roelke and Spatharis, 2015a, 2015b). Recently, Sakavara et al. (2018) also showed that assemblage-like structures occur numerically in a wide range of spectral modes of resource fluctuations.

The important role that coastal ecosystem characteristics play in the distribution of phytoplankton taxa has been highlighted for several coastal ecosystems (Harding, 1994; Brush et al., 2021). The cyclical behaviour of seasonal phytoplankton dynamics is considered one of the most obvious features of this influence (Mozetič et al., 1998; Cerino et al., 2019; Salgado-Hernanz et al., 2019). In particular, in the nearshore environment, the usual pattern of environmental factors is a short period of time with fluctuations on the order of 2 to 4 months (Winder and Cloern, 2010). This rate of fluctuation has been recently described as characteristic as well for the phytoplankton community in the northern Adriatic in agreement with the expected fluctuation rate of environmental parameters (Vascotto et al., 2021). Cyclic patterns for phytoplankton communities have been recognized for this area of the Mediterranean (Bernardi Aubry et al., 2012), but these communities have also been described as sensitive to erratic behaviour of environmental forces (Malej et al., 1997). Partial phase synchronization together with chaotic dynamics is a feature of biological populations in extensive ecological systems where diffusive migration is possible (Blasius et al., 1999). The northern Adriatic can be considered such an ecological system, as it is located in the meteorological mesoscale region (Orlanski, 1975) and its waters are connected by the main cyclonic circulation of the Northern Adriatic (Poulain et al., 2001; Petelin et al., 2013). On the other hand, recent studies of marine ecosystems suggest that phytoplankton diversity varies strongly within meso- and submesoscale distances (10–100 km) and that large-scale environmental conditions have a relevant influence on assemblage formation (Levy et al., 2015; Levy et al., 2018; Francé et al., 2021).

As we have seen so far, there is a gap between the theoretical models for the role of the cyclicity of environmental conditions in shaping succession (Reynolds, 2006) and formation (Sakavara et al., 2018) of phytoplankton assemblages with examples from the field (Vascotto et al., 2021). Furthermore, the complexity of patterns in phytoplankton phenology (Cloern and Jassby, 2010) does not allow for simple conclusions about the behaviour of multivariable objects such as phytoplankton assemblages. Nevertheless, it is crucial for the modelling of phytoplankton patterns to investigate in more detail the relationships between phytoplankton assemblages and environmental factors, their explanatory power and their harmonic properties. Our working hypothesis is that a model based on the regularity of mesoscale environmental factors can predict the structure and temporal distribution of the phytoplankton community when assemblages are used as the level of community organisation/composition in the analyses.

At two sampling stations of the northern Adriatic LTER (Long-Term Ecological Research) sites in the Slovenian part of the Gulf of Trieste (GoT) and the Italian Gulf of Venice (GoV) (Fig. 1), the phytoplankton community has been actively sampled for decades. The sites are located 100 km apart, thus ideal to study the synchronization between the phytoplankton community and environmental factors, and the extent of these relationships at the mesoscale. Since cyclic, seasonal, and periodic patterns all belong to the family of autocorrelation patterns, Tobler's first law applies: *"Everything is related to everything else, but near things are more related than distant things"* (Tobler, 1970). The analysis of autocorrelation patterns has emerged as a spatial technique in geographic studies, but from the analytical point of view, the use of time instead of space as a dimension of interest is equivalent (Legendre and Legendre, 2012).

In this work, we have studied the importance of autocorrelative processes in the northern Adriatic from the point of view of environmental forces in the time domain. We used the periodic and non-periodic components of these forces to model the time series of the phytoplankton community in the GoT on the eastern side of the northern Adriatic. We then attempted to extend the predictive capacity of our model to the western side of the northern Adriatic (GoV) at the boundary of the mesoscale domain.

2. Material and methods

2.1. Study area

The northern Adriatic basin is defined as the area north of the 100-m isobath of the Adriatic Sea and represents the largest shelf area in the Mediterranean Sea (Gačic et al., 2001). This basin is under the influence of intense lateral (river discharge and southward transport) and surface (wind and air temperature) stresses (Poulain et al., 2001). The water column of the northern Adriatic is seasonally mixed and stratified (Poulain et al., 2001), and in many areas the euphotic zone exceeds the depth of the upper mixed layer for most of the year (Talaber et al., 2014). The northern Adriatic is under the influence of two main winds, the "Bora" and the "Jugo" (Scirocco), the first blowing from the northeast and the second from the southeast. Bora is a strong katabatic wind that affects the water column in two ways: mixing and cooling, while Jugo is a constant wind with maximum speed in the eastern part of the basin and has a chaotic effect on the current circulation in the GoT (Malačič and Petelin, 2001).

The Slovenian LTER station (Fig. 1: 000F; 45.54 N, 13.55 E; 22 m depth) is located at the southern entrance of the Gulf of Trieste (GoT), which is a shallow basin with an average depth of 21 m (Malačič et al., 2006). The Italian LTER station (Fig. 1: AAOT, 45.32 N, 12.50 E, 16 m depth) is located offshore of the Venice Lagoon in the Gulf of Venice (GoV). Both gulfs are under the influence of freshwater (Zhang et al., 2020): GoT is influenced by the Soča River (Malačič and Petelin, 2001) and occasionally by the Po River plume (Vilicic et al., 2013), while GoV

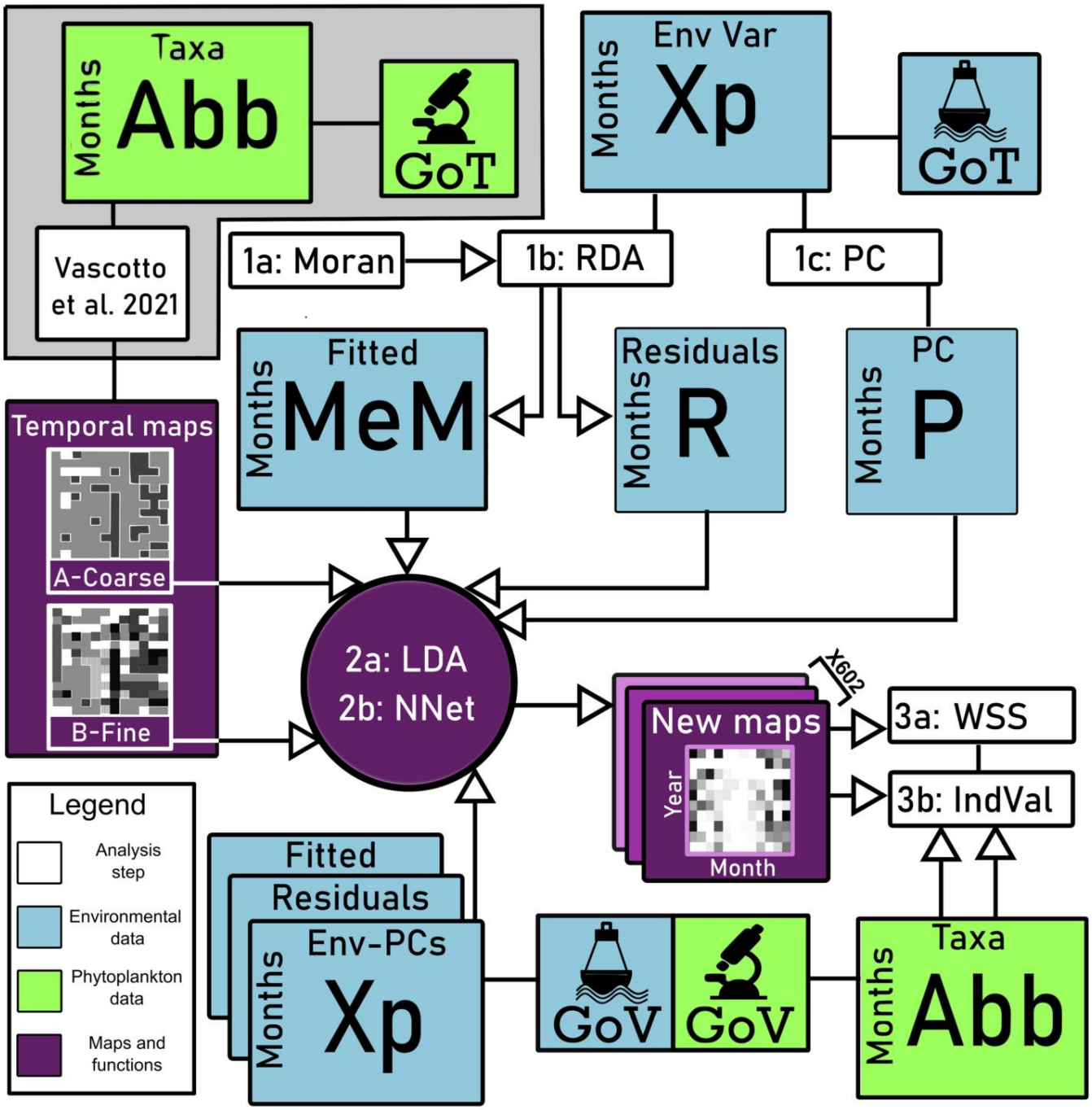

Fig. 2. Flowchart of the analysis. Each box represents either a data matrix, an analysis step, or the classification functions and temporal maps. In the boxes representing data matrices, the names of the variables and the names of the objects are given at the top and left of each box. In the boxes representing the analysis steps, the name of the analysis and the code used in the text are given to refer to it. In the upper left part of the diagram, the grey area contains all data and analyses already included in Vascotto et al., 2021. The temporal maps below the grey area represent the results of that analysis as well as the starting point for the present analysis. The circle represents both the linear discriminant analysis and the neural networks. Note that several arrows point to this circle area, but for each iteration of the analysis, the algorithm presented here uses only one of the two original maps (coarse or fine), only one of the three GoT environment matrices for training (MeM, R, or P), and only one of the three GoV environment matrices for prediction. Each of the 602 predicted temporal maps is then tested separately with GoV phytoplankton data (Abb).

is influenced by Po River plume (Poulain et al., 2001). Rivers like Tagliamento, Livenza, Piave, Brenta and Adige contribute to river discharge in northern Adriatic but, all together, they sum to only a minor fraction of the Po runoff (Cozzi and Giani, 2011).

2.2. Data

A 12-year time series from 2005 to 2017 and comprising 130 taxa from station 000F (Fig. 1) was collected and stored as part of routine sampling in the Slovenian national monitoring programme. The data is produced on a monthly basis. Phytoplankton structure and abundance

Table 1
Environmental data used in the analysis: raw data, the operation applied to the raw data and the parameter obtained.

Original data	Operation	Parameter	Name
Rain (mm)	Cumulative sum	Rain	Rain
	Coefficient of variance	Rain variance	Rain_var
Temperature air (C)	Mean	Temperature	T_air
Temperature surface (C)	Mean(Surface-Bottom)/Depth	Thermocline strength	T_grad
Temperature bottom (C)			
River outflow (m^3/s)	Mean	River	River
	Coefficient of variance	River variance	River_var
Salinity surface	Mean	Salinity	Sal
Wind speed (m/s)	Mean	Wind	Wind
Wind speed and direction (m/s, Θ)	Mean(speed*cos(Θ))	N.S. component	N.S.
Wind speed and direction (m/s, Θ)	Mean(speed*sin(Θ))	E.W. component	E.W.

data of station 000F were analysed in a previous study Vascotto et al. (2021) where a temporal maps of assemblages and their indicative taxa were obtained (Fig. 2: Temporal maps A and B, more information present in Supplementary material S16). From Vascotto et al. (2021) we had two possible partition systems available, a coarse phytoplankton assemblage partition (Fig. 2: Temporal map A) from which two main assemblages were used and a fine phytoplankton assemblage partition (Fig. 2: Temporal map B) from which six main assemblages were used. We reduced the number of assemblages from Vascotto et al. (2021) because only assemblages that covered at least six samplings/months were used. These phytoplankton assemblages were the starting point for the present analysis.

For the GoT, we also collected data on rain, wind direction and strength, salinity, air temperature, Soča river flow, sea surface and bottom temperature and stored them in an environmental table (Fig. 2: Xp). The data covered the same time period (2005–2017), more details are given in the Supplementary material S1. These data come from the oceanographic buoy Vida, located at a distance of 1.16 km from station 000F (wind, air temperature, water temperature and salinity; https://www.nib.si/mbp/en/oceanographic-data-and-measurements/buoy-2) and from the database of Slovenian Environment Agency (rain, river discharge; https://www.arso.gov.si/en/).

For the GoV, we also collected data on precipitation rain, wind direction and strength, salinity, air temperature, sea surface and bottom temperature form data collected onboard of Acqua Alta Oceanographic Tower (AAOT) by mean of WMO certified meteo station and Seabird SBE 19 CTD casts (Fig. 2: Xp). The environmental dataset covered the period between 2010 and 2019, more details are given in the Supplementary material S11. Phytoplankton structure and abundance data from the station AAOT covered the years from 2010 to 2018 and comprised >300 taxa (Fig. 2: Abb). The data was produced on a monthly basis.

The temporal density of the environmental data was on the order of hours, so we merged the data from the 30 days prior to each phytoplankton sampling to calculate the new variables as summarised in Table 1. The transformed data accounted for environmental conditions between phytoplankton sampling events.

The differences between the averages of the environmental parameters in the two sites were tested using a t.test, while the presence of linear trends was tested using the F-statistic of the Pearson R squared value (Legendre and Legendre, 2012).

2.3. Analysis

2.3.1. Decomposition of environmental data

Autocorrelation of environmental parameters was investigated using distance-based Moran eigenvector maps (Legendre and Legendre, 2012). We used the eigenvectors maps (Fig. 2: 1a Moran) to remove significant autocorrelation components from the detrended GoT environmental data by performing a redundancy analysis (Fig. 2: 1b RDA) between relevant eigenvectors and environmental data (Legendre and Legendre, 2012). In this way, we generated two datasets: one with the fitted values containing the periodic component (Fig. 2: MeM) and the other with residuals containing the non-periodic part (Fig. 2: R). Moreover, we calculated the global Moran's I to estimate the autocorrelation for each environmental variable (Legendre and Legendre, 2012). Finally we used the variation portioning approach (Legendre and Legendre, 2012) to assess the power of GoT environmental components in explaining the variance of the GoV environmental data, that have been decomposed in periodic and non-periodic components prior the variation portioning analysis. We used the R package "adespatial" (Dray et al., 2016) to compute the eigenvectors maps and the Moran's I of each environmental parameter. We used the R package "vegan" (Oksanen et al., 2013) to apportioning the variation among GoT and GoV components and to produce the resulting Venn diagrams.

Apart from periodic and non periodic components of the environmental data, also the complete environmental dataset was used after the decomposition with principal component analysis (Fig. 2: 1c PCA). From the three environmental datasets, the first three principal components were retained (Fig. 2: MeM, R, P). The use of the three first axes was dictated by the small number of objects to model in certain assemblages.

Modelling the relationship between environment and phytoplankton assemblages.

To examine linear relationships between the phytoplankton assemblage partitions (coarse and fine) obtained from Vascotto et al. (2021) in form of an occurrence vector and all three environmental datasets (MeM, R, P), we used linear discriminant analysis (Fig. 2: 2a LDA). The significance of these relationships was evaluated using Wilks Λ (Legendre and Legendre, 2012). The discriminant functions obtained from the LDA of both partitions were then used to reclassify the objects of each assemblage and evaluate the success rate of these functions.

The environmental parameters from GoV were analysed following the same procedure (Fig. 2: Xp) to obtain the complete, periodic and non periodic environmental datasets. The statistically significant LDA discriminant functions obtained in GoT (Wilks Λ with $p < 0.05$) were then applied to forecast the presence of phytoplankton assemblages in GoV using the corresponding environmental dataset from GoV.

To overcome the linearity constraints of LDA analysis, we used Neural networks (Fig. 2: 2b NNet) modelling approach. Also here, the NNets were trained on complete, periodic and non periodic environmental datasets with coarse and fine phytoplankton assemblage partitions from GoT. The resulting six classification functions were used to forecast phytoplankton assemblages in GoV using the corresponding environmental datasets (Fig. 2: Xp). The six parallel tests were each repeated 100 times. The training-to-test ratio was 80–20 %.The NNets were built using the TensorFlow package (Abadi et al., 2015) in Python 3.8. The architecture of the NNets consisted of three layers enabled by linear rectifiers (ReLU) and softmax function. The search optimization algorithm (Adam) attempted to minimise cross entropy by using L1 and L2 regularizations to avoid overfitting.

To characterize each assemblage in terms of environmental conditions for both GoT and GoV, we calculated the average value of environmental parameters and their variances in the samples/months representing a certain assemblage. The environmental parameters were represented as standardized values in bar plots.

2.3.2. Evaluation of phytoplankton assemblages

To evaluate the forecasted assemblages in GoV, we calculated the IndVal index with the corresponding *p*-value (Fig. 2: 3b IndVal) on the GoV phytoplankton community data (Fig. 2: Abb). The IndVal is an index that takes into account the fidelity and the specificity of a certain taxon in a cluster of samples (Dufrene and Legendre, 1997). In our case it was calculated for taxa in the forecasted phytoplankton assemblages resulting from the statistically significant LDA classification functions

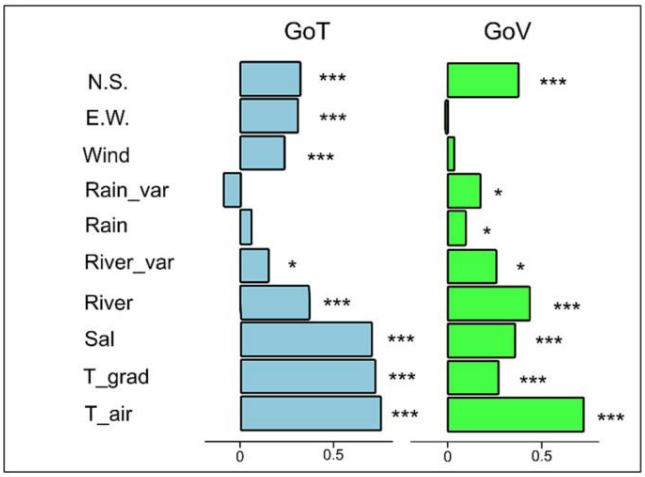

Fig. 3. Global Moran's I for the environmental data in GoT and in GoV. The significance of each value is encoded with stars: * correspond to significant Moran's I (p.value <0.05), *** correspond to highly significant results (p. value <0.01).

(2) and all NNet classification functions (600) (Fig. 2: New Maps). The average p-value of IndVal was used to score each forecasted phytoplankton assemblages. In parallel, we also calculated the within-group sum of squares (WSS) over the chi-square transformed matrix of abundances (Legendre and Legendre, 2012). The chi-square values represent the deviations of a certain taxon in a sample from its expected abundance while the WSS represents the homogeneity of such values inside the clusters of samples. Values close to one indicate a poor classification of the samples variance, in this case taxa deviations, while values close to zero would indicate a perfect classification of the variance. IndVal *p*-values and WSS values for the six parallel outcome groups (coarse and fine phytoplankton assemblage partitions per complete, periodic and non periodic components of environmental datasets) were represented with box-plots and differences tested with the Kruskal-Wallis test. Pairwise differences were tested for significance using the Tukey-Kramer test for independent samples. The forecasted assemblages obtained using the complete environmental dataset were chosen to be explored further in the discussion since they represented the best possible predictions.

3. Results

3.1. Environmental conditions

The environment in the two neighbouring areas in the northern Adriatic was relatively stable during the study period. Of the 10 variables considered in GoT and in GoV, none showed a positive or negative long-term trend, with the exception of the mean discharge of the Soča River in GoT which showed a slightly positive trend (Supplementary material S 5). With respect to the average values, some environmental parameters were significantly different at the two sites. The thermocline appeared to be stronger in GoV (0.193 °C/m on average) than in GoT (0.130 °C/m) (p-value <0.01), and the water in GoV was less salty (34.1 vs 36.6, p-value <0.01). In addition, the Po River discharge and its coefficient of variance were higher than the Soča river discharge. On the contrary, air temperature, wind speed, rain and its coefficient of variance were similar in the two sites (p-value >0.05). The wind roses of wind speed and direction (Supplementary materialS6) indicate that the main winds in the GoT had a strong NEE contribution and a secondary component from the south (S and SSE). Winds in the GoV also had a large contribution from the northeast quadrant (NNE and NE) and secondary components from the southern quadrants.

Most environmental variables exhibited some degree of periodicity

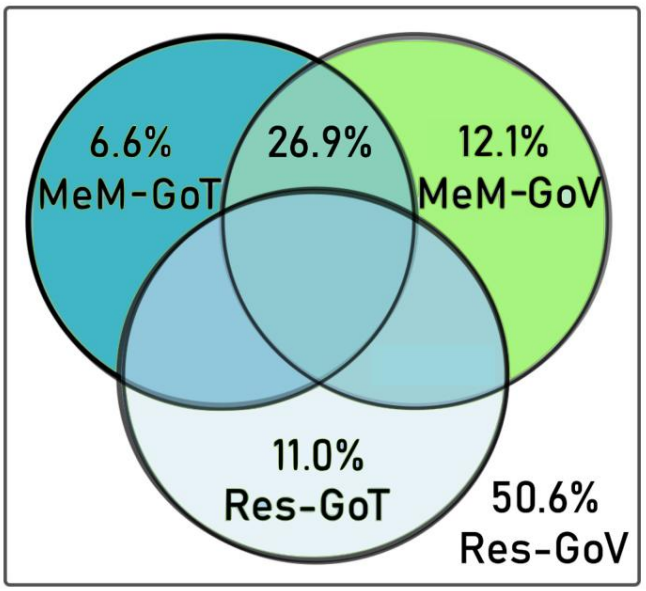

Fig. 4. Venn diagram of the variance partition of the environmental dataset from GoV. Variance is partitioned between the two periodic components of the two environments (MeM-Got and MeM-GoV) and the residuals of the environmental variables from GoT (Res-GoT). The intersections with no value represent zero or negative values which together with the remaining values sum up to 100 %.

in both study areas (Fig. 3). Overall, periodicity explained a relevant proportion of the variance in environmental data (46 % in GoT and 39 % in GoV- More details are given in the Supplementary material). Periodicity in environmental parameters was less pronounced in GoV compared to GoT, as indicated by generally lower Moran's I in Fig. 3. In GoT, three parameters, i.e. salinity, air temperature, and thermocline strength, showed the most pronounced cyclic behaviour, while rain and rain variability seem to show mainly erratic behaviour. On the contrary, the rain pattern was somewhat more regular in GoV. In addition, in GoV the average wind speed and the strength of the east-west components showed a more pronounced erratic behaviour. The same was true for the thermocline and salinity.

The combination of the periodic components from GoV (Fig. 4: MeM-GoV) and from GoT (Fig. 4: MeM-GoT) explained 45.6 % of the variance in the GoV environmental data. The periodic components of GoV and GoT shared ~26.9 % of the explained variance. The remaining variance was partially explained (11.0 %) by the non-periodic components of the environmental data from GoT (Fig. 4: Res-GoT). The residual variance (Res -GoV 50.6 % in Fig. 4) corresponds to the variance of local non-periodic events.

Table 2
Results of LDA on the two phytoplankton assemblage partitions from Vascotto et al. (2021) with three different environmental datasets from GoT. The bold values correpsond to LDA configuration that resulted significative (p-value < 0.05).

Phytoplankton assemblage partition from Vascotto et al. (2021)	Environmental dataset	Wilks Λ	p-value
Coarse (2 assemblages)	Complete (principal components)	0.98	0.69
	Periodic component	0.96	0.33
	Non-periodic component	0.97	0.51
Fine (6 assemblages)	Complete (principal components)	**0.73**	**0.0037**
	Periodic component	**0.67**	**0.001**
	Non-periodic component	0.87	0.25

Table 3
The efficiency of the LDA and NNets in reclassification in % of correctly classified GoT objects. In the second column the original encoding from Vascotto et al., 2021 are reported in order to facilitate the comparison. The results refer to the reclassification obtained using the complete environmental dataset.

Assemblage	Original encoding	LDA	NNets
A	Group IX	4 %	40 %
B	Group IV	70 %	92 %
C	Group XI	13 %	66 %
D	Group XII	0 %	70 %
E	Group III	75 %	100 %
F	Group VII	67 %	78 %
Weighted mean		21 %	60 %

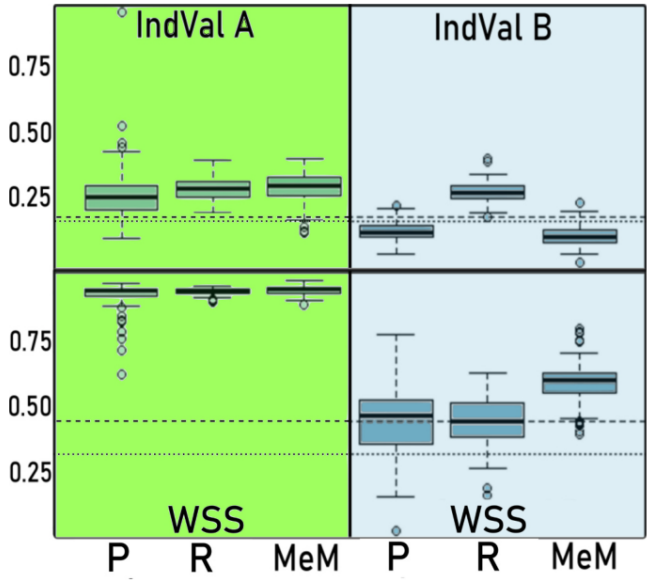

Fig. 5. Boxplots of average IndVal p-values (upper panel) and WSS values (lower panel) for the Neural network predicted phytoplankton assemblages in GoV. The green left panel represents the results obtained from the coarse phytoplankton assemblage partition from Vascotto et al. (2021), blue right panel refers to results obtained from fine phytoplankton assemblage partition from Vascotto et al. (2021). Each panel includes from left to right the results got using complete environmental dataset (P), its non periodic (R) and periodic component (MeM). Horizontal lines in the right panel represent the average IndVal p-value and WSS for the assemblages predicted with two statistically significant discriminant functions of the LDA: Dotted lines represent the predicted assemblages with complete environmental dataset, dashed lines represent the predicted assemblages with periodic component.

3.2. *Efficiency of linear and non-linear classification functions for predicting phytoplankton assemblages*

From the results of Vascotto et al. (2021) only assemblages present at least in six months were retained from further analysis. This corresponded to two assemblages from the coarse partition and six from the fine one. The six assemblages covered 128 months of the total 152 we had at our disposal. No significant linear relationship with environmental variables in GoT was found when performing linear discriminant analysis (LDA) with two assemblages from the coarse phytoplankton assemblage partition, neither with complete environmental dataset nor with data decomposed in periodic and non-periodic components (Table 2). On the contrary, when using the fine phytoplankton assemblage partition from Vascotto et al. (2021), the six assemblages discriminated a relevant part of the variance of the principal components of the complete environmental dataset and of its periodic part while there was no relationship with the non-periodic component of the environmental dataset (Table 2).

However, the classification functions obtained from the LDA with two statistically significant settings (for complete environmental dataset and periodic component) were only able to correctly reclassify on average 21 % of the objects in the associated assemblages. But, when looking at the reclassification results at the level of single assemblage, the success of correct classification was quite high for 3 assemblages and very low for the remaining 3 (Table 3). The Neural Networks (NNets) were able to correctly reclassify on average 60 % of the objects using its non-linear classification functions (Table 3). For the three assemblages for which LDA performed poorly (A, C, D) the reclassification of the NNets is greatly improved.

3.3. *Evaluation and composition of predicted phytoplankton assemblages in Gulf of Venice*

Both classification functions resulted from LDA (only from the two statistically significant settings; see Table 2) and from Neural networks (from all six settings) on GoT data were used to forecast the assemblages in GoV. We first present the evaluation of the predicted phytoplankton assemblages within the coarse and the fine phytoplankton assemblage partition by neural networks, using the mean IndVal *p*-values and WSS values obtained with the complete environmental dataset (Fig. 5, P) and with its periodic (Fig. 5, MeM) and non-periodic components (Fig. 5, R). For both IndVal p-values and WSS, the differences between the six groups were significant (Kruskal-Wallis test; p-value <0.001). The IndVal p-values and the WSS values we obtained from the coarse phytoplankton assemblage partition (Fig. 5, left) were generally higher than those obtained from the fine phytoplankton assemblage partition (Fig. 5, right). While there were no substantial differences between the three cases (P, R and MeM) within the coarse phytoplankton assemblage partition (Fig. 5, left), a different pattern emerged within the group of fine phytoplankton assemblage partition (Fig. 5, right). The IndVal p-values obtained using complete environmental dataset (Fig. 5: IndVal B, P) and its periodic components (Fig. 5: IndVal B, MeM) were significantly lower than those obtained using the non-periodic component (Fig. 5: IndVal B, R) (Tukey-Kramer test; p-value <0.001). In the case of evaluation with the WSS values, they were significantly higher for the assemblages obtained with periodic component of environmental data (Tukey-Kramer test; p-value <0.001).

In comparison, the mean IndVal p-values of assemblages predicted by LDA discriminant functions (Fig. 5; horizontal lines in right upper panel) were lower than those obtained by neural network either for the coarse phytoplankton assemblages or for the fine phytoplankton assemblages using the non periodic component. The mean WSS values (Fig. 5; horizontal lines in right lower panel) indicate that the results for the assemblages predicted by LDA using the complete environmental dataset are better than those using its periodic part, mirroring the results from neural networks.

The best results in terms of average *p* values were obtained for the assemblages predicted by neural networks using the periodic components, although no significant difference was found in comparison to the results from the complete environmental dataset (Fig. 5; IndVal B, P and MeM). On the contrary, from the point of view of WSS the assemblages predicted by neural network using the complete dataset performed better than those using the periodic components (Tukey-Kramer test; p-value <0.001). Therefore, as the best synthesis the assemblages predicted for GoV by neural network with the use of the complete environmental dataset is further analysed in the following.

In Fig. 6, the similarities, and differences between the "original" phytoplankton assemblages (GoT) and those predicted for GoV are presented together with the environmental conditions. Assemblages are presented as clusters of sampling dates characterised by certain phytoplankton taxa (Fig. 6, temporal maps). Environmental conditions associated to these assemblages are presented as standardized average values of environmental parameters and their variances in the samples/

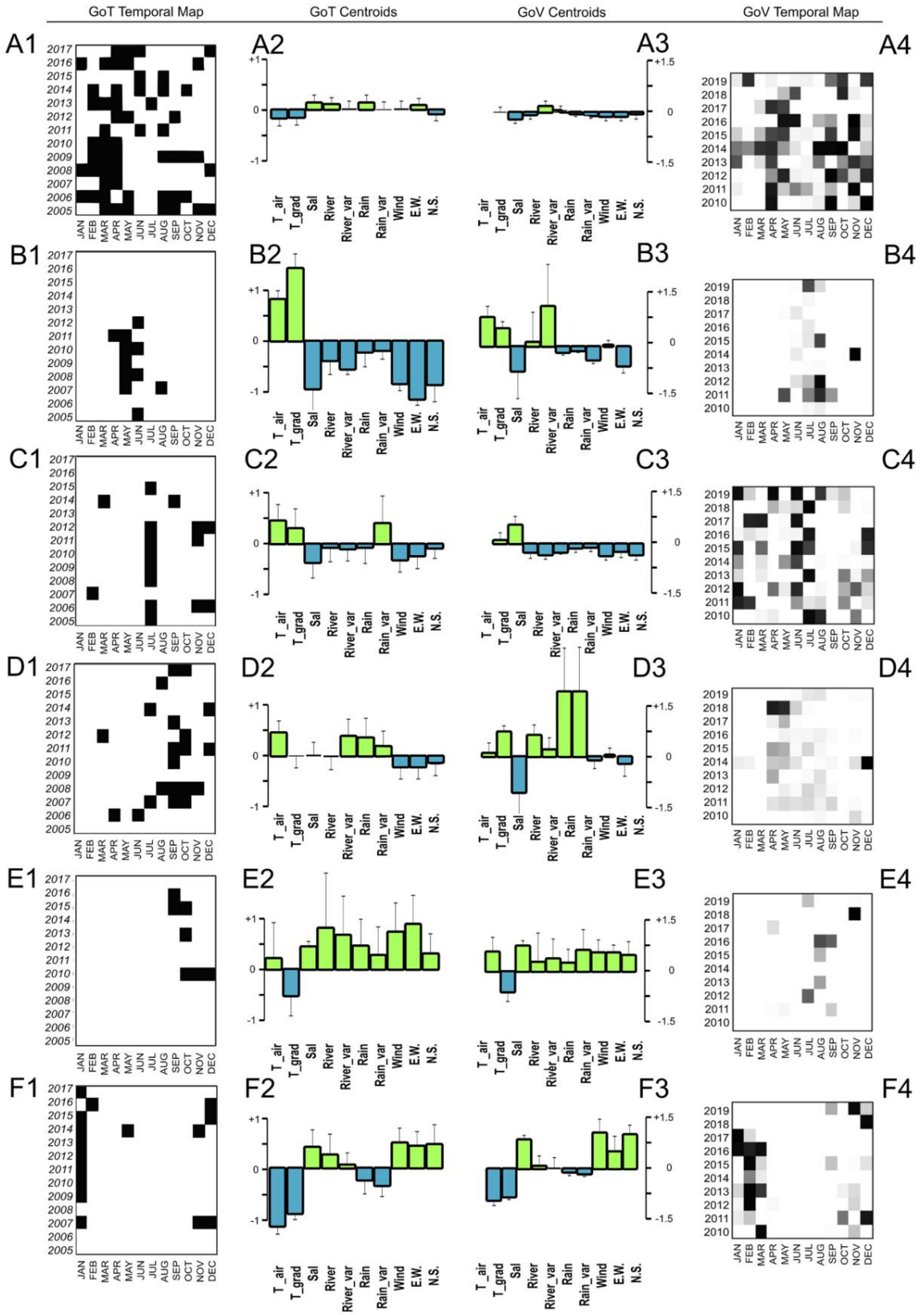

Fig. 6. Phenology of the six phytoplankton assemblages and the corresponding environmental conditions. A1-F1: temporal distribution of phytoplankton assemblages in GoT (from Vascotto et al., 2021); A2-F2: environmental characteristic in GoT; A3-F3: environmental characteristic in GoV; A4-F4: temporal distribution of predicted phytoplankton assemblages in GoV. The bar charts represent environmental variables in standardized values (mean + sd). Note the different scales on y axes. The temporal maps for GoV and GoT are expressed in probability (darker the colour, the higher the probability that a certain month belongs to an assemblage). The temporal map of GoT had probability either 0 or 1 having been already defined at the beginning of the study.

Table 4
The indicative taxa of phytoplankton assemblages. For GoT the indicative taxa are represented by the IndVal (from Vascotto et al., 2021). An IndVal value >0.2 is a sign of indicativity for a certain assemblage. Taxa are ordered in decreasing order of IndVal. For GoV, only taxa with the highest IndVal values are shown.

GoT		GoV	
Taxa	Indval	Taxa	IndVal
A			
Cryptophyceae	0.08	Coccolithophyceae	0.34
Phytoflagellates	0.06	*Lessardia elongata*	0.29
Prasinophyceae	0.06	*Diplopsalis* group	0.28
Meringosphaera mediterranea	0.05	*Chaetoceros diversus*	0.23
Prorocentrum cordatum	0.05	*Leptocylindrus danicus*	0.23
Gymnodinium spp.	0.05	*Protoperidinium steinii*	0.23
Chlorophyceae	0.04	Dinophyceae	0.22
Gyrodinium spp.	0.03	*Amphora* spp.	0.20
Ophiaster hydroideus	0.03	*Paulinella ovalis*	0.20
B			
Cyclotella spp.	0.44	*Cyclotella* spp.	0.42
Prorocentrum gracile	0.20	*Cyclotella caspia*	0.38
Prorocentrum cordatum	0.13	*Eutreptia lanowii*	0.37
Chaetoceros simplex	0.13	*Calciosolenia brasiliensis*	0.28
Prasinophyceae	0.12	*Dactyliosolen fragilissimus*	0.24
Heterocapsa group	0.11	*Tripos fusus*	0.23
C			
Proboscia alata	0.45	*Thalassionema nitzschioides*	0.56
Chaetoceros spp.	0.38	*Chaetoceros* spp.	0.31
Rhizosolenia spp.	0.19	*Emiliania huxleyi*	0.28
Hemiaulas hauckii	0.13	*Cerataulina pelagica*	0.26
Thalassionema nitzschioides	0.11	*Thalassiosira* spp.	0.26
Euglenophyceae	0.11	*Leptocylindrus minimus*	0.22
Nitzschia spp.	0.10	*Nitzschia longissima*	0.22
Guinardia striata	0.09	*Pseudo-nitzschia delicatissima* group	0.22
Phytoflagellates	0.07	*Chaetoceros affinis*	0.21
Gymnodinium spp.	0.07	*Bacteriastrum* spp.	0.20
D			
Nitzschia spp.	0.14	*Pyramimonas* spp.	0.33
Guinardia striata	0.12	*Ebria tripartita*	0.28
Dactyliosolen fragilissimus	0.10	*Calcidiscus leptoporus*	0.27
Syracosphaera pulchra	0.09	*Leucocryptos marina*	0.25
Hemiaulas hauckii	0.09	*Prorocentrum gracile*	0.25
Coccolithophyceae	0.09	*Prorocentrum cordatum*	0.24
Proboscia alata	0.07	*Cocconeis scutellum*	0.23
Rhabdosphaera stylifera	0.06	Cryptophyceae	0.23
Phytoflagellates	0.06	*Chaetoceros simplex*	0.21
Pseudo-nitzschia delicatissima group	0.06	*Protoperidinium* spp.	0.21
E			
Pseudo-nitzschia delicatissima group	0.65	*Gyrodinium spirale*	0.77
Nitzschia spp.	0.28	*Gyrodinium* spp.	0.51
Syracosphaera pulchra	0.28	*Cochlodinium* sp.	0.47
Calciosolenia murrayi	0.24	*Guinardia striata*	0.45
Dactyliosolen fragilissimus	0.20	*Torodinium robustum*	0.42
Gyrodinium spp.	0.18	*Nitzschia sigma*	0.35
Tripos fusus	0.18	*Oxytoxum* spp.	0.31
Calciosolenia brasiliensis	0.17	*Pleurosigma* spp.	0.31
Ophiaster hydroideus	0.16	*Psammodictyon panduriforme*	0.31
Rhizosolenia spp.	0.13	*Pseudo-nitzschia seriata* group	0.31
Tripos furca	0.13	Bacillariophyceae	0.30
Pseudo-nitzschia seriata group	0.11	*Chaetoceros curvisetus*	0.29
Euglenophyceae	0.10	*Gymnodinium* spp.	0.29
Prorocentrum triestinum	0.10	*Chaetoceros danicus*	0.28
Guinardia striata	0.08	*Dactyliosolen blavyanus*	0.28
Rhabdosphaera stylifera	0.08	*Hemiaulus hauckii*	0.28
Gymnodinium spp.	0.08	*Hermesinum adriaticum*	0.28
Gonyaulax spp.	0.08	*Katodinium glaucum*	0.28
Leptocylindrus mediterraneus	0.07	*Paralia sulcata*	0.28
Cerataulina pelagica	0.07	*Proboscia alata*	0.26
F			
Emiliania huxleyi	0.11	*Skeletonema costatum* s.l.	0.35
Ophiaster hydroideus	0.07	*Dictyocha fibula*	0.29
Diploneis crabro	0.07	*Asterionellopsis glacialis*	0.29
Prasinophyceae	0.06	*Diploneis crabro*	0.25
Meringosphaera mediterranea	0.06	*Dactyliosolen phuketensis*	0.21

Table 4 (*continued*)

GoT		GoV	
Taxa	Indval	Taxa	IndVal
Proboscia alata	0.07	*Heterocapsa* group	0.25
Heterocapsa group	0.07	*Nitzschia* spp.	0.23
Emiliania huxleyi	0.07	*Chaetoceros decipiens*	0.22
Pleurosigma normanii	0.06	Phytoflagellates	0.22
Diploneis crabro	0.06	*Guinardia flaccida*	0.21
Cryptophyceae	0.06	*Rhizosolenia imbricata*	0.21

months occupied by the assemblage (Fig. 6, env. centroids). For the predicted phytoplankton assemblages in GoV, the indicative taxa are presented with the appertaining IndVal index (Table 4). The indicative taxa of phytoplankton assemblages in GoT are presented by IndVal (Table 4, from Vascotto et al., 2021).

The first phytoplankton assemblage we describe (Fig. 6, A1) was originally defined as the base community in GoT (Vascotto et al., 2021). This and the remaining assemblages of GoT were defined on the basis of the community composition following the method described in Supplementary material in S 16. It is scattered during whole time-series but more concentrated in the first half of the year. The predicted phenology for this assemblage in GoV was similar to that in GoT in that it occurred throughout the year (Fig. 6, A4). Another similarity concerns the fact that in both GoT and GoV this assemblage had a mix of indicative taxa from different phytoplankton classes. While in GoT these were mostly belonging to the phytoflagellates, in GoV most indicative taxa were coccolithophores, diatoms and dinoflagellates (Table 4, A). In both areas, the environmental conditions for this assemblage were characterised by parameters fluctuating around the overall mean, but with standardized values not exceeding ±0.20.

In GoT, the spring phytoplankton assemblage (Fig. 6, B1) was mainly characterised by the presence of diatom *Cyclotella* spp. and small dinoflagellates of the genera *Prorocentrum* and *Heterocapsa* (Table 4, B). This assemblage was present in stratified waters (T_grad standardized average at 1.24 from the overall mean) with low surface salinity (standardized average at −0.75), relatively high air temperature (standardized average at 0.71) and weak winds. Using the classification functions obtained by neural networks, the presence of this assemblage in GoV was predicted mainly for late spring-late summer period. Environmental conditions for this predicted assemblage were partly similar to those in GoT, with stratified (T_grad standardized average at 0.55) and warm (T_air standardized average at 0.90) waters, but with an important contribution of river discharge variability (River_var standardized average at 1.23). Also in the predicted assemblage, the most indicative taxa belonged to the genus *Cyclotella* (Table 4, B).

The third phytoplankton assemblage in GoT (Fig. 6, C1) represents a predominantly diatom assemblage (Table 4) with most occurrences in July but also in other seasons. The predicted phenology of this assemblage in GoV also indicates a scattered distribution throughout the year although the highest probability of occurrence was in summer months (Fig. 6, C4). Also here, the assemblage was dominated by the presence of diatoms (Table 4, C). Environmental conditions in both areas (Fig. 6, C2 and C3) were similar to those during the previous assemblage (B2) but with less pronounced values of parameters' standardized averages. In addition, there was also an important contribution of rain variability in GoT (standardized average at 0.35); while river discharge variability was not so important for this assemblage in GoV.

The fourth phytoplankton assemblage in GoT presented in Fig. 6 (D1) occurred primarily in the second half of the year, mainly in autumn and

was characterised by a mix of coccolithophores and large centric diatoms (Table 4, D). This assemblage could be easily associated with warmer periods under the influence of pulsating freshwater inputs due to rivers and rain (Fig. 6, D2). In GoV, the phenology of the predicted phytoplankton assemblage was different and characterised mainly by low probability of occurrence (Fig. 6, D4). The environmental conditions were mainly determined by exceptionally high values of rain (Rain standardized average at 1.99, Rain_var standardized average at 2.13, Fig. 6, D3). This assemblage differed from the original not only in its phenology but also in terms of indicative taxa, since here the contribution of phytoflagellates was substantial (Table 4, D).

The autumn in GoT was characterised also by another phytoplankton assemblage (Fig. 6, E1) which was defined by the presence of pennate diatoms, coccolithophores and thecate dinoflagellates (Table 4, E). This assemblage was only present from 2010 onwards and was delineated by well-mixed water column (T_grad standardized average at −0.45), with high river outflow (River standardized average at 0.72 and strong winds with *E*-W component (E-W standardized average at 0.78) (Fig. 6, E2). The occurrence of such assemblage in GoV was predicted for late summer-early autumn (Fig. 6, E4), with environmental conditions similar to that in GoT: mixed water column (T_grad standardized average at −0.63), relatively warm weather (T_air standardized average at 0.60) and high salinity (sal standardized average at 0.78) and strong winds (Fig. 6, E3). This predicted assemblage was associated with a long list of indicative taxa (Table 4, E) of predominantly naked forms of dinoflagellates and diatoms. Coccolithophores were not indicative for this assemblage in GoV.

Coccolithophores *Emiliania huxleyi* and *Ophiaster hydroideus* together with small diatoms dominated the winter assemblage in GoT (Table 4, F). This assemblage occurred primarily in December and January (Fig. 6, F1) and was associated with cold weather (T_air standardized average at −0.96) and mixed water column (T_grad standardized average at −0.86) most likely associated to strong winds (Wind standardized average at 0.43, E-W standardized average at 0.38, N-S standardized average at 0.40) (Fig. 6, F2). A very similar pattern of environmental conditions emerged for the predicted assemblage in GoV (Fig. 6, F3), which also shared a similar phenology (Fig. 6, F4). The associated taxa in GoV (Table 4, F) were dominated by the diatom *Skeletonema costatum s.l.* and lacked the presence of coccolithophores characteristic for GoT. A benthic diatom *Diploneis crabro* was indicative of the winter community in both areas.

4. Discussion

4.1. Considerations on data representativeness

In a highly variable environment such as the northern Adriatic, which is prone to rapidly changing small scale conditions (Jeffries and Lee, 2007), it is probable that at the scale of a hundred km (distance between the LTER stations) these conditions would be different. However, the two locations have been described in several regionalization studies belonging to the same recognizable space, which can be distinguished by its abiotic characteristics and associated biological assemblage (Ayata et al., 2018). To study the influence of environmental parameters and their variability on the phytoplankton community in the two study areas, it was crucial to take into consideration the representativeness of the environmental data. These were collected from the source closest to phytoplankton sampling stations: at the LTER station itself for some parameters and at the nearest meteorological station for others. The reason we chose to use environmental data from a single site closest to LTER was double. First, in this way we avoided the "fading" of localized extreme events as would come from averaging multiple sites over larger area. Second, data from more distant sites could have blurred environmental cycles by adding out-of-phase patterns. Because the goal of this study was to assess the importance of cyclic patterns of environmental parameters in shaping the phytoplankton community, we preferred the risk of underestimating the strength of these patterns to the opposite. Moreover, in this way, local extreme events and their influence on the model could also be taken into consideration.

Another consideration goes to the choice of environmental parameters, since the data we have used for the present analysis (some physical, meteorological and hydrological data) do not represent the totality of factors that influence the phytoplankton community in the northern Adriatic, e.g. physical, chemical and biological factors (Brush et al., 2021; Neri et al., 2022). The choice of parameters in this study was guided by the sufficient temporal frequency of data acquisition. At both LTER stations, the chemical parameters (i.e. nutrient concentrations) are sampled along with phytoplankton on a monthly basis, which poses two problems. First, the data represent the chemical status at the current time, and second, they are strongly influenced by randomness and measurement errors because of their small number. Since the rate of change of environmental parameters is higher than the rate of fluctuations in phytoplankton community (Hutchinson, 1941), using parameters from the day of sampling cannot provide a reliable picture of past conditions that determined a particular community. On the other hand, hydrological and meteorological data have the advantage of being recorded very frequently allowing to summarise the data over longer period (for example one month). In addition, most of the chosen data are indirect indicators of other relevant parameters, such as water column stability (T, salinity) and nutrient enrichment (river discharge and rain).

4.2. Patterns of mesoscale connectivity

Half of phytoplankton assemblages in GoT have been quite well characterised by linear relationships with the environmental parameters. Neural network improved the proportion of correct reclassifications in all six phytoplankton assemblages in GoT, indicating the existence of non-linear elements in the relationships between environment and phytoplankton, as well. The fact that the neural network was able to predict assemblages in GoV with similar indicative taxa indicates that these methods can be successfully applied to predict phytoplankton community structure at the mesoscale.

For assemblages with linear relationships, it was possible to find matching assemblages in GoV accompanied with similar or very similar environmental conditions. These assemblages were characterised, at least to some degree, by the same or related species in both environments. The assemblage that was in both areas dominated by *Cyclotella* species was characterised by a warm period and stratified water column. However, in GoV this assemblage was not predicted for late spring as in GoT, but mainly for summer and late summer. This phenological difference highlights the link between indicative taxa and environmental conditions, since the two assemblages are out of phase in both areas, but form under similar environmental conditions. However, besides thermal stratification also Po River discharges played a significant role for the formation of this assemblage in GoV.

Very similar environmental conditions and slightly different timing were characteristic also for the assemblage E. While in GoV this community was still dominated by diatoms, and dinoflagellates were characteristic for both areas, coccolithophores were exclusively typical for GoT. Such a rich and diverse community without a single dominant taxon is typical for the early autumn in the northern Adriatic (Bernardi Aubry et al., 2012; Marić et al., 2012; Cerino et al., 2019). One common element in both areas was the presence of species from the genus *Pseudo-nitzschia*, which are frequently mentioned as community-forming in the northern Adriatic (Marić et al., 2012; Godrijan et al., 2013; Cerino et al., 2019). However, *Pseudo-nitzschia* species were also present in other assemblages, such as D in GoT and C in GoV, indicating the opportunistic nature of this genus (Bernardi Aubry et al., 2012). Within the present study *Pseudo-nitzschia* species were just assigned into two groups, i.e. the *P. seriata* and the *P. delicatissima* group, which could have contributed to uncertainties in defining indicative taxa and their niches (Turk Dermastia et al., 2020).

Differently from the described out-of-phase conditions for the "*Cyclotella*" and "*Pseudo-nitzschia*" assemblage, the late autumn-winter period in GoT and GoV was similar in terms of environmental conditions (cold period, mixed water column, strong winds) and temporally synchronized. Although the indicative taxa for this assemblage were mainly different for the two areas, most of them are considered as characteristic for the autumn-winter period in the northern Adriatic basin (Bernardi Aubry et al., 2012; Marić et al., 2012; Godrijan et al., 2013; Cerino et al., 2019). The common presence of the benthic diatom *Diploneis crabro* is in line with the phenology of the genus *Diploneis* described previously in the area (Cibic et al., 2012) and can be explained in light of the mixed condition present in winter. Also, *Skeletonema costatum s.l.* and *Asterionellopsis glacialis* were found to be typical for a few assemblages in GoT that were not included in the model, but occurred under the same environmental conditions as the winter cluster F1 (Vascotto et al., 2021). *S. costatum s.l.*, which was the most indicative taxon for the winter in GoV, is considered to be responsible for the winter-early spring bloom across whole northern Adriatic (as *S. marinoi*), with increasing abundances towards its western part (Marić Pfannkuchen et al., 2018). However, the abundance of *S. costatum s.l.* decreased markedly in the GoT from 2013 onwards (Cerino et al., 2019; Vascotto et al., 2021). As concerns the coccolithophore *Emiliania huxleyi*, the main winter indicative species in GoT (Cabrini et al., 2012; Cerino et al., 2019; Vascotto et al., 2021), there was a recent decrease of its abundances in southern parts of the basin (Totti et al., 2019). It appears that winter conditions constitute a spatially uniform habitat at the mesoscale of the northern Adriatic and set favouring conditions for some common indicative taxa.

Fairly well temporally defined assemblage of relatively large, mostly colonial diatoms in the GoT formed also during summer (mainly in July) although with some appearance in winter and autumn too, but its appertaining environmental characteristics were not as good defined by linear discriminants as with previously discussed assemblages. Here, neural network significantly improved the predicting capacity and modelled a similar diatom dominated assemblage in GoV. Differences in phenology of this assemblage in the two areas can be justified by the underlying trophic differences. While in the GoV diatoms dominate the phytoplankton community most of the time (Bernardi Aubry et al., 2012) which was also predicted in our study, a recent July diatom peak has established in the GoT (Mozetič et al., 2012) and eastern part of the northern Adriatic (Marić et al., 2012), apparently governed by summer rain events. In GoT, a mixed community of nanoplanktonic phytoflagellates from different taxonomic groups predominantly dominates the phytoplankton community (Brush et al., 2021; Vascotto et al., 2021). The assemblage depicting this was the largest one considered in this study with indicative taxa from all groups. An assemblage with similar characteristics was predicted also for GoV, especially for spring and autumn, when also previous studies depicted a codominance among diatoms and other groups (Bernardi Aubry et al., 2012).

The last assemblage we discuss was found with a very different phenology and taxa composition in both areas. In GoT, this assemblage formed in conditions with relatively high rain and freshwater discharge pulses, which enriched the water column with nutrients and led to proliferation of large diatoms (Vascotto et al., 2021). On the contrary, a similar assemblage could not be predicted for GoV, where only three sampling dates were assigned with high probability to this group. These three sampling dates were characterised by extreme rainfall, which probably led the neural network to a local minimum outside of the range of the training data. Therefore, the extrapolation performed by the neural network was less accurate than interpolation (Maier and Dandy, 2000). This issue is particularly relevant in the case of the assemblage D but it almost certainly applies to all the six models to a certain degree.

4.3. Patterns of periodicity

The environmental conditions in GoT appear to be more periodic than in GoV. This can be partly explained by the shorter length of the time series in GoV (70 months versus 150 months in GoT) and the proportion of missing data. The Moran eigenvectors eliminate missing values in the time-series at the expense of some bias in the shortest and longest frequency vectors (Brind'Amour et al., 2018). Nevertheless, the periodic components of the GoT explained additional ~6.6 % variation in environmental parameters in GoV, thus suggesting a more equal role of autocorrelation in both areas. In GoV, the N-S component of the wind is as periodic as in GoT, as Bora and southern winds alternate (Supplementary material S 6). On the contrary, the *E*-W component does not show periodicity in GoV, probably because of the weaker dominance of the Jugo (Scirocco) among the southern winds (Poulain et al., 2001). The strength of the thermocline is more irregular in GoV, but this may be due to both the higher number of missing values for this specific factor compared to its counterpart in GoT and the coastal and meteorological influences (Alberotanza et al., 2004). The combination of these two parameters (E.W component and thermocline strength) is responsible for the slightly lower percentage of variance explained by periodic components in GoV overall. From the analysis of variance, it appears that a relatively large portion of variance in GoV is explained by the periodic components of the environmental parameters in GoT (~26.9 %). This shared variance expresses the extent to which the two environments are similar in periodicity. Temperature and thermocline cycles (rho = 0.82 and 0.57, respectively), along with seasonal variations in wind and rivers (rho = 0.63 and 0.49, respectively), are the source of the common periodicity. As expected, the non periodic components did not share explanatory power with the periodic components of GoT and GoV, but explained another 11.0 % of the variance of GoV non periodic components. This 11.0 % of the variance represents anomalous events that occurred at the mesoscale level. Rather than trying to determine which parameters are responsible for this anomaly, it is more important to note that unexplained non-periodic events in GoV account for ~50 % of the variance. This suggests that the two LTER sites do not share the majority of non-periodic events (11.0 % shared vs 50.6 %) but the environment in the northern Adriatic is mainly uniform in its periodic part (33.5 % vs 12.1 %).

Our results also confirm the relationship between the phytoplankton community in the GoT and the periodic components of the environmental parameters, which can be mirrored to a nearby area of the northern Adriatic (GoV). This could be confirmed only when a fine structure of the phytoplankton community in GoT was taken into consideration (i.e. the fine phytoplankton assemblage partition from Vascotto et al. (2021)). Although our results suggest that phytoplankton community is more structured by the periodic components of the environment, we should be cautious to argue the opposite as well, since we could not use all the assemblages from Vascotto et al. (2021). The short-lived assemblages that were excluded from the analysis could have represented the deviations resulted from the non-periodic components of the environment.

Current dynamics, as one of these important mesoscale engineers, determine water masses with similar histories whose lifetimes fall within the range of phytoplankton blooms; i.e.few weeks (d'Ovidio et al., 2010). In northern Adriatic such currents connect the two study areas by persistent cyclonic sub-gyres (Poulain et al., 2001; Petelin et al., 2013). Moreover, this circulation path is even strengthened during Bora events (Boicourt et al., 2021). Surface waters from GoT reach the western part of the northern Adriatic, while deeper waters from GoV are transported back to the eastern part with a branch entering the GoT (Malačič et al., 2012). This cyclonic circulation is responsible also for the occasional surface summer advection of riverine waters, nutrients and phytoplankton from the western to the eastern side of the Adriatic (Vilicic et al., 2013). Alternatively, during Scirocco events surface circulation is generally split in two branches, one entering the GoT and the other recirculating in a basin scale cyclonic gyre (Boicourt et al., 2021). The cyclonic connectivity could explain some of the features of the phytoplankton community in the northern Adriatic. In fact, two of the

assemblages occurring during windy months (assemblages E and F) presented a one-month delay in their phenology between the two sides of the basin indicating a synchronized change in water column conditions. Moreover, the first appearance of the assemblage E in September 2010, which corresponded to the long-lasting *Pseudo-nitzschia* bloom in GoT (Vascotto et al., 2021), matched one of the intrusion of Po River plume in GoT in August 2010 (Vilicic et al., 2013).

Stratification of the water column is another mesoscale characteristic that affects the phytoplankton community in northern Adriatic, acting in periodical patterns but differently in both areas. When the winter winds calm down, the stratification in the GoV moves eastward starting at the end of spring in the western part and reaching the strongest stratification condition at the end of summer (Degobbis et al., 2000). In GoT, on the contrary, the stratification reaches its maximum at the end of spring, when Soča River plume remains blocked in the surface layer of the gulf moving clockwise (Malačič and Petelin, 2009). Therefore, during stratified water column conditions in spring and summer the phytoplankton community seems to be more affected by local events, which can be seen in the temporally non-synchronized formation of assemblage B. Moreover, this assemblage disappeared after 2012 in GoT, when there was also an interruption of successive comparison of assemblage C in July. These changes were not mirrored by any change in GoV community succession, indicating that during this part of the year the two areas are less connected. Similar results were obtained in the Gulf of Naples from Ribera d'Alcalà et al. (2004) who observed that winter and autumn blooms were related to basin-wide meteorological events, whereas late spring-summer blooms were local phenomena, driven by lateral advection. It is possible, finally, that the increase in Soča River discharge (Supplementary material Fig. 5) could have affected these changes in GoT phytoplankton phenology.

The importance of seasonality for the northern Adriatic phytoplankton community has been highlighted several times in recent years (Mozetič et al., 1998; Cerino et al., 2019; Salgado-Hernanz et al., 2019). Besides confirming this importance, our work also extended the relevance of this relationship to assemblages' patterns. The succession of assemblages is linked to the seasonality of environmental forcing, both at mesoscale (Bora events) and at local scale (stratification and river discharge). Bora winds, which contribute to the cyclonic gyre connecting the basin at mesoscale, are decreasing in frequency and strength most likely due to global warming (Pirazzoli and Tomasin, 2002). On the other hand, anomalous meteorological events, such as marine heat waves, have increased in frequency in the last years (Boicourt et al., 2021) and have been forecasted to increase even more in near future (Lionello, 2012). It has been forecasted that future conditions of global temperature increase predicted by the International Panel on Climate Change (IPCC) will pose medium to high risk to the structure and phenology of Mediterranean marine ecosystems (Ali et al., 2022) our results seem to confirm this expectations. Increased stratification due to lack of winds and increased air temperature should lead, according the Magalef's succession model (Margalef, 1978), to the rise of motile and mixotrophic dinoflagellates over diatoms. Moreover, the enhanced stratification could also increase the chance of episodic outburst of phytoplankton biomass during high river discharge (Lowery, 1998; Rabalais et al., 2014). Alternatively, such water column condition could lead to a main assemblage succession sensu Reynolds (2006) from high surface/volume colonist species to biomass conserving stress-tolerant species (Reynolds, 2006). The reduction in phytoplankton size in stratified conditions should also lead to a change in trophic fluxes with an increased importance of the microbial loop pathway for zooplankton grazing (Lewandowska et al., 2014). Moreover, the reduced connectivity between the two sides could increase the sensitivity of the habitat to local events such as droughts or freshwater pulses, which are mostly non-periodic. As concerns phytoplankton community, an increasing disorder in the succession of assemblages has been observed in the GoT in recent years (Vascotto et al., 2021) possibly indicating a loss in connectivity.

The 11th Workshop of International Association of Phytoplankton Taxonomy and Ecology (IAP) proposed 10 rules for the formation of community assembly (Reynolds et al., 2000). According to these, the factors determining a particular assemblage at a particular point of time are not only those determining the realised niche, but they also depend on the precedent state of the community and stochasticity (Reynolds et al., 2000). In the present study, the physical parameters considered are those associated with the formation of realised phytoplankton niches, e.g., temperature and salinity (Irwin et al., 2012; Brun et al., 2015), stratification and river discharge (Kemp and Villareal, 2018) and we found differences in taxonomic composition under similar environmental conditions and consequently similar realised niches. The presence in our results of different indicative phytoplankton taxa inside the same niche can be explained in the light of IAP's rules. Moreover, the differences in taxonomic composition under similar conditions seem to indicate a pattern of community succession consistent with the lumpy coexistence theory (Scheffer and van Nes, 2006). Within this theory, Sakavara et al. (2018) showed that assemblage-like structures arise from resource fluctuations (Sakavara et al., 2018). In line with this recent ecological theory, the periodic components of our niche-forming environmental parameters were key in building working models for the assemblages' phenology. There is a close relationship between IAP's rules and lumpy coexistence theory that has not been pointed out so far in literature. The concepts of niche and stochasticity coexist in both frameworks and both can explain the complex patterns seen in the formation of phytoplankton assemblages in our results.

5. Conclusions

In this study, we investigated the relative importance of environmental factors and temporal periodicity in governing the structure of the phytoplankton community in the northern Adriatic. We also aimed to determine whether the influence of these factors extends to the mesoscale. The results show that there is an overlap of phenomena in the northern Adriatic, with both widespread periodic processes and local non-periodic events affecting the phytoplankton community at the basin scale. A portion of the phytoplankton assemblages have similar indicative taxa or respond similarly to the environment at the basin-wide level. Here, autocorrelation contributes to the explanatory power of environmental factors and suggests that the northern Adriatic can be treated partially as a single environment when considering periodic patterns of recurrent phytoplankton assemblages. In the context of global climate change, the connectivity of this environment and the existence and succession of phytoplankton assemblages are threatened by the reduction of wind-driven circulation and the increasing disorder of environmental conditions. Both IAP's rules for community assembly and lumpy coexistence theory explain the taxa composition in our phytoplankton assemblages drawing a connection between the two models.

Declaration of generative AI in scientific writing

During the preparation of this work the authors used InstaText (https://instatext.io/) to check the grammar and style. After using this tool/service, the authors reviewed and edited the content as needed and take full responsibility for the content of the publication.

CRediT authorship contribution statement

Ivano Vascotto: Conceptualization, Formal analysis, Methodology, Writing – original draft, Writing – review & editing, Visualization. **Fabrizio Bernardi Aubry:** Supervision, Writing – review & editing. **Mauro Bastianini:** Data curation, Writing – review & editing. **Patricija Mozetič:** Supervision, Writing – review & editing. **Stefania Finotto:** Resources. **Janja Francé:** Conceptualization, Supervision, Writing – review & editing.

Declaration of competing interest

The authors declare that they have no known competing financial interests or personal relationships that could have appeared to influence the work reported in this paper.

Data availability

The raw environmental data from the GoT can be found at the following links; for the oceanographic data: https://www.nib.si/mbp/en/oceanographic-data-and-measurements/buoy-2/new-scalar-plots, for the river discharge data: https://www.arso.gov.si/en/water/data/,and for the meteorological data: https://meteo.arso.gov.si/met/sl/archive/.

The raw phytoplankton data and the environmental parameters from GoV are stored in the Marine Data Archive (MDA) https://marinedataarchive.org/ following the public directory path: ASSEMBLE Plus - Public/TA Data/North Adriatic Phytoplankton Assemblages/.

The assemblage's probability and Indicative Index results are stored in the Marine Data Archive (MDA) and are findable at IMIS record https://www.vliz.be/en/imis?module=dataset&dasid=8110.

The R code for the Moran's eigenvector decomposition and RDA as well as the Python code for the neural network construction and training can be found in the public repository GitHub at the following link: https://github.com/ivanovascotto/NorthAdriaticPhytoplanktonAssemblages.

Acknowledgements

The research leading to these results received funding from the European Union's Horizon 2020 research and innovation programme under grant agreement No 730984, ASSEMBLE Plus project and by Slovenian Research Agency (ARIS), grant number P1-0237.

The GoT and the GoV are included in the Italian (LTER-Italy) and Slovenian (LTER-Slovenia), European (LTER-Europe) and International (LTER-International) Long-Term Ecological Research (LTER)

networks: the time series analysed in this paper was gathered in the context of these networks. Phytoplankton data of the Slovenian LTER originates from the national monitoring program financed by the Slovenian Environment Agency of the Ministry of Environment and Spatial Planning.

Authors wish to thank Milijan Šiško for phytoplankton species identification and enumeration, the crew of R/V Sagita for the field work and curators of oceanographic buoy Vida for data generation.

Appendix A. Supplementary data

Supplementary data to this article can be found online at https://doi.org/10.1016/j.scitotenv.2023.169814.

References

Abadi, M., A. Agarwal, P. Barham, E. Brevdo, Z. Chen, C. Citro, G. S. Corrado, A. Davis, J. Dean, M. Devin, S. Ghemawat, I. Goodfellow, A. Harp, G. Irving, M. Isard, R. Jozefowicz, Y. Jia, L. Kaiser, M. Kudlur, J. Levenberg, D. Mané, M. Schuster, R. Monga, S. Moore, D. Murray, C. Olah, J. Shlens, B. Steiner, I. Sutskever, K. Talwar, P. Tucker, V. Vanhoucke, V. Vasudevan, F. Viégas, O. Vinyals, P. Warden, M. Wattenberg, M. Wicke, Y. Yu and X. Zheng (2015). "TensorFlow: Large-scale machine learning on heterogeneous systems.".

Alberotanza, L., Chiggiato, J., Profeti, G., 2004. Analysis of the seasonal stratification at the Acqua Alta oceanographic tower, northern Adriatic Sea. Int. J. Remote Sens. 25 (7–8), 1473–1480.

Ali, E., Cramer, W., Carnicer, J., Georgopoulou, E., Hilmi, N.J.M., Le Cozannet, G., Lionello, P., 2022. Cross-chapter paper 4: Mediterranean region. Climate change 2022: Impacts, adaptation and vulnerability. In: Pörtner, H.O., Roberts, D.W., Tignor, M., et al. (Eds.), Contribution of Working Group II to the Sixth Assessment Report of the Intergovernmental Panel on Climate Change. Cambridge University Press, Cambridge, UK and New York, NY, USA, pp. 2233–2272.

Ayata, S.-D., Irisson, J.-O., Aubert, A., Berline, L., Dutay, J.-C., Mayot, N., Nieblas, A.-E., D'Ortenzio, F., Palmiéri, J., Reygondeau, G., Rossi, V., Guieu, C., 2018. Regionalisation of the Mediterranean basin, a MERMEX synthesis. Prog. Oceanogr. 163, 7–20.

Bernardi Aubry, F., Cossarini, G., Acri, F., Bastianini, M., Bianchi, F., Camatti, E., De Lazzari, A., Pugnetti, A., Solidoro, C., Socal, G., 2012. Plankton communities in the northern Adriatic Sea: patterns and changes over the last 30 years. Estuar. Coast. Shelf Sci. 115, 125–137.

Blasius, B., Huppert, A., Stone, L., 1999. Complex dynamics and phase synchronization in spatially extended ecologicals ystems. Nature 27, 354–359.

Boicourt, W.C., Ličer, M., Li, M., Vodopivec, M., Malačič, V., 2021. Sea State: Recent Progress in the Context of Climate Change. Coastal Ecosystems in Transition: A Comparative Analysis of the Northern Adriatic and Chesapeake Bay. John Wiley & Sons, Malone C. Thomas, A. Malej and J. Faganeli.

Brind'Amour, A., Mahévas, S., Legendre, P., Bellanger, L., 2018. Application of Moran eigenvector maps (MEM) to irregular sampling designs. Spatial Statistics 26, 56–68.

Brun, P., Vogt, M., Payne, M.R., Gruber, N., O'Brien, C.J., Buitenhuis, E.T., Le Quéré, C., Leblanc, K., Luo, Y.-W., 2015. Ecological niches of open ocean phytoplankton taxa. Limnol. Oceanogr. 60 (3), 1020–1038.

Brush, M.J., Mozetič, P., Francé, J., Aubry, F.B., Djakovac, T., Faganeli, J., Harris, L.A., Niesen, M., 2021. Phytoplankton Dynamics in a Changing Environment. John Wiley & Sons.

Cabrini, M., Fornasaro, D., Cossarini, G., Lipizer, M., Virgilio, D., 2012. Phytoplankton temporal changes in a coastal northern Adriatic site during the last 25 years. Estuar. Coast. Shelf Sci. 115, 113–124.

Cerino, F., Fornasaro, D., Kralj, M., Giani, M., Cabrini, M., 2019. Phytoplankton temporal dynamics in the coastal waters of the North-Eastern Adriatic Sea (Mediterranean Sea) from 2010 to 2017. Nature Conserv. 34, 343–372.

Cibic, T., Comici, C., Bussani, A., Del Negro, P., 2012. Benthic diatom response to changing environmental conditions. Estuar. Coast. Shelf Sci. 115, 158–169.

Cloern, J.E., Jassby, A.D., 2010. Patterns and scales of phytoplankton variability in estuarine-coastal ecosystem. Estuar. Coasts 33, 230–241.

Cozzi, S., Giani, M., 2011. River water and nutrient discharges in the northern Adriatic Sea: current importance and long term changes. Cont. Shelf Res. 31 (18), 1881–1893.

Degobbis, D., Precali, R., Ivancic, I., Smodlaka, N., Fuks, D., Kveder, S., 2000. Long-term changes in the northern Adriatic ecosystem related to anthropogenic eutrophication. Int. J. Environ. Pollut. 13 (1–6), 495–533.

d'Ovidio, F., De Monte, S., Alvain, S., Dandonneau, Y., Levy, M., 2010. Fluid dynamical niches of phytoplankton types. Proc. Natl. Acad. Sci. U. S. A. 107 (43), 18366–18370.

Dray, S., G. Blanchet, D. Borcard, G. Guenard, T. Jombart, G. Larocque, P. Legendre, N. Madi and H. H. Wagner (2016). "adespatial: Multivariate Multiscale Spatial Analysis. R package version 0.0–7.".

Dufrene, M., Legendre, P., 1997. Species assemblages and Indicator species: the need for a flexible asymmetrical approach. Ecol. Monogr. 67 (3), 345.

Francé, J., Varkitzi, I., Stanca, E., Cozzoli, F., Skejić, S., Ungaro, N., Vascotto, I., Mozetič, P., Ninčević Gladan, Ž., Assimakopoulou, G., Pavlidou, A., Zervoudaki, S., Pagou, K., Basset, A., 2021. Large-scale testing of phytoplankton diversity indices for environmental assessment in Mediterranean sub-regions (Adriatic, Ionian and Aegean seas). Ecol. Indic. 126, 107630.

Gačic, M., Lascaratos, A., Manca, B.B., Mantziafau, A., 2001. Adriatic deep water and interaction with the easter mediterranean sea. Physical oceanography of the Adriatic Sea; past present future. B. Cushman-Roisin, M. Gačić, P.-M. Poulain and A. Artegiani, Kluwer Academic Publishers. 6, 111–142.

Godrijan, J., Marić, D., Tomažić, I., Precali, R., Pfannkuchen, M., 2013. Seasonal phytoplankton dynamics in the coastal waters of the North-Eastern Adriatic Sea. J. Sea Res. 77, 32–44.

Harding, L., 1994. Long-term trends in the distribution of phytoplankton in Chesapeake Bay: roles of light, nutrients and streamflow. Mar. Ecol.: Prog Ser. 104, 267–291.

Hubbel, S.P., 2005. The neutral theory of biodiversity and biogeography and Stephen jay Gould. Paleobiology 31 (2), 122–132.

Hutchinson, G.E., 1941. Ecological aspects of succession in natural populations. Am. Nat. 75 (760), 406–418.

Irwin, A.J., Nelles, A.M., Finkel, Z.V., 2012. Phytoplankton niches estimated from field data. Limnol. Oceanogr. 57 (3), 787–797.

Jeffries, M.A., Lee, C.M., 2007. A climatology of the northern Adriatic Sea's response to bora and river forcing. J. Geophys. Res. 112.

Jenkins, D.G., Ricklefs, R.E., 2011. Biogeography and ecology: two views of one world. Philos. Trans. R. Soc. Lond. Ser. B Biol. Sci. 366 (1576), 2331–2335.

Kemp, A.E.S., Villareal, T.A., 2018. The case of the diatoms and the muddled mandalas: time to recognize diatom adaptations to stratified waters. Prog. Oceanogr. 167, 138–149.

Legendre, P., Legendre, L., 2012. Numerical ecology. Elsevier.

Levy, M., Jahn, O., Dutkiewicz, S., Follows, M.J., d'Ovidio, F., 2015. The dynamical landscape of marine phytoplankton diversity. J. R. Soc. Interface 12 (111), 20150481.

Levy, M., Franks, P.J.S., Smith, K.S., 2018. The role of submesoscale currents in structuring marine ecosystems. Nat. Commun. 9 (1), 4758.

Lewandowska, A.M., Boyce, D.G., Hofmann, M., Matthiessen, B., Sommer, U., Worm, B., 2014. Effects of sea surface warming on marine plankton. Ecol. Lett. 17 (5), 614–623.

Lionello, P., 2012. The climate of the venetian and north Adriatic region: variability, trends and future change. Phys. Chem. Earth 40-41 (1–8).

Lowery, T.A., 1998. Modelling estuarine eutrophication in the context of hypoxia, nitrogen loadings, stratification and nutrient ratios. J. Environ. Manag. 52 (3), 289–305.
Maier, H.R., Dandy, G.C., 2000. Neural networks for the prediction and forecasting of water resources variables: a review of modelling issues and applications. Environ. Model Softw. 15, 101–124.
Malačič, V., Petelin, B., 2001. In: Cushman-Roisin, B., Gačić, M., Poulain, P.-M., A. (Eds.), Regional Studies. Physical Oceanography of the Adriatic Sea: Past, Present, and Future. Artegiani, Kluwer Academic Publishers, pp. 167–181.
Malačič, V., Petelin, B., 2009. Climatic circulation in the Gulf of Trieste (northern Adriatic). J. Geophys. Res. Oceans 114 (C7).
Malačič, V., Celio, M., Čermelj, B., Bussani, A., Comici, C., 2006. Interannual evolution of seasonal thermohaline properties in the Gulf of Trieste (northern Adriatic) 1991–2003. J. Geophys. Res. 111 (C8).
Malačič, V., Petelin, B., Vodopivec, M., 2012. Topographic control of wind-driven circulation in the northern Adriatic. J. Geophys. Res. Oceans 117 (C6).
Malej, A., Mozetič, P., Malačič, V., Turk, V., 1997. Response of summer phytoplankton to episodic meteorological events (gulf of Trieste, Adriatic Sea). Mar. Ecol. 18 (3), 273–288.
Margalef, R., 1978. Life-forms of phytoplankton as survival alternatives in an unstable environment. Oceanol. Acta 1 (4), 493–509.
Marić Pfannkuchen, D., Godrijan, J., Smodlaka Tanković, M., Baričević, A., Kužat, N., Djakovac, T., Pustijanac, E., Jahn, R., Pfannkuchen, M., 2018. The ecology of one cosmopolitan, one newly introduced and one occasionally advected species from the genus Skeletonema in a highly structured ecosystem, the northern Adriatic. Microb. Ecol. 75, 674–687.
Marić, D., Kraus, R., Godrijan, J., Supić, N., Djakovac, T., Precali, R., 2012. Phytoplankton response to climatic and anthropogenic influences in the north-eastern Adriatic during the last four decades. Estuar. Coast. Shelf Sci. 115, 98–112.
Martin, A.P., 2003. Phytoplankton patchiness: the role of lateral stirring and mixing. Prog. Oceanogr. 57 (2), 125–174.
May, R., 1976. Simple mathematical models with very complicated dynamics. Nature 261 (459–467).
Mozetič, P., Fonda Umani, S., Cataletto, B., Malej, A., 1998. Seasonal and inter-annual plankton variability in the Gulf of Trieste (northern Adriatic). J. Mar. Sci. 55 (711–722).
Mozetič, P., Francé, J., Kogovšek, T., Talaber, I., Malej, A., 2012. Plankton trends and community changes in a coastal sea (northern Adriatic): bottom-up vs. top-down control in relation to environmental drivers. Estuar. Coast. Shelf Sci. 115, 138–148.
Neri, F., Romagnoli, T., Accoroni, S., Campanelli, A., Marini, M., Grilli, F., Totti, C., 2022. Phytoplankton and environmental drivers at a long-term offshore station in the northern Adriatic Sea (1988–2018). Cont. Shelf Res. 242, 104746.
Oksanen, J., Blanchet, F.G., Kindt, R., Legendre, P., Minchin, P.R., O'hara, R.B., Simpson, G.L., Solymos, P., Stevens, M.H.H., Wagner, H., Oksanen, M.J., 2013. Package 'vegan. Community ecology package, version 2 (9), 1–295.
Orlanski, I., 1975. A rational subdivision of scales for atmospheric processes. Bull. Am. Meteorol. Soc. 56 (5), 527–530.
Petelin, B., Kononenko, I., Malačič, V., Kukar, M., 2013. Multi-level association rules and directed graphs for spatial data analysis. Expert Syst. Appl. 40 (12), 4957–4970.
Pirazzoli, P.A., Tomasin, A., 2002. Recent evolution of surge-related events in the northern Adriatic area. J. Coast. Res. 537–554.
Platt, T., Denmann, K.L., 1975. Spectral analysis in ecology. Annu. Rev. Ecol. Syst. 6, 189–210.
Poulain, P.-M., Kourafalou, V.H., Cushman-Roisin, B., 2001. In: Cushman-Roisin, B., Gačić, M., Poulain, P.-M., A. (Eds.), Northern Adriatic Sea. Physical Oceanography of the Adriatic Sea: Past, Present, and Future. Artegiani, Kluwer Academic Publishers, pp. 167–181.
Ptacnik, R., Solimini, A.G., Andersen, T., Tamminen, T., Brettum, P., Lepistö, L., Willén, E., Rekolainen, S., 2008. Diversity predicts stability and resource use efficiency in natural phytoplankton communities. Proc. Nat. Acad. Sci. U.S.A 105 (13), 5134–5138.
Rabalais, N.N., Cai, W.-J., Carstensen, J., Conley, D.J., Fry, B., Hu, X., Quinones-Rivera, Z., Rosenberg, R., Slomp, C.P., Turner, R.E., 2014. Eutrophication-driven deoxygenation in the coastal ocean. Oceanography 27 (1), 172–183.
Reynolds, C., 1980. Phytoplankton assemblages and their periodicity in stratifying Lake systems. Holoartic Ecol. 3 (3), 141–159.
Reynolds, C.S., 2006. The Ecology of Phytoplankton. Cambridge University Press.
Reynolds, C., Dokulil, M., Padisák, J., 2000. Understanding the assembly of phytoplankton in relation to the trophic spectrum: where are we now? Hydrobiologia 424, 147–152.
Ribera d'Alcalà, M., Conversano, F., Corato, F., Licandro, P., Mangoni, O., Marino, D., Mazzochi, M.G., Modigh, M., Montresor, M., Nardella, M., Saggiomo, V., Sarno, D., Zingone, A., 2004. Seasonal patterns in plankton communities in a pluriannual time series at a coastal Mediterranean site (gulf of Naples): an attempt to discern recurrences and trends. Sci. Mar. 68 (1), 65–83.
Ricklefs, R.E., Jenkins, D.G., 2011. Biogeography and ecology: towards the integration of two disciplines. Philos. Trans. R. Soc. Lond. Ser. B Biol. Sci. 366 (1576), 2438–2448.
Roelke, D.L., Spatharis, S., 2015a. Phytoplankton assemblage characteristics in recurrently fluctuating environments. PLoS One 10 (3), e0120673.
Roelke, D.L., Spatharis, S., 2015b. Phytoplankton succession in recurrently fluctuating environments. PLoS One 10 (3), e0121392.
Sakavara, A., Tsirtsis, G., Roelke, D.L., Mancy, R., Spatharis, S., 2018. Lumpy species coexistence arises robustly in fluctuating resource environments. PNAS 115 (4), 738–743.
Salgado-Hernanz, P.M., Racault, M.F., Font-Muñoz, J.S., Basterretxea, G., 2019. Trends in phytoplankton phenology in the Mediterranean Sea based on ocean-colour remote sensing. Remote Sens. Environ. 221, 50–64.
Scheffer, M., van Nes, E.H., 2006. Self-organized similarity, the evolutionary emergence of groups of similar species. Proc. Natl. Acad. Sci. U. S. A. 103 (16), 6230–6235.
Soininen, J., 2010. Species turnover along abiotic and biotic gradients: patterns in space equal patterns in time? BioScience 60 (6), 433–439.
Stone, L., 1993. Period-doubling reversals and chaos in simple ecological models. Nature 365, 617–620.
Talaber, I., Francé, J., Mozetič, P., 2014. How phytoplankton physiology and community structure adjust to physical forcing in a coastal ecosystem (northern Adriatic Sea). Phycologia 53 (1), 74–85.
Tobler, W.R., 1970. A computer movie simulating urban growth in the Detroit region. Econ. Geogr. 46, 234–240.
Totti, C., Romagnoli, T., Accoroni, S., Coluccelli, A., Pellegrini, M., Campanelli, A., Grilli, F., Marini, M., 2019. Phytoplankton communities in the northwestern Adriatic Sea: Interdecadal variability over a 30-years period (1988–2016) and relationships with meteoclimatic drivers. J. Mar. Syst. 193, 137–153.
Turk Dermastia, T., Cerino, F., Stankovic, D., France, J., Ramsak, A., Znidaric Tusek, M., Beran, A., Natali, V., Cabrini, M., Mozetic, P., 2020. Ecological time series and integrative taxonomy unveil seasonality and diversity of the toxic diatom pseudo-nitzschia H. Peragallo in the northern Adriatic Sea. Harmful Algae 93, 101773.
Vallina, S.M., Follows, M.J., Dutkiewicz, S., Montoya, J.M., Cermeno, P., Loreau, M., 2014. Global relationship between phytoplankton diversity and productivity in the ocean. Nat. Commun. 5, 4299.
Vascotto, I., Mozetič, P., Francé, J., 2021. Phytoplankton time-series in a LTER site of the Adriatic Sea: methodological approach to decipher community structure and indicative taxa. Water 13 (15), 2045.
Vilicic, D., Kuzmic, M., Tomažić, I., Ljubešić, Z., Bosak, S., Precali, R., Djakovac, T., Marić, D., Godrijan, J., 2013. Northern Adriatic phytoplankton response to short Po River discharge pulses during summer stratified conditions. Mar. Ecol. 34 (4), 451–466.
Winder, M., Cloern, J.E., 2010. The annual cycles of phytoplankton biomass. Philosophical Transaction of The Royal Society 365, 3215–3226.
Zhang, Q., Cozzi, S., Palinkas, C., Giani, M., 2020. Recent status and long-term trends in freshwater discharge and nutrient inputs. Coastal Ecosystems in Transition: A Comparative Analysis of the Northern Adriatic and Chesapeake Bay 7–19.

Chapter 4

Traits Distribution and Dynamic

4.1 Phytoplankton Morphological Traits and Biomass Outline Community Dynamics in a Coastal Ecosystem (Gulf of Trieste, Adriatic Sea)

This chapter broadens the investigation on phytoplankton phenology and ecology using other types of measures. Individual-based biological data collected in the LTER site in the Gulf of Trieste between April 2020 and March 2021 is presented. In this study, inverted microscopy was used to measure individual cell size (maximum linear dimension), biovolume, and biomass, categorizing phytoplankton cells by taxonomic groups and morphological shapes. The differences between taxonomical and traits classification were observed as well as the differences between abundance and biomass parameters. Starting from the level of individual phytoplankton cells and the level of main taxonomic groups, the chapter explores the distribution of these parameters at the level of the whole community. Statistical tests assess the unimodality or bimodality of the size and biomass distributions, while the conformity of these distributions to power-law models is evaluated. Diversity metrics and environmental data are integrated to broaden the comparison and to investigate the ecological drivers of community dynamics. The phenology of these parameters as well as their distributions are discussed considering the connections between environment and phytoplankton community.

Key findings include:

I. Community composition: The phenology of abundances and biomasses mostly matched while their contribution to total diversity did not.

II. Shape as a diversity proxy: The shape trait proved effective as a substitute for taxonomy in assessing the diversity of the phytoplankton community.

III. Organization of phytoplankton size classes: Seasonal dynamics was evident, with bimodal size distributions during blooms and unimodal patterns during low biomass periods.

IV. Trophic network shifts: Deviations from the power-law distribution of biomass indicated shifts between stable trophic networks and unconstrained growth phases.

The findings indicate that individual morphological traits are useful to understand the dynamics of the phytoplankton community. They serve as proxies for diversity assessments and reflect the interplay between ecological drivers and the stability of trophic networks in coastal ecosystems.

Goal:

I. Explore the (de)coupling of individual cell traits (biomass, size, shape and taxonomy) of the phytoplankton community in the Gulf of Trieste.

Hypothesis:

I. The individual cell traits of the phytoplankton biomass follow a power law. Deviations from this are linked to trophic conditions and can be interpreted on the basis of data on cell size, shape and taxonomy.

The goal is accomplished, and the hypothesis is confirmed by the results presented in this chapter.

The research work is presented in the following publication and is listed below:

Vascotto, I., Mozetič, P., & Francé, J. (2024). Phytoplankton morphological traits and biomass outline community dynamics in a coastal ecosystem (Gulf of Trieste, Adriatic Sea). Community Ecology, 1-14.

Ivano Vascotto contributed to this paper as follows: conceptualization, formal analysis, methodology, writing – original draft, writing – review & editing, visualization.

Community Ecology
https://doi.org/10.1007/s42974-024-00215-4

ORIGINAL ARTICLE

Phytoplankton morphological traits and biomass outline community dynamics in a coastal ecosystem (Gulf of Trieste, Adriatic Sea)

Ivano Vascotto[1,2,3] · Patricija Mozetič[3] · Janja Francé[3]

Received: 31 January 2024 / Accepted: 10 September 2024

Abstract
Trait-based ecology has recently gained increasing importance in phytoplankton research. In particular, the taxonomic and morphological traits, such as size and shape of phytoplankton cells, can help to unveil the ecological processes and their drivers in the pelagic domain. Our study aims to shed light on the trophodynamics of phytoplankton communities in a coastal ecosystem in the northern Adriatic Sea (Gulf of Trieste) using data on individual traits such as biomass, size and shape of phytoplankton taxa during a one-year study. The phytoplankton parameters were investigated at the levels of the whole community, groups, and individual cells, analysing also the probability distributions of biomass and size of the latter level. The results showed good agreement between abundance and biomass data, as well as individual size and biomass with differences partly explained by cell shapes. We have emphasized the role of the local freshwater source in bottom-up control, alternating with top-down control of phytoplankton dynamics through taxonomic and morphological diversity. The predominant bimodal and non-power law distribution, especially during and around the biomass peaks, confirmed the importance of nano- and microphytoplankton size classes and the role of blooms in destabilizing the trophic webs. We suggest that the analyses of distribution types of individual cell size and biomass can be appropriate to spot ecological processes driving to unconstrained phytoplankton proliferation or to periods of trophic web stability.

Keywords Phytoplankton · Biomass · Size · Power law · Northern Adriatic

Introduction

Phytoplankton communities play an important role in marine ecosystems, as they are the gateway to pelagic food chains and are critical to biogeochemical cycling in the seas and oceans (Falkowski et al., 2003; Hays et al., 2005). The common characteristics used to describe phytoplankton communities and their dynamics are biomass, abundance, and taxonomic composition, with biomass, expressed as chlorophyll-a concentration, being largely used in ecological studies because it overwhelms all photoautotrophic microorganisms regardless of their size and taxonomic affiliation. As such, chlorophyll-a biomass is a suitable indicator for assessing the ecological or trophic status of water bodies in the context of various environmental policies (e.g. European Directives 2000/60/ EC and 2008/56/ EC) (Varkitzi et al., 2018). On the other hand, biomass in the form of cellular carbon is used as a crucial parameter to define the phytoplankton component in the study of biogeochemical cycles or in ecosystem modelling (Aumont et al., 2015; Falkowski et al., 2003). Carbon biomass is usually calculated from cell biovolume through standard conversion factors (Menden-Deuer & Lessard, 2000; Socal et al., 2010), and biovolume in turn depends on cell size, which is therefore a very important measurable phytoplankton trait (Finkel et al., 2009). Indeed, according to the "metabolic theory" of Brown (2004), body size is one of the three key factors along with temperature and stoichiometry that influence individual's metabolism and consequently community ecology. Body, i.e. cell size in phytoplankton, was recognized to offer potential advantages over standard taxonomic descriptors in community organization studies (Vadrucci et al., 2007),

✉ Ivano Vascotto
ivascotto@ogs.it

[1] Jozef Stefan International Postgraduate School, Jamova Cesta 39, 1000 Ljubljana, Slovenia

[2] National Institute of Oceanography and Applied Geophysics, Borgo Grotta Gigante, 42/C, 34010 Sgonico, TS, Italy

[3] National Institute of Biology, Marine Biology Station Piran, Fornače 41, 6330 Piran, Slovenia

Published online: 02 October 2024

and is, along with the associated value of biovolume of critical importance in allometric studies (Beardall et al., 2009; Niklas, 2004; Verdy et al., 2009). In addition, cell size is among the functional traits that regulate competitive ability (e.g. nutrient uptake rates, growth rates) (Nock et al., 2016) and has as such a pivotal role in the field of trait based ecology of phytoplankton (Litchman & Klausmeier, 2008).

When coming to distributional properties, phytoplankton biomass is often assumed to follow the power law (Kostadinov et al., 2009, 2010; Kriest & Evans, 1999; Niklas, 2004), which has been shown to be correct on a global scale (Perkins et al., 2019). Under such an assumption, the biomass is uniformly distributed along log-scaled body size classes and its distribution describes a line in a log–log frequency biomass diagram (Sheldon et al., 1972). Since the literature on power law distribution of phytoplankton size uses the term "size" in the sense of "body size", "biovolume" or "biomass" (Andersen et al., 2016; Finkel et al., 2009; Heneghan et al., 2019; Marquet et al., 2005), it is not clear whether the body size parameters of phytoplankton (for example length, diameter), also follow a power law. It has been suggested that the power law distribution can emerge from stable trophic networks (Bascompte, 2007; Newman, 2005) and that deviations from this distribution indicate the presence of ecological processes and human impacts operating at specific organism sizes and spatial scales (Armstrong, 1999; Cavender-Bares et al., 2001; Hatton et al., 2021). When biomass is assessed at the mesoscale, deviations from the power law are found in nearshore marine waters and in freshwater ecosystem (Sprules, 1988; Witek & Krajewska-Soltys, 1989). Such deviations have been associated with the seasonal blooms (Witek & Krajewska-Soltys, 1989) and with shifts from bottom-up to top-down control (Sprules, 1988). From these studies, it emerges that knowledge about cell size distribution provides valuable information not only about the phytoplankton community, but also about the state of its ecological relationships with other biological components (for example, zooplankton).

Referring to the cell size as maximum linear dimension (MLD), phytoplankton is usually classified in one of the three phytoplankton size classes (PSCs): picoplankton (0.2–2 µm), nanoplankton (2–20 µm) and microplankton (20–200 µm) (Sieburth et al., 1978). In the marine environment, the apportionment of biomass among PSCs is influenced by various biotic and abiotic factors, where, in general, the pico-fraction is advantaged at higher temperatures (Andersson et al., 1994), the nanofraction is advantaged at low nutrient concentrations, while microfraction is advantaged during nutrient pulses and in exploiting vertical gradients (Sommer et al., 2017). Also, the nanofraction is more affected by grazing by protists and pelagic tunicates, while the microfraction is more affected by larger zooplanktonic grazers (Sommer et al., 2017).

In addition to size, other morphological, behavioural and physiological traits are important in defining the properties of resource acquisition and predator avoidance, namely mixotrophy, motility, shape, life forms (single cell vs. colony), and surface to volume ratio (Durante et al., 2019; Leonilde et al., 2017; Roselli & Litchman, 2017; Weithoff & Gaedke, 2016). In this context, cell shape not only plays a crucial role in defining the biomass of a cell, but also have an influence on the efficiency of resource utilization in phytoplankton as well (Ryabov et al., 2022). In fact, elongated shapes allow for a greater surface area to volume ratio, which maximizes nutrient uptake and improves chloroplast packing (Naselli-Flores & Barone, 2011). Shape irregularities in the form of spines, appendages and flagella (Sonnet et al., 2022) also prevent sinking, increase resistance to grazing and improve the displacement capacity of cells towards better nutrient and light conditions (Durante et al., 2019; Stanca et al., 2013). As a morpho-functional trait, shape is more effective than a simple taxonomic hierarchy in grouping ecologically similar species (Roselli et al., 2022) and, together with size, determine the morphological optimum for speciation and thus maximum diversity (Ryabov et al., 2022). The temporal dynamics of phytoplankton shape composition have been described as highly variable over the course of the year and without clear seasonality (Sonnet et al., 2022), but opposite results have been published as well (Stanca et al., 2013).

Estimates of phytoplankton cellular carbon based on time-consuming measurements of species biovolume are not routinely assessed in ecological time series in the area of interest (Gulf of Trieste, northern Adriatic Sea) and have been used only sporadically in studies on the partitioning of organic carbon among different compartments of the coastal ecosystem (Malej et al. 2003). In this work, we investigate the first annual time series of phytoplankton cell size and biomass by direct microscopic measurements, which were assessed at the level of total community, groups and individual cells (Fig. 1). In addition, we analysed the distributional properties of phytoplankton individual cell size (as MLD) and biomass and their consistency with the power law to infer the fate of phytoplankton biomass in the pelagic trophic interactions. To supplement this, we examined the diversity of taxa and their shape, which highlight important ecological processes and help interpret the trophodynamics since the trophic status and structure of the phytoplankton community in the Gulf of Trieste changed significantly after the turn of the century (Brush et al., 2021; Mozetič et al., 2012).

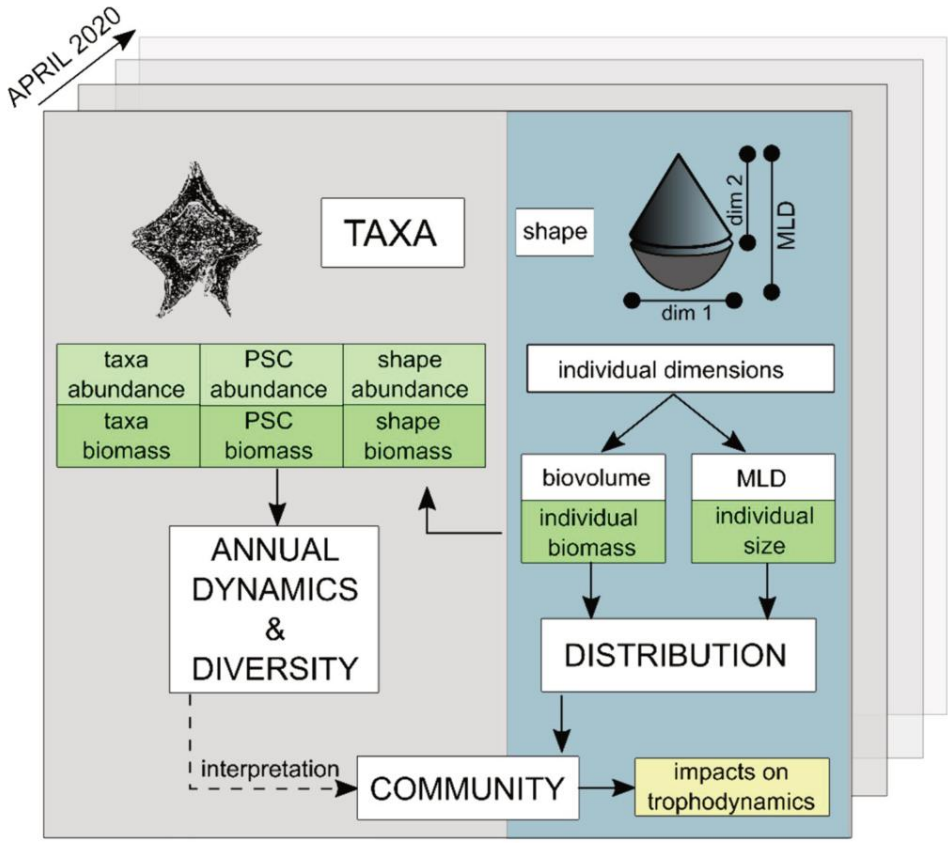

Fig. 1 Scheme of the relations between analysed phytoplankton parameters, the estimation methods, and objectives of the study. In green the parameters estimated in this study, in yellow the goals. (MLD = Maximum Linear Dimension; PSC = Phytoplankton Size Class)

Material and methods

The study area

The Gulf of Trieste (GoT) is a shallow basin surrounded by land at the north-eastern tip of the Adriatic Sea. This basin is very shallow (about 20 m on average) and is strongly influenced by meteorological conditions. The water column in the GoT is seasonally mixed and stratified (Malačič et al., 2006), and the euphotic zone considerably exceeds the depth of the upper mixed layer (Talaber et al., 2014). The sampling station 000F is located at the southern entrance of the GoT (Fig. 2) and represents the Slovenian long-term ecological research (LTER) site. The waters around the LTER station are generally crossed by the North Adriatic Dense Water (NAdDW) current and influenced by the river plume of the largest freshwater source in the GoT—the Soča (Isonzo) River (Fig. 2)(Zhang et al., 2020).

Phytoplankton exhibits strong seasonal fluctuations and large interannual variability in GoT and broader in the northern Adriatic (Brush et al., 2021; Totti et al., 2019). Usually, phytoplankton shows two seasonal peaks, first in late spring, which is inconstant and short-lived, and second larger and more constant in autumn (Vascotto et al., 2021). During blooms, phytoplankton community is mainly dominated by

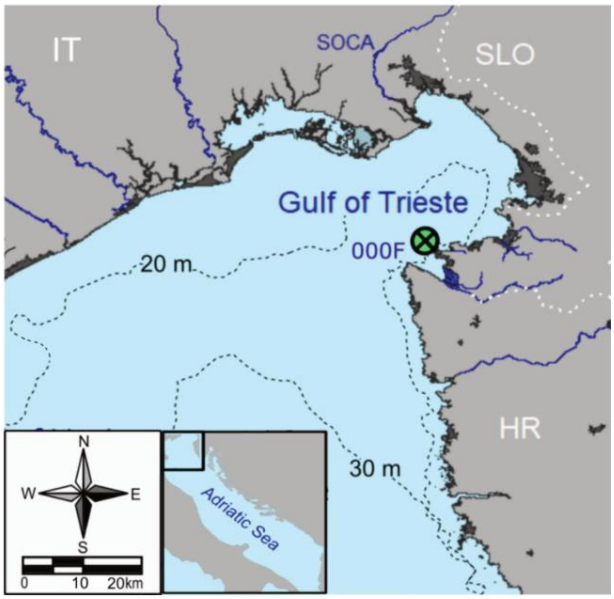

Fig. 2 Map of the study site: the sampling stations, 000F, represent the LTER site, Gulf of Trieste—Slovenia

diatoms, while during periods of low chlorophyll-a concentrations small cells (nanoflagellates, coccolithophores) prevail (Brush et al., 2021; Talaber et al., 2018). In this area, a trend towards oligotrophication and a decline in production has been observed in early 2000s (Mozetič et al., 2010), leading to the situation of low phytoplankton biomass strongly influenced by meteoclimatic variability (Brush et al., 2021). Recently, more irregularity was observed in the formation of typical assemblages that was attributed to mesoscale climatic and hydrological drivers (Vascotto et al., 2021). Daily flows of the Soča River, measured approx. 45 km upstream, were downloaded from the web page of the Environmental Agency of the Republic of Slovenia (https://vode.arso.gov.si/hidarhiv/pov_arhiv_tab.php).

Biomass determination

Size, biovolume and cellular carbon

A year-long campaign of monthly sampling was conducted at sampling station 000F from April 2020 to March 2021. Phytoplankton samples were collected at the surface with Niskin bottles and fixed with neutralized formaldehyde. 50 ml of samples were then analysed with an inverted microscope ZEISS AxioObserver.Z1 using the Utermöhl method (Utermöhl, 1958), with either counting and measuring phytoplankton cells in a minimum of 100 fields at 400× magnification or alternatively counting and measuring 1000 phytoplankton cells in a sample. After examining the sample at 400× magnification, half sedimentation chamber was scanned at 100× magnification to check for bigger specimens. Phytoplankton cells were determined to the lowest taxonomic level possible and assigned to one of the main phytoplankton groups (diatoms, dinoflagellates, coccolithophores, silicoflagellates, cryptophytes, chlorophytes and unidentified phytoflagellates).

Currently, the most used method for estimating the biomass of a phytoplankton does not rely only on size, in fact, it is based on the assignment of each taxon to a three-dimensional shape (Olenina et al., 2006; Sun & Liu, 2003; Vadrucci et al., 2007). The dimensions of these shapes and the inferred biovolume and biomass are measured under the microscope, in parallel with taxonomic identification and enumeration. This method uses the formula of geometric models or shapes that most closely resemble the actual shape of the organism. During this process, one is often faced with the dilemma whether to assign the shape of a phytoplankton cell to a complex but similar geometric model or rather to a simple, easily measured but dissimilar shape (Sun & Liu, 2003). The importance of choosing the right shape formula is emphasized by the fact that due to the geometric relationship between size and volume, there is a wide range of nine orders of magnitude for the cell biovolume of phytoplankton (Sutton, 1997).

To measure the biovolume, each phytoplankton species/taxon was first assigned to a shape according to the Helsinki Commission (HELCOM) classification system (Olenina et al., 2006) and found in the Nordic Microalgae website (Karlson et al., 2020). The taxa that were not present in the HELCOM list were assigned to the most similar shape and are, together with the complete list, reported in the Supplementary Materials (Table S1). Using ZEISS ZEN 3.0 software, the dimensions (length, width, diameter etc.) of each cell were measured individually, then the biovolume was calculated according to the formula assigned to a certain shape. When we found colonies in our samples, each cell of the colony was measured individually. The final biomass values (in pg C) were obtained using the Mendel-Deuer conversion factors (Menden-Deuer & Lessard, 2000; Socal et al., 2010). The size classes were obtained grouping the individual cell biomass and their abundances in the two classes (nano and micro) depending on their maximum linear dimension (MLD Fig. 1). Hereafter, to refer to the phytoplankton results measured by microscopy, the term Utermöhl phytoplankton will be used. The parameters measured in our study were taxa abundance (cell/L), shapes abundance (cell/L), taxa biomass (mg C /m^3), shapes biomass (mg C /m^3), individual cell biomasses (pg C), and individual cell sizes (MLD, µm) (Fig. 1).

Chlorophyll-a

The same monthly surface samples were used to determine chlorophyll-a (Chl-a) concentration. 400 mL of each sample was filtered through Whatman GF/F filters, and filters were frozen until analysis. Chl-a concentrations corrected for phaeopigments were then determined fluorometrically (Holm-Hansen et al., 1965) in 90% acetone extracts using a Turner Designs Trilogy fluorometer.

Analyses of data

The coherence among trends of different phytoplankton groups and among estimation methods was investigated using the Pearson determination coefficient (R^2) computed in the linear model II framework. The linear model II was obtained using the R package < lmodel2 > (Legendre & Legendre, 2012). The differences among medians were tested using the nonparametric rank test based on quantiles from the R package < EnvStats.R > . The community diversity was calculated using the Shannon diversity index (H') with the R package < vegan.R > (Oksanen et al., 2018). For every month, the taxa biomass, taxa abundance, shape biomass and shape abundance were transformed in proportions. Each

contribution to the community compositions p_i was used in the equation below to obtain the diversity values.

$$H' = -\sum_{k=0}^{n} p_i \ln p_i$$

To test whether nano- and microplankton subpopulations formed two distinct distributions, the unimodality or bimodality of the distributions of log size and log biomass was tested using the method of (Hartigan & Hartigan, 1985) embedded in the R package < diptest.R > (Maechler et al., 2021). In case unimodality of a distribution was not met, the distribution was split into two using the Gaussian mixture models method of the R package < mclust.R > (Fraley et al., 2022). For each of resulting distributions (the original one in case of unimodality and the two split distributions in case of bimodality), the agreement with the power law was tested (bootstrap, Supplementary Material Figure S1). When the test results significative, the tested distribution is not a power law (p-value < 0.05); on the contrary, if the test results have a p-value > 0.05, then the distribution could be a power law or other similar distributions (exponential and lognormal) (Clauset et al. (2009). In case of p-value > 0.05, the lognormal and exponential distributions were tested against the power law using the method developed by Clauset et al. (2009), included in the < poweRlaw.R > package (Gillespie, 2015). In case the test was not passed against one or both alternative distributions (exponential or power law), the support for the power law was considered as moderate, while in case both p-values were lower than 0.05, the support was considered as good. After Clauset et al. (2009), the support for power law was classified in "none", "moderate" and "good". The flowchart of the power law related analysis is schematized in the Supplementary Materials (Figure S1).

Results

Annual pattern of phytoplankton parameters

During the study period, a total of 10,030 cells were identified down to the lowest possible taxonomic level, counted and measured using an inverted microscope. The total abundance of phytoplankton exhibited three peaks (Fig. 3A). The highest abundance was observed in June 2020, while two minor peaks were observed in October–November 2020 and March 2021. The total carbon biomass followed the abundance pattern with very similar dynamics: the biomass peaked in June (89.4 mg C/m^3).

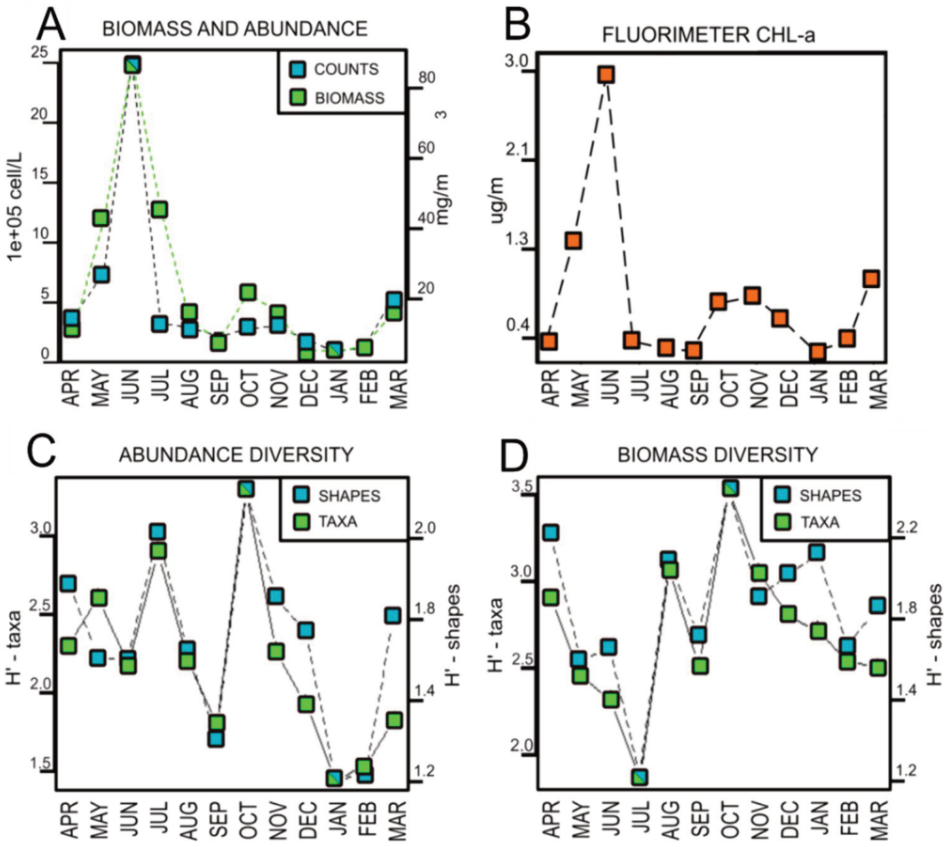

Fig. 3 Annual pattern of phytoplankton characteristics at the station 000F in the period April 2020–March 2021. **A** abundance (left axis) and carbon biomass (right axis); **B** chlorophyll-a concentration; **C** Shannon diversity index calculated using abundance of taxa (left axis) and abundance of shapes (right axis); **D** Shannon diversity index calculated using biomass of taxa (left axis) and biomass of shapes (right axis)

Chl-a concentrations (Fig. 3B) peaked synchronously with total carbon biomass and abundance in June 2020, which was followed by a summer low. The second minor peak in November 2020 was again followed by a decline in late autumn and winter, when the concentration reached the low in January 0.21 mg/m^3 to then increase again in March 2021. The Chl-a concentrations were significantly correlated with total carbon biomass ($R^2 = 0.74$, p-value < 0.01).

Phytoplankton diversity, which was calculated based on the abundance of taxa (Fig. 3C), was fluctuating but with relatively high values during spring and summer and reached its maximum during the peak in October 2020 ($H' = 3.2$). The minimum diversity was calculated in January 2021 ($H' = 1.7$) and was also low in September 2020. Very similar was the pattern of diversity calculated with the abundance of cell shapes ($R^2 = 0.76$, p-value = < 0.01), which slightly differed only in April–May 2020 and March 2021. Phytoplankton diversity based on the carbon biomass of taxa displayed a different temporal pattern (Fig. 3D). It decreased from high values in April 2020 and reached its minimum in July ($H' = 2.0$). The trend then reversed, and diversity peaked again in August and October 2020 (up to $H' = 3.5$), only to decline again in the winter months. Similar pattern was also observed for the diversity calculated with carbon biomass of different cell shapes ($R^2 = 0.83$, p-value = < 0.01). The autumn peak in phytoplankton abundance and carbon biomass, recorded in October/November, corresponded to the maximum in shape diversity for both shape abundance ($H' = 2.36$) and biomass ($H' = 2.16$).

The June and October/November peaks were characterized by an increase in the median of the individual cell sizes, while the March peak corresponded to a non-significant decrease (p-value > 0.05) (Fig. 4 and Supplementary Material Table S2). From the perspective of individual cell biomass, only the October/November period was characterized by an increase in average values while the March peak was characterized by a significant decrease (Fig. 4 and Supplementary Material Table S2). Both June and October peaks were preceded by an increase in freshwater inputs from the main river while the March peak was accompanied by a significant decrease in freshwater inputs (Supplementary Material Figure S2 and Table S2).

Phytoplankton size classes and main taxa

Phytoplankton size classes contributed differently to the community with respect to biomass and abundance. Microfraction (MLD > 20 µm) accounted for an average of 60% of the Utermöhl phytoplankton biomass, while nanofraction (MLD 2 – 20 µm) accounted for the remaining (Supplementary Material Table S3). Microphytoplankton share in the carbon biomass rose during the peaks to almost 90% in July 2020 and up to 80% in November 2020. The contribution of nanophytoplankton biomass was the highest during early spring (up to 72% in April 2020) and in December 2020 (71%). As expected, much higher contribution accounted for nanophytoplankton in case of abundance (Supplementary Material Table S4), where it accounted for an average of 80% of the total abundance. The contribution of microphytoplankton abundance was the highest during peaks (up to 30% in June and July and up to 44% in November).

The community composition in terms of phytoplankton main groups was during peaks characterized by the prevalence of diatoms, which dominated both in biomass (up to

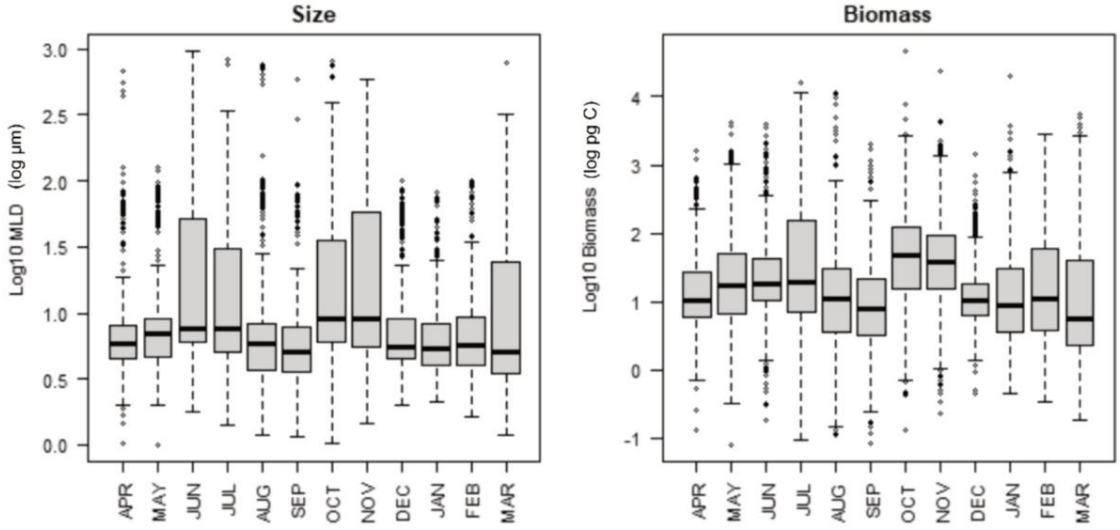

Fig. 4 Annual pattern of individual phytoplankton cell size (in terms of MLD; left) and biomass (in terms of carbon biomass; right) at the station 000F in the period April 2020–March 2021

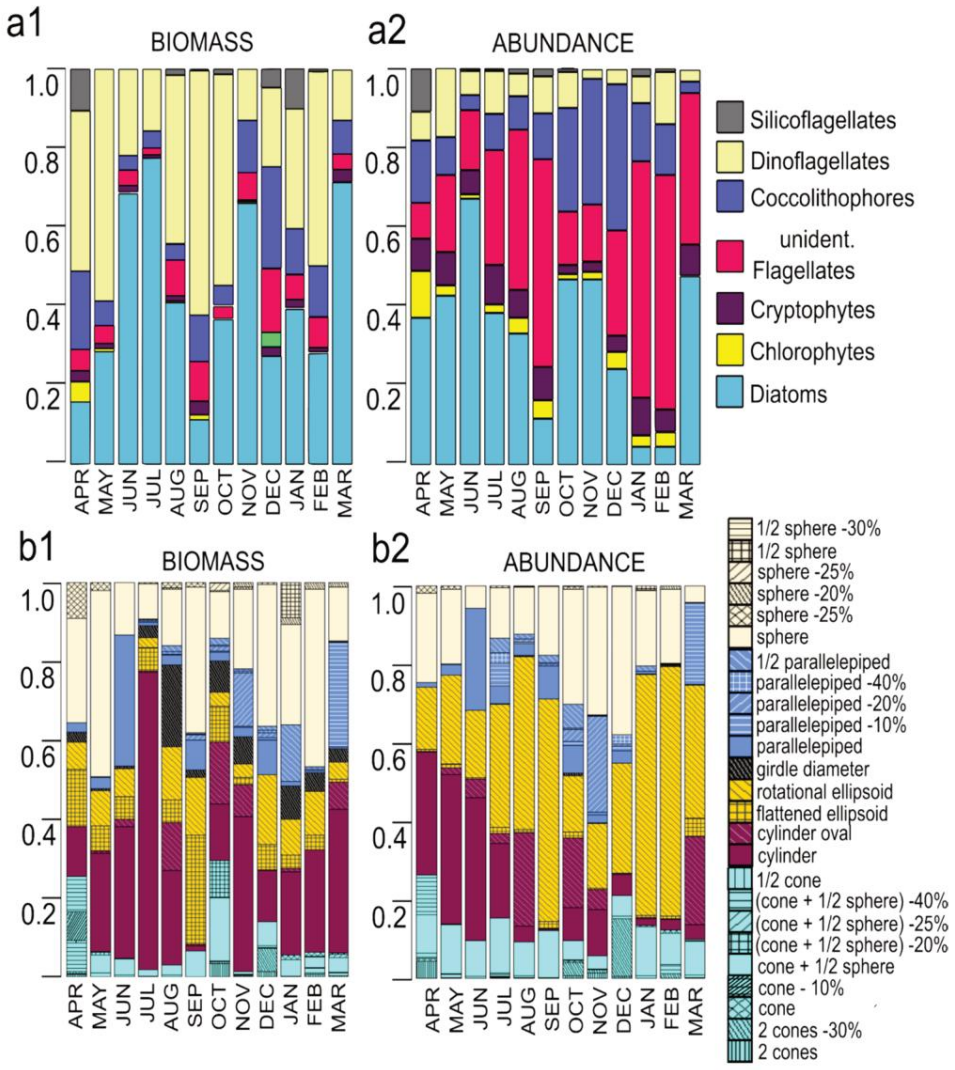

Fig. 5 Phytoplankton community composition at the station 000F in the period April 2020–March 2021: **a1** contribution of main groups to total biomass, **a2** contribution of main groups to total abundance; **b1** contribution of shapes to total biomass, **b2** contribution of shapes to total abundance

77%; Fig. 5a1) and abundance (up to 68%; Fig. 5a2). The share of dinoflagellates was, on the other hand, the highest during non-bloom periods, but only in terms of biomass (up to 55% in September; Fig. 5a1), while the non-bloom periods were dominated by flagellates in terms of abundance (up to 60%; Fig. 5a2). Coccolithophore share to abundance was the most important during autumn months (up to 37%; Fig. 5a2). Unidentified nanoflagellates and coccolithophores together with cryptophytes accounted for less biomass than dinoflagellates alone. Other groups had minor contributions for the total phytoplankton abundance and biomass (Fig. 5 and Supplementary Material Tables S3 and S4). The most uniform contribution of phytoplankton groups to the community was observed in the periods of the lowest biomass (April and December, Fig. 5).

Total carbon biomass and abundance were significantly correlated ($R^2 = 0.82$, p-value < 0.01), which was also mostly true when separately considering main phytoplankton groups. For cryptophytes and chlorophytes, biomass correlated almost perfectly with abundance (R^2 close to 1), and for dinoflagellates, correlation was also quite high ($R^2 = 0.86$, p-value < 0.01). For diatoms, the correlation was positive but not significant as it was strongly driven by the June peak ($R^2 = 0.77$, p-value > 0.01), and for the coccolithophores, the correlation was lower but nonetheless significant ($R^2 = 0.60$, p-value < 0.01). Biomass and abundance were positively correlated also for both PSCs (micro-size class $R^2 = 0.69$, p-value < 0.01; nanosize class $R^2 = 0.89$, p-value < 0.01).

Phytoplankton cell shapes

During the study period, 25 different shapes were registered that can be divided in six groups: nine shapes closely related to cones, two cylinders, two ellipsoids, five parallelepipeds, six spheres, and one unique shape of the genus *Tripos*, denoted as girdle diameter. In general, individual cell size

and individual biomass of phytoplankton cells were significantly correlated ($R^2 = 0.53$, p-value < 0.01). However, this correlation was stronger for spheres, ellipsoids and girdle diameter ($R^2 = 0.81$, 0.91 and 1.00, respectively) than for cylinders, parallelepipeds and cones ($R^2 = 0.77$, 0.20 and 0.10, respectively). The shape influenced the relation between total abundance and biomass as well. In fact, depending on the shape type, the correlation was stronger (parallelepipeds, ellipsoids and spheres $R = 0.99$, 0.77, 0.68, respectively) or weaker (girdle, cylinders and cones $R^2 = 0.47$, 0.42, 0.30, respectively).

There was substantial variation in the dominance of different shapes during the study period (Fig. 5b1, b2 and Supplementary Material Tables 5 and 6). Cylinders and parallelepipeds, associated with diatoms, dominated the abundance (41% and 26%, respectively) and biomass (35 and 33%, respectively) peak in June 2020, and their contribution was quite similar also during smaller March 2021 peak. Differently, all shapes contributed more or less uniformly to the autumn peak, especially in October 2020. The contribution of cylinders to biomass was the highest in months following the phytoplankton peaks July and November 2020 (75 and 39%, respectively), while their contribution to the abundance during these months was much smaller. In the months with the phytoplankton lows, both biomass and abundance were dominated by ellipsoids (up to 42% of biomass in September 2020) and spheres (up to 45% of biomass in February 2021 and 38% of abundance in December 2020). In absolute terms, spherical shapes reached their maximum biomass and abundance in May 2020, when their contribution to biomass also peaked (47%). The contribution of the genus *Tripos*-shape denominated girdle diameter to biomass was very variable, reaching the peak in August 2020 (21%), while its contribution to the abundance was negligible.

Distributions of individual cell size and biomass

The phytoplankton cell size in terms of MLD ranged from 2 to 821.5 µm. The largest cells in each sample belonged to diatoms. The carbon biomass of individual phytoplankton cells ranged from 0.08 to 46,529 pg C. In contrast to the linear dimension, the majority of taxa with the highest carbon biomass belonged to the dinoflagellates, with one specimen of *Protoperidinium depressum* having the highest biomass. The distributions of phytoplankton individual cell sizes passed the Hartigan test for unimodality in only four cases: April and September 2020, January, and February 2021, which corresponds to periods of the lowest total biomass and abundance (see Fig. 3A). For these months, a unique average cell size was estimated, which varied between 7 and 11 µm MLD (one solid vertical line in Fig. 6 and Supplementary material Table 9). In other months, the individual cell size was characterized by a bimodal distribution. In these months, the average cell size in the subpopulation of smaller cells ranged from around 5 to 7 µm MLD, whereas the average cell size in the subpopulation of larger cells was more variable and ranged from 18 to 78 µm MLD (Fig. 6, Supplementary material Table S7). Only the distributions of November 2020, December 2020, and February 2021 as well as the subpopulation of larger cells in May 2020 and smaller cells in June 2020 conformed to a power law (p-value > 0.05; Supplementary material Table S7. Of these, only the distributions of the small cells in June, November and December did not conform to the alternative distributions, i.e. lognormal and exponential (p-value < 0.05), indicating a good support for power law.

The distributions of individual cell biomass did not pass the Hartigan test for unimodality only in June, July and October 2020, and March 2021 (two dashed vertical lines in Fig. 6 and Supplementary material Table S7), which corresponds to months of phytoplankton biomass peaks. Only the distributions of April, January, and February and the small cells in June conformed to a power law distribution (p-value > 0.05; Supplementary material Table S7). For all three, it was not possible to discriminate the distribution from at least one of the two alternative distributions (p-value > 0.05; Supplementary material Table S7) indicating a moderate support for power law.

Discussion

In this paper, we present an annual characterization of the phytoplankton community in terms of taxonomy (main groups), morphology (size and shape) and diversity, which, in combination with their distributional properties, allows conclusions to be drawn about the ecology of the pelagic community at the LTER site in the Gulf of Trieste (northern Adriatic Sea). Our results on phytoplankton size (MLD), biovolume and biomass add to the total of around 40 such datasets found worldwide (Harrison et al., 2015) and are, to the best of our knowledge, one of the few existing for the Mediterranean Sea.

The general pattern of two annual peaks of phytoplankton abundance and biomass, one in the spring and one in the autumn, match with the known phytoplankton phenology in the Gulf of Trieste, where seasonal outbursts are associated with water column freshening and mixing (Cabrini et al., 2012; Cerino et al., 2019; Mozetič et al., 2012). The late appearance of spring phytoplankton peak during our study is also consistent with findings in this area, where late spring to summer diatom-dominated blooms recently substituted late winter or spring blooms (Cerino et al., 2019; Eker-Develi et al., 2022; Godrijan et al., 2013; Mozetič et al., 2012). Moreover, the minor relative importance of the autumn bloom is consistent with recent changes of phytoplankton

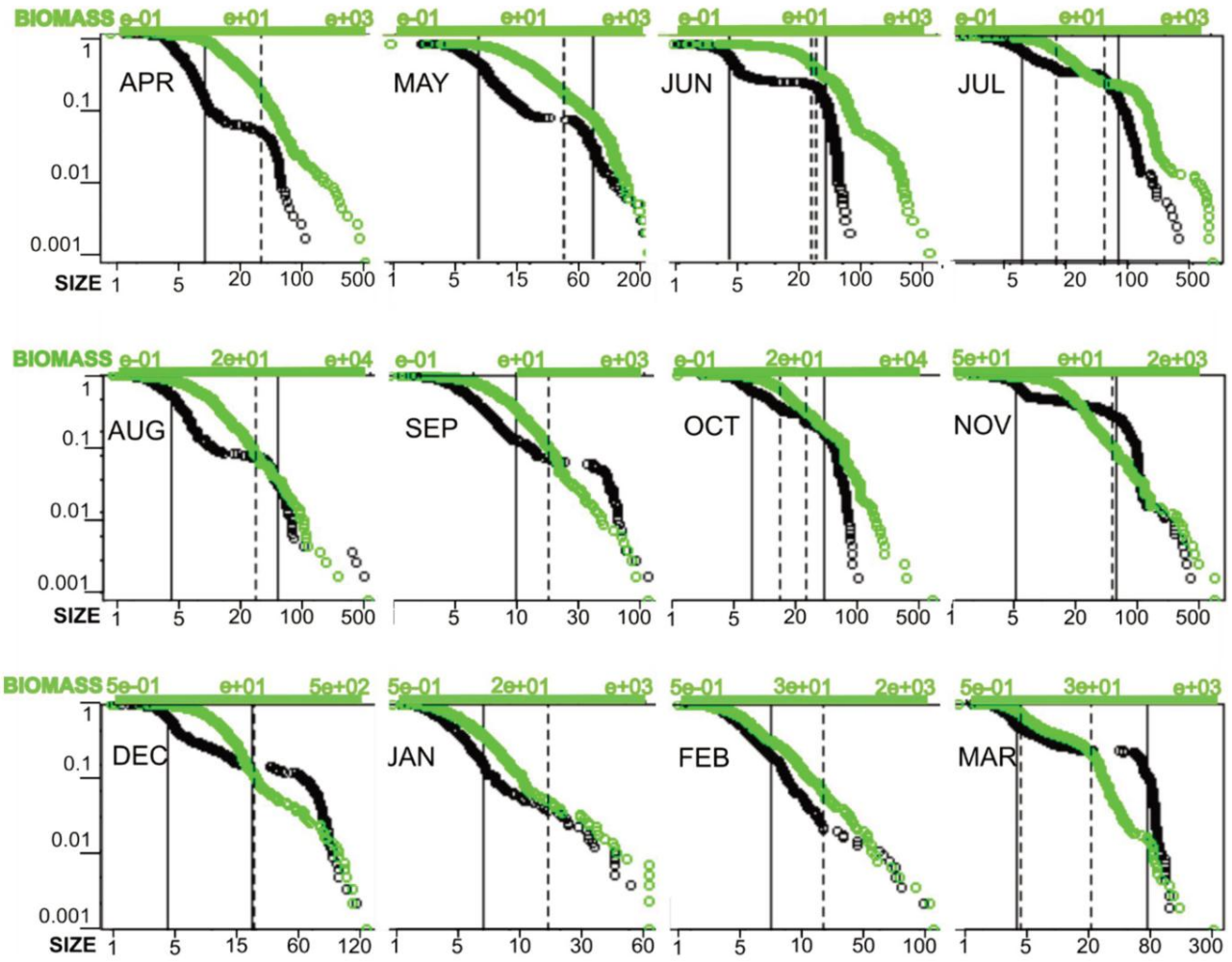

Fig. 6 Log–log cumulative distribution plots for individual cell size (in µm, black dots) and individual cell biomass (in pg C, green dots). The solid vertical line represents the average size, if there are two lines, they represent the average size of the two subpopulations. The dashed vertical line represents the average biomass; when there are two lines, they represent the average biomass of the two subpopulations. Note the different scale on *x* axes

annual dynamics, as either the biomass (in terms of Chl-a) or the abundances of main phytoplankton groups diminished after the break of the century (Brush et al., 2021). The community appeared to be more diverse during the autumn peak both functionally (shapes) and taxonomically in comparison to the spring period, which can be explained by the mechanisms causing the blooms. In the study area, the spring season is characterized by a stratified water column caused mainly by freshwater inputs, which enrich the surface layer with nutrients and cause diatom blooms mostly dominated by a small number of species (Brush et al., 2021). In autumn season, mixed conditions prevail, which redistribute nutrients from deeper water layers (Vascotto et al., 2024) and allow for a more complex and diverse community compared to other seasons (Vascotto et al., 2021). Active mixing can also favour the diversity by bringing specimens from the deeper layers into the surface, which was sampled in this study. Such an increase in diversity could also reflect the accumulation of species at the end of the phytoplankton succession cycle (Reynolds, 1980).

The range of cellular carbon of the Utermöhl phytoplankton (2.5–89 mg C/m^3) is similar to that found in the eutrophic western part of the northern Adriatic (Bernardi Aubry et al., 2006; Pugnetti et al., 2008), while the values in the southern Adriatic are much lower (Cerino et al., 2012). This is consistent with the known gradient of increasing phytoplankton biomass along the south-north axis of the Adriatic Sea (Bernardi Aubry et al., 2006; Fonda Umani, 1996). Since our data cover only the surface layer, it is not possible to draw conclusions about the dynamics of phytoplankton in the lower water layers. In the Gulf of Trieste, in particular, the dynamics of the biomass in the lower layers are different

from the surface during the stratified water column (Flander-Putrle et al., 2021; Talaber et al., 2014).

Depending on the taxa and their shape, the relation between individual size and individual biomass as well as the relation between total abundance and biomass showed different degrees of coherence. The significant correlation between phytoplankton abundance and biomass suggests the possibility of using abundance data as a proxy for biomass, and size (MLD) as a parameter (or trait) to estimate the individual biomass (Hillebrand et al., 1999). Although similar matchups for the marine environment between biomass and abundance have already been obtained before (Bernardi Aubry et al., 2006), there are also cases where satisfying agreement between the two parameters has not been achieved (Eker-Develi et al., 2022). Still, the output of this more demanding method, i.e. individual cell size, shape and biomass, can tell us other valuable information on the status and fit of the phytoplankton community in relation to energy flow, carbon export and carbon pump (Juranek et al., 2020). However, the major drawback when using Utermöhl method is the neglection of the pico-fraction. A previous study on PSCs based on HPLC pigments in GoT has shown that the pico-fraction makes the highest contribution (up to 30%) to the total biomass in the periods with the lowest Chl-a concentration. This contribution can be up to 30% of the total Chl-a in August and January, when cyanobacteria and chlorophytes predominate, respectively (Flander-Putrle et al., 2021). The relative importance of picophytoplankton may even increase in the future, as the biomass of picophytoplankton has recently increased significantly in all water layers of the GoT (Flander-Putrle et al., 2021).

The distributions of individual cell size and biomass were quite variable during the study period and often presented a mismatch between the size (MLD) and biomass suggesting nonlinear relationship between the two traits. This mismatch was also depicted by the results of the distribution tests (see Supplementary Material Table S7). It has to be stressed, however, that the power low test cannot perform at its best when the tested distribution does not span several orders of magnitude (Clauset et al., 2009), as was the case for the cell size subpopulations in our study. More specifically, for the size subpopulations of May, June, November and December that passed the test, special care must be taken before claiming that the distributions really corresponded to a power law. Nevertheless, two important characteristics can be drawn from the results: (i) unimodality was more common during periods of low phytoplankton biomass and abundance, meaning that phytoplankton community size and biomass could be described by one average value, and (ii) bimodality was more common during peaks, when more than one average value of biomass and size have to be used for describing the community. Moreover, the unimodal individual cell biomass distributions in the months with lower biomass (April, January and February) showed tendency to the power law, while during the months with higher biomass characterized by bi- or even tri-modality, the individual cell biomass distributions mostly conformed to other types of curves (log-normal or exponential) and only once to power law.

Apart from temporal differences between distributions, it is important to note that bimodality was a more common characteristic of the individual cell size (MLD) while unimodality was more frequent for individual cell biomass. Bimodality of individual cell size support the "classic" division of Utermöhl phytoplankton into nano- and micro-size classes, but specific variations during the study period indicate different underlying ecological processes. For example, November 2020 showed a distinct second change in slope in the range between 100 and 500 µm (see Fig. 6), indicating a possible third mode of distribution in the mesoplankton size class/or fraction. Indeed, big cylindrical cells of diatoms from the genera *Guinardia*, *Pseudosolenia*, *Hemiaulus* and *Rhizosolenia* were present in that period along with other diatoms in the micro-size fraction, most probably in relation to favourable conditions of a mixed nutrient enriched water column (Svensson et al., 2014) that allowed a highly diversified autumn community (see Fig. 5). Conversely, in the cases where the distribution of individual cell size was unimodal during periods of low phytoplankton biomass and abundance (i.e. in April, September, January and February), the community was dominated by nano-sized phytoplankton. In such cases, the distinction between nanoplankton and microplankton is hardly seen in data and appears to be more of an artefact than a meaningful ecological trait.

On the contrary, the biomass of individual cells was either uniformly (when the power law applies) or unimodally distributed in most cases, except in peak periods when two (October 2020) or even three (June, July 2020 and March 2021) subpopulations were present as shown by the cumulative distribution plots of biomass (see Fig. 6). Our results show that phytoplankton biomass in coastal waters deviates very often from the power law, not only in correspondence to the seasonal blooms. Indeed, the assumption of energy flow from smaller to larger organisms, which characterize the food networks resulting in power low distributions, does not hold for the size spectrum occupied by phytoplankton (Witek & Krajewska-Soltys, 1989). More specifically, phytoplankton biomass can grow exponentially when unimpeded by grazers in coastal waters (Irigoien et al., 2005), which deforms the expected power law distribution for the whole plankton range (Witek & Krajewska-Soltys, 1989). Similar results were obtained in our study, where size-specific blooms caused deviations from the power law inside the phytoplankton size spectrum itself (e.g. predominant cylinder and parallelepiped shapes characteristic for diatoms during June-July bloom).

The alternation between the bimodally and the unimodally power law distributed communities reflects the seasonal switches between unconstrained and constrained phytoplankton growth. In the first case, when the GoT is influenced by a high river discharge, the phytoplankton community is characterized by high biomass, bigger cells, clear separation between size classes, and higher contribution of diatoms in the microplankton size fraction. Such communities are richer in taxa and more diverse in terms of cell shapes, which indicates functional differentiation, especially in autumn. It has been argued that phytoplankton blooms, or peaks in our case, can be considered trophic "loopholes" as phases in the phytoplankton life cycles when species can proliferate exponentially unconstrained (Irigoien et al., 2005). During phytoplankton peaks, biomass increases in a specific range that is characteristic of the blooming taxa causing the deviation of the overall distribution of individual cell biomass from the power law.

Conversely, in more oligotrophic conditions, the phytoplankton community is characterized by smaller cells with a lower biomass, no clear separation between size classes, lower diversity, and a higher contribution of pico- and nanofractions. These communities, in which distributions of individual cell size and biomass more often conform to the power law, appear during lower freshwater outflows and during winter. Apart from scarce resources (nutrient and light availability), grazers like microzooplankton and heterotrophic nanoflagellates with similar growth rates to those of phytoplankton exert top-down control, maintaining phytoplankton biomass at low levels (Monti et al., 2012). Such communities can be considered in the final stage of a stable food web, which is organized in trophic networks that exhibits self-organized criticality (Bascompte, 2007) implying distributions conforming to the power law (Newman, 2005). In other words, in the post-bloom period where there are less resources available, grazers can "catch up" leading phytoplankton biomass to decrease and the distribution of individual cell biomass returns to the power law. These outcomes suggest that analyses of the distribution types of individual cell size and biomass can be seen as a useful tool to identify imbalances in the trophic network also in the coastal environment.

Conclusions

In this paper, we present a comprehensive characterization of the morphological traits (size and shape) and biomass of phytoplankton at the LTER site in the Gulf of Trieste (northern Adriatic Sea), which provided an insight into ecological processes driving the evolution of the phytoplankton community in time. Overall, the observed annual pattern of total phytoplankton abundance, carbon biomass and chlorophyll-a corresponded well to the expected phytoplankton dynamics in this area. The individual cell size distributions confirmed the subdivision of the phytoplankton community into nano- and micro-size fraction, especially in the periods during and around the abundance and biomass peaks. In contrast, the distribution of individual cell biomass was more often unimodal except during the peaks, showing that the biomass of phytoplankton cells usually presents a continuum. The conformity of the biomass distribution to the power law in the months of low biomass indicates a link to stable trophic networks controlled by consumers and resources, while the more frequently observed deviations reflect the unstable nature of the coastal environment driven by the irregular pulses of freshwater inflows.

Supplementary Information The online version contains supplementary material available at https://doi.org/10.1007/s42974-024-00215-4.

Funding Open access funding provided by Istituto Nazionale di Oceanografia e di Geofisica Sperimentale within the CRUI-CARE Agreement. This research was funded by Slovenian Research and Innovation Agency (ARIS), grant number P1-0237, and by the ARIS programme for young researcher 51986.

Data availability Part of data (chlorophyll-a) originates from the national monitoring programme financed by the Slovenian Environment Agency of the Ministry of Environment and Spatial Planning. The Soča River discharge data is available at https://vode.arso.gov.si/hidarhiv/pov_arhiv_tab.php.

Declarations

Conflict of interest The authors declare that they have no known competing financial interests or personal relationships that could have appeared to influence the work reported in this paper.

References

Andersen, K. H., Berge, T., Goncalves, R. J., Hartvig, M., Heuschele, J., Hylander, S., Jacobsen, N. S., Lindemann, C., Martens, E. A., Neuheimer, A. B., Olsson, K., Palacz, A., Prowe, A. E., Sainmont, J., Traving, S. J., Visser, A. W., Wadhwa, N., & Kiorboe, T. (2016). Characteristic sizes of life in the oceans, from bacteria to whales. *Annual Review of Marine Science, 8*, 217–241.

Andersson, A., Haecky, P., & Hagström, A. (1994). Effect of temperature and light on the growth of micro- nano- and pico-plankton: impact on algal succession. *Marine Biology, 120*(4), 511–520.

Armstrong, R. A. (1999). Stable model structures for representing biogeochemical diversity and size spectra in plankton communities. *Journal of Plankton Research, 21*(3), 445–464.

Aumont, O., Ethé, C., Tagliabue, A., Bopp, L., & Gehlen, M. (2015). PISCES-v2: An ocean biogeochemical model for carbon and ecosystem studies. *Geoscientific Model Development, 8*(8), 2465–2513.

Bascompte, J. (2007). Networks in ecology. *Basic and Applied Ecology, 8*(6), 485–490.

Beardall, J., Allen, D., Bragg, J., Finkel, Z. V., Flynn, K. J., Quigg, A., Rees, T. A. V., Richardson, A., & Raven, J. A. (2009). Allometry and stoichiometry of unicellular, colonial and multicellular phytoplankton. *New Phytologist, 181*(2), 295–309.

BernardiAubry, F., Acri, F., Bastianini, M., Bianchi, F., Cassin, D., Pugnetti, A., & Socal, G. (2006). Seasonal and interannual variations of phytoplankton in the Gulf of Venice (Northern Adriatic Sea). *Chemistry and Ecology, 22*(sup1), S71–S91.

Brown, J. H. (2004). Toward a metabolic theory of ecology. *Ecology, 85*(7), 1771–1789.

Brush, M. J., Mozetič, P., Francé, J., Aubry, F. B., Djakovac, T., Faganeli, J., Harris, L. A., & Niesen, M. (2021). *Phytoplankton dynamics in a changing environment*. Wiley.

Cabrini, M., Fornasaro, D., Cossarini, G., Lipizer, M., & Virgilio, D. (2012). Phytoplankton temporal changes in a coastal northern Adriatic site during the last 25 years. *Estuarine, Coastal and Shelf Science, 115*, 113–124.

Cavender-Bares, K. K., Rinaldo, A., & Chisholm, S. W. (2001). Microbial size spectra from natural and nutrient enriched ecosystems. *Limnology and Oceanography, 46*(4), 778–789.

Cerino, F., BernardiAubry, F., Coppola, J., La Ferla, R., Maimone, G., Socal, G., & Totti, C. (2012). Spatial and temporal variability of pico-, nano- and microphytoplankton in the offshore waters of the southern Adriatic Sea (Mediterranean Sea). *Continental Shelf Research, 44*, 94–105.

Cerino, F., Fornasaro, D., Kralj, M., Giani, M., & Cabrini, M. (2019). Phytoplankton temporal dynamics in the coastal waters of the north-eastern Adriatic Sea (Mediterranean Sea) from 2010 to 2017. *Nature Conservation, 34*, 343–372.

Clauset, A., Shalizi, C. R., & Newman, M. E. J. (2009). Power-law distributions in empirical data. *SIAM Review, 51*(4), 661–703.

Durante, G., Basset, A., Stanca, E., & Roselli, L. (2019). Allometric scaling and morphological variation in sinking rate of phytoplankton. *Journal of Phycology, 55*(6), 1386–1393.

Eker-Develi, E., Berthon, J.-F., & Free, G. (2022). Impact of environmental factors on phytoplankton composition and their marker pigments in the northern Adriatic Sea. *Oceanologia, 64*(4), 615–630.

Falkowski, P. G., Laws, E. A., Barber, R. T., & Murray, J. W. (2003). "Phytoplankton and their role in primary, new, and export production. In J. Michael & R. Fasham (Eds.), *Ocean biogeochemistry* (pp. 99–121). Springer.

Finkel, Z. V., Beardall, J., Flynn, K. J., Quigg, A., Rees, T. A. V., & Raven, J. A. (2009). Phytoplankton in a changing world: Cell size and elemental stoichiometry. *Journal of Plankton Research, 32*(1), 119–137.

Flander-Putrle, V., Francé, J., & Mozetič, P. (2021). Phytoplankton pigments reveal size structure and interannual variability of the coastal phytoplankton community (Adriatic Sea). *Water, 14*(1), 23.

Fonda Umani, S. (1996). Pelagic production and biomass in the Adriatic Sea. *Scientia Marina, 60*(2), 65–77.

Fraley, C., Raftery, A. E., Scrucca, L., Murphy, T. B., & Fop, M. (2022). *Gaussian mixture modelling for model-based clustering, classification, and density estimation*. Chapman and Hall.

Gillespie, C. S. (2015). Fitting heavy tailed distributions: The poweR-law package. *Journal of Statistical Software*. https://doi.org/10.18637/jss.v064.i02

Godrijan, J., Marić, D., Tomažić, I., Precali, R., & Pfannkuchen, M. (2013). Seasonal phytoplankton dynamics in the coastal waters of the north-eastern Adriatic Sea. *Journal of Sea Research, 77*, 32–44.

Harrison, P. J., Zingone, A., Mickelson, M. J., Lehtinen, S., Ramaiah, N., Kraberg, A. C., Sun, J., McQuatters-Gollop, A., & Jakobsen, H. H. (2015). Cell volumes of marine phytoplankton from globally distributed coastal data sets. *Estuarine, Coastal and Shelf Science, 162*, 130–142.

Hartigan, J. A., & Hartigan, P. M. (1985). The dip test of unimodality. *The Annals of Statistics, 13*(1), 70–84.

Hatton, I. A., Heneghan, R. F., Bar-On, Y. M., & Galbraith, E. D. (2021). The global ocean size spectrum from bacteria to whales. *Science Advances*. https://doi.org/10.1126/sciadv.abh3732

Hays, G. C., Richardson, A. J., & Robinson, C. (2005). Climate change and marine plankton. *Trends in Ecology & Evolution, 20*(6), 337–344.

Heneghan, R. F., Hatton, I. A., & Galbraith, E. D. (2019). Climate change impacts on marine ecosystems through the lens of the size spectrum. *Emerg Top Life Sci, 3*(2), 233–243.

Hillebrand, H., Dürselen, C. D., Kirschtel, D., Pollingher, U., & Zohary, T. (1999). Biovolume calculation for pelagic and benthic microalgae. *Journal of Phycology, 35*(2), 403–424.

Holm-Hansen, O., Lorenzen, C. J., Holmes, R. W., & Strickland, J. D. (1965). Fluorometric determination of chlorophyll. *ICES Journal of Marine Science, 30*(1), 3–15.

Irigoien, X., Flynn, K. J., & Harris, R. P. (2005). Phytoplankton blooms: A 'loophole' in microzooplankton grazing impact? *Journal of Plankton Research, 27*(4), 313–321.

Juranek, L. W., White, A. E., Dugenne, M., Henderikx Freitas, F., Dutkiewicz, S., Ribalet, F., Ferrón, S., Armbrust, E. V., & Karl, D. M. (2020). The importance of the phytoplankton "middle class" to ocean net community production. *Global Biogeochemical Cycles, 34*(12), e2020GB006702.

Karlson, B., A. Andreasson, M. Johansen, M. Karlberg, A. Loo and A.-T. Skjevik. (2020). Nordic microalgae. World-wide electronic publication, , from http://nordicmicroalgae.org.

Kostadinov, T. S., Siegel, D. A., & Maritorena, S. (2009). Retrieval of the particle size distribution from satellite ocean color observations. *Journal of Geophysical Research*. https://doi.org/10.1029/2009JC005303

Kostadinov, T. S., Siegel, D. A., & Maritorena, S. (2010). Global variability of phytoplankton functional types from space: Assessment via the particle size distribution. *Biogeosciences, 7*(10), 3239–3257.

Kriest, I., & Evans, G. T. (1999). Representing phytoplankton aggregates in biogeochemical models. *Deep-Sea Research, 46*(1), 1841–1859.

Legendre, P., & Legendre, L. (2012). *Numerical ecology*. Elsevier.

Leonilde, R., Elena, L., Elena, S., Francesco, C., & Alberto, B. (2017). Individual trait variation in phytoplankton communities across multiple spatial scales. *Journal of Plankton Research, 39*(3), 577–588.

Litchman, E., & Klausmeier, C. A. (2008). Trait-based community ecology of phytoplankton. *Ann. Rev. Ecol. Evol. Syst., 39*(1), 615–639.

Maechler, M., P. Rousseeuw, A. Struyf, M. Hubert and K. Hornik. (2021). Cluster: Cluster analysis basics and extensions.

Malačič, V., Celio, M., Čermelj, B., Bussani, A., & Comici, C. (2006). Interannual evolution of seasonal thermohaline properties in the Gulf of Trieste (northern Adriatic) 1991–2003. *Journal of Geophysical Research*. https://doi.org/10.1029/2005JC003267

Marquet, P. A., Quinones, R. A., Abades, S., Labra, F., Tognelli, M., Arim, M., & Rivadeneira, M. (2005). Scaling and power-laws in ecological systems. *Journal of Experimental Biology, 208*(Pt 9), 1749–1769.

Menden-Deuer, S., & Lessard, E. J. (2000). Carbon to volume relationships for dinoflagellates, diatoms, and other protist plankton. *Limnology and Oceanography, 45*(3), 569–579.

Monti, M., Minocci, M., Milani, L., & Umani, S. F. (2012). Seasonal and interannual dynamics of microzooplankton abundances in the Gulf of Trieste (Northern Adriatic Sea, Italy). *Estuarine, Coastal and Shelf Science, 115*, 149–157.

Mozetič, P., Francé, J., Kogovšek, T., Talaber, I., & Malej, A. (2012). Plankton trends and community changes in a coastal sea (northern Adriatic): Bottom-up vs. top-down control in relation to environmental drivers. *Estuarine, Coastal and Shelf Science, 115*, 138–148.

Mozetič, P., Solidoro, C., Cossarini, G., Socal, G., Precali, R., Francé, J., Bianchi, F., De Vittor, C., Smodlaka, N., & Fonda Umani, S. (2010). Recent trends towards oligotrophication of the northern Adriatic: evidence from chlorophyll a time series. *Estuaries and Coasts, 33*(2), 362–375.

Naselli-Flores, L., & Barone, R. (2011). Invited review-fight on plankton! Or, phytoplankton shape and size as adaptive tools to get ahead in the struggle for life. *Cryptogamie, Algologie, 32*(2), 157–204.

Newman, M. E. J. (2005). Power laws, Pareto distributions and Zipf's law. *Contemporary Physics, 46*(5), 323–351.

Niklas, K. J. (2004). Plant allometry: Is there a grand unifying theory? *Biological Reviews of the Cambridge Philosophical Society, 79*(4), 871–889.

Nock, C. A., Vogt, R. J., & Beisner, B. E. (2016). *Functional traits* (pp. 1–8). Wiley.

Oksanen, J., Blanchet, F. G., Friendly, M., Kindt, R., Legendre, P., McGlinn, D., Minchin, P. R., O'Hara, R. B., Simpson, G. L., Solymos, P., Stevens, M. H. H., Szoecs, E., & Wagner, H. (2018). Package 'vegan.' *Community Ecology Package, Version, 2*(9), 1–295.

Olenina, I., S. Hajdu, L. Edler, A. Andersson, N. Wasmund, S. Busch, J. Göbel, S. Gromisz, S. Huseby, M. Huttunen, A. Jaanus, P. Kokkonen, I. Ledaine and E. Niemkiewicz. (2006). Biovolumes and size-classes of phytoplankton in the Baltic Sea HELCOM. Baltic Sea Environment Proceeding. 106(144).

Perkins, D. M., Perna, A., Adrian, R., Cermeno, P., Gaedke, U., Huete-Ortega, M., White, E. P., & Yvon-Durocher, G. (2019). Energetic equivalence underpins the size structure of tree and phytoplankton communities. *Nature Communications, 10*(1), 255.

Pugnetti, A., Bazzoni, A. M., Beran, A., BernardiAubry, F., Camatti, E., Celussi, M., Coppola, J., Crevatin, E., Negro, P. D., & Paoli, A. (2008). Changes in biomass structure and trophic status of the plankton communities in a highly dynamic ecosystem (Gulf of Venice, Northern Adriatic Sea). *Marine Ecology, 29*(3), 367–374.

Reynolds, C. (1980). Phytoplankton assemblages and their periodicity in stratifying lake systems. *Holoartic Ecology, 3*(3), 141–159.

Roselli, L., Bevilacqua, S., & Terlizzi, A. (2022). Using null models and species traits to optimize phytoplankton monitoring: An application across oceans and ecosystems. *Ecological Indicators, 138*, 108827.

Roselli, L., & Litchman, E. (2017). Phytoplankton traits, functional groups and community organization. *Journal of Plankton Research, 39*(3), 491–493.

Ryabov, A., Blasius, B., Hillebrand, H., Olenina, I., & Gross, T. (2022). Estimation of functional diversity and species traits from ecological monitoring data. *Proc Natl Acad Sci U S A, 119*(43), e2118156119.

Sheldon, R. W., Prakash, A., & Sutcliffe, W. H. (1972). The size distribution of particles in the ocean. *Limnology and Oceanography, 17*(3), 327–340.

Sieburth, J., Smetacek, V., & Lenz, J. (1978). Pelagic ecosystem structure: Heterotrophic compartments of the plankton and their relationship to plankton size fractions. *Limnology and Oceanography, 23*, 1256–1263.

Socal, G., I. Buttino, A. Penna, C. Totti, M. Cabrini and O. Mangoni. (2010). Metodologie di studio del Plancton marino.

Sommer, U., Charalampous, E., Genitsaris, S., & Moustaka-Gouni, M. (2017). Benefits, costs and taxonomic distribution of marine phytoplankton body size. *Journal of Plankton Research, 39*(3), 494–508.

Sonnet, V., Guidi, L., Mouw, C. B., Puggioni, G., & Ayata, S. D. (2022). Length, width, shape regularity, and chain structure: Time series analysis of phytoplankton morphology from imagery. *Limnology and Oceanography, 67*(8), 1850–1864.

Sprules, W. G. (1988). Effects of trophic interactions on the shape of pelagic size spectra: With 5 figures in the text. *Internationale Vereinigung Für Theoretische und Angewandte Limnologie: Verhandlungen, 23*(1), 234–240.

Stanca, E., Cellamare, M., & Basset, A. (2013). Geometric shape as a trait to study phytoplankton distributions in aquatic ecosystems. *Hydrobiologia, 701*(1), 99–116.

Sun, J., & Liu, D. (2003). Geometric models for calculating cell biovolume and surface area for phytoplankton. *Journal of Plankton Research, 25*(11), 1331–1346.

Sutton, J. (1997). Gibrat's legacy. *Journal of Economic Literature, 35*(1), 40–59.

Svensson, F., Norberg, J., & Snoeijs, P. (2014). Diatom cell size, coloniality and motility: Trade-offs between temperature, salinity and nutrient supply with climate change. *PLoS ONE, 9*(10), e109993.

Talaber, I., Francé, J., Flander-Putrle, V., & Mozetič, P. (2018). Primary production and community structure of coastal phytoplankton in the Adriatic Sea: Insights on taxon-specific productivity. *Marine Ecology Progress Series, 604*, 65–81.

Talaber, I., Francé, J., & Mozetič, P. (2014). How phytoplankton physiology and community structure adjust to physical forcing in a coastal ecosystem (northern Adriatic Sea). *Phycologia, 53*(1), 74–85.

Totti, C., Romagnoli, T., Accoroni, S., Coluccelli, A., Pellegrini, M., Campanelli, A., Grilli, F., & Marini, M. (2019). Phytoplankton communities in the northwestern Adriatic Sea: Interdecadal variability over a 30-years period (1988–2016) and relationships with meteoclimatic drivers. *Journal of Marine Systems, 193*, 137–153.

Utermöhl, H. (1958). Vervollkommung der quantitativen phytoplankton-methodik. *Zur Mitteilungen Internationale Vereinigung Fuer Theoretische und Ange-Wandte Limnologie, 9*, 1–38.

Vadrucci, M. R., Cabrini, M., & Basset, A. (2007). Biovolume determination of phytoplankton guilds in transitional water ecosystems of Mediterranean Ecoregion. *Transitional Waters Bulletin., 2*, 83–102.

Varkitzi, I., Francé, J., Basset, A., Cozzoli, F., Stanca, E., Zervoudaki, S., Giannakourou, A., Assimakopoulou, G., Venetsanopoulou, A., Mozetič, P., Tinta, T., Skejic, S., Vidjak, O., Cadiou, J. F., & Pagou, K. (2018). Pelagic habitats in the Mediterranean Sea: A review of good environmental status (GES) determination for plankton components and identification of gaps and priority needs to improve coherence for the MSFD implementation. *Ecological Indicators, 95*, 203–218.

Vascotto, I., Aubry, F. B., Bastianini, M., Mozetič, P., Finotto, S., & Francé, J. (2024). Exploring the mesoscale connectivity of

phytoplankton periodic assemblage's succession in northern Adriatic pelagic habitats. *Science of the Total Environment, 913*, 169814.

Vascotto, I., Mozetič, P., & Francé, J. (2021). Phytoplankton time-series in a LTER site of the Adriatic Sea: Methodological approach to decipher community structure and indicative taxa. *Water, 13*(15), 2045.

Verdy, A., Follows, M., & Flierl, G. (2009). Optimal phytoplankton cell size in an allometric model. *Marine Ecology Progress Series, 379*, 1–12.

Weithoff, G., & Gaedke, U. (2016). Mean functional traits of lake phytoplankton reflect seasonal and inter-annual changes in nutrients, climate and herbivory. *Journal of Plankton Research*. https://doi.org/10.1093/plankt/fbw072

Witek, Z., & Krajewska-Soltys, A. (1989). Some examples of the epipelagic plankton size structure in high latitude oceans. *Journal of Plankton Research, 11*(6), 1143–1155.

Zhang, Q., Cozzi, S., Palinkas, C., & Giani, M. (2020). Recent status and long-term trends in freshwater discharge and nutrient inputs. *Coastal Ecosystems in Transition: A Comparative Analysis of the Northern Adriatic and Chesapeake Bay*. https://doi.org/10.1002/9781119543626.ch2

Chapter 5

Conclusions

This dissertation presents the dynamics of the phytoplankton community in the northern Adriatic Sea, presented in three interconnected scientific papers. The overarching aim was to build on previous studies in the area and map the variability of phytoplankton while clarifying the factors that drive it in this ecologically significant and complex marine environment. The research focused on the Slovenian LTER site in the Gulf of Trieste, with later extension to the wider northern Adriatic basin. The dissertation addressed three main hypotheses: (1) the predictability of successional patterns of phytoplankton assemblages characterized by indicative taxa and shaped by environmental conditions in the Gulf of Trieste; (2) the mesoscale connectivity of such assemblages at the scale of the northern Adriatic, driven by periodic and non-periodic events; and (3) the importance of individual cell traits, in exploring and interpreting the presented dynamics of the phytoplankton community.

5.1 Refinement of Analytical Methods

One of the main characteristics of phytoplankton distribution is its high variability in structure and abundance, with some species occasionally reaching very high abundances and many others being either persistent or only occasionally present in low numbers. This complex pattern observed in ecological datasets makes it difficult to determine which species can be excluded from the dataset to simplify the analysis. The index proposed in this dissertation (FREVE) allows to discard "rare" species while preserving the information structure of the dataset.

Clustering techniques further simplify patterns in phytoplankton datasets, although the choice of mathematical distance must be carefully considered. High variability in abundance often leads to numerous zeros in the datasets. Clustering methods based on Euclidean distances are strongly influenced by these zeros and can distort the results. The dissertation shows that chi-squared distances effectively mitigate this problem by converting the abundances into values that represent deviations from the expected abundances.

The clusters identified with this approach are characterized by the presence of indicative species, where the ensemble of species defining a cluster is called an assemblage. An index of representativeness is proposed based on the position of the cluster centroids in the chi-squared transformed data set. This index proves to be more stable against variations in cluster structure than the widely used IndVal index.

5.2 The Phenology of the Recurrent Phytoplankton Assemblages in the Gulf of Trieste

Clustering allowed us to visualize the seasonal separation of the diatom-dominated community during peak periods, with an inconstant and short-lived spring peak and a longer and more diverse autumn bloom, from the mixed community dominated by nanoplanktonic flagellates. Furthermore, a more refined exploration of the cluster structure showed recurring assemblages in the analysed time series, some of which exhibited pronounced seasonality. In addition, several short-lived assemblages were identified whose presence increased in the later years of the time series, possibly indicating an increasing instability of the ecosystem.

5.3 Relationships between Phytoplankton Assemblages and Environmental Factors

In this dissertation, the investigation of the relationship between environmental conditions and short-lived assemblages was not possible due to the limited statistical size, so the focus was on the structure of the most common assemblages. The analysis revealed that assemblages are influenced by both periodic and non-periodic components of environmental conditions. Periodic components were particularly useful for explaining assemblage patterns and predicting them at the mesoscale, providing a link to the seasonality observed in the phenology of recurrent assemblages.

The assemblages showed both linear and non-linear responses to environmental conditions. The phenology of assemblages in the northern Adriatic was in some cases synchronized across the basin, especially in winter and autumn when the community appeared connected. In spring and summer, however, local phenomena dominated the dynamics.

Predictions of changes in the phytoplankton community did not always correspond to the exact occurrence of the predicted species within the assemblages. This discrepancy can be explained by ecological theories such as the lumpy coexistence theory, which assumes that species composition is influenced by both environmental conditions and pre-existing community structure. Consequently, the outcome of competition for resources depends on both these interacting factors.

5.4 Diversity Patterns and Individual Phytoplankton Cell Traits

The techniques applied to the time series of abundance data could also be used for other types of phytoplankton data, such as cell size, biomass and cell shape. The dissertation has shown that diversity patterns change when the unit of measurement changes from abundance to biomass, even when the seasonal succession of the main phytoplankton groups remain similar. This result underlines the need for caution when interpreting and analyzing data of different types.

Comparisons between abundance and biomass data revealed remarkable differences, especially for nano- and microphytoplankton taxa, which swapped their role as dominant

components of the community. Also, the alternative biological traits (shape), compared to taxonomic affiliation were found to retain the major compositional patterns.

Furthermore, this work has shown fluctuations in the distribution of community biomass thorough the year, moving from a power-law distribution to a multimodal distribution. During periods of resource scarcity, such as summer (low nutrients) or winter (low light), biomass followed a power-law distribution as grazing pressure kept populations under control. In contrast, periods of abundant resources led to species blooms and multimodal biomass distributions. Thus, the influence of environmental factors extended beyond the assemblage's structure to the distribution of individual cell sizes and biomasses. These results emphasize the crucial role of environmental conditions in shaping the structure and dynamics of phytoplankton communities.

5.5 A Conceptual Model of the Distribution of Phytoplankton Assemblages and Influencing Factors in a Highly Dynamic Coastal Environment

In summary, the distribution of phytoplankton communities in the Gulf of Trieste exhibits a partially predictable seasonal succession driven by environmental forces and mesoscale connectivity and can be conceptualized as follows. The baseline community is mainly represented in terms of abundance by nano-sized phytoflagellates and less by small diatoms and coccolithophores, while the biomass of this community is occasionally dominated by dinoflagellates. The distribution of phytoplankton biomass and size in these periods of resource scarcity (nutrients or light) or grazing pressure often corresponds to a power law. Conversely, diatoms dominate during peaks, both in biomass and numbers, where the first peak in spring is inconstant and short-lived and the second in autumn being longer and more diverse. Peaks in biomass are associated with larger cells that often exhibit multimodal distribution patterns and reflect trophic "loopholes" in the ecosystem. These shifts highlight the influence of both top-down and bottom-up processes on community dynamics. Community phenology is largely shaped by periodic events such as nutrient inputs from mixing and river discharge, as well as non-periodic disturbances such as droughts and/or prolonged climatic anomalies, which contribute to the emergence of ephemeral or erratic assemblages that have become more common in recent years.

At the mesoscale, the Gulf of Trieste shows a partial connection with the northern Adriatic mediated by physical processes such as cyclonic gyres and wind-driven circulation. Winter and autumn show a basin-wide synchronization of phytoplankton dynamics due to widespread meteorological events, while spring and summer are dominated by local phenomena that disrupt basin-wide connectivity. Stratification, influenced by seasonal wind patterns and freshwater inputs, acts as a key driver of assemblage variability, with stronger effects observed in late spring and summer.

In short, the dissertation showed that:

I. The complexity of the coastal phytoplankton community can be reduced at the level of the main groups of co-occurring species (assemblages).
II. The succession of the phytoplankton assemblages is driven at mesoscale by periodic components of the environmental variables and locally by erratic events.
III. Individual traits are a useful tool to observe the phenology of the overmentioned assemblages and interpret it considering their trophodynamic state.

This dissertation advances the field of marine phytoplankton ecology by providing robust evidence of the interactions between physical and biological processes in the northern Adriatic Sea. The use of ecological modeling has proven helpful in unraveling the complex dynamics of the ecosystem and predicting responses to environmental change. These results have implications for coastal management, particularly in addressing challenges related to climate change, and form the basis for future research where plankton studies should be extended to the entire size and trophic spectrum.

Appendix A

Supplementary Material to Chapter 3

A.1 Gulf of Trieste (GoT) Data

Gaps

Phytoplankton was sampled regularly at 0 m, 5 m, 15 m and near the bottom at 21 m. Sampling occurred regularly every month, with few gaps. A total of 152 months were sampled for a total of 540 sampled depths. For each month of the time series environmental data was collected and only months with data for all the parameters were retained for the analysis. The environmental data consisted of 140 sampled months. Presence and gaps in the series are presented in the Figure 1.

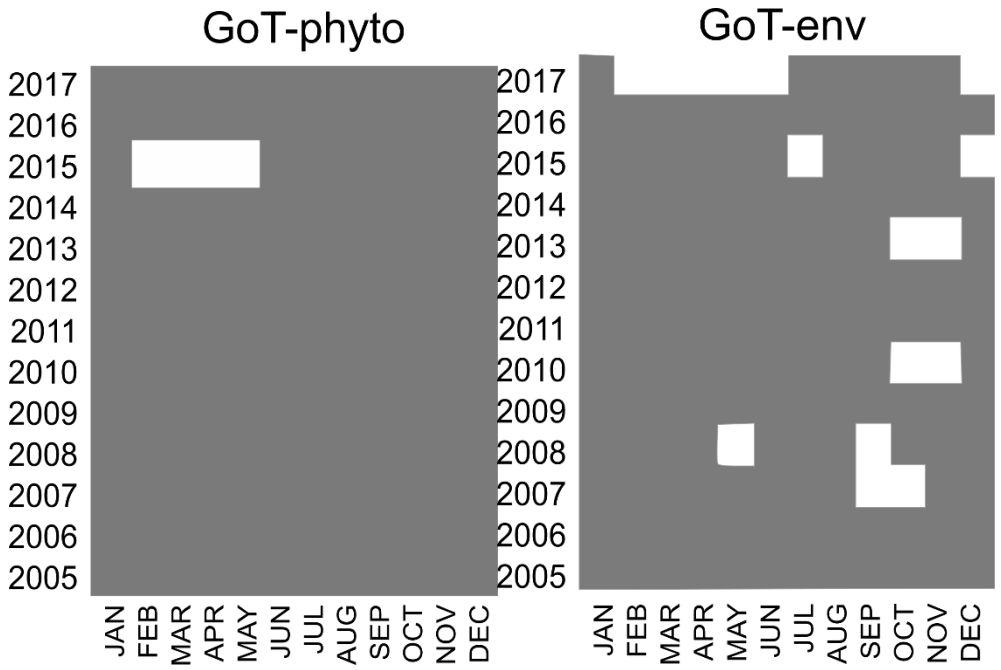

A.1 Presence of data for the Gulf of Trieste (GoT) time series: phytoplankton data (left) and environmental data (right). Gaps are represented as white boxes.

Phytoplankton data

In GoT, a total 130 taxa were determined, the taxa richness of the major groups is presented in the Figure 2. The majority of the identified taxa belonged to the diatoms (Bacillariophyta), dinoflagellates (Miozoa) and coccolithophores (Haptophyta).

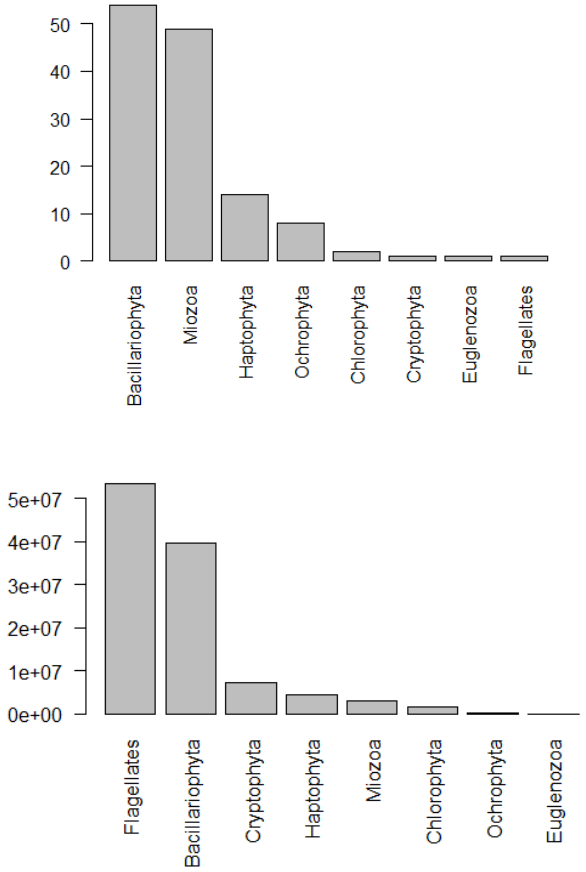

A.2 Frequency distributions of the major phytoplankton groups found in the Gulf of Trieste (GoT) in the period 2005-2017: taxa richness (left) and taxa abundance (right).

The group identified as flagellates was not rich in number of identified taxa (since it comprised mostly non-identified flagellated phytoplankton cells) but was among the most abundant groups, as such it is presented along the three major groups in the phenology diagrams in Figure 3.

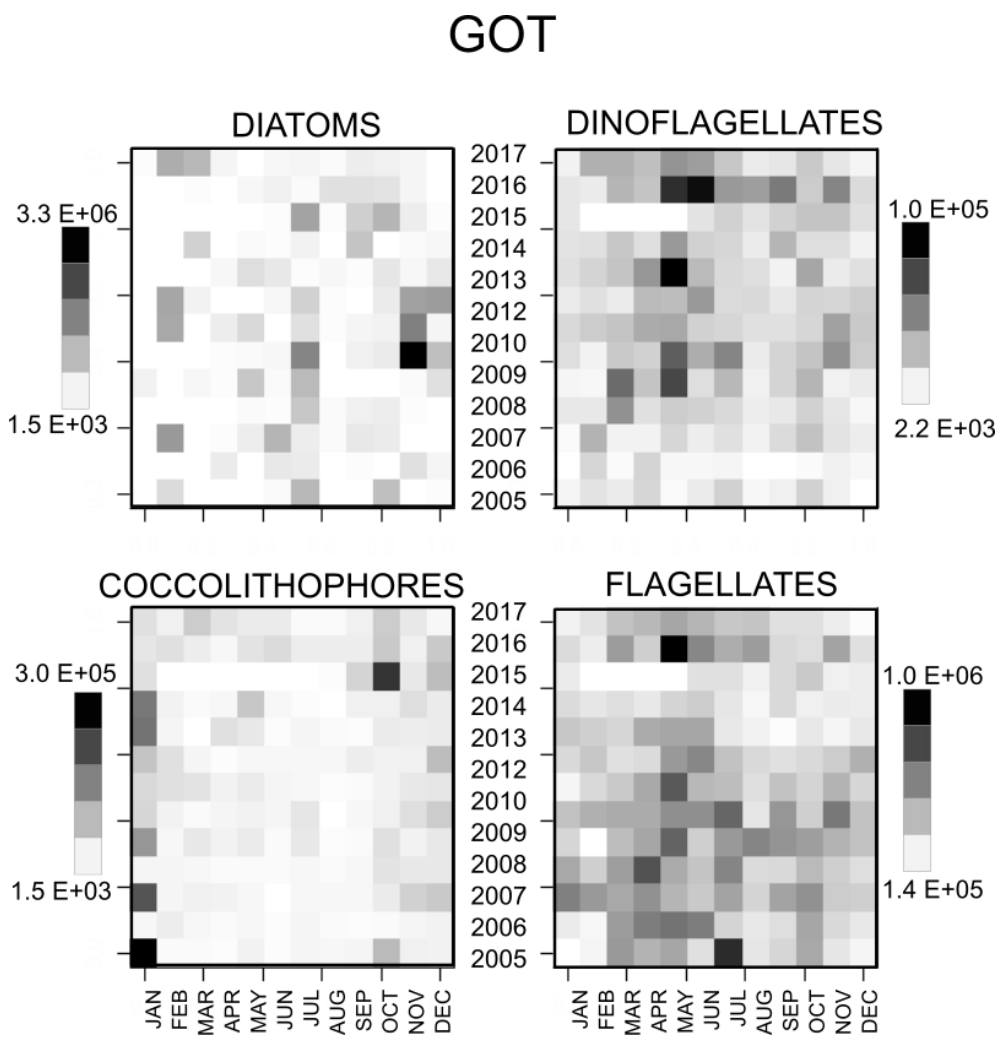

A.3 Phenology of the major phytoplankton groups in the Gulf of Trieste (GoT) in the period 2005-2017: each box represents a sampling month, the abundance value (in cells/L) corresponds to the integrated average among the sampled depths of each month.

Environmental data

The frequency distributions of the monthly averaged environmental data in the GoT in the period 2005-2017 are presented in Figure 4, while the raw environmental data is presented in Figure 5. Additionally, the rose of winds representative for the GoT in the period 2005-2017 is presented in Figure 6 (left panel).

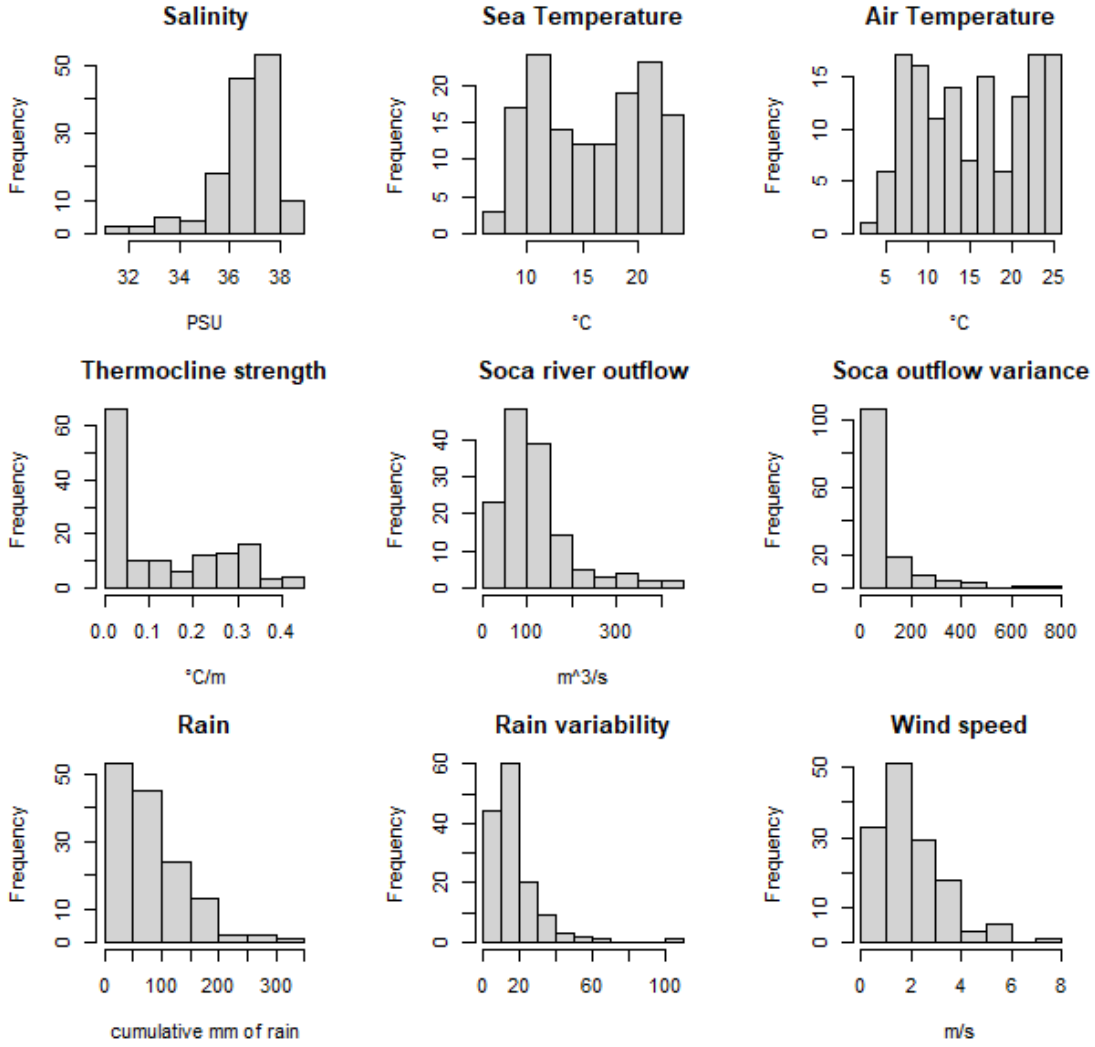

A.4 Histograms of the monthly averaged environmental data of the Gulf of Trieste (GoT) used in the analysis.

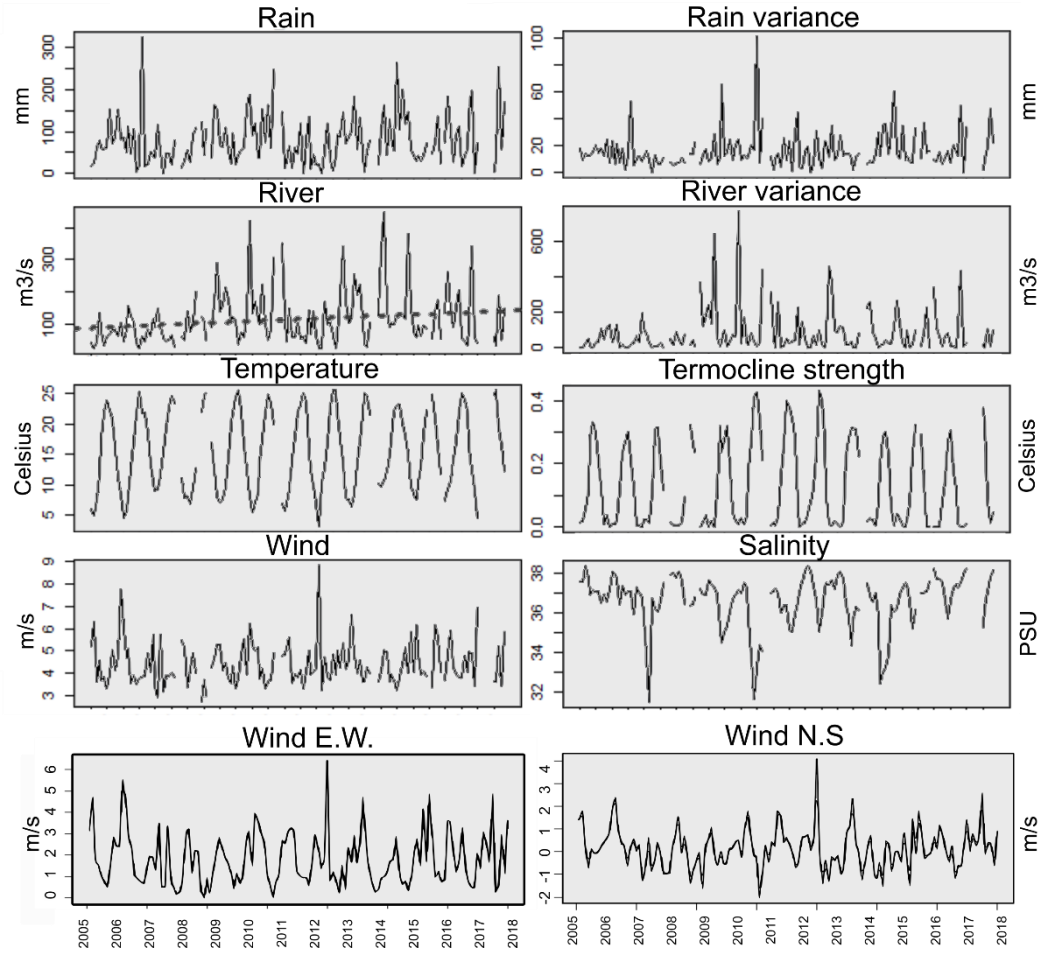

A.5 Time series of environmental parameters from the Gulf of Trieste (GoT) in the period 2005-2017. The dashed line represents the statistically significant linear trend found for the river discharge.

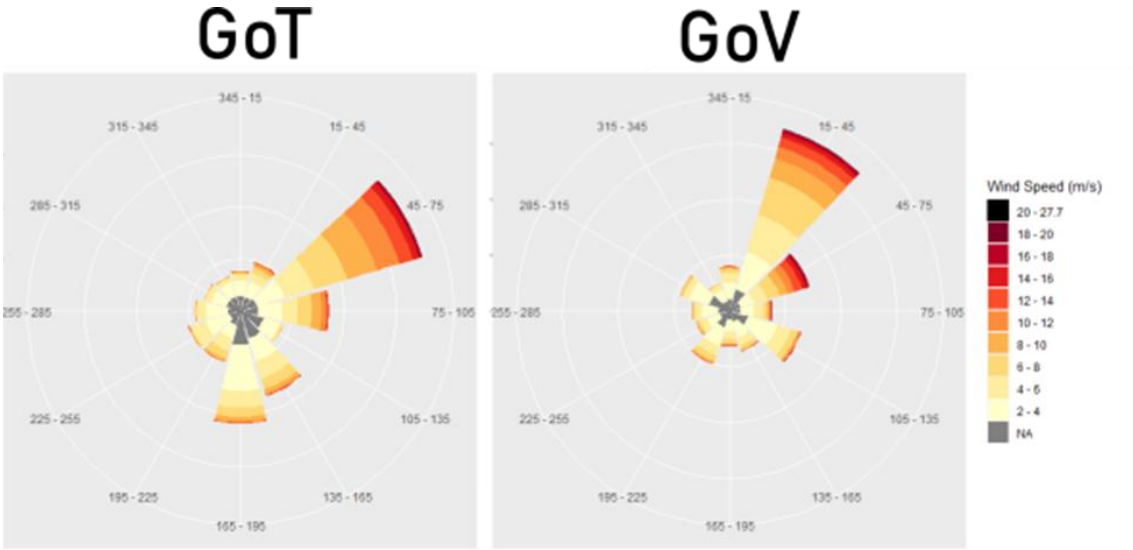

A.6 Rose of winds representative for the study areas in the study period: Gulf of Trieste – GoT (left) and Gulf ov Venice - GoV (right). The colours represent the speed of the wind

events, the orientations represent the direction of the wind events, and the width of each colour band represents the proportion of wind of a certain speed in a certain direction.

Phytoplankton-environment relationships

The effects of each environmental variable over the logarithm of the abundance of the major phytoplankton groups for the GoT in the period 2005-2017 are presented in Figures 7, 8, 9 and 10. The relationship was explored using the smoothed transformation of the environmental variable in the context of generalized additive modelling analysis (GAM).

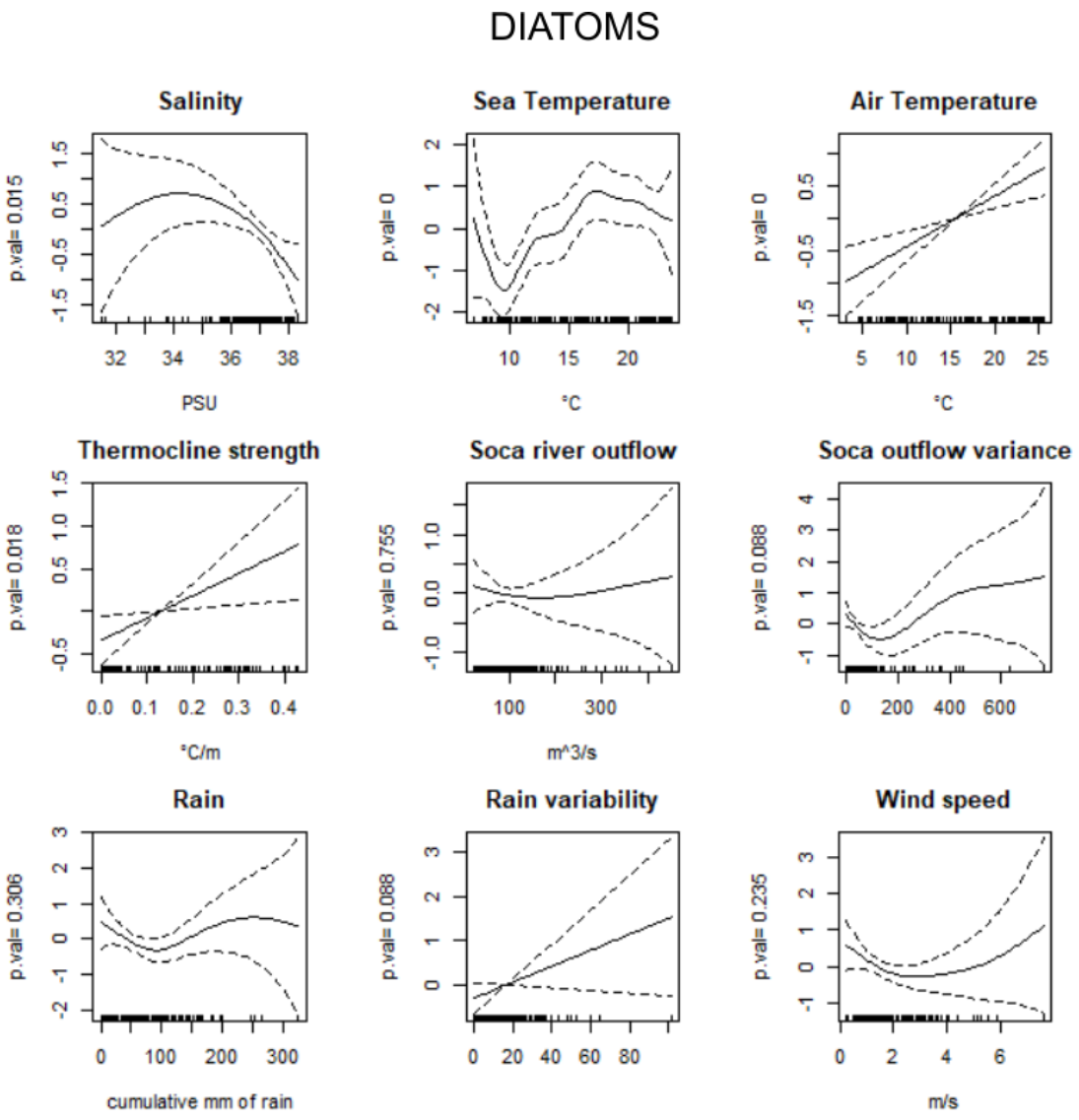

A.7 Generalized additive models (GAMs) of the logarithm of the abundances of diatoms (y axis) in relation to environmental parameters (x axes) for the Gulf of Trieste (GoT). The dashed lines represent the interval of the residual distribution, the solid line represents the smoothed relation between the environmental variable and the abundance of the taxa. Next to the y axis, the p.value of the relationship is reported.

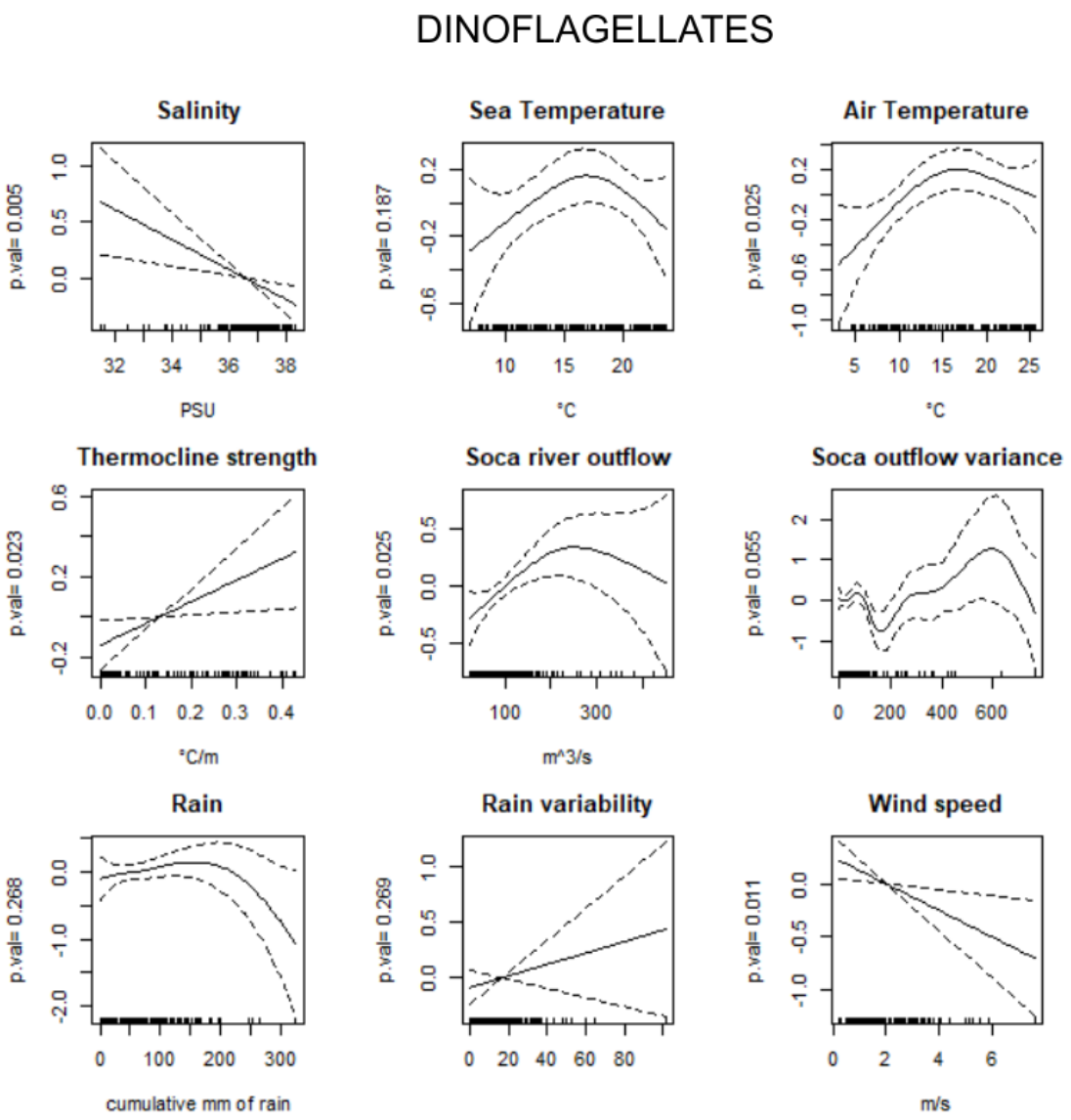

A.8 Generalized additive models (GAMs) of the logarithm of the abundances of dinoflagellates (y axis) in relation to environmental parameters (x axes) for the Gulf of Trieste (GoT). the dashed lines represent the interval of the residual distribution, the solid line represents the smoothed relation between the environmental variable and the abundance of the taxa. Next to the y axis, the p.value of the relationship is reported.

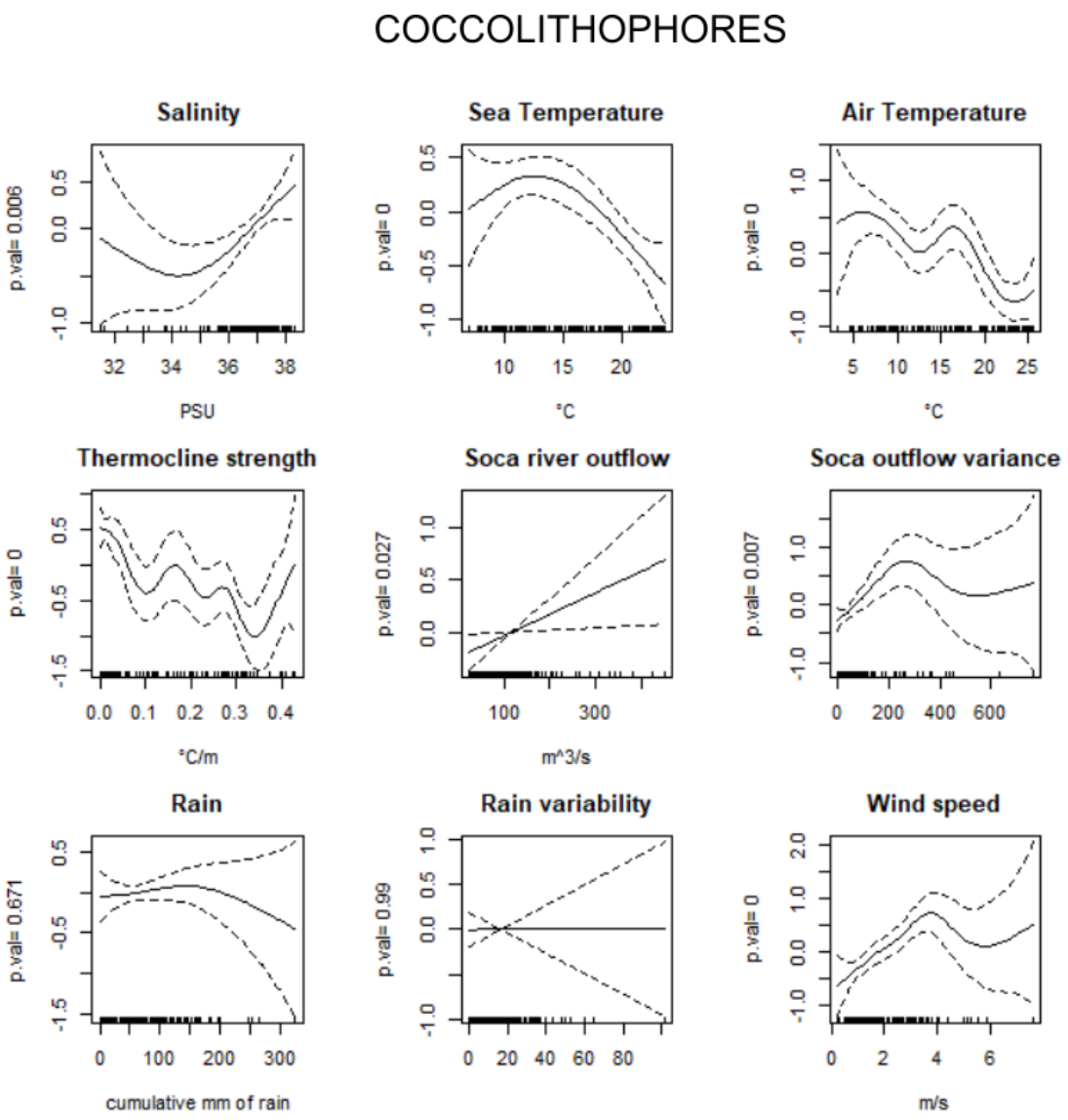

A.9 Generalized additive models (GAMs) of the logarithm of the abundances of coccolithophores (y axis) in relation to environmental parameters (x axes) for the Gulf of Trieste (GoT). The dashed lines represent the interval of the residual distribution, the solid line represents the smoothed relation between the environmental variable and the abundance of the taxa. Next to the y axis, the p.value of the relationship is reported.

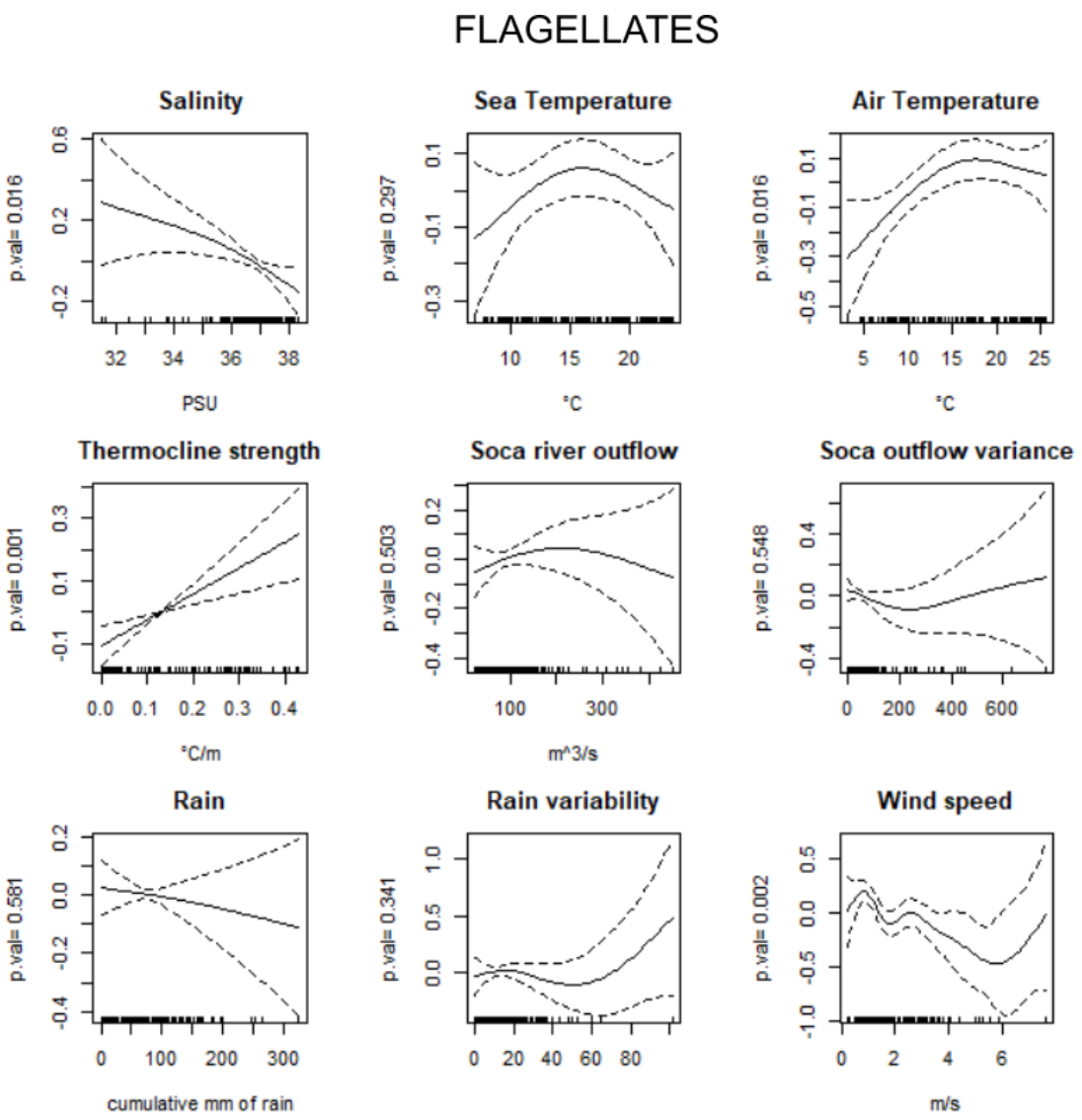

A.10 Generalized additive models (GAMs) of the logarithm of the abundances of flagellates (y axis) in relation to environmental parameters (x axes) for the Gulf of Trieste (GoT). The dashed lines represent the interval of the residual distribution, the solid line represents the smoothed relation between the environmental variable and the abundance of the taxa. Next to the y axis, the p.value of the relationship is reported.

A.2 Gulf of Venice (GoV) Data

Gaps

Phytoplankton was regularly sampled at 0 m and near the bottom at 15 meters, and occasionally at 10-meters depth. Sampling occurred regularly every month, with more gaps with respect to GoT. A total of 77 months were sampled for a total of 156 sampled depths. For each month of the time series environmental data was collected and only months with data for all the parameters were retained for the analysis. The environmental data consisted of 93 sampled months. Presence and gaps in the GoV time series are presented in the Figure 11.

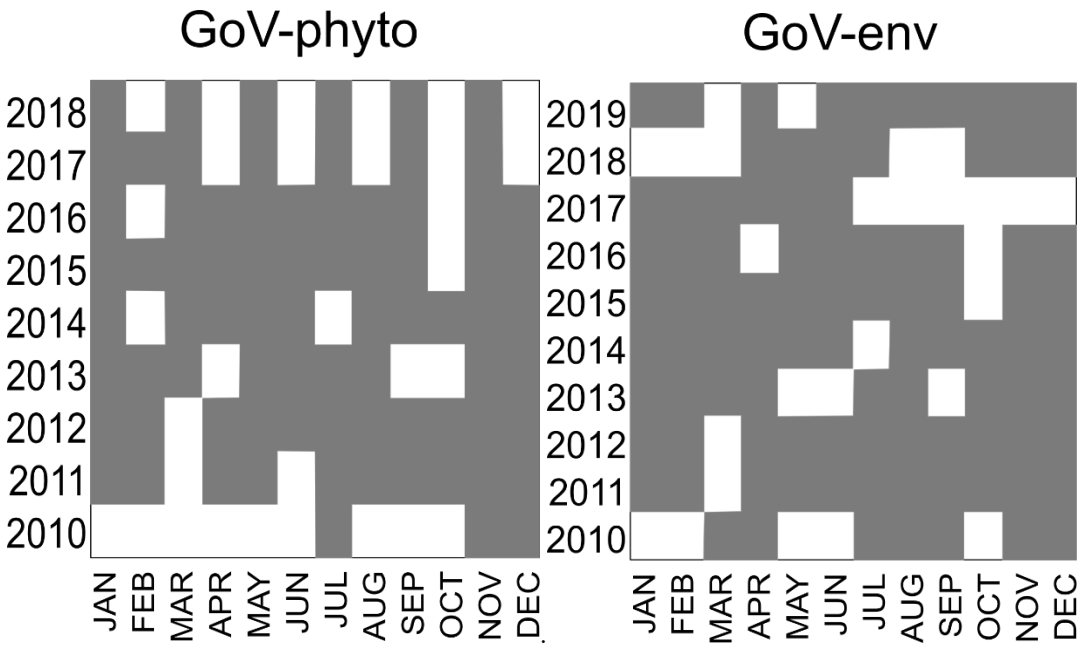

A11 Presence of data for the Gulf of Venice (GoV) time series: phytoplankton data (left) and environmental data (right). Gaps are represented as white boxes.

Phytoplankton data

In GoV a total 332 taxa were determined, the taxa richness of the major phytoplankton groups is presented in the Figure 12. Most of the identified taxa belonged to diatoms (Bacillariophyta), dinoflagellates (Miozoa) and coccolitophores (Haptophyta).

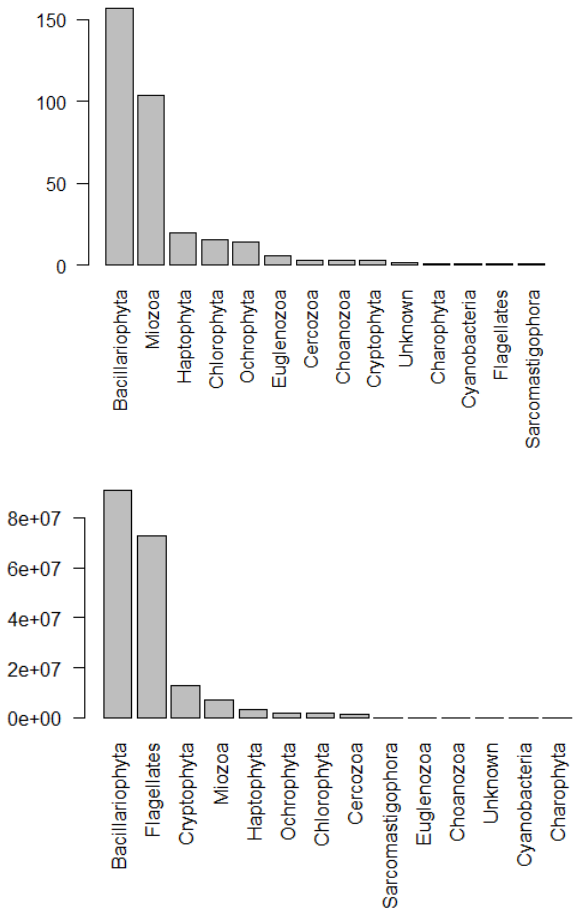

A.12 Frequency distributions of the major phytoplankton groups found in the Gulf of Venice (GoV) in the period 2010-2018: taxa richness (left) and taxa abundance (right).

Again, the group identified as flagellates, was not rich in number of identified taxa but was among the most abundant groups. As such, it is presented along the other three major groups in the phenology diagrams in Figure 13.

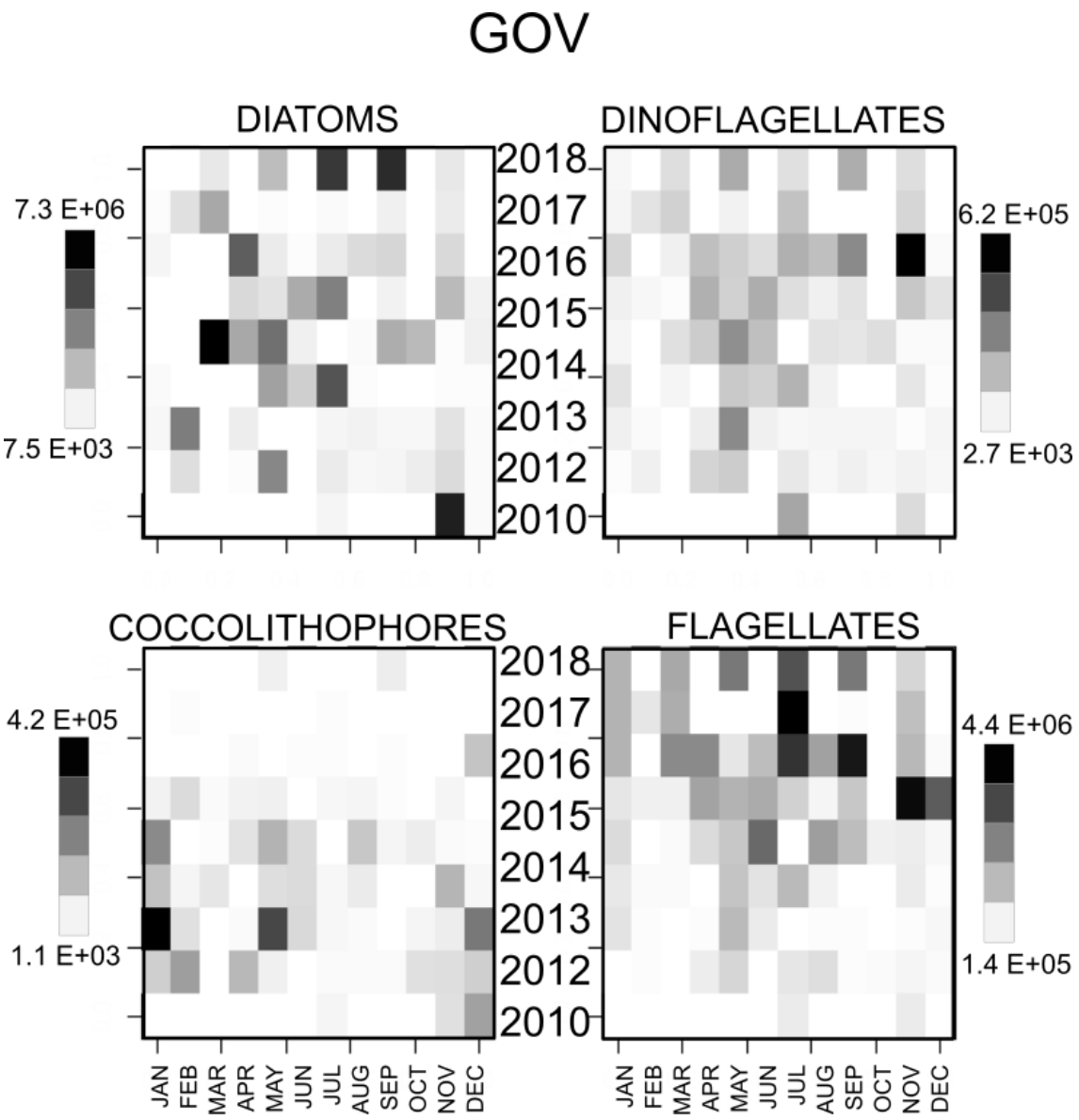

A.13 Phenology of the major phytoplankton groups in the Gulf of Venice (GoV) in the period 2010-2018: each box represents a sampling month, the abundance value (in cells/L) corresponds to the integrated average among the sampled depths of each month.

Environmental data

The frequency distributions of the monthly averaged sampled environmental data in the GoV in the period 2010-2018 are presented in S 14. Additionally, the raw environmental data is presented in S 15 and the rose of winds representative for the GoV is presented in S6 (right panel).

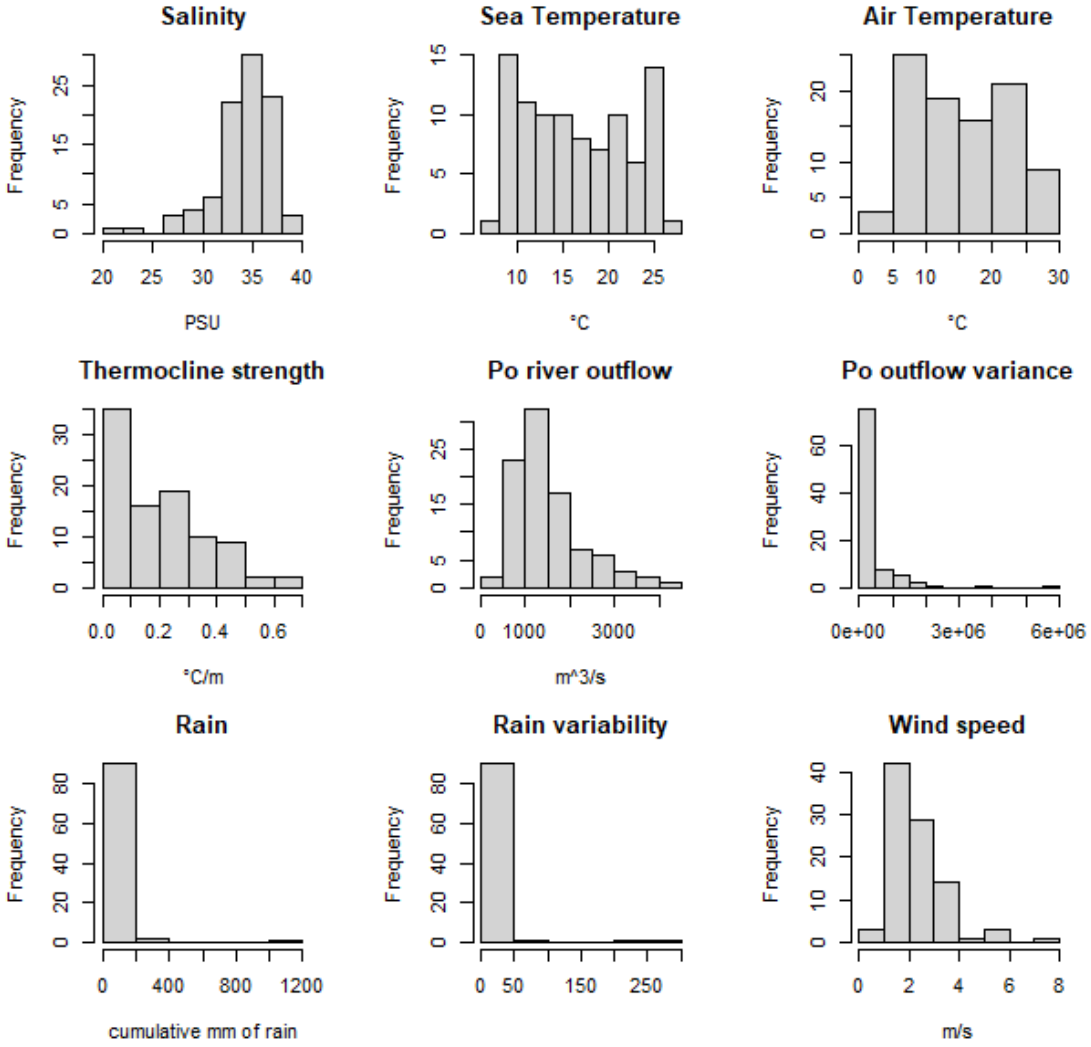

A.14 Histograms of the monthly averaged environmental data of the Gulf of Trieste (GoT) used in the analysis.

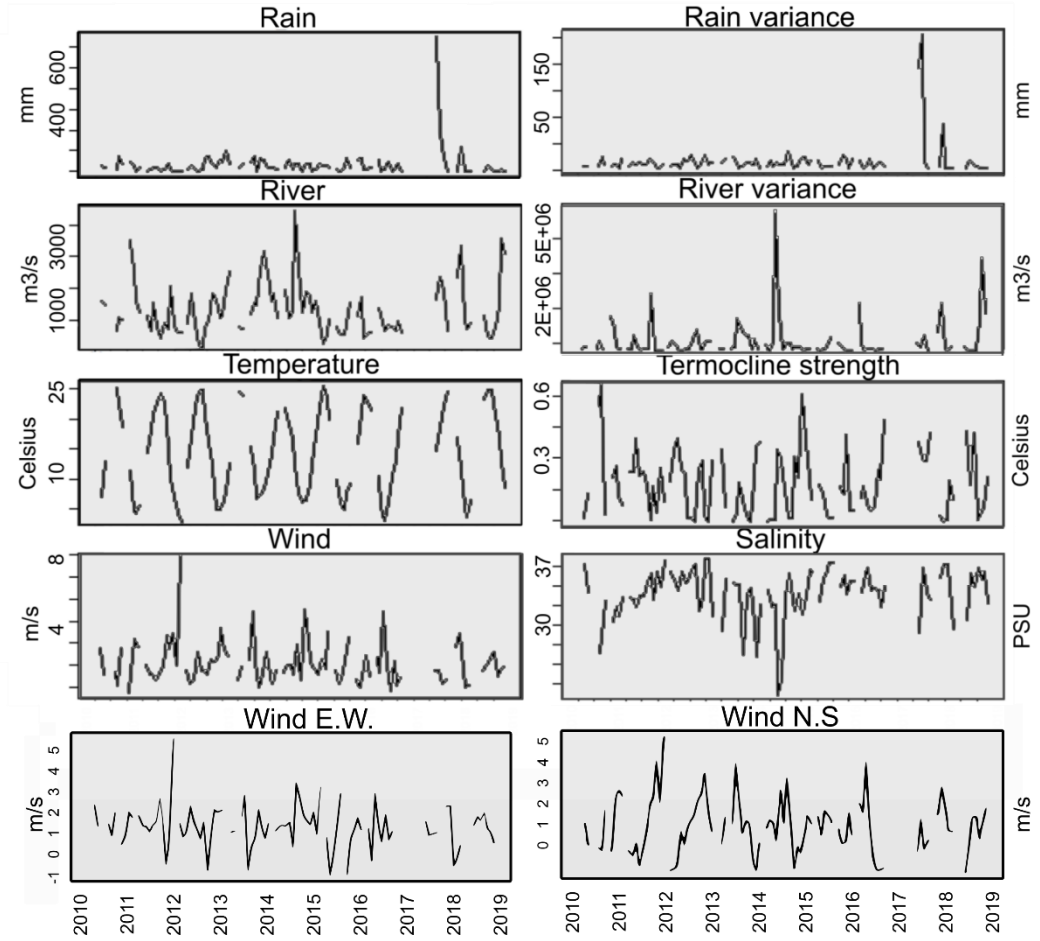

A.15 Time series of environmental parameters from the Gulf of Venice (GoV) in the period 2010-2018. No statistically significant linear trends were found.

A.3 Summary of Results from Vascotto et al. (2021)

The main results of the study of Vascotto et al (2021) used as starting point for the current work can be divided into two sections, methodological and ecological. From the methodological perspective, the flowchart of analysis steps and results is presented in S 16. The presented procedure produced temporal clusters that were highly representative of the information present in the original data on the phytoplankton community in the GoT, and, as such, they were a good reduction of the complexity of the original data. From the ecological perspective, the study showed that two main structural level are present in the GoT phytoplankton data: (i) a coarse phytoplankton assemblage partition with a succession between the mixed phytoplankton community dominated by flagellates and the diatom-dominated community, and (ii) a fine phytoplankton assemblage partition of several clusters (18) each of them characterized by different combinations of taxa. The study highlighted the presence of both seasonality and erratic behaviour in the temporal distribution of these clusters. Moreover, the study emphasized a tendency toward a loss in seasonality in the cluster's presence during the last years of the time series. Several ecological interpretations of the distribution of clusters are given in Vascotto et al. (2021), which were based on the expert knowledge on the ecological distribution of the species composing the clusters but with no direct comparison with environmental data.

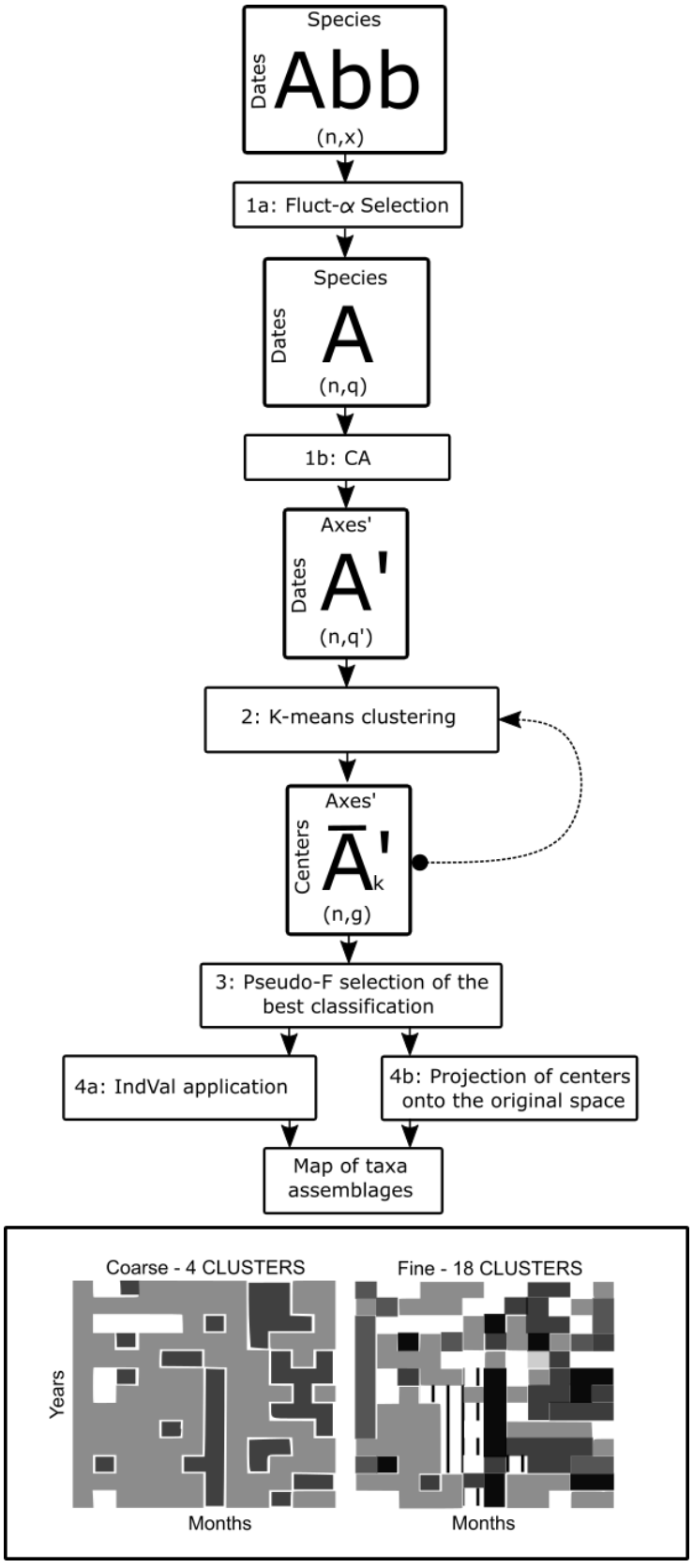

A.16 Flowchart of the main analysis steps used in Vascotto et al. (2021) to obtain the temporal maps used in the present study.

A.4 Moran's Eigenvectors Map

A.4.1 Gulf of Trieste (GoT)

Hereafter, the results from the function mem.select of the R package "adespatial" applied over the GoV environmental variables, where by default, only MEMs associated to positive eigenvalues are considered and a forward selection (based on R2 statistic) is performed after a global test. The results comprise:

Principal component analysis of environmental data with instrumental variables (Moran eigenvector's map)

Total inertia: 4.65

Eigenvalues:

Ax1	Ax2	Ax3	Ax4	Ax5
3.04300	0.83380	0.37275	0.20494	0.09945

Projected inertia (%):

Ax1	Ax2	Ax3	Ax4	Ax5
65.437	17.930	8.016	4.407	2.138

Cumulative projected inertia (%):

Ax1	Ax1:2	Ax1:3	Ax1:4	Ax1:5
65.44	83.37	91.38	95.79	97.93

(Only 5 dimensions (out of 10) are shown)

Total unconstrained inertia : 9.929

Inertia of GoT **explained** by mem.gab.sel$MEM.select (%): 46.84

Decomposition per axis:

	iner	inercum	inerC	inercumC	ratio	R2	lambda
1	4.08	4.08	3.98	3.98	0.976	0.764	3.043
2	2.24	6.32	2.18	6.16	0.974	0.383	0.834

Significative Moran eigenvector components:

variables	order	R2	R2Cum	AdjR2Cum	pvalue
MEM25	25	0.13356000	0.1335600	0.1272814	0.001
MEM27	27	0.08078460	0.2143446	0.2028752	0.001
MEM26	26	0.05014940	0.2644940	0.2482696	0.001
MEM2	2	0.02590105	0.2903950	0.2693697	0.002
MEM24	24	0.02372070	0.3141157	0.2885230	0.002
MEM49	49	0.01820666	0.3323224	0.3022016	0.005
MEM37	37	0.01708701	0.3494094	0.3149084	0.008
MEM29	29	0.01441787	0.3638273	0.3249770	0.015
MEM21	21	0.01411012	0.3779374	0.3348715	0.009
MEM6	6	0.01260542	0.3905428	0.3432981	0.019
MEM7	7	0.01200764	0.4025505	0.3512071	0.031
MEM4	4	0.01198130	0.4145318	0.3592119	0.031
MEM53	53	0.01152278	0.4260545	0.3668380	0.042

MEM11	11	0.01103493	0.4370895	0.3740435	0.050
MEM44	44	0.01091094	0.4480004	0.3812263	0.031
MEM13	13	0.01066228	0.4586627	0.3882448	0.043

Global test:0.4197059

A.4.2 Gulf of Venice (GoV)

Hereafter, the results from the function mem.select of the R package "adespatial" applied over the GoV environmental variables, where by default, only MEMs associated to positive eigenvalues are considered and a forward selection (based on R2 statistic) is performed after a global test. The results comprise:

Principal component analysis of environmental data with instrumental variables (Moran eigenvector's map)

Total inertia: 4.095

Eigenvalues:

Ax1	Ax2	Ax3	Ax4	Ax5
1.6145	1.1322	0.5974	0.2809	0.2595

Projected inertia (%):

Ax1	Ax2	Ax3	Ax4	Ax5
39.428	27.648	14.589	6.861	6.338

Cumulative projected inertia (%):

Ax1	Ax1:2	Ax1:3	Ax1:4	Ax1:5
39.43	67.08	81.66	88.53	94.86

(Only 5 dimensions (out of 10) are shown)

Total unconstrained inertia: 9.892

Inertia of GoV explained by mem.gab.sel$MEM.select (%): 41.39

Decomposition per axis:

	iner	inercum	inerC	inercumC	ratio	R2	lambda
1	2.92	2.92	2.57	2.57	0.881	0.627	1.61
2	2.18	5.10	2.18	4.75	0.932	0.520	1.13

Significative Moran eigenvector components:

variables	order	R2	R2Cum	AdjR2Cum	pvalue
MEM2	2	0.07131429	0.07131429	0.06110895	0.001
MEM19	19	0.05290006	0.12421435	0.10475244	0.001
MEM17	17	0.04994147	0.17415582	0.14631838	0.001
MEM35	35	0.03186540	0.20602122	0.16993127	0.007
MEM21	21	0.02856463	0.23458585	0.19059653	0.013
MEM5	5	0.02762451	0.26221036	0.21073666	0.007
MEM44	44	0.02692030	0.28913066	0.23058848	0.012
MEM12	12	0.02327883	0.31240948	0.24692467	0.013
MEM41	41	0.02081899	0.33322847	0.26092794	0.044
MEM6	6	0.02081143	0.35403990	0.27526428	0.017

MEM1	1	0.02058433	0.37462423	0.28969665	0.042
MEM18	18	0.02017050	0.39479473	0.30401394	0.017
MEM32	32	0.01914136	0.41393609	0.31749519	0.022

Global test: 0.3663597

A.4.3 Redundancy analysis:

The redundancy analysis is used as canonical method to explain the structure of the environmental table by spatial variables obtained by the function mem.select. For instance, Redundancy Analysis (RDA) is available in functions pcaiv (package ade4) or rda (package vegan). RDA is applied using selected MEMs as explanatory variables to study the spatial patterns in environmental variables. The permutation test based on the percentage of variation explained by the spatial predictors (R2) is highly significant in both cases (S17):

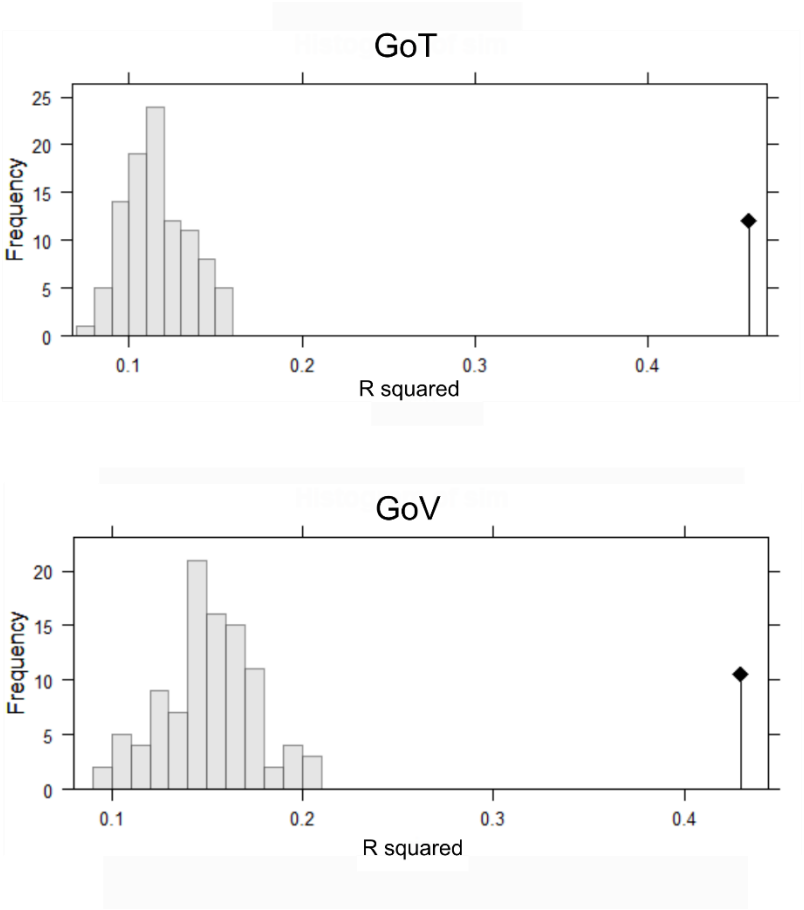

A.17 The frequency histograms of RDA permutation test using random permutations for the periodic components environmental data of the Gulf of Trieste – GoT (upper panel) and Gulf of Venice – GoV (lower panel). The tested values is represented by the solid line and the diamond shape point.

A.4.4 Fitted and residual values

From the RDA between environmental variables and significative moran eigenfunctions (obtained be mem.select) we obtain the environmental fitted and residual values. The fitted values correspond to the periodic components used in this study. The residuals of the RDA correspond to the non-periodic components of the environmental variables used in this study. The axes of decomposition of the fitting over GoT and GoV are presented respectively in S18 and S19.

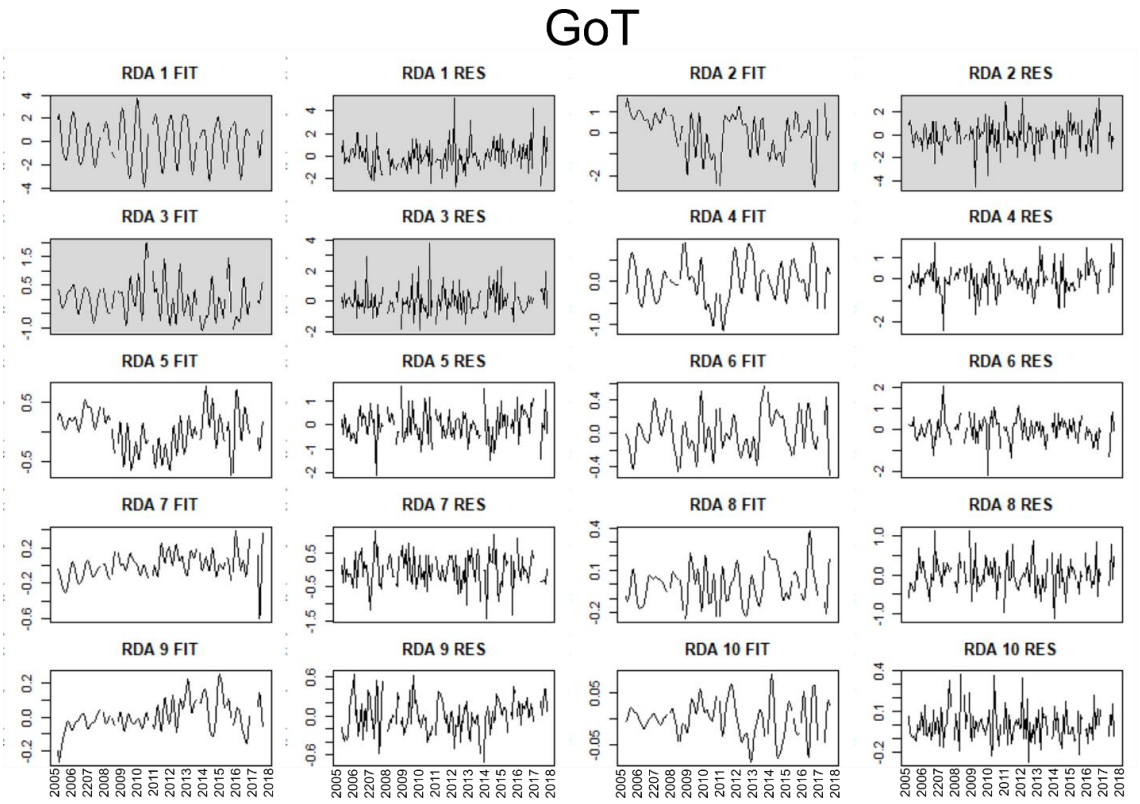

A.18 Fitted (FIT) and residuals (RES) axes of the RDA results for the environmental data of the Gulf of Trieste – GoT. The fitted axes represent the periodic components, the residual axes represent the non-periodic part. The plots with grey background represent the ones that were retained for the modelling of the cluster presence with the linear discriminant analysis and neural network.

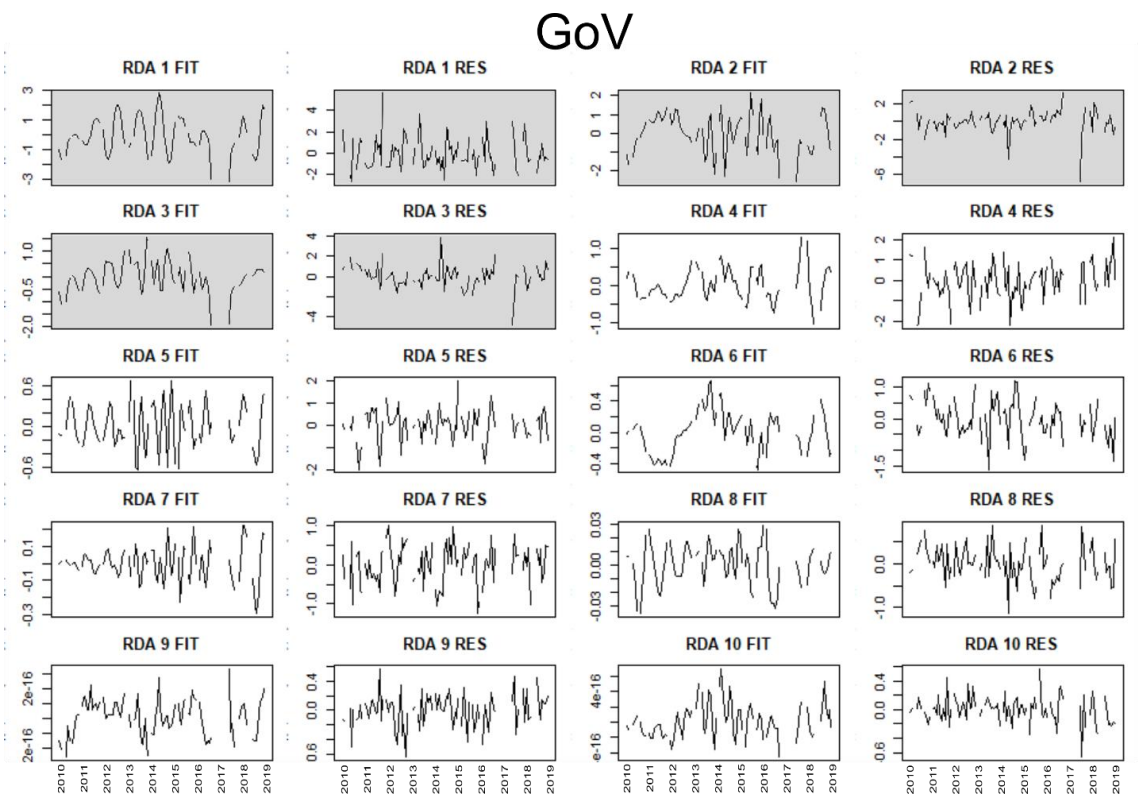

A.19 Fitted (FIT) and residuals axes (RES) of the RDA results for the environmental data of the Gulf of Venice – GoV. The fitted axes represent the periodic components, the residual axes represent the non-periodic part. The plots with grey background represent the ones that were retained for the modelling of the cluster presence with the linear discriminant analysis and neural network.

Appendix B

Supplementary Material to Chapter 4

Table A1 List of shapes and formulas associated to the taxa found in this study. The shapes were associated to the taxa following either the HELCOM list, or by following the most resembling shape principle.

N	Taxa	Shape	Formula	SOURCE
1	*Achnanthes*	parallelepiped	l*w*h	HELCOM
2	*Actinomonas*	sphere	pi/6*d**3	this study
3	*Alexandrium*	rotational ellipsoid	pi/6*d**2*l	HELCOM
4	*Alexandrium minutum*	rotational ellipsoid	pi/6*d**2*l	HELCOM
5	*Amphidinium*	flattened ellipsoid	pi/6*l*d1*d2	HELCOM
6	*Anoplosolenia brasiliensis*	2 cones-30%	pi/12*d**2*h*0.7	this study
7	*Apedinella radians*	sphere	pi/6*d**3	HELCOM
8	*Archaeperidinium c.f.*	sphere	pi/6*d**3	this study
9	*Azadinium caudatum*	cone + half sphere	pi/12*d**2*(h+d/2)	this study
10	*Bacillariophyceae*	cylinder	pi/4*d**2*h	this study
11	*Bacteriastrum*	cylinder	pi/4*d**2*h	this study
12	*Bacteriastrum furcatum*	cylinder	pi/4*d**2*h	this study
13	*Bacteriastrum hyalinum*	cylinder	pi/4*d**2*h	HELCOM
14	*Bacteriastrum mediterraneum*	cylinder	pi/4*d**2*h	this study
15	*Calciosolenia murray*	2 cones-30%	pi/12*d**2*h*0.7	this study
16	*Calyptosphaera*	sphere	pi/6*d**3	this study
17	*Calyptosphaera hyalinus*	sphere	pi/6*d**3	this study
18	*Calyptosphaera oblonga*	rotational ellipsoid	pi/6*d**2*l	this study
19	*Calyptosphaera spheroidea*	sphere	pi/6*d**3	this study
20	*Cerataulina pelagica*	cylinder	pi/4*d**2*h	HELCOM
21	*Ceratium candelabrum*	girdle diameter	2.3038*d**2.532	this study
22	*Ceratium extensum*	girdle diameter	2.3038*d**2.532	this study
23	*Ceratium furca*	girdle diameter	2.3038*d**2.532	HELCOM
24	*Ceratium fusus*	girdle diameter	2.3038*d**2.532	HELCOM
25	*Ceratium horridum*	girdle diameter	2.3038*d**2.532	HELCOM
26	*Ceratium lineatum*	girdle diameter	2.3038*d**2.532	HELCOM
27	*Ceratium longirostrum*	girdle diameter	2.3038*d**2.532	this study
28	*Ceratium macroceros*	girdle diameter	2.3038*d**2.532	HELCOM
29	*Ceratium trichoceros*	girdle diameter	2.3038*d**2.532	this study

30	*cf Fragilariopsis*	cylinder	pi/4*d**2*h	this study
31	*Chaetoceros*	oval cylinder	pi/4*d1*d2*h	HELCOM
32	*Chaetoceros affinis*	oval cylinder	pi/4*d1*d2*h	HELCOM
33	*Chaetoceros brevis*	oval cylinder	pi/4*d1*d2*h	HELCOM
34	*Chaetoceros constrictus*	oval cylinder	pi/4*d1*d2*h	HELCOM
35	*Chaetoceros curvisetus*	oval cylinder	pi/4*d1*d2*h	HELCOM
36	*Chaetoceros danicus*	oval cylinder	pi/4*d1*d2*h	HELCOM
37	*Chaetoceros decipiens*	oval cylinder	pi/4*d1*d2*h	HELCOM
38	*Chaetoceros decipiens/lorenzianus*	oval cylinder	pi/4*d1*d2*h	this study
39	*Chaetoceros didymus*	oval cylinder	pi/4*d1*d2*h	HELCOM
40	*Chaetoceros eibenii*	oval cylinder	pi/4*d1*d2*h	HELCOM
41	*Chaetoceros rostratus*	oval cylinder	pi/4*d1*d2*h	this study
42	*Chaetoceros similis*	oval cylinder	pi/4*d1*d2*h	HELCOM
43	*Chaetoceros simplex*	oval cylinder	pi/4*d1*d2*h	HELCOM
44	*Chaetoceros socialis*	oval cylinder	pi/4*d1*d2*h	HELCOM
45	*Chaetoceros throndsenii*	oval cylinder	pi/4*d1*d2*h	HELCOM
46	*Chaetoceros throndsenii var. trisetosa*	oval cylinder	pi/4*d1*d2*h	this study
47	*Chaetoceros tortissimus*	oval cylinder	pi/4*d1*d2*h	this study
48	*Chaetoceros vixvisibilis*	oval cylinder	pi/4*d1*d2*h	this study
49	*Chaetoceros wighamii*	oval cylinder	pi/4*d1*d2*h	HELCOM
50	*Chlorophyceae*	sphere	pi/6*d**3	HELCOM
51	*Choanoflagellatea*	flattened ellipsoid	pi/6*l*d1*d2	HELCOM
52	*Chrysochromulina*	sphere	pi/6*d**3	HELCOM
53	*Chrysophyceae*	sphere	pi/6*d**3	HELCOM
54	*Coscinodiscus*	cylinder	pi/4*d**2*h	HELCOM
55	*Cryptophyceae*	cone + half sphere	pi/12*d**2*(h+d/2)	HELCOM
56	*Cyclotella*	cylinder	pi/4*d**2*h	HELCOM
57	*Cylindrotheca closterium*	2 cones-30%	pi/12*d**2*h*0.7	HELCOM
58	*Dactyliosolen blavyanus*	cylinder	pi/4*d**2*h	HELCOM
59	*Dactyliosolen fragilissimus*	cylinder	pi/4*d**2*h	HELCOM
60	*Dactyliosolen phuketensis*	cylinder	pi/4*d**2*h	HELCOM
61	*Diatom*	parallelepiped	l*w*h	this study
62	*Dictyocha*	sphere	pi/6*d**3	HELCOM
63	*Dictyocha crux*	sphere	pi/6*d**3	this study
64	*Dictyocha fibula*	half sphere	pi/12*d**3	HELCOM
65	*Dinobryon*	rotational ellipsoid	pi/6*d**2*l	HELCOM
66	*Dinobryon faculiferum*	rotational ellipsoid	pi/6*d**2*l	HELCOM
67	*Dinophyceae*	sphere	pi/6*d**3	HELCOM
68	*Dinophysis*	flattened ellipsoid	pi/6*l*d1*d2	HELCOM
69	*Diplopsalis*	sphere	pi/6*d**3	HELCOM
70	*Dunaliella*	rotational ellipsoid	pi/6*d**2*l	this study
71	*Ebria tripartita*	half sphere-30%	pi/12*d**3*0.7	HELCOM
72	*Emiliania huxleyi*	sphere	pi/6*d**3	HELCOM
73	*Euglena*	cone	pi/12*d**2*h	HELCOM

74	*Flagellates*	rotational ellipsoid	pi/6*d**2*l	HELCOM
75	*Gonyaulax*	sphere-25%	pi/6*d**3*0.75	HELCOM
76	*Gonyaulax polygramma*	rotational ellipsoid	pi/6*d**2*l	HELCOM
77	*Guinardia flaccida*	cylinder	pi/4*d**2*h	HELCOM
78	*Guinardia striata*	cylinder	pi/4*d**2*h	HELCOM
79	*Gymnodinium*	flattened ellipsoid	pi/6*l*d1*d2	HELCOM
80	*Gyrodinium*	flattened ellipsoid	pi/6*l*d1*d2	HELCOM
81	*Haslea wawrikae*	2 cones-30%	pi/12*d**2*h*0.7	this study
82	*Hemiaulus hauckii*	cylinder	pi/4*d**2*h	this study
83	*Heterocapsa*	cone + half sphere	pi/12*d**2*(h+d/2)	HELCOM
84	*Leptocylindrus*	cylinder	pi/4*d**2*h	HELCOM
85	*Leptocylindrus danicus*	cylinder	pi/4*d**2*h	HELCOM
86	*Leptocylindrus mediterraneus*	cylinder	pi/4*d**2*h	HELCOM
87	*Leptocylindrus minimus*	cylinder	pi/4*d**2*h	HELCOM
88	*Licmophora*	half parallelepiped	l*w*h/2	HELCOM
89	*Lioloma pacificum*	parallelepiped	l*w*h	this study
90	*Melosira*	cylinder	pi/4*d**2*h	HELCOM
91	*Meringosphaera mediterranea*	sphere	pi/6*d**3	HELCOM
92	*Mesoporos perforatus*	sphere-20%	pi/6*d**3*0.9	HELCOM
93	*Meuniera membranacea*	oval cylinder	pi/4*d1*d2*h	HELCOM
94	*Minidiscus*	cylinder	pi/4*d**2*h	this study
95	*Naked Dinoflagellate*	cylinder	pi/4*d**2*h	this study
96	*Naked Dinoflagellate*	cone + half sphere - 40%	pi/12*d**2*(h+d/2)*0.6	this study
97	*Naked Dinoflagellate*	sphere	pi/6*d**3	this study
98	*Naked Dinoflagellate*	rotational ellipsoid	pi/6*d**2*l	this study
99	*Naked Dinoflagellate*	flattened ellipsoid	pi/6*l*d1*d2	this study
100	*Naked Dinoflagellate*	(cone + half sphere)-25%	pi/12*d**2*(h+d/2)*0.75	this study
101	*Navicula*	parallelepiped-40%	l*w*h*0.6	HELCOM
102	*Nitzschia*	half parallelepiped	l*w*h/2	HELCOM
103	*Nitzschia cf. acicularis*	rotational ellipsoid	pi/6*d**2*l	this study
104	*Nitzschia longissima*	2 cones	pi/12*d**2*h	HELCOM
105	*Noctiluca scintillans*	sphere	pi/6*d**3	HELCOM
106	*Oblea rotunda*	sphere-10%	pi/6*d**3*0.9	HELCOM
107	*Octactis octonaria*	sphere	pi/6*d**3	this study
108	*Ophyaster hydroideus*	sphere	pi/6*d**3	this study
109	*Oxytoxum*	2 cones	pi/12*d**2*h	HELCOM
110	*Oxytoxum longiceps*	2 cones	pi/12*d**2*h	this study
111	*Papposphaera lepida*	sphere	pi/6*d**3	this study
112	*Periphyllophora mirablis*	sphere	pi/6*d**3	this study
113	*Phaeocystis*	sphere	pi/6*d**3	HELCOM
114	*Pleurosigma*	half parallelepiped	l*w*h/2	HELCOM
115	*Pleurosigma normanii*	half parallelepiped	l*w*h/2	this study

116	*Podolampas palmipes*	girdle diameter	2.3038*d**2.532	this study
117	*Prasinophyceae*	rotational ellipsoid	pi/6*d**2*l	this study
118	*Proboscia alata*	cylinder	pi/4*d**2*h	HELCOM
119	*Prorocentrum*	cone-10%	pi/12*d**2*h*0.9	HELCOM
120	*Prorocentrum balticum*	sphere-10%	pi/6*d**3*0.9	HELCOM
121	*Prorocentrum compressum*	flattened ellipsoid	pi/6*l*d1*d2	HELCOM
122	*Prorocentrum dactylus*	cone-10%	pi/12*d**2*h*0.9	this study
123	*Prorocentrum lima*	flattened ellipsoid	pi/6*l*d1*d2	HELCOM
124	*Prorocentrum micans*	flattened ellipsoid	pi/6*l*d1*d2	HELCOM
125	*Prorocentrum minimum*	cone-10%	pi/12*d**2*h*0.9	HELCOM
126	*Prorocentrum triestinum*	flattened ellipsoid	pi/6*l*d1*d2	HELCOM
127	*Protoperidinium*	(cone + half sphere)-25%	pi/12*d**2*(h+d/2)*0.75	HELCOM
128	*Protoperidinium bipes*	half cone	pi/24*d**2*h	HELCOM
129	*Protoperidinium brevipes*	cone + half sphere	pi/12*d**2*(h+d/2)	HELCOM
130	*Protoperidinium cerasus*	cone + half sphere	pi/12*d**2*(h+d/2)	HELCOM
131	*Protoperidinium curvipes*	cone + half sphere	pi/12*d**2*(h+d/2)	HELCOM
132	*Protoperidinium depressum*	(cone + half sphere)-20%	pi/12*d**2*(h+d/2)*0.8	HELCOM
133	*Protoperidinium divergens*	(cone + half sphere)-20%	pi/12*d**2*(h+d/2)*0.8	HELCOM
134	*Protoperidinium quarnerense/ovatum*	rotational ellipsoid	pi/6*d**2*l	this study
135	*Protoperidinium steinii*	(cone + half sphere)-25%	pi/12*d**2*(h+d/2)*0.75	HELCOM
136	*Prymnesiophyceae*	sphere	pi/6*d**3	this study
137	*Pseliodinium vaubanii*	girdle diameter	2.3038*d**2.532	this study
138	*Pseudanabaena cf. galeata*	cylinder	pi/4*d**2*h	this study
139	*Pseudo-nitzschia pseudodelicatissima g.*	parallelepiped-10%	l*w*h*0.9	this study
140	*Pseudo-nitzschia seriata g.*	parallelepiped-20%	l*w*h*0.8	this study
141	*Pseudosolenia calcar-avis*	cylinder	pi/4*d**2*h	HELCOM
142	*Raphidophyceae*	cone + half sphere - 40%	pi/12*d**2*(h+d/2)*0.6	this study
143	*Rhizosolenia*	cylinder	pi/4*d**2*h	HELCOM
144	*Rhizosolenia fallax*	cylinder	pi/4*d**2*h	this study
145	*Rhizosolenia ostenfeldii*	cylinder	pi/4*d**2*h	this study
146	*Scripsiella*	cone + half sphere	pi/12*d**2*(h+d/2)	this study
147	*Skeletonema*	cylinder	pi/4*d**2*h	HELCOM
148	*Syracosphaera*	sphere	pi/6*d**3	this study
149	*Syracosphaera pulchra*	sphere	pi/6*d**3	this study
150	*Thalassionema nitzschioides*	parallelepiped	l*w*h	HELCOM
151	*Thalassiosira*	cylinder	pi/4*d**2*h	HELCOM
152	*Thalassiosira nordenskioeldii*	cylinder	pi/4*d**2*h	HELCOM
153	*Torodinium robustum*	flattened ellipsoid	pi/6*l*d1*d2	HELCOM
154	*Unknown*	parallelepiped	l*w*h	this study
155	*Unknown*	sphere	pi/6*d**3	this study

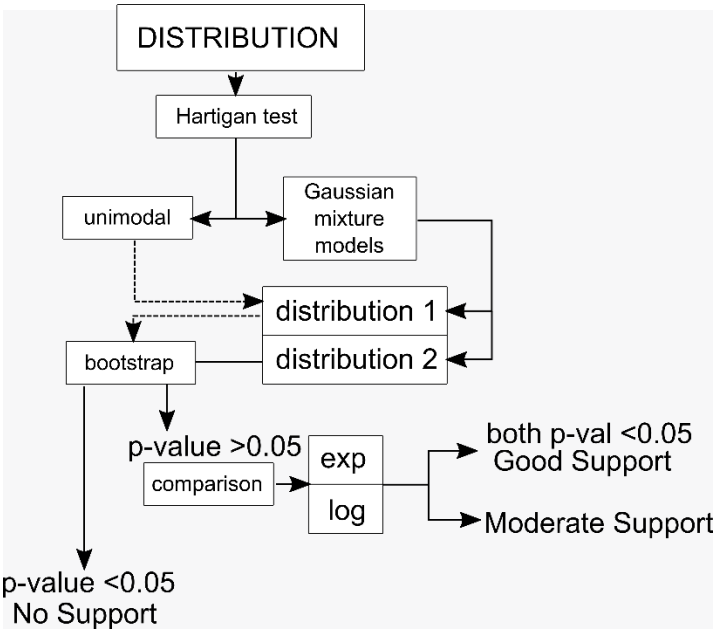

Figure A20: Flowchart of the power law related statistical analysis.

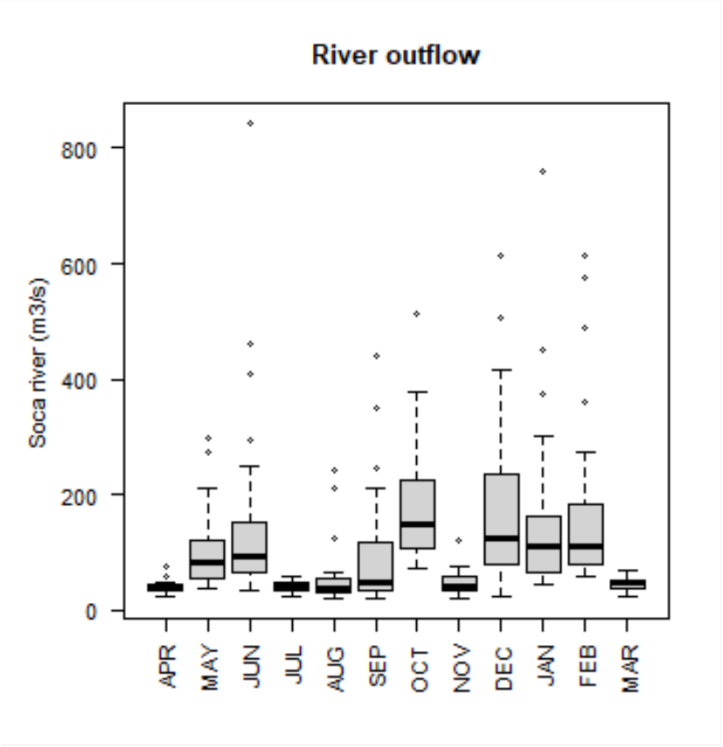

Figure A21 Annual pattern of outflow of the local river in the study period.

Table A2: p-values of the quantileTest over the difference between medians of each month compared to the previous for Soča River flow, individual phytoplankton cell size and biomass. The significative results are signed in bold.

	River	Size (MLD)	Biomass
APR	-	-	-
MAY	**0.000**	0.455	0.455
JUN	0.351	**0.080**	0.263
JUL	**0.000**	0.186	0.265
AUG	0.155	0.153	**0.037**
SEP	**0.027**	0.124	**0.014**
OCT	**0.001**	**0.047**	**0.003**
NOV	**0.000**	0.351	0.080
DEC	**0.000**	0.186	0.186
JAN	0.400	0.306	0.306
FEB	0.456	**0.044**	0.072
MAR	**0.000**	0.119	**0.044**

Table A3: Monthly values of carbon biomass (in mg C m^{-3}) for phytoplankton size classes (PSCs) and main groups at station 000F in the period April 2020 - March 2021 estimated by the Utermöhl method

	Apr	**May**	**Jun**	**Jul**	**Aug**	**Sep**	**Oct**	**Nov**	**Dec**	**Jan**	**Feb**	**Mar**
PSCs												
Microplankton	2.80	15.81	53.29	39.02	7.98	3.01	14.84	11.59	0.79	1.87	2.36	9.15
Nanoplankton	7.23	25.48	36.06	5.34	3.78	2.65	4.75	2.91	1.95	0.61	1.50	4.50
Main groups												
diatoms	1.58	11.75	61.18	34.31	4.80	0.64	7.16	9.56	0.75	0.97	1.08	9.73
chlorophytes	0.51	0.31	0.29	0.06	0.06	0.07	0.05	0.07	0.07	0.01	0.02	0.02
cryptophytes	0.30	0.61	1.67	0.32	0.16	0.19	0.07	0.06	0.10	0.05	0.04	0.45
flagellates	0.53	1.84	3.42	0.76	1.06	0.58	0.62	1.01	0.44	0.15	0.30	0.52
haptophytes	1.97	2.56	3.17	1.95	0.49	0.65	0.96	1.91	0.71	0.29	0.50	1.14
dinoflagellates	4.08	24.22	19.57	6.94	5.02	3.50	10.47	1.89	0.54	0.75	1.90	1.78
silicoflagellates	1.06	0.00	0.06	0.02	0.17	0.02	0.26	0.00	0.13	0.25	0.03	0.02

Table A4: Monthly values of abundances (in 1000 cell L^{-1}) for phytoplankton size classes (PSCs) and main groups at station 000F in the period April 2020 - March 2021 estimated by the Utermöhl method.

	Apr	**May**	**Jun**	**Jul**	**Aug**	**Sep**	**Oct**	**Nov**	**Dec**	**Jan**	**Feb**	**Mar**
PSCs												
Microplankton	23.85	68.24	734.06	91.28	25.34	18.73	76.62	114.83	28.70	2.97	3.52	114.31
Nanoplankton	324.54	650.71	1795.24	195.99	217.56	152.00	159.08	148.04	123.90	44.77	66.12	364.64
Main groups												
diatoms	130.24	307.18	1701.00	110.37	83.44	20.51	110.89	123.09	36.72	2.22	3.25	230.53
chlorophytes	41.65	20.00	30.00	6.96	10.38	8.38	3.36	5.83	7.17	1.45	2.67	1.22
cryptophytes	29.28	60.00	157.50	28.52	17.69	14.86	5.61	6.60	6.04	4.52	4.00	38.78
flagellates	30.52	139.29	377.50	82.43	100.81	91.43	31.72	37.71	40.46	28.39	41.58	184.90
haptophytes	55.67	70.71	97.50	27.13	21.92	20.95	62.06	83.54	56.35	7.04	8.98	14.69
dinoflagellates	24.74	122.49	153.30	30.46	13.99	16.12	21.59	6.49	5.40	3.17	9.32	13.32

silicoflagellates	38.76	0.71	17.50	2.09	3.12	3.43	1.96	0.39	0.46	0.96	0.59	2.04

Table A5: Monthly values of abundances (in 1000 cell L^{-1}) for phytoplankton cell shapes at station 000F in the period April 2020 - March 2021 estimated by the Utermöhl method.

	Apr	May	Jun	Jul	Aug	Sep	Oct	Nov	Dec	Jan	Feb	Mar
2 cones	15.26	0.00	0.00	0.35	0.00	0.00	1.72	3.54	0.79	0.00	0.00	0.00
2 cones-30%	0.41	0.00	0.00	0.70	0.00	0.00	7.93	2.22	22.30	0.00	0.81	1.18
cone	2.06	1.43	2.50	0.70	0.38	0.38	1.12	0.00	0.00	0.00	0.00	0.00
cone-10%	4.95	7.14	10.00	2.09	1.54	0.00	0.37	0.39	1.13	0.32	1.73	3.27
cone + half sphere	34.23	90.00	232.50	40.35	21.58	20.95	11.67	8.93	7.96	5.99	5.50	41.63
cone + half sphere-20%	0.00	0.08	0.00	0.00	0.00	0.00	0.04	0.00	0.00	0.00	0.00	0.00
cone + half sphere-25%	0.00	0.00	0.04	0.00	0.00	0.00	0.00	0.00	0.00	0.00	0.02	0.04
cone + half sphere - 40%	35.46	0.00	0.00	0.00	0.00	0.00	0.00	0.00	0.00	0.00	0.00	2.04
cone half	0.00	0.71	0.00	0.00	0.00	0.00	0.00	0.00	0.00	0.16	0.59	0.32
cylinder	110.04	275.00	920.76	54.91	10.23	0.66	19.84	31.09	8.22	0.81	1.96	17.76
cylinder oval	0.41	12.14	120.24	7.46	59.37	0.38	42.15	13.54	0.08	0.10	0.12	109.40
ellipsoid flattened	1.65	7.29	10.48	4.17	2.20	3.09	3.74	0.86	0.42	0.30	0.43	22.88
ellipsoid rotational	55.67	162.86	432.50	90.09	110.77	99.43	33.84	43.71	42.64	29.23	44.74	163.87
girdle diameter	0.41	0.12	0.28	0.90	0.60	0.08	1.39	0.12	0.00	0.12	0.25	0.16
parallelepiped	4.12	18.61	660.00	12.87	7.69	14.86	16.94	5.26	4.91	0.34	0.06	1.10
parallelepiped-10%	0.00	0.00	0.00	16.70	0.77	0.00	2.61	1.94	1.89	0.00	0.00	100.41
parallelepiped-20%	0.00	0.00	0.00	0.00	2.31	0.76	6.83	64.47	0.83	0.00	0.00	0.16
parallelepiped-40%	0.00	1.43	0.00	7.65	0.00	0.76	0.87	0.39	3.40	0.00	0.19	0.41
parallelepiped half	0.00	0.00	0.00	10.78	3.08	3.09	14.69	0.28	0.04	0.65	0.13	0.04
sphere	79.59	137.14	145.00	36.87	30.08	30.86	69.45	86.10	57.60	9.15	13.27	20.41
sphere-10%	6.60	6.43	0.00	1.39	0.38	0.38	1.50	0.78	0.38	0.00	0.00	0.00
sphere-20%	0.00	0.00	0.00	0.00	0.00	0.00	0.00	0.04	0.00	0.11	0.59	0.41
sphere-25%	0.00	0.00	0.00	0.00	0.00	0.00	0.37	0.00	0.00	0.00	0.00	0.00
sphere half	0.00	0.00	0.00	0.00	0.00	0.00	0.00	0.00	0.00	0.45	0.00	0.00
sphere half - 30%	0.00	0.00	0.00	0.00	0.38	0.00	0.12	0.00	0.00	0.00	0.00	0.00

Table A6: Monthly values of carbon biomass (in mg C m^{-3}) for phytoplankton cell shapes at station 000F in the period April 2020 - March 2021 estimated by the Utermöhl method.

	Apr	May	Jun	Jul	Aug	Sep	Oct	Nov	Dec	Jan	Feb	Mar
2 cones	0.07	0.00	0.00	0.00	0.00	0.00	0.66	0.05	0.04	0.00	0.00	0.00
2 cones-30%	0.02	0.00	0.00	0.02	0.00	0.00	0.12	0.03	0.16	0.00	0.02	0.04

cone	0.06	0.03	0.03	0.01	0.00	0.00	0.01	0.00	0.00	0.00	0.00	0.00
cone-10%	0.79	0.37	0.44	0.08	0.06	0.00	0.01	0.01	0.02	0.00	0.07	0.12
cone + half sphere	0.73	1.94	3.67	0.72	0.31	0.37	3.14	0.12	0.17	0.10	0.11	0.52
cone + half sphere-20%	0.00	0.28	0.00	0.00	0.00	0.00	1.86	0.00	0.00	0.00	0.00	0.00
cone + half sphere-25%	0.00	0.00	0.05	0.00	0.00	0.00	0.00	0.00	0.00	0.00	0.00	0.10
cone + half sphere - 40%	0.90	0.00	0.00	0.00	0.00	0.00	0.00	0.00	0.00	0.00	0.00	0.02
cone half	0.00	0.03	0.00	0.00	0.00	0.00	0.00	0.00	0.00	0.03	0.04	0.05
cylinder	1.26	10.31	29.95	33.44	2.81	0.08	2.82	5.68	0.35	0.52	1.00	4.96
cylinder oval	0.00	0.18	1.56	0.16	1.42	0.02	3.07	1.18	0.00	0.02	0.00	0.95
ellipsoid flattened	1.45	2.65	5.19	2.62	0.67	1.56	1.77	0.27	0.18	0.08	0.14	0.10
ellipsoid rotational	0.68	3.69	6.23	1.13	1.60	0.83	0.70	0.50	0.49	0.23	0.43	0.60
girdle diameter	0.27	0.21	0.68	1.33	2.44	0.10	1.53	0.99	0.00	0.21	0.19	0.45
parallelepiped	0.23	1.23	29.67	0.32	0.29	0.43	0.46	0.35	0.24	0.03	0.02	0.08
parallelepiped-10%	0.00	0.00	0.00	0.20	0.01	0.00	0.04	0.04	0.02	0.00	0.00	3.62
parallelepiped-20%	0.00	0.00	0.00	0.00	0.08	0.08	0.25	1.95	0.03	0.00	0.00	0.02
parallelepiped-40%	0.00	0.03	0.00	0.14	0.00	0.00	0.05	0.07	0.02	0.00	0.01	0.01
parallelepiped half	0.00	0.00	0.00	0.06	0.19	0.03	0.34	0.09	0.03	0.36	0.03	0.02
sphere	2.66	19.52	11.90	3.95	1.69	2.08	2.31	2.92	0.98	0.63	1.74	1.86
sphere-10%	0.91	0.82	0.00	0.19	0.03	0.07	0.04	0.09	0.02	0.00	0.00	0.00
sphere-20%	0.00	0.00	0.00	0.00	0.00	0.00	0.00	0.16	0.00	0.04	0.06	0.17
sphere-25%	0.00	0.00	0.00	0.00	0.00	0.00	0.38	0.00	0.00	0.00	0.00	0.00
sphere half	0.00	0.00	0.00	0.00	0.00	0.00	0.00	0.00	0.00	0.22	0.00	0.00
sphere half - 30%	0.00	0.00	0.00	0.00	0.16	0.00	0.04	0.00	0.00	0.00	0.00	0.00

Table A7: Monthly individual cell size and biomass distribution: mean value, the p.value for the power law test (P-law), the p.value for the likelihood test against the Log-normal distribution (Log), the p.value for the likelihood test against the Exponential distribution (Exp) and the Support for the Power law (G=Good, M=Moderate). s - subpopulation of the small cells, l - subpopulation of the large cells for a specific month

	Individual cell size (MDL)					**Individual cell biomass**				
Month	**mean (in µm)**	**p-value**	**exp**	**log**	**power law support**	**mean (in pg C)**	**p-value**	**exp**	**log**	**power law support**
April	10.64	0.00				28.78	**0.47**	**0.00**	0.95	**M**
May -S	6.59	0.02				57.60	0.00			
May -L	78.03	**0.57**	**0.03**	0.94	**M**					
June -S	6.46	**0.37**	**0.00**	**0.00**	**G**	16.30	**0.93**	0.25	0.91	**M**
June -L	65.77	0.02				19.47	0.00			
July -S	6.75	0.00				8.60	0.00			

July -L	76.84	0.00				40.28	0.00			
August -S	5.19	0.00				48.64	0.00			
August -L	78.01	0.01								
September	11.24	0.00				31.05	0.00			
October -S	7.23	0.00				11.60	0.00			
October -L	47.51	0.00				27.33	0.00			
November - S	5.31	**0.14**	**0.00**	**0.00**	**G**	52.68	0.02			
November - L	58.78	**0.56**	0.46	0.87	**M**					
December - S	4.93	**0.06**	**0.00**	**0.00**	**G**	18.20	0.02			
December - L	18.64	**0.84**	0.31	0.93	**M**					
January	7.13	0.00				37.49	**0.20**	**0.00**	0.97	**M**
February	7.96	**0.14**	**0.00**	0.94	**M**	48.62	**0.67**	**0.00**	0.57	**M**
March -S	4.25	0.00				2.45	0.00			
March -L	78.54	0.00				32.49	0.00			

References

Abonyi, A., Z. Horváth and R. Ptacnik (2018). "Functional richness outperforms taxonomic richness in predicting ecosystem functioning in natural phytoplankton communities." Freshwater Biology 63(2): 178-186.

Adl, S. M., D. Bass, C. E. Lane, J. Lukeš, C. L. Schoch, A. Smirnov, S. Agatha, C. Berney, M. W. Brown and F. Burki (2019). "Revisions to the classification, nomenclature, and diversity of eukaryotes." Journal of Eukaryotic Microbiology 66(1): 4-119.

Aiken, C. M. and S. A. Navarette (2014). "Coexistence of competitors in marine metacommunities: environmental variability, edge effects, and the dispersal niche." Ecology 95(8): 2289–2302.

Akinnawo, S. O. (2023). "Eutrophication: Causes, consequences, physical, chemical and biological techniques for mitigation strategies." Environmental Challenges 12: 100733.

Alster, A., R. Kaplan-Levy, S. Barinova and T. Zohary (2024). "Analyzing semiquantitative phytoplankton counts." Hydrobiologia 851(4): 1079-1090.

Andersen, K. H., T. Berge, R. J. Goncalves, M. Hartvig, J. Heuschele, S. Hylander, N. S. Jacobsen, C. Lindemann, E. A. Martens, A. B. Neuheimer, K. Olsson, A. Palacz, A. E. Prowe, J. Sainmont, S. J. Traving, A. W. Visser, N. Wadhwa and T. Kiorboe (2016). "Characteristic Sizes of Life in the Oceans, from Bacteria to Whales." Ann Rev Mar Sci 8: 217-241.

Anderson, T. R. (2005). "Plankton functional type modelling: running before we can walk?" Journal of Plankton Research 27(11): 1073-1081.

Archibald, J. M., A. G. Simpson, C. H. Slamovits, L. Margulis, M. Melkonian, D. J. Chapman and J. O. Corliss (2017). Handbook of the Protists, Springer Cham, Switzerland.

Armstrong, R. A. (1999). "Stable model structures for representing biogeochemical diversity and size spectra in plankton communities." Journal of Plankton Research 21(3): 445–464.

Aumont, O., C. Ethé, A. Tagliabue, L. Bopp and M. Gehlen (2015). "PISCES-v2: an ocean biogeochemical model for carbon and ecosystem studies." Geoscientific Model Development 8(8): 2465-2513.

Azam, F., T. Fenchel, J. G. Field, J. S. Gray, L.-A. Meyer-Reil and F. Thingstad (1983). "The ecological role of water-column microbes in the sea." Marine ecology progress series. Oldendorf 10(3): 257-263.

Azam, F. and F. Malfatti (2007). "Microbial structuring of marine ecosystems." Nature Reviews Microbiology 5(10): 782-791.

Beardall, J., D. Allen, J. Bragg, Z. V. Finkel, K. J. Flynn, A. Quigg, T. A. V. Rees, A. Richardson and J. A. Raven (2009). "Allometry and stoichiometry of unicellular, colonial and multicellular phytoplankton." New Phytol 181(2): 295-309.

Belmonte, G., P. Castello, M. R. Piccinni, S. Quarta, F. Rubino, S. Geraci and F. Boero (1997). "Resting stages in marine sediments off the Italian coast." Oceanographic Literature Review 44(2): 114-114.

Belmonte, G. and F. Rubino (2019). Resting cysts from coastal marine plankton. Oceanography and Marine Biology: An Annual Review. 57: 1-88.

Bernardi Aubry, F., F. Acri, M. Bastianini, F. Bianchi, D. Cassin, A. Pugnetti and G. Socal (2006). "Seasonal and interannual variations of phytoplankton in the Gulf of Venice (Northern Adriatic Sea)." Chemistry and Ecology 22(sup1): S71-S91.

Bernardi Aubry, F., A. Berton, M. Bastianini, G. Socal and F. Acri (2004). "Phytoplankton succession in a coastal area of the NW Adriatic, over a 10-year sampling period (1990–1999)." Continental shelf research 24(1): 97-115.

Bernardi Aubry, F., G. Cossarini, F. Acri, M. Bastianini, F. Bianchi, E. Camatti, A. De Lazzari, A. Pugnetti, C. Solidoro and G. Socal (2012). "Plankton communities in the northern Adriatic Sea: Patterns and changes over the last 30 years." Estuarine, Coastal Shelf Sci. 115: 125-137.

Boicourt, W. C., M. Ličer, M. Li, M. Vodopivec and V. Malačič (2021). Sea State: Recent Progress in the Context of Climate Change. Coastal Ecosystems in Transition: A Comparative Analysis of the Northern Adriatic and Chesapeake Bay. Malone C. Thomas, A. Malej and J. Faganeli, John Wiley & Sons.

Boje, R. and M. Tomczak (1978). Ecosystem analysis and the definition of boundaries in upwelling regions. Upwelling ecosystems, Springer.

Brewin, R. J. W., N. J. Hardman-Mountford, S. J. Lavender, D. E. Raitsos, T. Hirata, J. Uitz, E. Devred, A. Bricaud, A. Ciotti and B. Gentili (2011). "An intercomparison of bio-optical techniques for detecting dominant phytoplankton size class from satellite remote sensing." Remote Sensing of Environment 115(2): 325-339.

Brown, J. H. (2004). "Toward a metabolic theory of ecology." Ecology 85(7): 1771-1789.

Brush, M. J., P. Mozetič, J. Francé, F. B. Aubry, T. Djakovac, J. Faganeli, L. A. Harris and M. Niesen (2021). Phytoplankton Dynamics in a Changing Environment, John Wiley & Sons.

Brussaard, C. P. (2004). "Viral control of phytoplankton populations--a review." J Eukaryot Microbiol 51(2): 125-138.

Cabrini, M., D. Fornasaro, G. Cossarini, M. Lipizer and D. Virgilio (2012). "Phytoplankton temporal changes in a coastal northern Adriatic site during the last 25 years." Estuarine, Coastal Shelf Sci. 115: 113-124.

Calbet, A. (2001). "Mesozooplankton grazing effect on primary production: a global comparative analysis in marine ecosystems." Limnology and Oceanography 46(7): 1824-1830.

Calbet, A. and M. R. Landry (2004). "Phytoplankton growth, microzooplankton grazing, and carbon cycling in marine systems." Limnology and Oceanography 49(1): 51-57.

Cavender-Bares, K. K., A. Rinaldo and S. W. Chisholm (2001). "Microbial size spectra from natural and nutrient enriched ecosystems." Limnology and Oceanography 46(4): 778-789.

Cerino, F., D. Fornasaro, M. Kralj, M. Giani and M. Cabrini (2019). "Phytoplankton temporal dynamics in the coastal waters of the north-eastern Adriatic Sea (Mediterranean Sea) from 2010 to 2017." Nature Conservation 34: 343-372.

Ciavatta, S., S. Kay, R. J. Brewin, R. Cox, A. Di Cicco, F. Nencioli, L. Polimene, M. Sammartino, R. Santoleri and J. Skakala (2019). "Ecoregions in the Mediterranean Sea through the reanalysis of phytoplankton functional types and carbon fluxes." Journal of Geophysical Research: Oceans 124(10): 6737-6759.

Clauset, A., C. R. Shalizi and M. E. J. Newman (2009). "Power-Law Distributions in Empirical Data." SIAM Review 51(4): 661-703.

Claustre, H. (1994). "The trophic status of various oceanic provinces as revealed by phytoplankton pigment signatures." Limnol. Oceanogr. 39: 1206–1210.

Clayton, S., S. Dutkiewicz, O. Jahn and M. J. Follows (2013). "Dispersal, eddies, and the diversity of marine phytoplankton." Limnology and Oceanography: Fluids and Environments 3(1): 182-197.

Cloern, J. E. (1996). "Phytoplankton bloom dynamics in coastal ecosystems: a review with some general lessons from sustained investigation of San Francisco Bay, California." Reviews of Geophysics 34(2): 127-168.

Cloern, J. E. and A. D. Jassby (2008). "Complex seasonal patterns of primary producers at the land-sea interface." Ecol Lett 11(12): 1294-1303.

Cloern, J. E. and A. D. Jassby (2010). "Patterns and scales of phytoplankton variability in estuarine-coastal ecosystem." Estuaries and Coasts 33: 230-241.

Condie, S. and R. Condie (2016). "Retention of plankton within ocean eddies." Global Ecology and Biogeography 25(10): 1264-1277.

Connell, J. H. (1978). "Diversity in tropical rain forests and coral reefs: high diversity of trees and corals is maintained only in a nonequilibrium state." Science 199(4335): 1302-1310.

Cozzi, S. and M. Giani (2011). "River water and nutrient discharges in the Northern Adriatic Sea: Current importance and long term changes." Continental Shelf Research 31(18): 1881-1893.

Crise, A., S. Querin and V. Malačič (2006). "A strong bora event in the Gulf of Trieste: a numerical study of wind driven circulation in stratified conditions with a preoperational model." Acta Adriatica: International Journal of Marine Sciences 47(Supplement): 185-206.

d'Ortenzio, F. and M. Ribera d'Alcalà (2009). "On the trophic regimes of the Mediterranean Sea: a satellite analysis." Biogeosciences 6(2): 139-148.

D'asaro, E., C. Lee, L. Rainville, R. Harcourt and L. Thomas (2011). "Enhanced turbulence and energy dissipation at ocean fronts." science 332(6027): 318-322.

De Vargas, C., S. Audic, N. Henry, J. Decelle, F. Mahé, R. Logares, E. Lara, C. Berney, N. Le Bescot and I. Probert (2015). "Eukaryotic plankton diversity in the sunlit ocean." Science 348(6237): 1261605.

Degobbis, D., R. Precali, I. Ivancic, N. Smodlaka, D. Fuks and S. Kveder (2000). "Long-term changes in the northern Adriatic ecosystem related to anthropogenic eutrophication." International journal of environment and pollution 13(1-6): 495-533.

Di Cicco, A., M. Sammartino, S. Marullo and R. Santoleri (2017). "Regional Empirical Algorithms for an Improved Identification of Phytoplankton Functional Types and Size Classes in the Mediterranean Sea Using Satellite Data." Frontiers in Marine Science 4.

Durante, G., A. Basset, E. Stanca and L. Roselli (2019). "Allometric scaling and morphological variation in sinking rate of phytoplankton." J Phycol 55(6): 1386-1393.

Durham, W. M., E. Climent, M. Barry, F. De Lillo, G. Boffetta, M. Cencini and R. Stocker (2013). "Turbulence drives microscale patches of motile phytoplankton." Nature communications 4(1): 2148.

Elliott, J., A. Irish and C. Reynolds (2001). "The effects of vertical mixing on a phytoplankton community: a modelling approach to the intermediate disturbance hypothesis." Freshwater Biology 46(10): 1291-1297.

Falkowski, P. G., E. A. Laws, R. T. Barber and J. W. Murray (2003). "Phytoplankton and Their Role in Primary, New, and Export Production." 99-121.

Field, C. B., M. J. Behrenfeld, J. T. Randerson and P. Falkowski (1998). "Primary production of the biosphere: integrating terrestrial and oceanic components." science 281(5374): 237-240.

Filatov, D. A. (2019). "Extreme Lewontin's Paradox in Ubiquitous Marine Phytoplankton Species." Mol Biol Evol 36(1): 4-14.

Finkel, Z. V., J. Beardall, K. J. Flynn, A. Quigg, T. A. V. Rees and J. A. Raven (2009). "Phytoplankton in a changing world: cell size and elemental stoichiometry." Journal of Plankton Research 32(1): 119-137.

Flander-Putrle, V., J. Francé and P. Mozetič (2021). "Phytoplankton Pigments Reveal Size Structure and Interannual Variability of the Coastal Phytoplankton Community (Adriatic Sea)." Water 14(1): 23.

Flynn, K. J., A. Mitra, W. H. Wilson, S. A. Kimmance, D. R. Clark, A. Pelusi and L. Polimene (2022). "'Boom-and-busted'dynamics of phytoplankton–virus interactions explain the paradox of the plankton." New Phytologist 234(3): 990-1002.

Fogg, G. E. (1982). "Nitrogen Cycling in the Sea Waters." Philosophical Transactions of the Royal Society of London. Series B: Biological Sciences 296(1082): 511-520.

Ford, D. A., J. van der Molen, K. Hyder, J. Bacon, R. Barciela, V. Creach, R. McEwan, P. Ruardij and R. Forster (2017). "Observing and modelling phytoplankton community structure in the North Sea." Biogeosciences 14(6): 1419-1444.

Francé, J., I. Varkitzi, E. Stanca, F. Cozzoli, S. Skejić, N. Ungaro, I. Vascotto, P. Mozetič, Ž. Ninčević Gladan, G. Assimakopoulou, A. Pavlidou, S. Zervoudaki, K. Pagou and A. Basset (2021). "Large-scale testing of phytoplankton diversity indices for environmental assessment in Mediterranean sub-regions (Adriatic, Ionian and Aegean Seas)." Ecological Indicators 126: 107630.

Franco, P. and A. Michelato (1992). Northern Adriatic Sea: oceanography of the basin proper and of the western coastal zone. Marine coastal eutrophication, Elsevier: 35-62.

Franks, P. J. (1992). "Phytoplankton blooms at fronts: patterns, scales, and physical forcing mechanisms." Rev. Aquat. Sci 6(2): 121-137.

Gačić, M., A. Lascaratos, B. B. Manca and A. Mantziafau (2001). Adriatic deep water and interaction with the easter mediterranean sea. Physical Oceanography of the Adriatic Sea; Past Present Future. B. Cushman-Roisin, M. Gačić, P.-M. Poulain and A. Artegiani, Kluwer Academic Publishers. 6: 111-142.

Glibert, P. M. (2019). "Phytoplankton in the aqueous ecological theater: Changing conditions, biodiversity, and evolving ecological concepts." Journal of Marine Research 77(Supplement): 83-197.

Godrijan, J., D. Marić, I. Tomažić, R. Precali and M. Pfannkuchen (2013). "Seasonal phytoplankton dynamics in the coastal waters of the north-eastern Adriatic Sea." J. Sea Res. 77: 32-44.

Griffiths, J. R., M. Kadin, F. J. Nascimento, T. Tamelander, A. Törnroos, S. Bonaglia, E. Bonsdorff, V. Brüchert, A. Gårdmark and M. Järnström (2017). "The importance of benthic–pelagic coupling for marine ecosystem functioning in a changing world." Global change biology 23(6): 2179-2196.

Grilli, F., S. Accoroni, F. Acri, F. Bernardi Aubry, C. Bergami, M. Cabrini, A. Campanelli, M. Giani, S. Guicciardi and M. Marini (2020). "Seasonal and interannual trends of oceanographic parameters over 40 years in the northern Adriatic Sea in relation to nutrient loadings using the EMODnet chemistry data portal." Water 12(8): 2280.

Grime, J. P. (1977). "Evidence for the existence of three primary strategies in plants and its relevance to ecological and evolutionary theory." The american naturalist 111(982): 1169-1194.

Groß, E., J. Di Pane, M. Boersma and C. L. Meunier (2022). "River discharge-related nutrient effects on North Sea coastal and offshore phytoplankton communities." Journal of Plankton Research 44(6): 947-960.

Guiry, M. D. (2024). How many species of algae are there? A reprise. Four kingdoms, 14 phyla, 63 classes and still growing. Journal of Phycology, 60(2), 214-228.

Hatton, I. A., R. F. Heneghan, Y. M. Bar-On and E. D. Galbraith (2021). "The global ocean size spectrum from bacteria to whales." Science Advances 7.

Hays, G. C., A. J. Richardson and C. Robinson (2005). "Climate change and marine plankton." Trends Ecol Evol 20(6): 337-344.

Heneghan, R. F., I. A. Hatton and E. D. Galbraith (2019). "Climate change impacts on marine ecosystems through the lens of the size spectrum." Emerg Top Life Sci 3(2): 233-243.

Herbert, R. A. (1999). "Nitrogen cycling in coastal marine ecosystem." FEMS Microbiology Review 23(563-590).

Horner-Devine, A. R., R. D. Hetland and D. G. MacDonald (2015). "Mixing and transport in coastal river plumes." Annual Review of Fluid Mechanics 47: 569-594.

Hossain, M. S., A. K. Gain and K. G. Rogers (2020). Sustainable coastal social-ecological systems: how do we define “coastal”?, Taylor & Francis. 27: 577-582.

Hubbel, S. P. (2005). "The Neutral Theory of Biodiversity and Biogeography and Stephen Jay Gould." Paleobiology 31(2): 122-132.

Huisman, J. and F. J. Weissing (1999). "Biodiversity of plankton by species oscillation and chaos." Nature 402.

Huppert, A., B. Blasius and L. Stone (2002). "A Model of Phytoplankton Blooms." The American Naturalist 159(2): 156-171.

Hutchinson, G. E. (1941). "Ecological Aspects of Succession in Natural Populations." Am. Nat. 75(760): 406-418.

Hutchinson, G. E. (1961). "The Paradox of the Plankton " Am. Nat. 95(882): 137-145.

IOCCG (2000). " Remote Sensing of Ocean Colour in Coastal, and Other Optically-Complex, Waters. Sathyendranath, S. (ed.), Reports of the International Ocean-Colour Coordinating Group, No. 3, IOCCG, Dartmouth, Canada.".

Irigoien, X., K. J. Flynn and R. P. Harris (2005). "Phytoplankton blooms: a 'loophole' in microzooplankton grazing impact?" Journal of Plankton Research 27(4): 313-321.

Jeffrey, S. and M. Vesk (2005). "Introduction to marine phytoplankton and their pigment signatures."

Jenkins, D. G. and R. E. Ricklefs (2011). "Biogeography and ecology: two views of one world." Philos Trans R Soc Lond B Biol Sci 366(1576): 2331-2335.

Kemp, A. E. S. and T. A. Villareal (2018). "The case of the diatoms and the muddled mandalas: Time to recognize diatom adaptations to stratified waters." Prog. Oceanogr. 167: 138-149.

Kostadinov, T. S., D. A. Siegel and S. Maritorena (2009). "Retrieval of the particle size distribution from satellite ocean color observations." Journal of Geophysical Research 114(C9).

Kostadinov, T. S., D. A. Siegel and S. Maritorena (2010). "Global variability of phytoplankton functional types from space: assessment via the particle size distribution." Biogeosciences 7(10): 3239-3257.

Kremp, A. (2001). "Effects of cyst resuspension on germination and seeding of two bloom-forming dinoflagellates in the Baltic Sea." Marine Ecology Progress Series 216: 57-66.

Kruk, C., M. Devercelli, V. L. M. Huszar, E. Hernández, G. Beamud, M. Diaz, L. H. S. Silva and A. M. Segura (2017). "Classification of Reynolds phytoplankton functional groups using individual traits and machine learning techniques." Freshwater Biology 62(10): 1681-1692.

Le Quéré, C., S. P. Harrison, I. C. Prentice, E. T. Buitenhuis, O. Aumont, L. Bopp, H. Claustre, L. C. Da Cunha, R. Geider, X. Giraud, C. Klaas, K. E. Kohfeld, L. Legendre, M. Manizza, T. Platt, R. B. Rivkin, S. Sathyendranath, J. Uitz, A. J. Watson and D. Wolf-Gladrow (2005). "Ecosystem dynamics based on plankton functional types for global ocean biogeochemistry models." Global Change Biology 11: 2016-2040.

Legendre, P. and L. Legendre (2012). Numerical ecology, Elsevier.

Litchman, E. and C. A. Klausmeier (2008). "Trait-Based Community Ecology of Phytoplankton." Ann. Rev. Ecol. Evol. Syst. 39(1): 615-639.

Litchman, E., C. A. Klausmeier, O. M. Schofield and P. G. Falkowski (2007). "The role of functional traits and trade-offs in structuring phytoplankton communities: scaling from cellular to ecosystem level." Ecology letters 10(12): 1170-1181.

Malačič, V. and B. Petelin (2001). Regional Studies. Physical Oceanography of the Adriatic Sea: Past, Present, And Future. B. Cushman-Roisin, M. Gačić, P.-M. Poulain and A. Artegiani, Kluwer Academic Publishers: 167-181.

Malačič, V. and B. Petelin (2009). "Climatic circulation in the Gulf of Trieste (northern Adriatic)." Journal of Geophysical Research: Oceans 114(C7).

Malačič, V., B. Petelin and M. Vodopivec (2012). "Topographic control of wind-driven circulation in the northern Adriatic." Journal of Geophysical Research: Oceans 117(C6).

Mangolte, I., M. Lévy, S. Dutkiewicz, S. Clayton and O. Jahn (2022). "Plankton community response to fronts: winners and losers." Journal of Plankton Research 44(2): 241-258.

Mangoni, O., M. Modigh, P. Mozetič, A. Bergamasco, P. Rivaro and V. Saggiomo (2008). "Structure and photosynthetic properties of phytoplankton assemblages in a highly

dynamic system, the Northern Adriatic Sea." Estuarine, Coastal and Shelf Science 77(4): 633-644.
Mansour, J. S. and K. Anestis (2021). "Eco-evolutionary perspectives on mixoplankton." Frontiers in Marine Science 8: 666160.
Marcus, N. H. and F. Boero (1998). "Minireview: The importance of benthic-pelagic coupling and the forgotten role of life cycles in coastal aquatic systems." Limnology and Oceanography 43(5): 763-768.
Margalef, R. (1978). "Life-forms of phytoplankton as survival alternatives in an unstable environment." Oceanol. Acta 1(4): 493-509.
Margalef, R. (1978). "Life-forms of phytoplankton as survival alternatives in an unstable environment." Oceanologica acta 1(4): 493-509.
Margalef, R. (1978). What is an upwelling ecosystem?, Springer.
Margalef, R., M. Estrada and D. Blasco (1979). "Functional morphology of organisms involved in red tides, as adapted to decaying turbulence [Dinoflagellates, Algae]." Developments in marine biology.
Marić, D., R. Kraus, J. Godrijan, N. Supić, T. Djakovac and R. Precali (2012). "Phytoplankton response to climatic and anthropogenic influences in the north-eastern Adriatic during the last four decades." Estuarine, Coastal Shelf Sci. 115: 98-112.
Marquet, P. A., R. A. Quinones, S. Abades, F. Labra, M. Tognelli, M. Arim and M. Rivadeneira (2005). "Scaling and power-laws in ecological systems." J Exp Biol 208(Pt 9): 1749-1769.
Martin, A. P. (2003). "Phytoplankton patchiness: the role of lateral stirring and mixing." Progress in Oceanography 57(2): 125-174.
Martin, A. P., K. J. Richards, A. Bracco and A. Provenzale (2002). "Patchy productivity in the open ocean." Global Biogeochemical Cycles 16(2): 9-1-9-9.
May, R. (1976). "Simple mathematical models with very complicated dynamics." Nature 261(459-467).
McGill, B. J., B. J. Enquist, E. Weiher and M. Westoby (2006). "Rebuilding community ecology from functional traits." Trends Ecol Evol 21(4): 178-185.
McManus, M. A. and C. B. Woodson (2012). "Plankton distribution and ocean dispersal." J Exp Biol 215(Pt 6): 1008-1016.
Medlin, L. K. (2016). "Evolution of the diatoms: major steps in their evolution and a review of the supporting molecular and morphological evidence." Phycologia 55(1): 79-103.
Menden-Deuer, S. and E. J. Lessard (2000). "Carbon to volume relationships for dinoflagellates, diatoms, and other protist plankton." Limnol. Oceanogr. 45(3): 569–579.
Mitra, A., K. J. Flynn and M. J. Fasham (2007). "Accounting for grazing dynamics in nitrogen-phytoplankton-zooplankton (NPZ) models." Limnology and Oceanography 52(2): 649-661.
Mozetič, P., J. Francé, T. Kogovšek, I. Talaber and A. Malej (2012). "Plankton trends and community changes in a coastal sea (northern Adriatic): Bottom-up vs. top-down control in relation to environmental drivers." Estuarine, Coastal Shelf Sci. 115: 138-148.
Mozetič, P., C. Solidoro, G. Cossarini, G. Socal, R. Precali, J. Francé, F. Bianchi, C. De Vittor, N. Smodlaka and S. Fonda Umani (2010). "Recent Trends Towards Oligotrophication of the Northern Adriatic: Evidence from Chlorophyll a Time Series." Estuaries and Coasts 33(2): 362-375.
Mullin, M. M. and E. R. Brooks (1976). "Some consequences of distributional heterogeneity of phytoplankton and zooplankton1." Limnology and Oceanography 21(6): 784-796.
Niklas, K. J. (2004). "Plant allometry: is there a grand unifying theory?" Biol Rev Camb Philos Soc 79(4): 871-889.
Nock, C. A., R. J. Vogt and B. E. Beisner (2016). "Functional Traits." 1-8.
Olenina, I., S. Hajdu, L. Edler, A. Andersson, N. Wasmund, S. Busch, J. Göbel, S. Gromisz, S. Huseby, M. Huttunen, A. Jaanus, P. Kokkonen, I. Ledaine and E. Niemkiewicz (2006).

"Biovolumes and size-classes of phytoplankton in the Baltic Sea HELCOM." Balt.Sea Environ. Proc. 106(144).

Paytan, A. and K. McLaughlin (2007). "The Oceanic Phosphorus Cycle." Chem. Rev. 107: 563-576.

Perkins, D. M., A. Perna, R. Adrian, P. Cermeno, U. Gaedke, M. Huete-Ortega, E. P. White and G. Yvon-Durocher (2019). "Energetic equivalence underpins the size structure of tree and phytoplankton communities." Nat Commun 10(1): 255.

Petelin, B., I. Kononenko, V. Malačič and M. Kukar (2013). "Multi-level association rules and directed graphs for spatial data analysis." Expert Systems with Applications 40(12): 4957-4970.

Pielou, E. C. (1977). Mathematical ecology, John Wiley & Sons.

Platt, T. and K. L. Denmann (1975). "Spectral Analysis in Ecology." Annual Review of Ecology and Systematics 6: 189-210.

Platt, T. and S. Sathyendranath (1999). "Spatial structure of pelagic ecosystem processes in the global ocean." Ecosystems 2: 384-394.

Poulain, P.-M., V. H. Kourafalou and B. Cushman-Roisin (2001). Northern Adriatic Sea. Physical Oceanography of the Adriatic Sea: Past, Present, And Future. . B. Cushman-Roisin, M. Gačić, P.-M. Poulain and A. Artegiani, Kluwer Academic Publishers: 167-181.

Ptacnik, R., A. G. Solimini, T. Andersen, T. Tamminen, P. Brettum, L. Lepistö, E. Willén and S. Rekolainen (2008). "Diversity predicts stability and resource use efficiency in natural phytoplankton communities." Proceedings of the National Academy of Science of the United States of America 105(13): 5134-5138.

Rangel-Buitrago, N., F. Galgani and W. J. Neal (2024). "Addressing the global challenge of coastal sewage pollution." Marine Pollution Bulletin 201: 116232.

Rao, C. R. (1982). "Diversity And Dissimilarity Coefficents: A Unified Apporach." J. Theor. Pop. Biol. 21(24-33).

Raven, J. (1998). "The twelfth Tansley Lecture. Small is beautiful: the picophytoplankton." Functional ecology 12(4): 503-513.

Rengefors, K., A. Kremp, T. B. H. Reusch and A. M. Wood (2017). "Genetic diversity and evolution in eukaryotic phytoplankton: revelations from population genetic studies." Journal of Plankton Research.

Reynolds, C. (1980). "Phytoplankton Assemblages and Their Periodicity in Stratifying Lake Systems." Holoartic Ecology 3(3): 141-159.

Reynolds, C. (2006). The Ecology of Phytoplankton, Cambridge University Press, Cambridge.

Reynolds, C., M. Dokulil and J. Padisák (2000). "Understanding the assembly of phytoplankton in relation to the trophic spectrum: where are we now?" Hydrobiologia 424: 147-152.

Reynolds, C. S. (2006). The ecology of phytoplankton, Cambridge University Press.

Reynolds, C. S. and A. J. Elliott (2002). "Phytoplankton diversity: discontinuous assembly responses to environmental forcing." Internationale Vereinigung für theoretische und angewandte Limnologie: Verhandlungen 28(1): 336-344.

Reynolds, C. S., V. Huszar, C. Kruk, L. Naselli-Flores and S. Melo (2002). "Towards a functional classification of the freshwater phytoplankton." Journal of Plankton Research 24(5): 417-428.

Rocchini, D., M. Marcantonio, D. Da Re, G. Bacaro, E. Feoli, G. M. Foody, R. Furrer, R. J. Harrigan, D. Kleijn, M. Iannacito, J. Lenoir, M. Lin, M. Malavasi, E. Marchetto, R. S. Meyer, V. Moudry, F. D. Schneider, P. Šímová, A. H. Thornhill, E. Thouverai, S. Vicario, R. K. Wayne, C. Ricotta and T. Gillespie (2021). "From zero to infinity: Minimum to maximum diversity of the planet by spatio-parametric Rao's quadratic entropy." Global Ecology and Biogeography 30(5): 1153-1162.

Roelke, D. L. and S. Spatharis (2015). "Phytoplankton assemblage characteristics in recurrently fluctuating environments." PLoS One 10(3): e0120673.

Roelke, D. L. and S. Spatharis (2015). "Phytoplankton succession in recurrently fluctuating environments." PLoS One 10(3): e0121392.

Rojo, C. and M. Alvarez-Cobelas (2000). "A plea for more ecology in phytoplankton ecology." Hydrobiologia 424: 141–146.

Roselli, L. and E. Litchman (2017). "Phytoplankton traits, functional groups and community organization." Journal of Plankton Research 39(3): 491-493.

Sakavara, A., G. Tsirtsis, D. L. Roelke, R. Mancy and S. Spatharis (2018). "Lumpy species coexistence arises robustly in fluctuating resource environments." PNAS 115(4): 738-743.

Salmaso, N., L. Naselli-Flores and J. Padisák (2015). "Functional classifications and their application in phytoplankton ecology." Freshwater Biology 60(4): 603-619.

Scheffer, M. and E. H. van Nes (2006). "Self-organized similarity, the evolutionary emergence of groups of similar species." Proc Natl Acad Sci U S A 103(16): 6230-6235.

Sheldon, R. W., A. Prakash and W. H. Sutcliffe (1972). "The Size Distribution of Particles in the Ocean." Limnology and Oceanography 17(3): 327-340.

Shikata, T., S. Nagasoe, T. Matsubara, S. Yoshikawa, Y. Yamasaki, Y. Shimasaki, Y. Oshima, I. R. Jenkinson and T. Honjo (2008). "Factors influencing the initiation of blooms of the raphidophyte Heterosigma akashiwo and the diatom Skeletonema costatum in a port in Japan." Limnology and Oceanography 53(6): 2503-2518.

Sieburth, J., V. Smetacek and J. Lenz (1978). "Pelagic ecosystem structure: Heterotrophic compartments of the plankton and their relationship to plankton size fractions." Limnol. Oceanogr. 23: 1256–1263

Smayda, T. J. and C. S. Reynolds (2001). "Community assembly in marine phytoplankton: application of recent models to harmful dinoflagellate blooms." Journal of plankton research 23(5): 447-461.

Smayda, T. J. and C. S. Reynolds (2003). "Strategies of marine dinoflagellate survival and some rules of assembly." Journal of Sea Research 49(2): 95-106.

Socal, G., I. Buttino, A. Penna, C. Totti, M. Cabrini and O. Mangoni (2010). Metodologie di studio del Plancton marino.

Soetaert, K., J. J. Middelburg, P. M. Herman and K. Buis (2000). "On the coupling of benthic and pelagic biogeochemical models." Earth-Science Reviews 51(1-4): 173-201.

Soininen, J. (2010). "Species Turnover along Abiotic and Biotic Gradients: Patterns in Space Equal Patterns in Time?" BioScience 60(6): 433-439.

Sournia, A., M. J. Chretiennot-Dinet and M. Ricard (1991). "Marine phytoplankton: how many species in the world ocean?" Journal of Plankton Research 13(5): 1093-1099.

Stirn, J. (1993). "Man-made eutrophication in the Mediterranean Sea." Prospettive e proposte mediterranee-Rivista di Economia, Agricoltura e Ambiente.

Stone, L. (1993). "Period-doubling reversals and chaos in simple ecological models." Nature 365: 617-620.

Sullivan, J. M., M. A. McManus, O. M. Cheriton, K. J. Benoit -Bird and J. P. Ryan (2010). "Layered organization in the coastal ocean: An introduction to planktonic thin layers and the LOCO project." Continental Shelf Research 30: 1-6.

Talaber, I., J. Francé, V. Flander-Putrle and P. Mozetič (2018). "Primary production and community structure of coastal phytoplankton in the Adriatic Sea: insights on taxon-specific productivity." Marine Ecology Progress Series 604: 65-81.

Talaber, I., J. Francé and P. Mozetič (2014). "How phytoplankton physiology and community structure adjust to physical forcing in a coastal ecosystem (northern Adriatic Sea)." Phycologia 53(1): 74-85.

Thompson, P. A. and J. Carstensen (2023). "Global observing for phytoplankton? A perspective." Journal of Plankton Research 45(1): 221-234.

Titocci, J., M. Bon and P. Fink (2022). "Morpho-functional traits reveal differences in size fractionated phytoplankton communities but do not significantly affect zooplankton grazing." Microorganisms 10(1): 182.

Totti, C., T. Romagnoli, S. Accoroni, A. Coluccelli, M. Pellegrini, A. Campanelli, F. Grilli and M. Marini (2019). "Phytoplankton communities in the northwestern Adriatic Sea: Interdecadal variability over a 30-years period (1988–2016) and relationships with meteoclimatic drivers." Journal of Marine Systems 193: 137-153.

Treguer, P. J. and C. L. De La Rocha (2013). "The world ocean silica cycle." Ann Rev Mar Sci 5: 477-501.

Turk Dermastia, T., F. Cerino, D. Stankovic, J. France, A. Ramsak, M. Znidaric Tusek, A. Beran, V. Natali, M. Cabrini and P. Mozetic (2020). "Ecological time series and integrative taxonomy unveil seasonality and diversity of the toxic diatom Pseudo-nitzschia H. Peragallo in the northern Adriatic Sea." Harmful Algae 93: 101773.

Uitz, J., H. Claustre, A. Morel and S. B. Hooker (2006). "Vertical distribution of phytoplankton communities in open ocean: An assessment based on surface chlorophyll. ." J. Geophys. Res. Oceans 111.

Utermöhl, H. (1958). "Vervollkommung der quantitativen Phytoplankton-Methodik. ." Zur Mitteilungen Internationale Vereinigung fuer Theoretische und Ange-wandte Limnologie 9: 1-38.

Vadrucci, M. R., M. Cabrini and A. Basset (2007). "Biovolume determination of phytoplankton guilds in transitional water ecosystems of Mediterranean Ecoregion." Transitional Waters Bulletin(2): 83-102.

Vallina, S. M., M. J. Follows, S. Dutkiewicz, J. M. Montoya, P. Cermeno and M. Loreau (2014). "Global relationship between phytoplankton diversity and productivity in the ocean." Nat Commun 5: 4299.

Verdy, A., M. Follows and G. Flierl (2009). "Optimal phytoplankton cell size in an allometric model." Marine Ecology Progress Series 379: 1-12.

Vidussi, F., H. Claustre, B. B. Manca, A. Luchetta and J. C. Marty (2001). "Phytoplankton pigment distribution in relation to upper thermocline circulation in the Eastern Mediterranean Sea during winter." J. Geophys. Res. Oceans 106: 19939–19956.

Viličić, D., M. Kuzmic, I. Tomažić, Z. Ljubešić, S. Bosak, R. Precali, T. Djakovac, D. Marić and J. Godrijan (2013). "Northern Adriatic phytoplankton response to short Po River discharge pulses during summer stratified conditions." Marine ecology 34(4): 451-466.

von Dassow, P. and M. Montresor (2011). "Unveiling the mysteries of phytoplankton life cycles: patterns and opportunities behind complexity." Journal of Plankton Research 33(1): 3-12.

Weithoff, G. and B. E. Beisner (2019). "Measures and Approaches in Trait-Based Phytoplankton Community Ecology – From Freshwater to Marine Ecosystems." Frontiers in Marine Science 6.

Weithoff, G. and U. Gaedke (2016). "Mean functional traits of lake phytoplankton reflect seasonal and inter-annual changes in nutrients, climate and herbivory." Journal of Plankton Research.

Wilhelm, S. W. and C. A. Suttle (1999). "Viruses and nutrient cycles in the sea: viruses play critical roles in the structure and function of aquatic food webs." Bioscience 49(10): 781-788.

Winder, M. and J. E. Cloern (2010). "The annual cycles of phytoplankton biomass." Philosophical Transaction of The Royal Society 365: 3215-3226.

Witek, Z. and A. Krajewska-Soltys (1989). "Some examples of the epipelagic plankton size structure in high latitude oceans." Journal of Plankton Research 11(6): 1143-1155.

Zapata, M. (2005). "Recent advances in pigment analysis as applied to picophytoplankton." Vie et Milieu 55(3): 233-248.

Zapata, M., S. Fraga, F. Rodríguez and J. L. Garrido (2012). "Pigment-based chloroplast types in dinoflagellates." Marine Ecology Progress Series 465: 33-52.

Zapata, M., S. W. Jeffrey, S. W. Wright, F. Rodríguez, J. L. Garrido and L. Clementson (2004). "Photosynthetic pigments in 37 species (65 strains) of Haptophyta: implications for oceanography and chemotaxonomy." Marine Ecology Progress Series 270: 83-102

Bibliography

Journal Articles

Vascotto, I., Mozetič, P. & Francé, J. (2021). Phytoplankton Time-Series in a LTER Site of the Adriatic Sea: Methodological Approach to Decipher Community Structure and Indicative Taxa. Water, **13**: 2045.

Vascotto, I., Aubry, F. B., Bastianini, M., Mozetič, P., Finotto, S., & Francé, J. (2024). Exploring the mesoscale connectivity of phytoplankton periodic assemblage's succession in northern Adriatic pelagic habitats. Science of the Total Environment, **913**: 169814.

Vascotto, I., Mozetič, P., & Francé, J. (2024). Phytoplankton morphological traits and biomass outline community dynamics in a coastal ecosystem (Gulf of Trieste, Adriatic Sea). Community Ecology, **25**(3): 389-402.

Turk Dermastia, T., Vascotto, I., Francé, J., Stanković, D., & Mozetič, P. (2023). Evaluation of the rbcL marker for metabarcoding of marine diatoms and inference of population structure of selected genera. Frontiers in Microbiology, **14**: 1071379.

Francé, J., Varkitzi, I., Stanca, E., Cozzoli, F., Skejić, S., Ungaro, N., Vascotto, I., Mozetič, P., Gladan, Ž. N., & Assimakopoulou, G. (2021). Large-scale testing of phytoplankton diversity indices for environmental assessment in Mediterranean sub-regions (Adriatic, Ionian and Aegean Seas). Ecological Indicators, **126**: 107630.

Biography

The author was born on June 22, 1990 in Trieste (Italy), where he lived and studied. He attended Guglielmo Oberdan High School and after graduating he continued his studies at the University of Trieste (UNITS). In 2015, he completed his undergraduate studies in Science and Technology for Environment and Nature, acquiring basic knowledge in natural sciences. His thesis, titled "*Dynamics of pico- and nanoplankton on the mesoscale in front of Terra Nova Bay (Ross Sea, Antarctica)*", was based on the research he conducted during his traineeship at the National Institute of Oceanography and Applied Geophysics (OGS) under the mentorship of Dr. Celussi and the supervision of Prof. Fonda Umani. Two years later, he obtained his Master's degree in Environmental Biology at the same university with a thesis on seagrasses (title: "*Functional redundancy of seagrasses in Mediterranean lagoons: carbon, oxygen and nutrient cycles*"). This work was based on the traineeship at the IFREMER (L'Institut Français de Recherche pour l'Exploitation de la Mer) in the French town of Séte as part of the six-month Erasmus+ program. This research was conducted under the mentorship of Dr. Le Fur, Dr Ouisse and Dr. Malet and under the supervision of Prof. Falace. In 2018 he obtained a position as a young researcher at the Marine Biology Station Piran (National Institute of Biology), where he focused on the ecology of phytoplankton. The same year he enrolled in the postgraduate program in Ecotechnology at the Jožef Stefan International Postgraduate School. Since 2023 he is employed, under the mentorship of Dr. Agnetta, as post-doc at the National Institute of Oceanography and Applied Geophysics (OGS).